

NASA-CR-193215

NASA-CR-193,215

JPL D-5574

(NASA-CR-193215) MODEL
DETERMINATION FOR LARGE SPACE
SYSTEMS WORKSHOP, VOLUME 2 (JPL)
434 p

N93-72760
--THRU--
N93-72775
Unclassified

NASA-CR-193215
19930075313

Z9/18 0163810

MODEL DETERMINATION FOR LARGE SPACE SYSTEMS WORKSHOP

HELD AT CALIFORNIA INSTITUTE OF TECHNOLOGY
MARCH 22-24, 1988

VOLUME 2

RAY-1102

EDISON READER CENTER

EDISON, CALIFORNIA

Sponsored by

Air Force Astronautics Laboratory
and
National Aeronautics and Space Administration
Office of Aeronautics and Space Technology

JPL

Jet Propulsion Laboratory
California Institute of Technology
Pasadena, California

JPL D-5574

MODEL DETERMINATION FOR LARGE SPACE SYSTEMS WORKSHOP

**HELD AT CALIFORNIA INSTITUTE OF TECHNOLOGY
MARCH 22-24, 1988**

VOLUME 2

Sponsored by

**Air Force Astronautics Laboratory
and
National Aeronautics and Space Administration
Office of Aeronautics and Space Technology**

JPL

**Jet Propulsion Laboratory
California Institute of Technology
Pasadena, California**

N93-72760#
N93-72775#

TABLE OF CONTENTS

	<u>Page</u>
Experimental Facilities for System Identification.	1
Dr. Alok Das and Roger C. Thompson	
Identification of Large Space Structure On Orbit - A Survey.	36
Dr. T. K. Hasselman	
Overview of Structural Parameter Identification for Large Space Structures Needs, Concepts, Limits, Potential.	54
Alex Berman	
On the Inclusion Principle and Spillover Effect in the Identification of Distributed Structures.	72
Mark A. Norris and L. Meirovitch	
System Identification Using Modal Residues & Roots	81
Bruce H. Wendler	
Modal Parameter Identification in Space Structure.	97
Haim Baruh and J. Boka	
Effects of Model Deficiencies on Parameter Estimation.	117
T. K. Hasselman	
Stiffnesses of a Solid-Rocket Motor from an Ambient Vibration Survey .	131
S. Rubin, G. Searle, and R. Wagner	
Time Domain Identification of Element Matrices	153
Vernon C. Matzen	
Probabilistic System Identification in the Time Domain	164
James L. Beck	
An Adaptive Identification and Control Scheme for Large Space Systems.	188
James V. Carroll	
Experimental Implementation of Adaptive Control for Flexible Space Structures	238
Gary A. McGraw	
On-Orbit System Parameter Identification	250
Stepan S. Simonian	
A Neurocomputing Approach to Model Determination of LSS.	263
Richard H. Travassos	

TABLE OF CONTENTS

	<u>Page</u>
Variational Modal Identification of Gyroscopic Distributed - Parameter Systems.	290
Larry M. Silverberg and Mark A. Norris	
Stability Analysis and Control of Tethered Satellites.	308
E. H. Abed and D. C. Liaw	
Parameter Identification of Material Constants in a Composite Shell Structure.	331
David R. Martinez and Thomas G. Carne	
Progress Toward a Unified Approach to Space Experiments for Material and Structures.	373
Robert L. Turner	
The Space Station Structural Characterization Experiment	401
James W. Johnson	

VOLUME 2

Some Instrumentation Requirement Issues for the Space Station Structural Characterization Experiment	437-1
Richard S. Pappa	
Application of the ITD Algorithm to Landsat Orbital Transient Responses.	474-2
R. R. Kauffman	
Modal Identification Using Single-Mode Projection Filters & Comparison with ERA and MLE Results.	509-3
Jen-Kuang Huang and Ji-Yao Shen	
ISE Structural Dynamic Experiments	524-4
M. H. Lock and S-Y. Clark	
A Stereo Triangulation System for Structural Identification: Analytical and Experimental Results.	558-5
J. L. Junkins, G. H. James, III, T. C. Pollock, and Z. H. Rahman	
A Unified Process for System Identification Based on Performance Assessment	570-6
C. Hyland and J. W. Shipley	
On-Orbit System Identification Overview.	596-7
Edward Mettler	

TABLE OF CONTENTS

	<u>Page</u>
Optimal Experiment Design for On-Orbit Identification.	616 -8
David S. Bayard	
In-Flight Identification of the Galileo Spacecraft Flexible Mode Characteristics	643 -9
Edward Wong	
Evaluation of a Methodology for Model Identification in the Time Domain	665 -10
R. T. Beck and J. L. Beck	
Non-Parametric Identification Experiment	690 -11
Yeung Yam	
Identification and Control Integration Strategies.	725 -12
Mark Milman, Edward Mettler, and David Bayard	
Formulation and Verification of Frequency Response System Identification Techniques for Large Space Structures	752 -13
J. R. Mitchell, V. L. Jones, and C. Plant	
Modal Model Reduction or Model Reduction of Large Space Structures in Frequency Domain.	800 -14
A.S.S.R. Reddy and Ruan Mifang	
Experimental Component Mode Synthesis with Nonlinear Joints.	827 -15
G. H. Blackwood and A. von Flotow	

VOLUME 3

Nonlinear Modelling, Identification and Estimation of Slew - Induced Structural Deformation	860
Thomas A. W. Dwyer, III and Fakhreddine Karray	
Nonlinear Damping Models in Flexible Structures.	877
A. V. Balakrishnan	
Effects of Mode Localization to the Dynamic Responses of Spacecraft with Disordered Appendages.	893
Bo Ping Wang and David F. H. Chu	
A Proposed Method for Enhanced Eigen-Pair Extraction Using the Finite Element Methods; Theory & Application	908
J. Jara-Almonte and L. D. Mitchell	
Determining State Space Models from Sequential Output Data	941
J. G. Lin	

TABLE OF CONTENTS

	<u>Page</u>
12 Meter Truss Modal Test. Doug Henderson & Michael Zeigler	955
Data Dependent Systems Methodology for Lumped Mass Modelling of Structures. Sudhakar M. Pandit	970
Uncertainties in Large Space Systems J. S. Fuh	982
Eigenvalue/Eigenvector Derivative for SAVI Nonlinear Time Domain Simulation Matthew Orr	992
A Note on the Limitation of Lattice Least Squares. C. L. Gustafson, J. T. Gillis, and G. A. McGraw	1011
Maximum Likelihood Identification for Large Structures Michael F. Barrett and Dale F. Enns	1021
Assessment and Control of Structural Damage. G. D. Jeong, N. Stubbs and J. T. P. Yao	1056
Structural Identification & Damage Assessment of Large Space Structures Richard B. Nelson and Michael E. Fourney	1099
Damage Assessment Technology for Large Space Systems J. C. Chen	1112
A Non-linear Hyper-Coherence Filter for Damage Assessment in Noisy Environment Jeny-Yi Jong and Tom Coffin	1129
The Assessment of Damage in Composites Using the Random Decrement System Identification Technique. N. E. Bedewi, D. N. Kung, J. C. S. Yang, and G-Z. Qi	1143
Summary of Analytical Model Improvement" Method and Related Technology Alex Berman and J. S. Fuh	1185
Dynamic Structural Correlation via Nonlinear Programming Techniques T. Ting and I. U. Ojalvo	1205

TABLE OF CONTENTS

	<u>Page</u>
Evaluation of Structural Integrity Using Integrated Testing and Analysis	1226
Robert N. Coppolino	
An Alternative to Guyan Reduction of Finite-Element Models	1241
Jiguan Gene Lin	
On-Orbit Parametric Identification Methodology	1258
F. Y. Hadaegh and D. S. Bayard	
Computational Requirements for On-Orbit Identification of Space Systems.	1281
Fred Y. Hadaegh	

omit to
P. 437

Attendant List

Prof. E. H. Abed
Electrical Engineering Department
University of Maryland
College Park, Maryland 20742
(301) 454-2496

Anthony K. Amos
AF Office of Scientific Research
AFWAL/FIBR
Wright-Patterson AFB, OH 45433-6553
(513) 255-7191

Peter M. Bainum
Dept. of Mechanical Engrg.
Howard University
2300 6th Street N.W.
Washington, D.C. 20059
(202) 636-6612

Prof. A. V. Balakrishnaw
Electrical Engineering Department
Univ. of California at Los Angeles
Los Angeles, CA 90024-1600

Siva S. Banda
Flight Dynamics Laboratory
AFWAL/FIGC
Wright-Patterson AFB, OH 45433
(513) 255-8677

Prof. H. T. Banks
Center for Control Sciences
Division of Applied Mathematics
Brown University
Providence, RI
(401) 863-3248

Prof. Menahem Baruch
Dept. of Civil Engineering
Univ. of Southern California
Los Angeles, CA 90089-0242
(213) 659-7561

Prof. Haim Baruh
Dept. of Mech. & Aerospace Eng'g.
Rutgers University
P.O. Box 909
Piscataway, New Jersey 08855-0909
(201) 932-3680

Dr. Michael F. Barrett
Honeywell Systems and Research Center
MN 65-2500
3660 Technology Drive
Minneapolis, MN 55418
(612) 782-7286

Dr. David S. Bayard
Jet Propulsion Laboratory
Mail Stop 198-330
4800 Oak Grove Drive
Pasadena, CA 91109
(818) 354-8208

Prof. James L. Beck
Mail Station 104-44
Department of Civil Engineering
Calif. Institute of Technology
Pasadena, CA 91125

Mr. R. T. Beck
Mail Station 104-44
Department of Civil Engineering
Calif. Institute of Technology
Pasadena, CA 91125

Dr. Nabih E. Bedewi
Advanced Technology & Research, Inc.
14900 Sweitzer Lane
Laurel, MD 20707
(301) 953-9200

Mr. H. Benaroya
Weidlinger Assoc.
333 Seventh Ave.
New York, NY 10001
(212) 563-5200

Mr. Alex Berman
Kaman Aerospace Corporation
P. O. Box 2
Bloomfield, CT 06002
(203) 243-7215

Andrew S. Bicos
McDonnell Douglas Astronautics Co.
5301 Bolsa Avenue
Huntington Beach, CA
(714) 896-8879

Attendant List

Mr. G. H. Blackwood
Room 37-335
Massachusetts Institute of Technology
77 Massachusetts Avenue
Cambridge, MA 02139
(617) 253-7472

Dr. Terry Brennan
The Aerospace Corp.
M4/976
P.O. Box 92957
Los Angeles, CA 90009
(213) 336-6810

Clark Briggs
Jet Propulsion Laboratory
Mail Stop 185-105
4800 Oak Grove Drive
Pasadena, CA 91109
(818) 354-8192

Thomas Carne
Sandia National Laboratory
Division 7544
Albuquerque, NM 87185
(505) 822-1738

Dr. James V. Carroll
Business & Tech. Systems, Inc.
36 Commerce Way, Suite 310
Woburn, MA 01801
(617) 932-8582

Mr. Leland Celestre
Rockwell Int'l., Rocketdyne Div.
6633 Canoga Ave., AC15
Canoga Park, CA 91303
(818) 710-6295

Gun-Shing Chen
Jet Propulsion Laboratory
Mail Stop 157-316
4800 Oak Grove Drive
Pasadena, CA 91109
(818) 354-3375

Jon Chrostowski
Engineering Mechanics Associates
3820 Del Amo Blvd.
Suite 318
Torrance, CA 90503
(213) 370-2551

David Fei Hon Chu
GE/Astro-Space Division
P.O. Box 800
Mail Stop 410-A36
Princeton, NJ 08540
(609) 426-3094

Mr. S-Y. Clark
R & D Associates
2301 Yale Blvd., S.E. Bldg. F
P. O. Box 9377
Albuquerque, New Mexico 87119
(505) 842-8911

Dr. Tom Coffin
Wyle Laboratories
7800 Governors Drive West
P.O. Box 1008
Huntsville, AL 35807-5101
(205) 837-4411

Dr. Robert N. Coppolino
Measurement Analysis Corporation
23852 Madison Street
Torrance, CA 90505
(213) 378-5261

Mr. Nelson G. Creamer
General Research Corp.
1215 Jefferson Davis Hwy.
Suite 906
Arlington, VA 22202
(703) 920-2004

John Dahlgren
Jet Propulsion Laboratory
Mail Stop 198-330
4800 Oak Grove Drive
Pasadena, CA 91109
(818) 354-4065

Dr. R. L. Dailey
TRW Space & Defense
One Space Park, 82/2325
Redondo Beach, CA 90278
(213) 535-3085

Mr. Eric Dale
Air Force Astronautics Lab.
AFAL/DYSS
Edwards AFB, CA 93523
(805) 275-548

Attendant List

Dr. Alok Das
Air Force Astronautics Lab.
AFAL/DYSS
Edwards AFB, CA 93523
(805) 275-5412

Dr. Cornelius J. Dennehy
Fairchild Space Company
20301 Century Blvd.
Mail Stop A-14
Germantown, MD 20874-1181
(301) 428-6049

Mr. Ralph Dornsife
USA -CERL - EM
P. O. Box 4005
Champaign, IL 61820
(217) 352-6511

John Doyle
California Institute of Technology
Mail Code 116-81
Pasadena, CA 91125
(818) 356-4808

Prof. Thomas A. W. Dwyer, III
AAE Dept.
University of Illinois
104 South Mathews Ave.
Urbana, IL 61801
(217) 333-2051

Lt. Sharon A. Eide
AF Flight Dynamics Laboratory
AFWAL/FIGC
Wright-Patterson AFB, OH 45433
(513) 255-8683

Daniel Eldred
Jet Propulsion Laboratory
Mail Stop 198-330
4800 Oak Grove Drive
Pasadena, CA 91109
(818) 354-6519

Dr. James L. Fanson
Jet Propulsion Laboratory
Mail Stop 157-316
4800 Oak Grove Drive
Pasadena, CA 91109
(818) 354-7014

Dr. Jens Fromm
DFVLR RF-PV
Linder Hohe
D-5000 Keln 90
Federal Republic of Germany

Mr. John A. Garba
Jet Propulsion Laboratory
Mail Stop 157-316
4800 Oak Grove Drive
Pasadena, CA 91109
(818) 354-2085

Steven Ginter
Honeywell, Inc.
3660 Technology Drive
Minneapolis, MN 55418
(612) 782-7290

Dr. Rafael Gluck
TRW Space & Technology Group
Bldg. R4/1408
One Space Park
Redondo Beach, CA 90505
(213) 297-3655

Robert Gordon
AFWAL/FIBG
Wright-Patterson AFB, OH 45433
(513) 255-5236

Mr. Richard W. Griffiths
G2 Corporation
P.O. Box 666
Pacific Palisades, CA 90272-0666
(213) 454-0777

Dr. C. L. Gustafson
Mail Station M4/974
The Aerospace Corporation
P.O. Box 92957-2957
Los Angeles, CA 90009
(213) 336-1824

Dr. Hari Hablani
Rockwell International
Satellite Systems Division
Seal Beach, CA
(213) 577-3876

Attendant List

Dr. Fred Hadaegh
Jet Propulsion Laboratory
Mail Stop 198-330
4800 Oak Grove Drive
Pasadena, CA 91109
(818) 354-8777

Prof. S. V. Hanagud
School of Aerospace Engr.
Georgia Institute of Technology
Atlanta, Georgia 30332
(404) 894-3000

Dr. T. K. Hasselman
Engr. Mech. Assoc., Inc.
3820 Del Amo Blvd.
Suite 318
Torrance, CA 90503
(213) 370-2551

Mr. Richard G. Helms
Jet Propulsion Laboratory
Mail Stop 157-316
4800 Oak Grove Drive
Pasadena, CA 91109
(818) 354-6507

Dr. Doug Henderson
AFWAL/FIBG
Flight Dynamics Laboratory
Wright Patterson AFB, Ohio 45433
(513) 255-5236

Mr. Charles Herget
Lawrence Livermore Laboratory
P.O. Box 808, L-86
Livermore, CA 94550
(415) 422-7786

Mr. Robert E. Holman
Hughes Aircraft
EO/E12/B106
P.O. Box 902
El Segundo, CA 90245
(213) 414-6656

Robert Hunt
USAF
AFWL/ARBC
Kirtland AFB, NM 87117
(505) 844-1705

Mr. David Hunt
SDRC
11055 Roselle Street
San Diego, CA 98121
(619) 450-1553

Dr. Stuart Hsu
Satellite Systems Division
Honeywell, Inc.
19019 North 59th Ave.
Glendale, AZ 85308
(602) 561-3485

Mr. D. C. Hyland
Harris Corporation
P. O. Box 94000
Melbourne, FL 32902
(305) 729-2138

Paul Ibanez
Anco Engineers
9937 Jefferson Blvd.
Culver City, CA 90232
(213) 204-5050

George James
Texas A&M University
Box 4305
College Station, TX 77844
(409) 845-3288

Garrett D. Jeong
Purdue University
School of Civil Engineering
West Lafayette, IN 47907-3399
(317) 742-0313

Dawn Johnson
Rocketdyne Division
Rockwell International
6633 Canoga Ave., MC-AC15
Canoga Park, CA 91304
(213) 710-4867

James W. Johnson
Langley Research Center
Mail Stop 288
Hampton, VA 23665
(804) 865-4834

Attendant List

Dr. Jeny-Yi Jong
Wyle Laboratories
7800 Governors Drive West
P.O. Box 1008
Huntsville, AL 35807-5101
(205) 837-4411

Dr. Alvar Kabe
The Aerospace Corp.
2350 East El Segundo Blvd.
M4/909
El Segundo, CA 90245-4691
(213) 336-7489

Dr. Daniel C. Kammer
SDRC
11055 Roselle St.
San Diego, CA 92121
(619) 450-1553

Dr. R. R. Kauffman
GE Astro Space Division
P. O. Box 8555
Bldg. 100, Room M4018
Philadelphia, PA 19101
(215) 354-1264

Randy Kendall
The Aerospace Corporation
2350 East El Segundo Blvd.
Mail Stop M4-971
El Segundo, CA 90254
(213) 336-5358

David A. Kienholz
CSA Engineering, Inc.
560 San Antonio Road
Palo Alto, CA 94306
(415) 494-7351

Robert J. Kinsey
The Aerospace Corporation
2350 East El Segundo Blvd.
Mail Stop M4-972
El Segundo, CA 90254
(213) 336-6306

Dr. Robert L. Kosut
Integrated Systems, Inc.
2500 Mission College Blvd.
Santa Clara, CA 95054
(408) 980-1500

Mr. Wallace T. Lee
Aerospace Corp.
Vehicle & Control Systems Div.
P.O. Box 92957, M4/911
Los Angeles, CA 90009
(213) 336-5482

George A. Lesieutre
Sparta, Inc.
23041 De La Carlota, Suite 400
Laguna Hills, CA 92653
(714) 768-8161

Prof. D. C. Liaw
Electrical Engineering Department
University of Maryland
College Park, Maryland 20742

Jiguang Gene Lin
Control Research Corp.
6 Churchill Lane
Lexington, MA 02173
(617) 863-0889

Damian Ludwiczak
NASA Lewis Research Center
21000 Brookpark Road
Mail Stop 86-10
Cleveland, OH 44135
(216) 433-2383

Malcolm Lock
R & D Associates
P.O. Box 9377
Albuquerque, NM 87119
(505) 842-8911

Dr. Michael S. Lukich
TRW Space & Defense
One Space Park, 82/2325
Redondo Beach, CA 90278
(213) 535-3085

Mr. Steve Lust
Hughes Aircraft - EDSG
P.O. Box 902
Mail Stop Bldg. E12, B106
El Segundo, CA 90245
(213) 414-6144

Attendant List

Patrick Mak
The Aerospace Corporation
2350 East El Segundo Blvd.
El Segundo, CA 90245
(213) 336-5717

Dr. David R. Martinez
Sandia National Laboratories
P.O. Box 5800
Division 1522
Albuquerque, NM 87185
(505) 844-1457

Sami F. Masri
School of Civil Engineering
Univ. of Southern California
Los Angeles, CA 90089-0242
(213) 743-6209

Prof. Vernon C. Matzen
Dept. of Civil Eng'g
North Carolina State Univ.
Box 7908
Raleigh, NC 27695-7908

Dr. Dennis J. McGovern
McDonnell Douglas Astronautics Co. - HB
5301 Bolsa Ave., M/S 365-13/3
Huntington Beach, CA 92647
(714) 896-1002

Dr. Gary A. McGraw
Aerospace Corp.
P.O. Box 92957, M/S M4/972
Los Angeles, CA 90009-2957

Prof. L. Meirovitch
Dept. of Eng'g Science & Mech.
Virginia Poly. Inst. & State Univ.
Blacksburg, VA 24061-0219

Mr. Edward Mettler
Jet Propulsion Laboratory
Mail Stop 157-410
4800 Oak Grove Drive
Pasadena, CA 91109
(818) 354-2071

Dr. Mark Milman
Jet Propulsion Laboratory
Mail Stop 198-330
4800 Oak Grove Drive
Pasadena, CA 91109
(818) 354-7548

Prof. J. R. Mitchell
Ohio University
Stocker Center
Athens, OH 45707
(614) 593-5199

Prof. L. D. Mitchell
Dept. of Mechanical Engineering
Virginia Poly. Inst. and State Univ.
Blacksburg, VA 24061
(703) 961-7461

Richard B. Nelson
UCLA
4532 Boelter Hall
Los Angeles, CA 90024
(213) 825-1412

Mr. Greg Norris
Air Force Astronautics Lab.
AFAL/DYSS
Edwards AFB, CA 93523
(805) 275-5526

Mark A. Norris
Virginia Tech.
ESM Department
Blacksburg, VA 24061
(703) 961-4576

Mr. Matthew Orr
Martin Marietta Space Systems
M/S B0560
P.O. Box 179
Denver, CO 80201
(303) 971-9740

Young H. Pak
McDonnell Douglas Astron. Co.
Mail Stop 218/13-3
5301 Bolsa Avenue
Huntington Beach, CA 92647
(714) 896-4682

Attendant List

Prof. Sudhakar M. Pandit
ME-EM Dept.
Michigan Technological University
Houghton, MI 49931
(612) 487-2153

Mr. Richard Pappa
NASA Langley Research Center
Mail Stop 230
Hampton, VA 23665
(804) 865-3196

Mr. Shayan Pazargadi
Wyle Laboratories
1841 Hillside Ave.
Norco, CA 91760
(714) 737-0871

Phil Reamy
USAF
AFWL/ARBC
Kirtland AFB, NM 07117-6008
(505) 844-2016

Prof. A.S.S.R. Reddy
Dept. of Mechanical Engineering
Howard University
Washington, D. C. 20059
(202) 636-6622

Dr. Lynn Rogers
USAF
AFWAL/FIBA
Wright Patterson AFB, Ohio 45433
(513) 255-5664

Prof. I. G. Rosen
Department of Mathematics
University of Southern California
Los Angeles, CA 90089-1113
(213) 743-8808

Ms. Heidi Rosner
TRW
One Space Park, R4/2190
Redondo Beach, CA 90266
(213) 535-1026

Mifang Ruan
Dept. of Mechanical Engrg.
Howard University
Washington, D. C. 20059
(202) 636-7124

Dr. S. Rubin
The Aerospace Corporation
M4/899
P.O. Box 92957
Los Angeles, CA 90009
(213) 336-6408

William C. Russell
Boeing Aerospace
P.O. Box 3999, M/S 82-97
Seattle, WA
(206) 773-2036

Celeste M. Satter
Jet Propulsion Laboratory
Mail Stop 157-410
4800 Oak Grove Drive
Pasadena, CA 91109
(818) 354-9246

Mr. Waid Schlaegel
Air Force Astronautics Lab.
AFAL/DYSS
Edwards AFB, CA 93523
(805) 275-5796

Mr. G. Searle
The Aerospace Corporation
M4/899
P.O. Box 92957
Los Angeles, CA 90009
(213) 336-5482

Mr. John J. Shi
Rocketdyne, Rockwell International
6633 Canoga Ave., FB49
Canoga Park, CA 91303
(818) 700-3893

Ramen P. Singh
Dynacs Engineering Co., Inc.
2280 US 19th North
Suite 111
Clearwater, FL 33575
(813) 799-4124

Attendant List

Dr. J. W. Shipley
Harris Corporation
Government Systems Sector
P. O. Box 37
Melbourne, FL 32902
(305) 727-4437

Prof. Larry M. Silverberg
Dept. of Mech. and Aerospace Eng'g
North Carolina State University
Box 7910
Raleigh, North Carolina 27695-7910
(919) 737-2365

Dr. S. S. Simonian
TRW, Inc.
One Space Park, M/S R4-1090
Redondo Beach, CA 90278
(213) 535-8756

Dr. Robert R. Strunce, Jr.
United Technologies
Strategic Defense Programs Office
2111 Wilson Blvd., Suite 800
Arlington, VA 22201
(703) 284-1823

Norris Stubbs
Dept. of Civil Engineering
Texas A & M University
College Station, TX 77840

Thomas Sutliff
NASA Lewis Research Center
Mail Stop 86-10
21000 Brookpark Road
Cleveland, OH 44135
(216) 433-3887

Dr. Lawrence W. Taylor
NASA Langley Research Center
MS-161
Hampton, VA 23665
(804) 865-4591

Roger C. Thompson
AFAL/DYSS
Edwards AFB, CA 93523
(805) 275-5412

Tienko Ting
University of Bridgeport
221 University Avenue
Bridgeport, CT 06601
(203) 576-4669

A. F. Tolivar
Jet Propulsion Laboratory
Mail Stop 198-330
4800 Oak Grove Drive
Pasadena, CA 91109
(818) 354-6215

Dr. John J. Tracy
McDonnell Douglas Astronautics Co.
Mail Stop 13-3
5301 Bolsa Ave.
Huntington Beach, CA 92647
(714) 896-3810

Dr. Richard H. Travassos
Systolic Systems, Inc.
2240 N. First Street
San Jose, CA 95131

Dr. G. T. Tseng
The Aerospace Corporation
P.O. Box 92957, MS M4/974
Los Angeles, CA 90009
(213) 336-6820

Dr. R. L. Turner
W. J. Schafer Associates
1901 N. Ft. Meyer Drive
Suite 800
Arlington, VA 22209
(703) 558-7900

Prof. F. E. Udwadia
Univ. of Southern California
University Park
Los Angeles, CA 90089-0242

V. B. Venkayya
AF Wright Aeronautical Lab.
AFWAL/FIBR
Wright-Patterson AFB, OH 45433

Attendant List

Dr. Frank Vigneron
Dir. of Space Mechanics
Communication Research Ctr.
Box 11490, Station H
Ottawa, Canada K2H 8S2
(613) 998-2741

Ben K. Wada
Jet Propulsion Laboratory
Mail Stop 157-5074800 Oak Grove Drive
Pasadena, CA 91109
(818) 354-3600

Mr. William B. Walton
ANCO Engineers, Inc.
9937 Jefferson Blvd.
Culver City, CA 90232
(213) 204-5050

Bo Ping Wang
Univ. of Texas at Arlington
Box 19023
Arlington, TX 76019
(817) 273-2021

Dr. S. J. Wang
Jet Propulsion Laboratory
Mail Stop 198-330
4800 Oak Grove Drive
Pasadena, CA 91109
(818) 354-7288

Mr. John Ward
Air Force Astronautics Lab.
AFAL/DYSS
Edwards AFB, CA 93523
(805) 275-5205

Mr. Carl Wellstein
Rockwell-Rocketdyne Div.
6633 Canoga Ave., M/S AC49
Canoga Park, CA 91403
(818) 700-4025

Dr. Bruce H. Wendler
Structural Gram
2736 N. Lamer Street
Burbank, CA 91504
(818) 842-9209

Donald M. Viberg
UCLA
7731 Boelter Hall
Los Angeles, CA 90024-1594
(213) 825-2214

Dr. Edward Wong
Jet Propulsion Laboratory
Mail Stop 198-326
4800 Oak Grove Drive
Pasadena, CA 91109
(818) 354-3053

Dr. Yeung Yam
Jet Propulsion Laboratory
Mail Stop 198-326
4800 Oak Grove Drive
Pasadena, CA 91109
(818) 354-0174

Chou-Chung Yu
McDonnell Douglas Astron. Co.
5301 Bolsa Avenue
Huntington Beach, CA 92647
(714) 896-2633

Dr. Michael Zeigler
AFWAL/FIBG
Flight Dynamics Laboratory
Wright Patterson AFB, Ohio 45433
(513) 255-5236

Karen R. Zinski
Rocketdyne
6633 Canoga Avenue
Canoga Park, CA 91304
(818) 710-4052

Jay-Chung Chen
Jet Propulsion Laboratory
Mail Stop 157-316
4800 Oak Grove Drive
Pasadena, CA 91109
(818) 354-2717

92261-396

**SOME INSTRUMENTATION REQUIREMENT ISSUES
FOR THE
SPACE STATION STRUCTURAL CHARACTERIZATION EXPERIMENT**

**Richard S. Pappa
Structural Dynamics Branch
NASA Langley Research Center
Hampton, Virginia**

**Presented at the
USAF/NASA Workshop on Model Determination for Large Space Systems
Pasadena, California
March 22-24, 1988**

51-19
163811
P-37

437

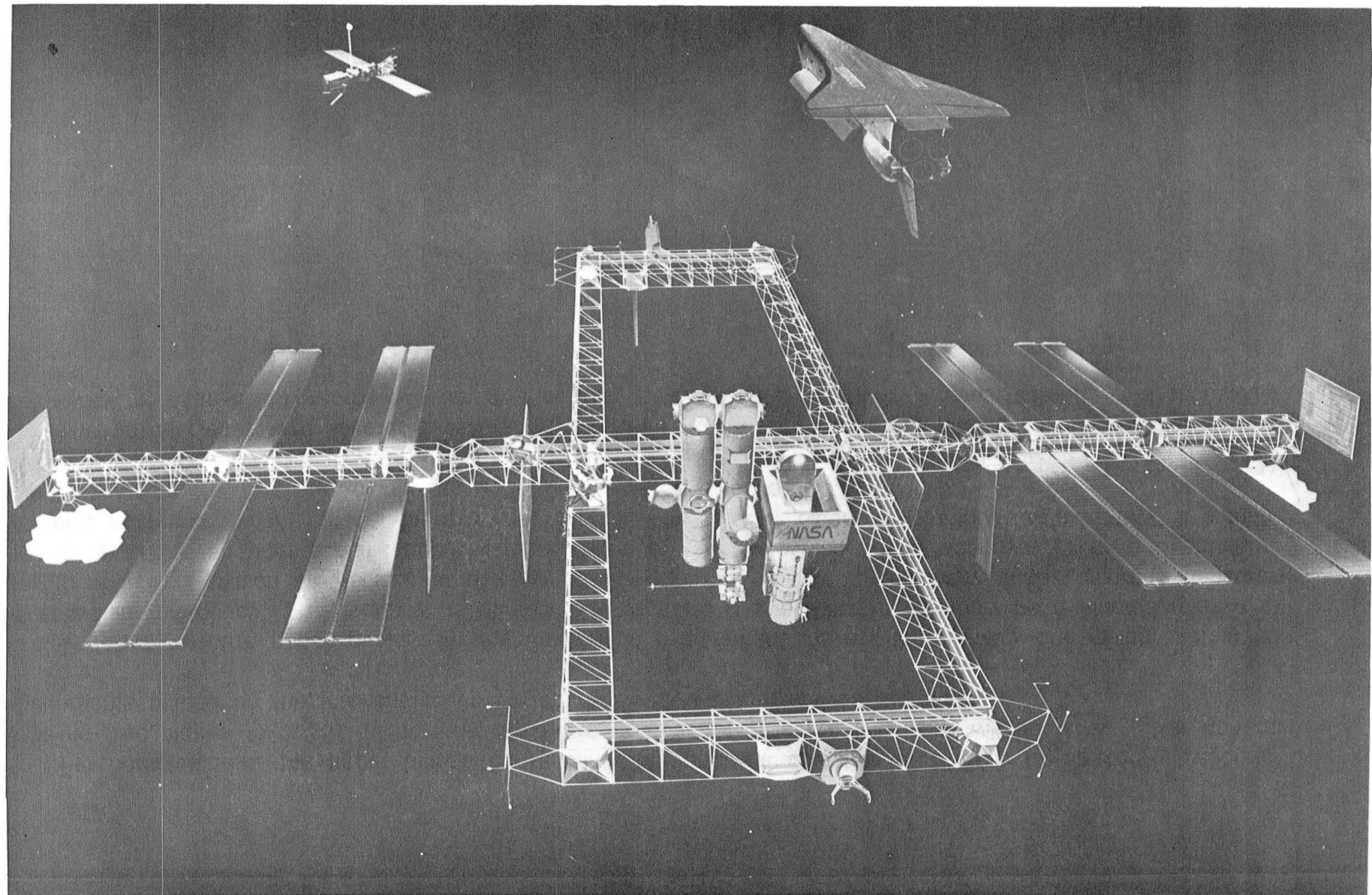
INTRODUCTION

The Space Station will provide unique opportunities to the Research and Technology (R&T) community as a national in-space research facility. Opportunities will exist for technology experiments in a variety of disciplines, including Dynamics and Control of Large Space Structures (LSS) (Reference 1).

The Space Station Structural Characterization Experiment (SSSCE), summarized in the previous talk at this Workshop (Reference 2), is an early Space Station technology experiment now under development. The objective of the experiment is to instrument and use the Space Station as a generic research test article, in support of R&T activities in the areas of Structural Dynamics and Control/Structure Interaction (CSI). Tests will be conducted, potentially, on each assembly flight configuration, as well as on the Phase I configuration. Structural dynamic response data will be measured and transferred to the ground for analysis. These measurements will support the development and in-space verification of system identification and analytical modeling techniques for future LSS, including the Evolutionary Space Station.

SSSCE is sponsored by NASA's Office of Aeronautics and Space Technology (OAST), with research and technology development objectives. As emphasized in Reference 2 and repeated here, SSSCE is a technology experiment which uses the Space Station as a generic LSS test article, and it does not represent, in any way, requirements within the Space Station Program.

Development of SSSCE is being directed by the LaRC Space Station Office, with Mr. James W. Johnson serving as project manager. The McDonnell Douglas Astronautics Company (MDAC) was recently awarded a study task to evaluate feasible approaches for conducting the experiment. That work, in conjunction with possible follow-on studies, will serve as the formal basis for developing the project. The data and issues discussed in this paper originated from in-house analyses and experiences, and are intended to complement, not supersede, the MDAC activity.



TOPICS

For completeness, the paper begins by restating the principal objective of SSSCE (In-Space Validation of Modeling Techniques for LSS), along with the basic approach (Modal Testing) that will be used. The general requirements placed on the instrumentation system to meet these objectives are given.

The body of the paper deals with instrumentation requirement issues, the primary one being: How do we establish "adequacy"? "Adequacy" is quoted to emphasize the fact that it can only be evaluated relative to specific objectives, which are difficult to develop so early in the project. Additionally, many different measures can be applied even after specific objectives are available. Those which gauge adequacy relative to structural dynamics model-refinement criteria, for example, may be considerably different from those related to CSI criteria. Work now in progress to help clarify and resolve the issues is described.

The paper closes with several questions concerning modal-testing objectives and limitations (ambiguities), a brief review of a previous on-orbit experiment--the Solar Array Flight Experiment (lessons learned), and concluding remarks.

TOPICS

- SSSCE
- GENERAL INSTRUMENTATION REQUIREMENTS
- REQUIREMENT ISSUES:
 1. How Do We Establish "Adequacy"?
 2. Other Ambiguities?
 3. Lessons Learned in Previous Programs?
- CONCLUDING REMARKS

SPACE STATION STRUCTURAL CHARACTERIZATION EXPERIMENT

The primary objective of SSSCE is to collect sufficient in-space data to validate various analytical modeling techniques for LSS. The basic approach is to conduct on-orbit modal testing (References 3-4).

This objective--to conduct modal testing in order to validate analytical models and modeling techniques--is a common goal of structural dynamics programs (References 5-6). Experience has shown, however, that the objective is often difficult to satisfy completely, with the level of success being highly dependent on the characteristics of the particular structure (i.e., the degree of nonlinearity, modal density, etc.). If modal test results are to be used to validate modeling techniques, they must accurately represent the characteristics of the structure. The challenge facing the experiment-definition activity now underway is to develop a viable testing and measurement strategy that will afford the highest probability of satisfying the stated objective, recognizing that some degree of uncertainty is inevitable.

The expression "Modal Testing" is being used throughout this project in a somewhat generic manner. For example, SSSCE does not intend to use experiment-unique actuators for excitation, as done in laboratory modal tests, unless all available Station excitation sources prove to be inadequate. Also, modal-parameter identification is only one of many types of data analysis that will be possible. The intent is to record all data in unprocessed form, to the extent possible, so that other types of system identification techniques can be applied as well.

SPACE STATION STRUCTURAL CHARACTERIZATION EXPERIMENT

Objective

To Collect In-Space Research Data to Characterize the Structural Dynamics of the Space Station, in Support of the Development of Analytical Models & Modeling Techniques for Large Space Structures.

Approach

On-Orbit Modal Testing of the Space Station at Each Stage of Assembly, to Identify:

Natural Frequencies

Damping

Mode Shapes

Nonlinearities

GENERAL INSTRUMENTATION REQUIREMENTS

General requirements for instrumentation are shown, along with a restatement of the three issues to be discussed. Most of the questions posed in this paper are related to Issue 1, and the asterisk is used to highlight this fact.

Both science and project-related requirements must be satisfied.

The science requirements consist of four primary items, all of which must be demonstrated to be "adequate." The issue of adequate coverage (i.e., how many sensors are needed, and where should they be located?) is of fundamental importance. The selections that are made could impact significantly the ultimate research benefits and opportunities resulting from the experiment. Performance requirements for sensors and data-acquisition hardware to detect and accurately record the dynamic response at these locations must then be assessed. Important issues here include: "What is the lowest level of vibration that must be measured?" and "What frequency range should be covered?". Dynamic response levels are expected to be much smaller (in terms of acceleration) than commonly encountered in the laboratory, and sensors to detect 1 micro-g or less may be needed. All of these issues related to coverage and performance must then be evaluated relative to the test configurations expected. As mentioned earlier, an attempt will be made to collect data on all assembly flight configurations, and on the Phase I configuration. Relocation of instrumentation between configurations would be costly, at best, implying that it should function effectively on early configurations as well as on subsequent ones. Optimization across all test configurations will require a measure of relative importance of the various configurations to be established. The final science requirement imposed on the instrumentation is that its performance must be adequately immune to errors in pre-test predictions. Satisfactory tolerance of all prediction errors must be demonstrated, including errors in natural frequencies, damping, mode shapes, and linearity.

Three project-related requirements are also shown. In addition to satisfying the science requirements mentioned above, the instrumentation system(s) must interfere as little as possible with other Station functions; their cost must be commensurate with the expected science benefits; and an adequate level of technology maturity must be demonstrated. To the extent possible, the science requirements will be established independently of project concerns, at least in the initial studies.

GENERAL INSTRUMENTATION REQUIREMENTS

- Adequate:
 - Coverage
 - Performance
 - Effectiveness For All Assembly Configurations, w/o Relocation
 - Tolerance of Pre-Flight Prediction Errors
- Minimum Interference With Space Station Project
- Acceptable Cost/Technology Maturity

Issues

- * 1. How Do We Establish "Adequacy"? (*Cont. on Next Chart*)
- 2. Other Ambiguities?
- 3. Lessons Learned in Previous Programs?

HOW DO WE CONFIDENTLY ESTABLISH INSTRUMENTATION "ADEQUACY"?

This figure shows four activities that will be used to help establish instrumentation "adequacy."

A formal experiment-definition study, currently underway at McDonnell Douglas, constitutes the primary effort. A simplified flow chart of the definition process will be presented in the following chart.

To assess instrumentation adequacy, it is necessary to understand the data requirements and--to some degree--the performance characteristics of various modal testing and identification techniques. As part of the MDAC study, a thorough review of this technology will be conducted. Ongoing research at LaRC in these areas will contribute additional information as well.

The third activity, modeling and simulation, is of central importance to the successful development of SSSCE. The principal work in this area to date has been performed using the Integrated Multidisciplinary Analysis Tool (IMAT) capability at LaRC (Reference 7). Detailed finite-element models of the structure, including control effects, will be used throughout the project. The results shown in this paper were generated using the IMAT-developed model of the NASA Reference Space Station configuration (Reference 8), as defined in the November 1987 Space Station Program-- Systems Engineering and Integration Data Book. McDonnell Douglas is currently using the IMAT model, as well, in their study.

The final item, ground tests, is not formally associated with the SSSCE experiment-development process at this time. Several opportunities will exist in the near future, however, to investigate candidate modal testing and identification techniques on various generic Space-Station components and models to be tested at LaRC (References 9-10). These tests will be performed under other work areas (R&T, DSMT, CSI). Application of proposed SSSCE procedures to real hardware, it is felt, will provide increased assurance of their effectiveness, and can serve to illustrate better--by example--the outstanding issues.

Work-in-progress in each of these areas will be discussed in the following charts.

HOW DO WE CONFIDENTLY ESTABLISH INSTRUMENTATION "ADEQUACY"?

(To Best Satisfy Research Objectives)

- Formal Experiment-Definition Study (MDAC)
- Better Definition of Data Requirements and Performance Characteristics of Various Modal Testing & Identification Techniques (MDAC/LaRC)
- Modeling and Simulation (LaRC/MDAC)
- Ground Tests (LaRC R&T)

*Work-in-Progress in Each of These Areas is Discussed in the
Following Charts.*

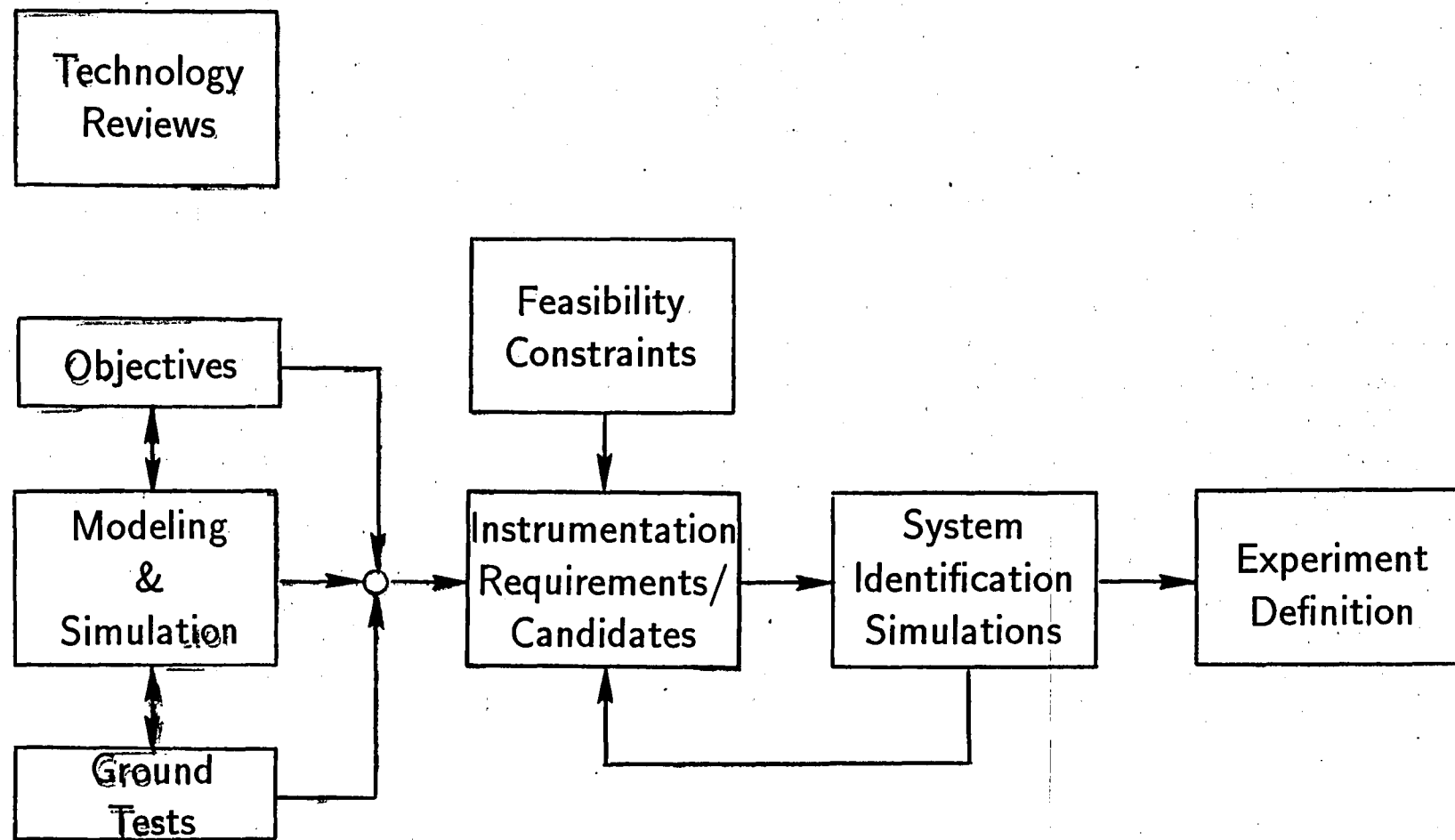
EXPERIMENT DEFINITION

A simplified block diagram of the experiment definition process is shown. Each of these areas constitutes a significant work item during the definition process. (As mentioned earlier, the Ground Test activity is not formally included in the SSSCE project, at this time, but will be conducted in conjunction with other projects.)

Note that Instrumentation Requirements/Candidates are affected by results generated in five other blocks, as well as by results from the Technology Reviews. Some fundamental issues are: How should these factors be weighted in order to develop a viable and effective set of requirements? If conflicting requirements are indicated, how should the selection be made? Do we understand the needs/concerns of all potential users of SSSCE data? The importance of developing an accurate set of instrumentation requirements cannot be overestimated because, once established, it will serve as the basis against which instrumentation hardware will be evaluated.

Other important issues are: How much fidelity is required in simulations? It is well known, for example, that the performance of commonly used modal identification techniques can be affected significantly by nonlinearities and closely spaced natural frequencies, particularly when occurring simultaneously. To what degree should we evaluate the effects of potential nonlinearities and errors in natural frequency predictions? Also, are we accounting for ambient sources of excitation with enough fidelity? If the baseline testing technique consists of the analysis of free-decay responses, for example, the amplitude of extraneous sources becomes very important.

EXPERIMENT DEFINITION



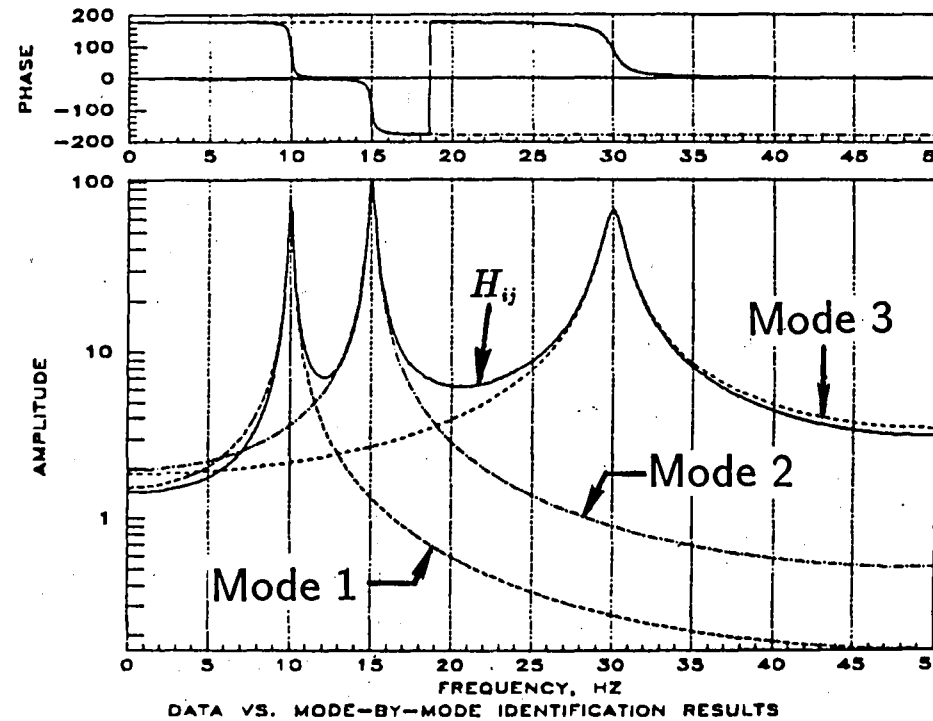
THE CHALLENGE OF MODAL IDENTIFICATION

One of the most difficult aspects of defining instrumentation requirements for SSSCE--or for any modal test for that matter--is that the desired end-product, the modal parameters, are not directly measurable quantities (such as temperature or strain, for example). The measurements that are made contain contributions from many modes. The challenge of modal identification is to correctly infer from the measured data the characteristic parameters of each of the individual, contributing modes. The accuracy with which this inference can be performed depends on many factors, including the characteristics of the data and the sophistication of the identification algorithm being used. These factors make it difficult to predict, with certainty, how well modal parameters will be identified in an experiment, based on the results of simulations. The strength with which the mode contributes to the measured response, relative to the instrumentation noise floor, is an important factor; however, it is not the only factor. When identification techniques are applied to simulated data, then, the findings generally constitute only necessary, but not sufficient, information. That is, other factors not included in the simulation can degrade the results further. When instrumentation requirements are defined for SSSCE, this uncertainty must be considered.

For completeness--to illustrate the potential difficulty of modal identification--the following three figures show the results of simple 3- and 10-mode simulations. The first figure illustrates the decomposition of a "measured" frequency response function into its individual modal contributions. The objective is to determine the value of each quantity listed below the plot, given only the frequency response function. In this simple example, the decomposition process is performed with virtually no error because noise-free, linear data were used. That is, the data satisfied exactly the assumed frequency-response equation shown in the figure. With experimental data, however, this assumption is always violated to some degree, resulting in reduced accuracy.

THE CHALLENGE OF MODAL IDENTIFICATION

(3-Mode Simulation)



$$H_{ij}(\omega) = \sum_{r=1}^N \frac{\phi_{ir}\phi_{jr}/m_r}{(\omega_{nr}^2 - \omega^2) + j2\zeta_r\omega_{nr}\omega}$$

$(H_{ij}(\omega))$ = Measured Frequency Response Function)

- How Many Modes? (N)
- Natural Frequencies? (ω_{nr})
- Damping Factors? (ζ_r)
- Mode Shape Coefficients? (ϕ_{xy})
- Modal Mass? (m_r)
- Nonlinearities?

10-MODE SIMULATION, WITH NOISE

This figure shows the results for a more-complex, 10-mode simulation with added noise. This data represents, more closely, a typical measurement from an actual structure.

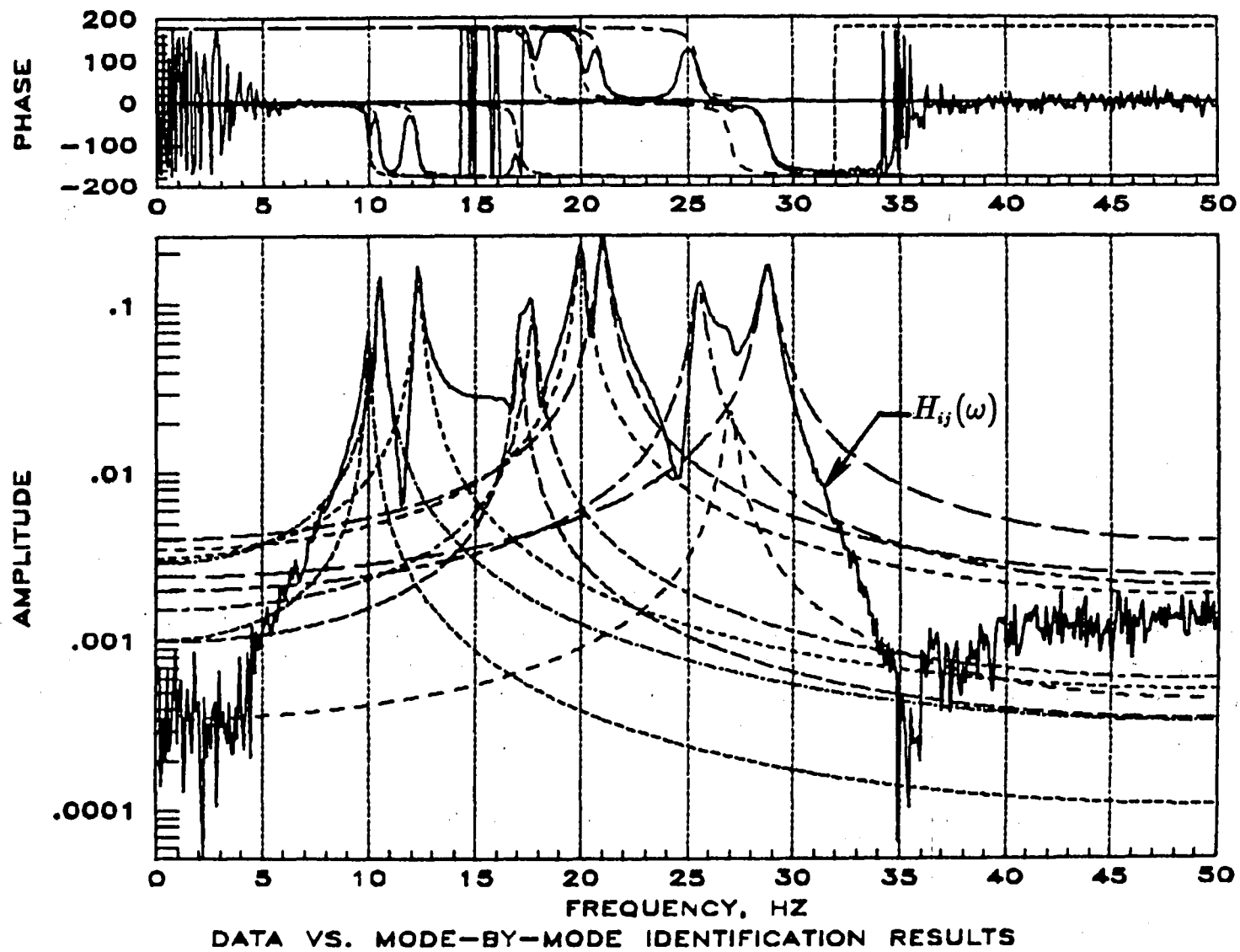
The only a-priori information is the "measured" frequency response function shown as a solid line. The individual modal contributions identified from this data are again plotted using dashed lines. Note that these results are all complex functions of frequency, consisting of both amplitude and phase. Perhaps surprisingly, the sum of the ten dashed lines, added vectorially, closely equals the solid line. (This comparison is shown on the next chart). The ten results are virtually identical to the functions used in constructing the simulated data.

As stated, this example more closely illustrates a typical modal identification challenge encountered in practice. With experimental data, however, the situation is often even worse. For example, each peak seen on the frequency response function can represent more than one mode. All that is certain is that each peak represents at least one mode. Errors in determining the number of contributing modes can significantly affect the identification results. Also, nonlinearities, which occur in some degree in all mechanical systems, cause the measurements to violate the basic linear-system equation shown previously, generating additional identification errors.

The identification results shown in this figure, and also in the previous one, were generated using the Eigensystem Realization Algorithm (ERA), a multi-input, multi-output, time domain algorithm developed at LaRC (References 11-12).

10-MODE SIMULATION, WITH NOISE

(ERA Identification Results)

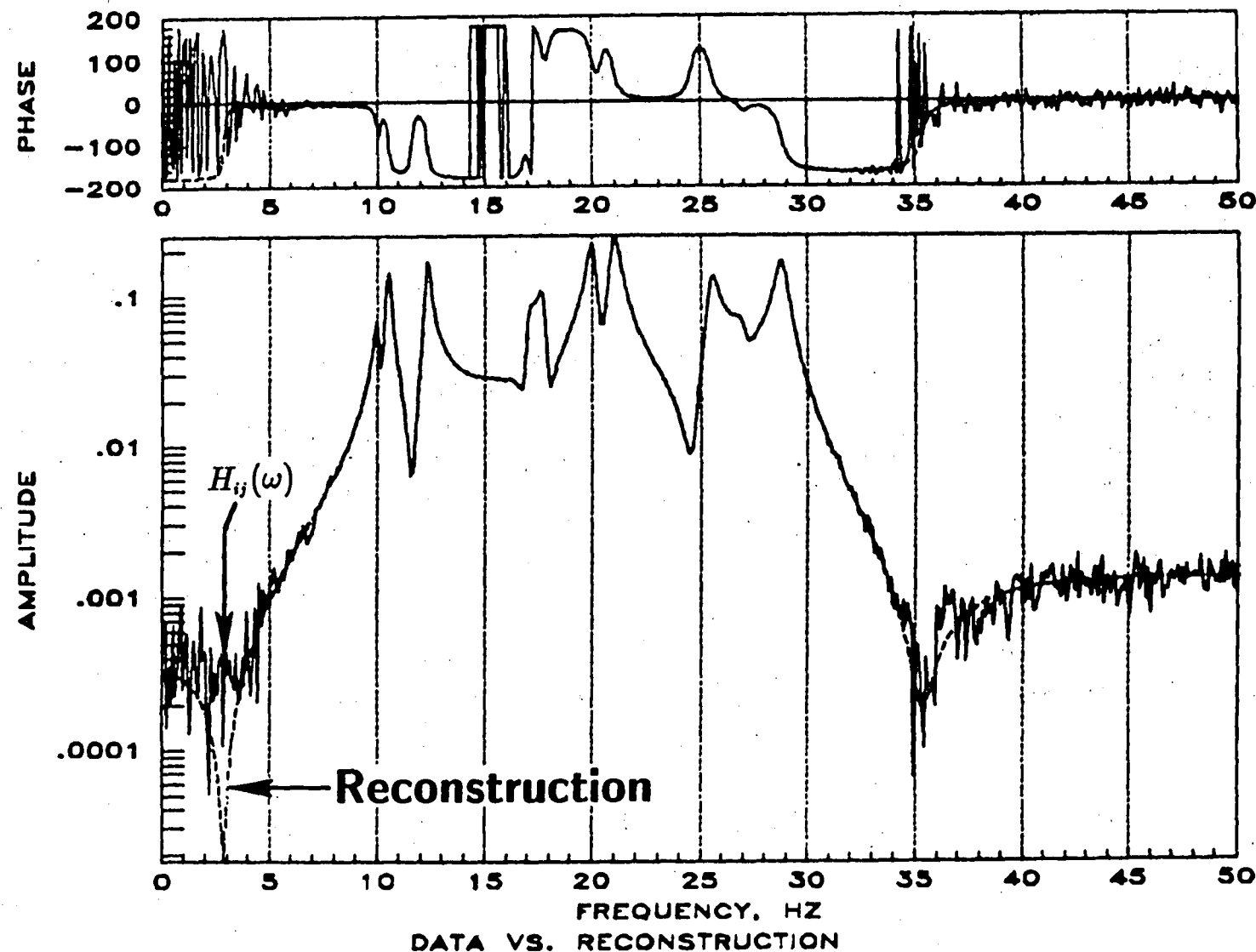


COMPARISON OF DATA WITH RECONSTRUCTION

The sum of the ten individual modes shown on the previous chart is compared with the original data used in the analysis in this figure. As stated, the sum (reconstruction) of the identified modes closely matches the "measured" data, even in regions of low signal amplitude. (That is, the reconstruction closely equals the analytical function--without added noise--over the entire bandwidth shown). The corresponding identified parameters, for all ten modes, were virtually identical to those used in constructing the simulated data.

COMPARISON OF DATA WITH RECONSTRUCTION

(Reconstruction = Sum of Identified Modes on Previous Chart)



STRUCTURAL-DYNAMIC COMPLEXITY: AN IMPORTANT ISSUE

As mentioned, experimental data can be even more complex than the 10-mode example just discussed. This is an important issue, and can affect instrumentation requirements considerably.

An example of such complex data is shown in the figure. These data are frequency response functions measured in the modal test of LDEF--the Long-Duration Exposure Facility. LDEF is a 30-ft-long passive satellite carrying experiments in each of 86 trays around its periphery. The structure was tested both with, and then without, the trays. With the trays installed an extremely high number of modes existed in the bandwidth of interest due to resonances of each individual tray. These results, shown in the upper plot, were virtually impossible to analyze. The difficulty resulted not only from the high modal density, but also from the fact that measurements were made only on the main structural beam members (using 142 accelerometers), and not on the trays themselves. Of course, to do so would have required a much larger number of sensors.

The trays were then removed and the structure re-tested. These results are shown in the lower figure. There are now approximately 30 modes below 55 Hz, compared with more than 100 in the first test configuration. The principal modes were identified using these frequency response functions, although the modal density was high enough to pose a significant challenge. Several weeks were devoted to data analysis, using various algorithms and other sets of data.

In its early stages of assembly, the Space Station will probably be less dynamically complex than LDEF with trays. In its operating configuration, however, many more dynamic degrees-of-freedom may arise in the bandwidth of interest due to the modes of individual subsystems and user payloads. This possibility is an important issue, and must be considered when establishing instrumentation requirements for SSSCE. Simulations using simplified structural models may falsely indicate adequate instrumentation.

STRUCTURAL-DYNAMIC COMPLEXITY: AN IMPORTANT ISSUE

STRUCTURAL DYNAMIC FREQUENCY RESPONSE CHARACTERISTICS OF LDEF

ACCELEROMETER

NO.

150

120

90

60

30

0

10 20 30 40 50

FREQUENCY, Hz

WITH TRAYS

150

120

90

60

30

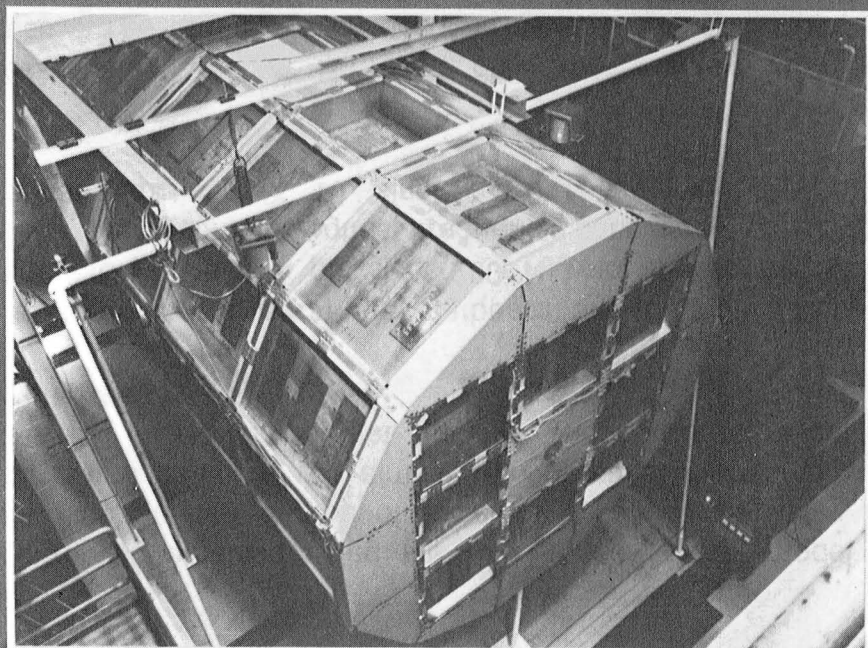
0

10 20 30 40 50

FREQUENCY, Hz

WITHOUT TRAYS

LDEF GROUND VIBRATION TEST



MODELING AND SIMULATION

The next three figures show representative analytical results obtained using the IMAT finite-element model of the Phase I configuration. The main intent is to briefly illustrate the degree of structural-dynamic complexity, based on current predictions. Measurements made on the actual structure will--almost without question--be more complex (not less complex) than these results. The analytical model is not yet detailed enough to represent accurately the dynamics of individual subsystems or user payloads.

The first figure shows response spectra measured at three locations on the starboard end of the Station due to an x-direction firing of the Reaction Control System (RCS) jets. A pulse of 200 N was applied for 50 msec to each thruster. This duration is short relative to the period of the highest frequency considered (2 Hz), so that the spectra shown are essentially frequency response functions (X 10, since a 10 N-sec impulse was used).

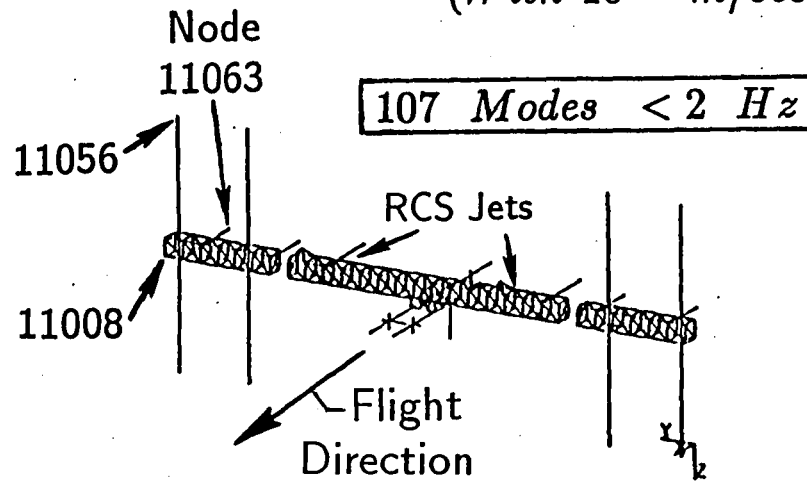
There are 107 modes, including six rigid-body modes, below 2 Hz. However, only approximately 20 of these modes involve primary bending and torsion of the truss. The others, which occur in several dense clusters, are predominantly appendage modes of the Photovoltaic Arrays and Radiators. A more-complete discussion of the analytical model and the modal characteristics is available in Reference 8.

Free-decay response histories generated in this simulation are being analyzed by various modal identification techniques, including ERA. The work is not yet complete, however, and is not discussed in this paper.

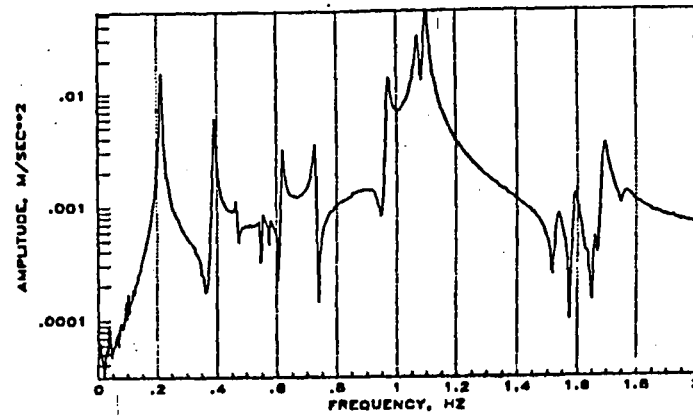
MODELING & SIMULATION

PREDICTED ACCELERATION RESPONSE SPECTRA DUE TO 50 MSEC FIRING OF X-DIRECTION RCS JETS

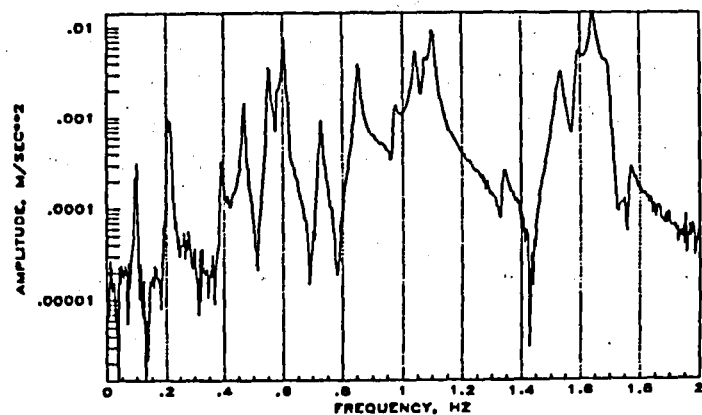
(With 10^{-5} m/sec^2 Sensor Noise Added)



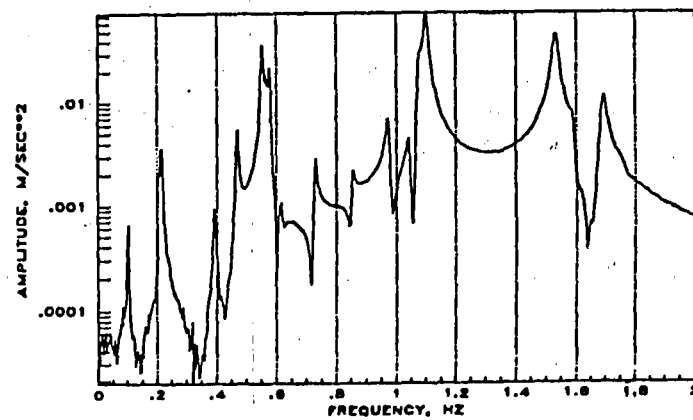
Finite-Element Model



Response DOF: 11008X



Response DOF: 11056Y



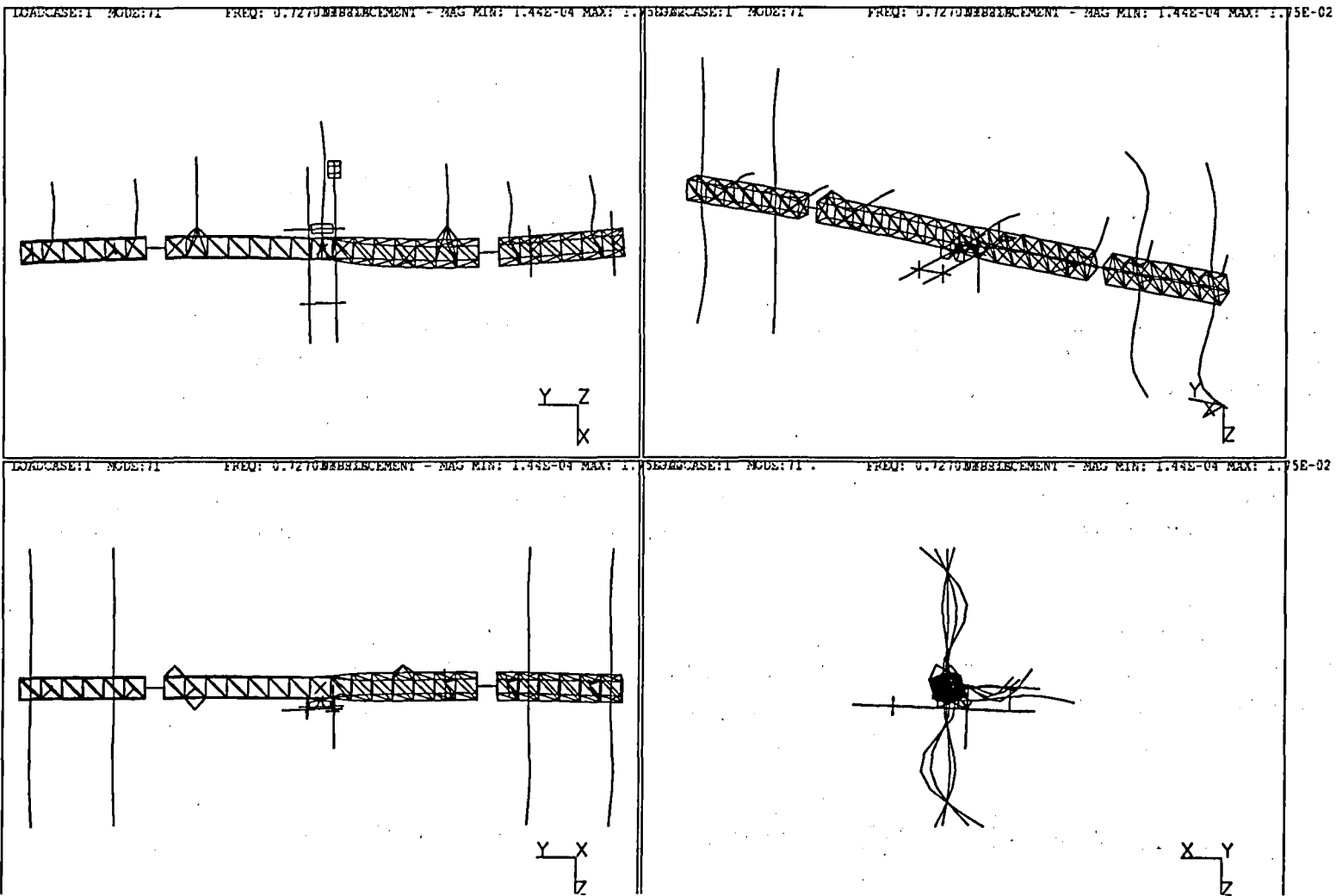
Response DOF: 11063Z

SAMPLE MODE SHAPE

A fairly representative mode shape is shown. This mode is one of the principal truss modes, involving torsion of the port side with significant participation in the appendages, as well.

Note that each appendage is moving somewhat differently. This complexity implies the need for a large number of sensors to characterize accurately. (Of course, the torsional motion of the truss alone could be identified with fewer sensors.) Many other modes involve complex appendage activity such as this. The number of appendages which need to be measured in order to provide "adequate" information for validating analytical modeling techniques is a key instrumentation requirement issue.

SAMPLE MODE SHAPE (0.727 Hz)



MODE-BY-MODE ACCELERATION UNIT-IMPULSE-RESPONSE AMPLITUDES

This figure shows impulse-response amplitudes at two locations at the starboard end of the Station, on a mode-by-mode basis, for excitation using the x-direction RCS jets. The upper and lower dotted lines correspond to response levels of $1E-3$ and $1E-6$ m/sec **2 , respectively. These are the amplitudes resulting from a 1 N-sec impulse applied by each thruster.

In operation, the thrusters will produce approximately 200 N, with a minimum pulse duration on the order of 50 msec. This corresponds to an impulse magnitude of 10 N-sec, and the resulting response amplitudes are 10 times larger than those shown in the figure.

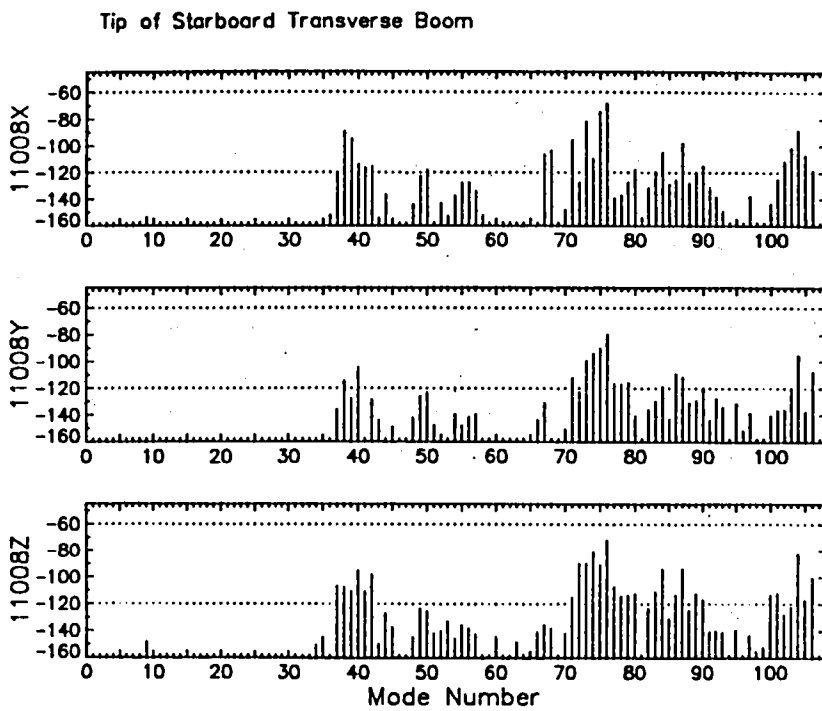
If these response amplitudes are expressed in gravity units, however, this factor of 10 is canceled approximately by the 9.8 conversion factor. Thus, the two dotted lines shown in the figure can be alternatively interpreted as response amplitudes of 1 milli-g and 1 micro-g, respectively, due to a 200 N, 50 msec RCS firing.

These levels have special significance: the lowest level that can be sensed by typical low-g accelerometers is approximately 1 micro-g. On the other hand, levels greater than 1 milli-g should be measurable with little difficulty and should provide strong signals for identification.

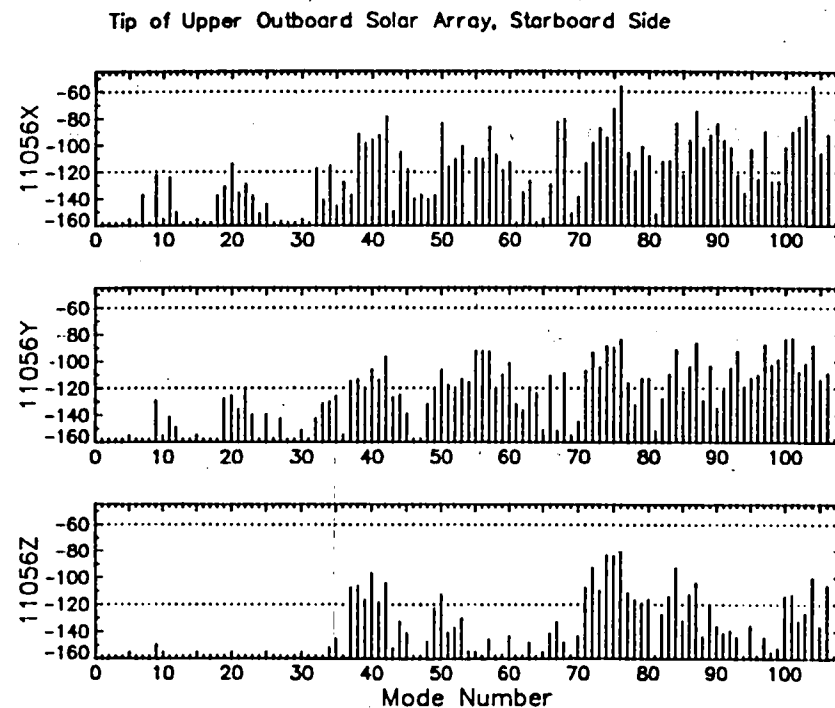
MODE-BY-MODE
ACCELERATION UNIT-IMPULSE-RESPONSE AMPLITUDES
DUE TO IN-PHASE FIRING OF X-DIRECTION RCS JETS

dB re $1 m/sec^2$

Response Node: 11008



Response Node: 11056



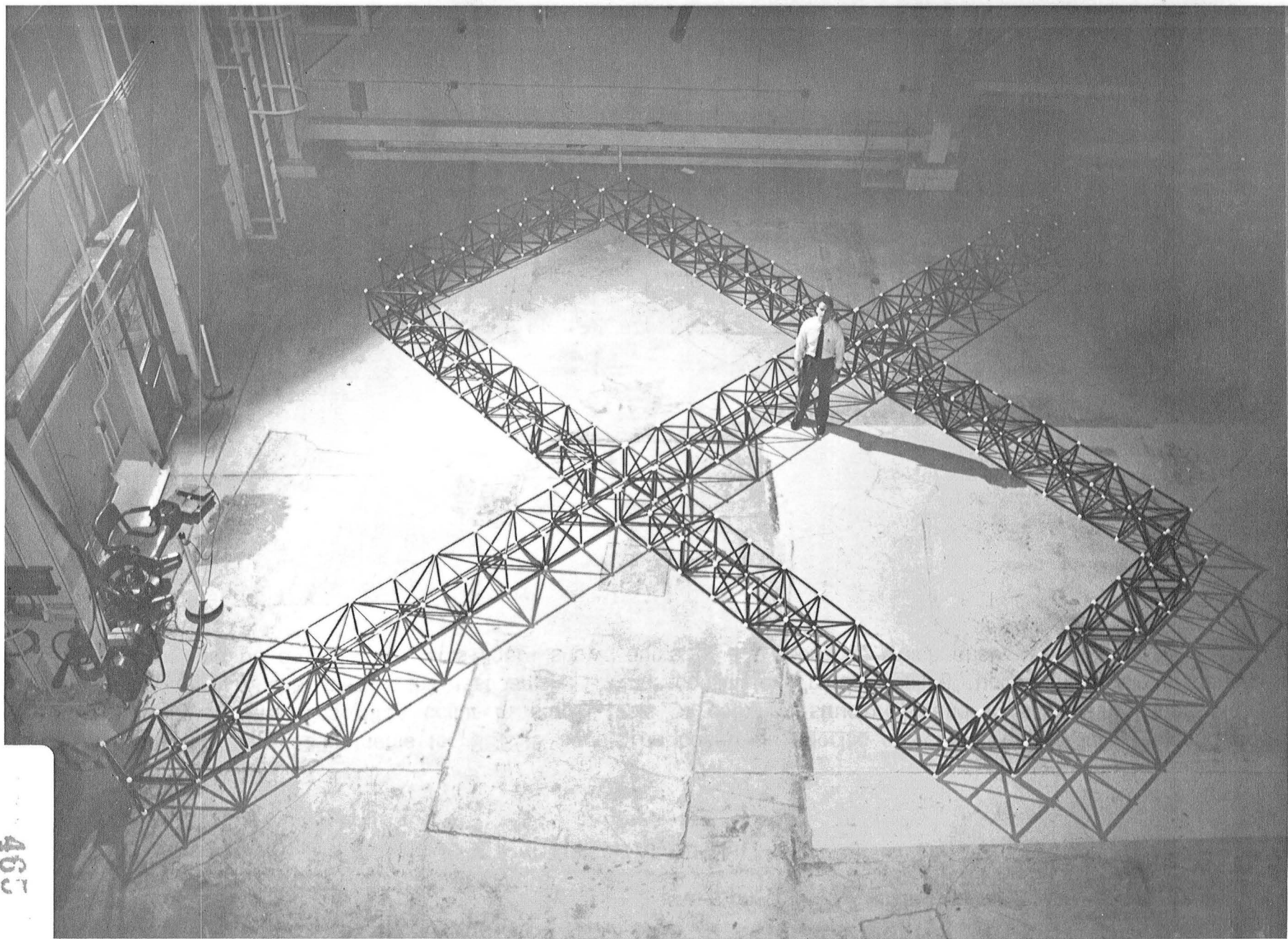
GROUND TESTS

As mentioned earlier, ground tests of generic Space Station components and models will be conducted at Langley under other work areas.

To the extent possible, the instrumentation and identification concepts considered for SSSCE will be applied in these experiments. This information will help assure experiment effectiveness. Unresolved issues, particularly those associated with experimental practicalities and limitations, should become clearer.

This figure shows the trusswork of a generic 1/10-scale Space Station model being prepared for testing. It will be suspended using long cables, and extensive modal testing will then be conducted. Following this program, a higher-fidelity model will be tested in the same facility.

GROUND TESTS
(1/10-Scale Dual-Keel Generic S. S. Model)



OTHER AMBIGUITIES

Instrumentation requirements for SSSCE should be based on specific objectives, to the fullest extend possible. Many uncertainties often occur in modal tests of complex structures, and it is usually impossible or impractical to fully characterize the test article. What constitutes "modal testing" under these circumstances? The answer can be ambiguous. This figure shows some of the questions which arise.

OTHER AMBIGUITIES

(To What Extent Do These Issues Affect Instrumentation Requirements?)

- Which Modes Are Important?
- Which Measurement Degrees-of-Freedom Are Sufficient (Best) to Characterize Mode Shapes?
- How Should Local Modes and Nonlinearities Be Handled?
- Are Structural-Dynamic Characteristics Invariant?
- Modal Mass Required?
- O. K. to Obtain Linear Combinations of Some Modes?
- O. K. to Miss Modes Altogether?
- Criteria For Assessing Modal-Identification Accuracy?
- Accuracy Requirements?

LESSONS LEARNED

Development of the technology to conduct on-orbit modal testing of Large Space Structures poses significant technical challenges. Many modal tests are conducted on the ground every year, and much can be learned from them. A small number of on-orbit experiments have already been conducted as well.

This figure shows results from the Solar Array Flight Experiment, conducted in September 1984. The test article is a 13-ft by 105-ft solar array which was extended from the Space Shuttle while in orbit. Vibration tests were conducted at two deployment lengths: 70 percent and 100 percent. When fully extended, the structure has more than 30 modes below 1 Hz, with the lowest at approximately 0.035 Hz. At 70-percent extension, the lowest mode increases to 0.059 Hz.

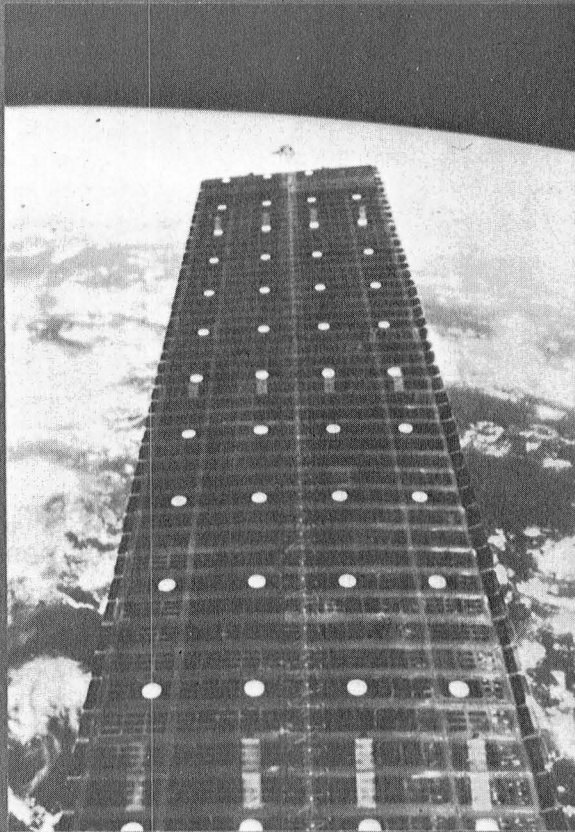
Free-response data were acquired by photogrammetric analysis of TV images. A least-squares triangulation process was applied to four simultaneous views of the array recorded with cameras at the corners of the cargo bay. Sixty locations on the array, consisting of six-inch white targets on the front and back surfaces, were measured. The analysis procedure extracted the centroid of each target. Vibrations were induced by maneuvering the Shuttle using its vernier reaction control system.

Overall, this project was very successful. The first several modes of each test configuration were characterized accurately, using this testing approach and ERA for data analysis. A more-complete description of the project is available in Reference 13.

The work described above was conducted at the Langley Research Center. An additional measurement system, consisting of a Retroreflector Field Tracker and 23 reflective targets mounted on the array, was also used. This capability was developed and used by the Marshall Space Flight Center. Their experiences are reported in Reference 14.

Another good source of additional information on experiences and Lessons Learned in structural dynamics test programs is Reference 15.

UNIQUE STRUCTURAL DYNAMICS MEASUREMENTS ACQUIRED FROM OAST-1 EXPERIMENT



Photogrammetry analysis

applied to recorded video images

Principal results:

- Measured frequencies very close to predictions
- Measured first-mode damping (3.5 %) higher than anticipated (0.5 %)
- Unexpected, marked transverse bowing occurred during darkness
- Residual, steady-state motion observed
- Measured displacement errors less than 0.1 in. at 100 ft

CONCLUDING REMARKS

Many issues often arise in modal testing and system identification projects. Experience has shown repeatedly the task of characterizing complex structural dynamics to be a difficult one. Inadequate or insufficient instrumentation only makes matters worse. It is important that the instrumentation requirements for SSSCE be established carefully. The needs, opinions, and other issues raised by the LSS R&T community should be addressed to the fullest extent possible. The ultimate research benefits and opportunities resulting from SSSCE will, undoubtedly, be affected significantly by the extent and performance of the instrumentation that is used.

CONCLUDING REMARKS

- *SSSCE is an OAST Experiment to Instrument and Use the Space Station For Conducting In-Space Research on LSS Structural Dynamics and Control/Structure Interaction.*
- *Instrumentation Requirements Should Reflect, to the Fullest Extent Possible, the Needs, Opinions, and Issues Raised by the LSS R&T Community.*
- *Instrumentation Selected For SSSCE Will Determine, In Large Part, the Potential Research Benefits and Opportunities.*

REFERENCES

1. Breckenridge, R. A., Russell, R. A., and Clark, L. G., "Space Station and Technology Experiments," AIAA Paper 86-2299, September 1986.
2. Johnson, J. W. and Cooper, P. A., "Space Station Structural Characterization Experiment," Presented at the USAF/NASA Workshop on Model Determination for Large Space Systems, Pasadena, CA, March 22-24, 1988.
3. Ewins, D. J., Modal Testing: Theory and Practice, John Wiley & Sons, New York, 1984.
4. Stroud, R. C., "Excitation, Measurement, and Analysis Methods for Modal Testing," Sound and Vibration, August 1987, pp. 12-27.
5. Chu, D. F. H. (ed.), Modal Testing and Model Refinement, ASME Publication AMD-Vol. 59, 1983.
6. Martinez, D. R. and Miller, A. K. (ed.), Combined Experimental/Analytical Modeling of Dynamic Structural Systems, ASME Publication AMD-Vol. 67, 1985.
7. Cooper, P. A., Stockwell, A. E., and Kim, Z. C., "Interdisciplinary Analysis Procedures in the Modeling and Control of Large Space-Based Structures," Presented at ASME Conference on Computers in Engineering, New York, NY, August 1987.
8. Sutter, T. R., Cooper, P. A., and Young, J. W., "Dynamics and Control Characteristics of a Reference Space Station Configuration," AIAA Paper 88-2485, To be Presented at the AIAA SDM Special Space Station Symposium, Williamsburg, VA, April 1988.
9. Letchworth, R. and McGowan, P. E., "COFS III: Multibody Dynamics and Control Technology," NASA CP-2447, Part 1, pp. 347-370.

REFERENCES, Cont.

10. Gronet, M. J. et al, "Preliminary Design, Analysis, and Costing of a Dynamic Scale Model of the NASA Space Station," NASA CR-4068, July 1987.
11. Juang, J. N. and Pappa, R. S., "An Eigensystem Realization Algorithm for Modal Parameter Identification and Model Reduction," Journal of Guidance, Control and Dynamics, Vol. 8, No. 5, September-October 1985, pp. 620-627.
12. Pappa, R. S. and Juang, J. N., "Some Experiences With the Eigensystem Realization Algorithm," Sound and Vibration, January 1988, pp. 30-34.
13. Brumfield, M. L., Pappa, R. S., Miller, J. B., and Adams, R. R., "Orbital Dynamics of the OAST-1 Solar Array Using Video Measurements," AIAA Paper 85-0758, April 1985.
14. Schock, R. W., "Solar Array Flight Dynamic Experiment," NASA TP-2598, May 1986.
15. Ryan, R. S., "Problems Experienced and Envisioned for Dynamical Physical Systems," NASA TP-2508, August 1985.



163812
5-13
P-35
GE Aerospace

APPLICATION OF THE ITD ALGORITHM TO LANDSAT ORBITAL TRANSIENT RESPONSES

R. R. KAUFFMAN
GENERAL ELECTRIC COMPANY, ASTRO SPACE DIVISION
PHILADELPHIA, PENNSYLVANIA

474
PRESENTED AT
THE USAF/NASA WORKSHOP ON MODEL DETERMINATION
FOR LARGE SPACE SYSTEMS
PASADENA, CALIFORNIA
22 - 24 MARCH 1988

N 9 3 - 2 2 7 6 2

INTRODUCTION

- **LANDSAT 4 SYSTEM DESCRIPTION**
- **FIVE DEGREE-OF-FREEDOM SYSTEM EXAMPLE PROBLEM**
- **ORBITAL FINITE ELEMENT MODEL ANALYSIS**
- **MEASURED ORBITAL DATA ANALYSIS**
- **SUMMARY**

This presentation is comprised of five sections. First there is a brief description of the LANDSAT spacecraft. This will include a discussion of the satellite's mission and the motion sensor system.

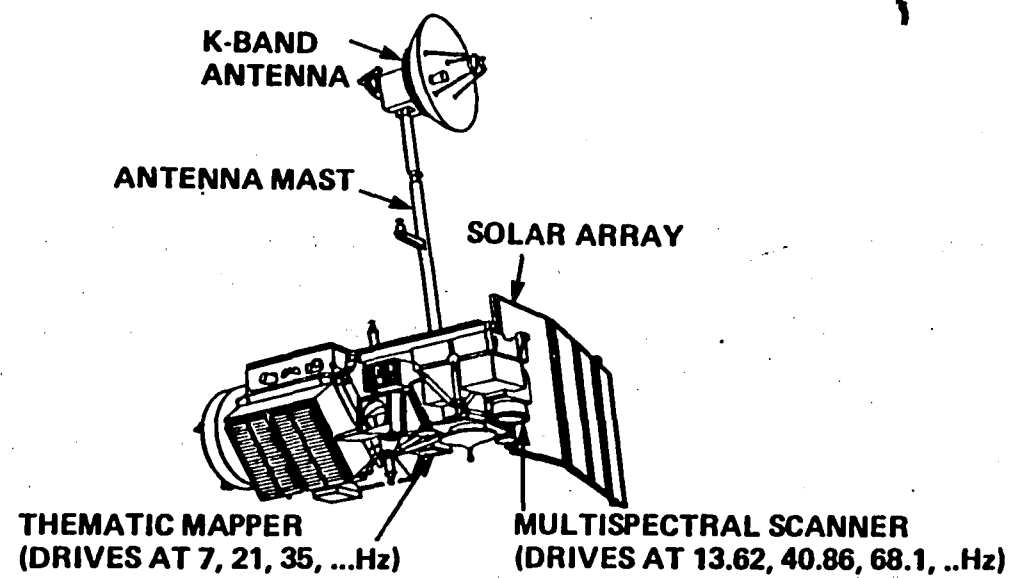
Next, the results of a study of the Ibrahim Time Domain (ITD) Algorithm which employed a five degree of freedom example problem will be related. This example problem was employed to become familiar with the algorithm and to explore its capabilities.

This will be followed by a discussion of the results of applying the ITD algorithm to an analytical simulation of the spacecraft in orbit. This simulation was used to give an upper bound on the expected accuracy of the algorithm when applied to actual orbital data.

Then the results of the analysis of the orbital data will be presented. This will include information on the frequency and damping as measured in orbit. The orbital frequencies will be compared to frequencies from a ground test verified finite element model. Results generally showed good agreement although some significant differences were found.

Finally, the results will be summarized and conclusions presented.

LANDSAT 4 SPACECRAFT



This chart presents the LANDSAT 4 spacecraft. The spacecraft is an earth resources satellite. The two sensors (the Thematic Mapper and the Multispectral Scanner) are labelled, along with the odd harmonics of the frequencies at which their scanning mirrors excite the structure. Also shown are several other major spacecraft subsystems.

Initial analyses indicated that on-board disturbances would result in unacceptable distortion of the Thematic Mapper images. Therefore, the motion of the Thematic Mapper was measured by an Angular Dispacement Sensor (ADS) and by attitude control system gyroscopes. The gyroscopes measured respones from zero through three Hz while the ADS measured data from three to one hundred and twenty five Hz. This data was transmitted from orbit and employed to remove motion induced distortion from the Thematic Mapper images.

In this study, the same information was used to characterize the modal characteristics of the Landsat 4 and Landsat 5 spacecraft while they were in orbit. Data was recorded for events in which either the Thematic Mapper or the Multi-Spectral Scanner was shut down which in theory will result in a free decay response of the structure. The data was then proccesed using both a fast Fourier transform and the Ibrahim Time Domain (ITD) algorithm.

478

IBRAHIM TIME DOMAIN (ITD)

- **METHOD DEVELOPED BY SAMIR IBRAHIM AND RICHARD PAPPA**
- **COMPUTER ALGORITHM SUPPLIED BY NASA Langley THROUGH RICHARD PAPPA**
- **STUDY WAS COMPRISED OF THREE MAIN PARTS**
 - 1) **FIVE DOF SYSTEM EXAMPLE PROBLEM**
 - 2) **ANALYTICAL ORBITAL FEM ANALYSIS**
 - 3) **ORBITAL DATA ANALYSIS**

The Ibrahim Time Domain algorithm that was employed was developed by Samir Ibrahim and Richard Pappa. The computer code was supplied by NASA Langley through Richard Pappa. The code employs free decay time history data to calculate the eigenvalues, eigenvectors, and damping of the system. In this study, the algorithm was applied to three separate systems: a five degree of freedom example problem, a transient response analysis of a Landsat finite element model, and measured orbital data from the two Landsat spacecraft.

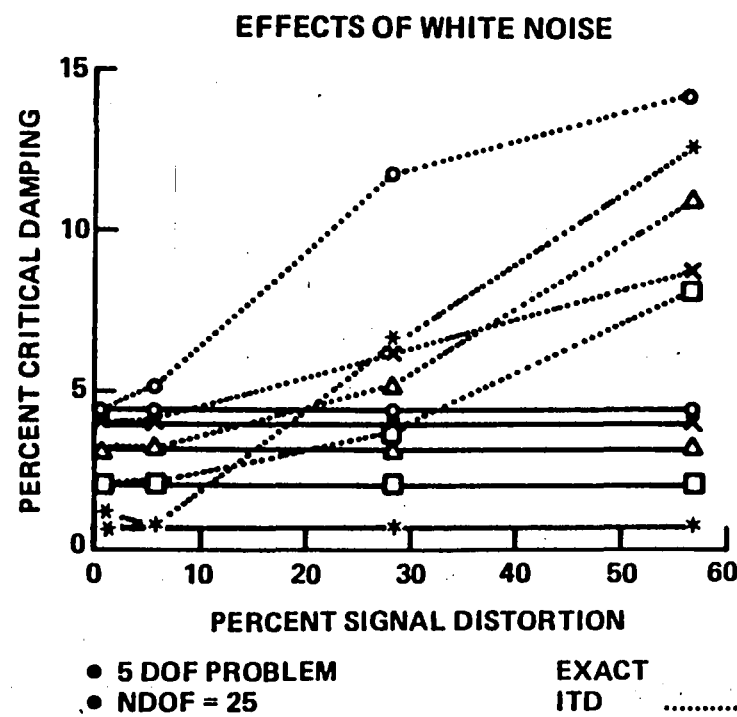
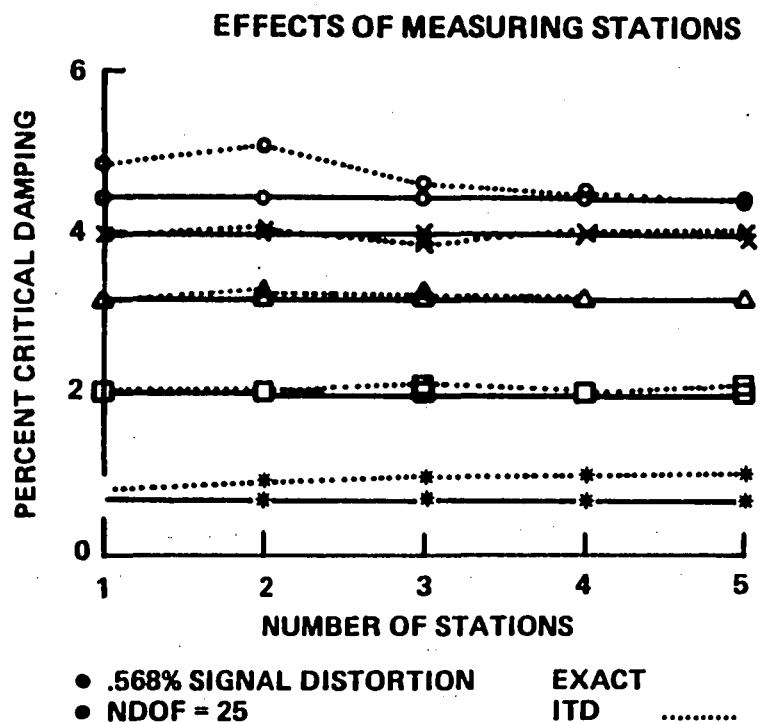
The five degree of freedom problem was employed to become familiar with the capabilities of the algorithm. The analytical model of Landsat was employed to determine an upper bound on the accuracy that could be expected from the measured orbital data. Finally, the orbital data was analyzed to characterize the orbital modal parameters of the two spacecraft.

FIVE DOF SYSTEM EXAMPLE PROBLEM

- **EXACT SOLUTION KNOWN**
- **BECOME FAMILIAR WITH THE CHARACTERISTICS OF THE ITD ALGORITHM**
- **INVESTIGATE THE EFFECTS OF NOISE IN THE DATA AND OF USER INPUT PARAMETERS**
- **DETERMINE THE ALGORITHMS ABILITY TO GENERATE MULTIPLE MODES/DATA CHANNEL**

The five degree of freedom problem had a known exact solution. Therefore, the values of various parameters in the algorithm could be varied to determine their effect upon the accuracy of the solution. The effects of noise in the data and the ability of the algorithm to determine multiple modes per channel of data were investigated.

RESULTS OF FIVE DOF ANALYSIS



This chart presents the results of the five degree of freedom study. The left half of the chart shows the effect of changing the number of channels of data has upon the calculated damping. The damping is plotted because it was the least accurately recovered parameter. As can be seen, even when only one measurement station was employed, results were fairly good for all five modes.

The right half of the chart presents the effect of adding white noise to the data. As can be seen, for noise to signal ratio below about five percent, good results were obtained. For higher levels of noise, the performance rapidly declines. Once again, the damping was the most sensitive parameter.

These results indicated that the ITD algorithm had the characteristics necessary for the next phase of the analysis. Therefore a finite element model of the Landsat spacecraft was employed to model the orbital conditions.

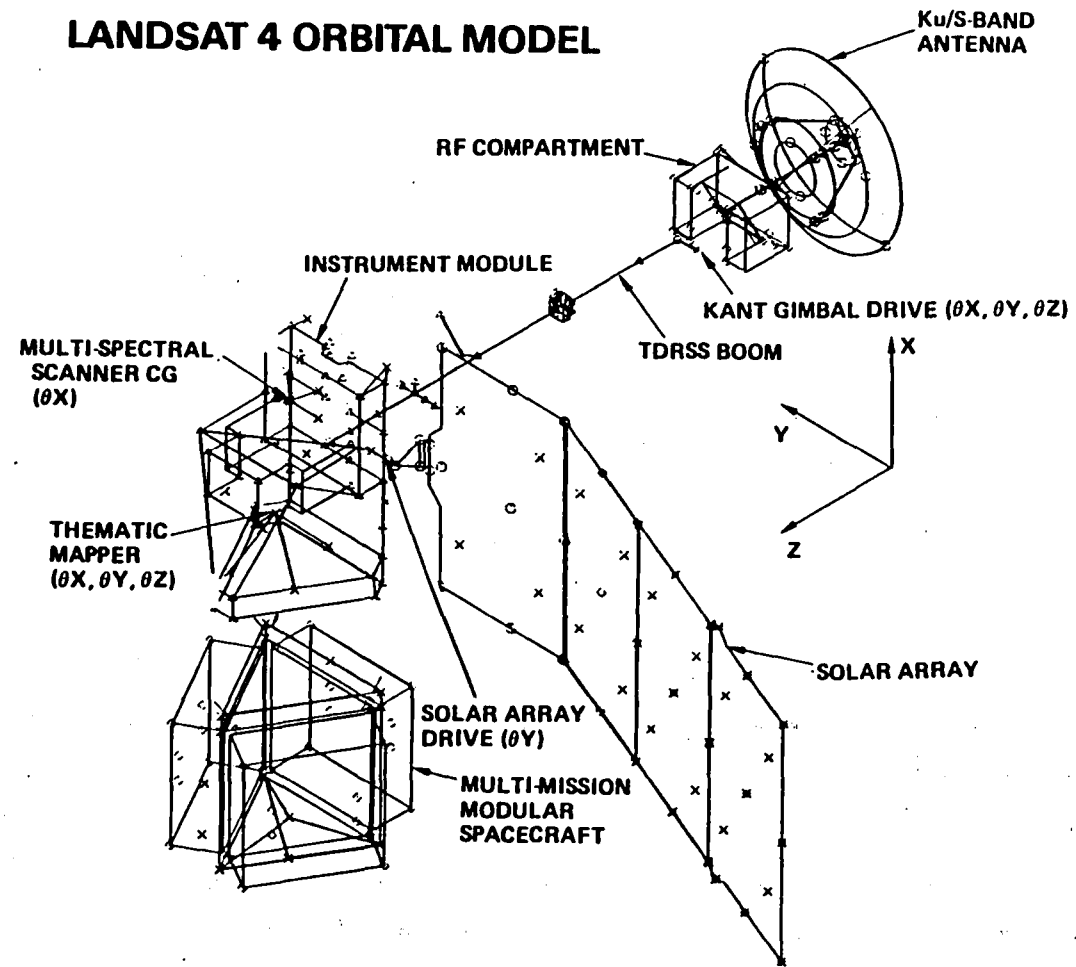
484

ANALYTICAL ORBITAL FEM ANALYSIS

- **SOURCES OF EXCITATION**
 - 1) THEMATIC MAPPER
 - 2) MULTI-SPECTRAL SCANNER
 - 3) KU/S BAND ANTENNA GIMBAL DRIVE
 - 4) SOLAR ARRAY DRIVE MOTOR
- **SIMULATE SOURCES OF EXCITATION**
- **GENERATE TRANSIENT RESPONSE TIME HISTORIES**
- **CALCULATE FAST FOURIER TRANSFORMS OF TIME HISTORY DATA**
- **INPUT TIME HISTORY DATA TO ITD**
- **COMPARE ITD RESULTS TO ORIGINAL ANALYTICAL MODAL PARAMETERS**

Response time histories of the NASTRAN finite element model of Landsat were developed for four forcing functions which represented the following disturbance sources: Thematic Mapper operation, Multi-Spectral Scanner operation, KU/S Band Antenna Gimbal Drive operation, and Solar Array Drive operation. These transient response time histories were then input to a fast Fourier transform to determine the frequency content and to ITD to determine the modal characteristics. The results of the modal parameters that were determined with the ITD algorithm are then compared to the original finite element model modal parameters. This will give an upper bound of how accurately the modal parameters can be recovered from measured orbital data.

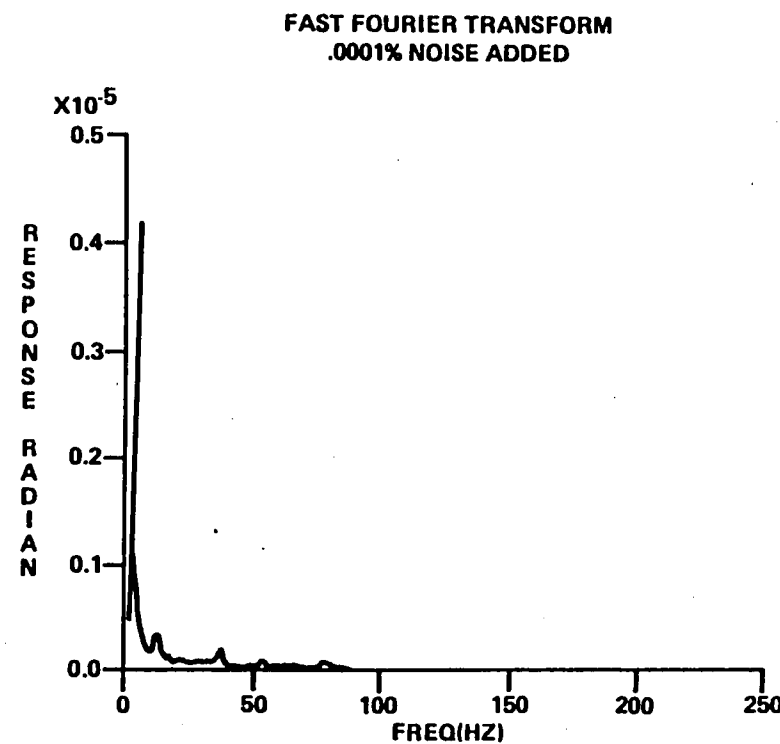
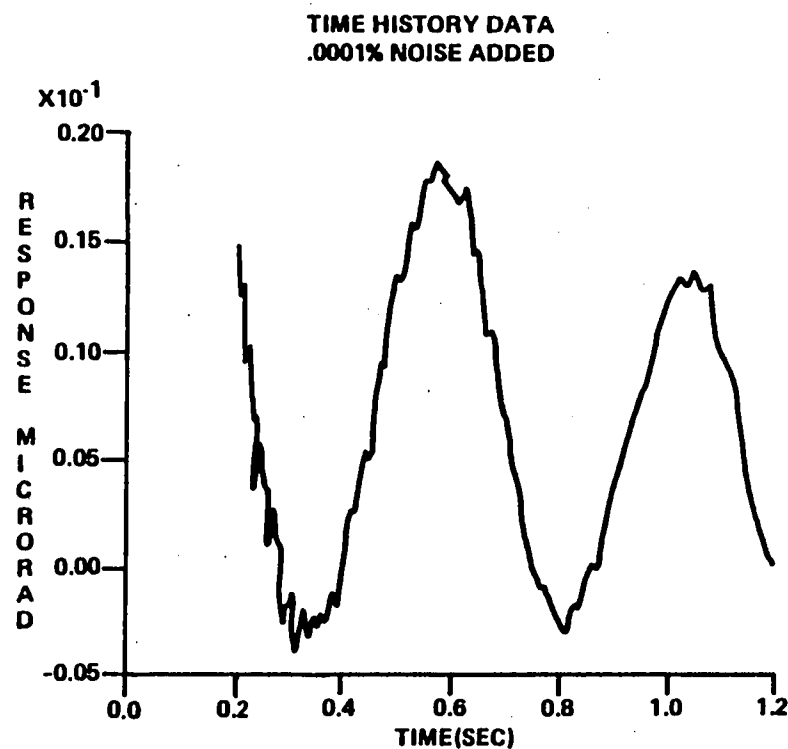
LANDSAT 4 ORBITAL MODEL



This chart sketches the orbital Landsat finite element model. Several major components are shown. The finite element model that was employed was tuned to match the results of modal tests. Also shown are the degrees of freedom that were employed in the transient response analysis. Forcing functions were applied to the K/US Band Antenna Drive in the theta-x, theta-y, and theta-z directions, to the Solar Array Drive in the theta-y direction, to the Multi-Spectral Scanner in the theta-x direction, and to the Thematic Mapper in the theta-x direction. Responses to these various forcing functions were recovered at the Thematic Mapper in the theta-x, theta-y, and theta-z directions.

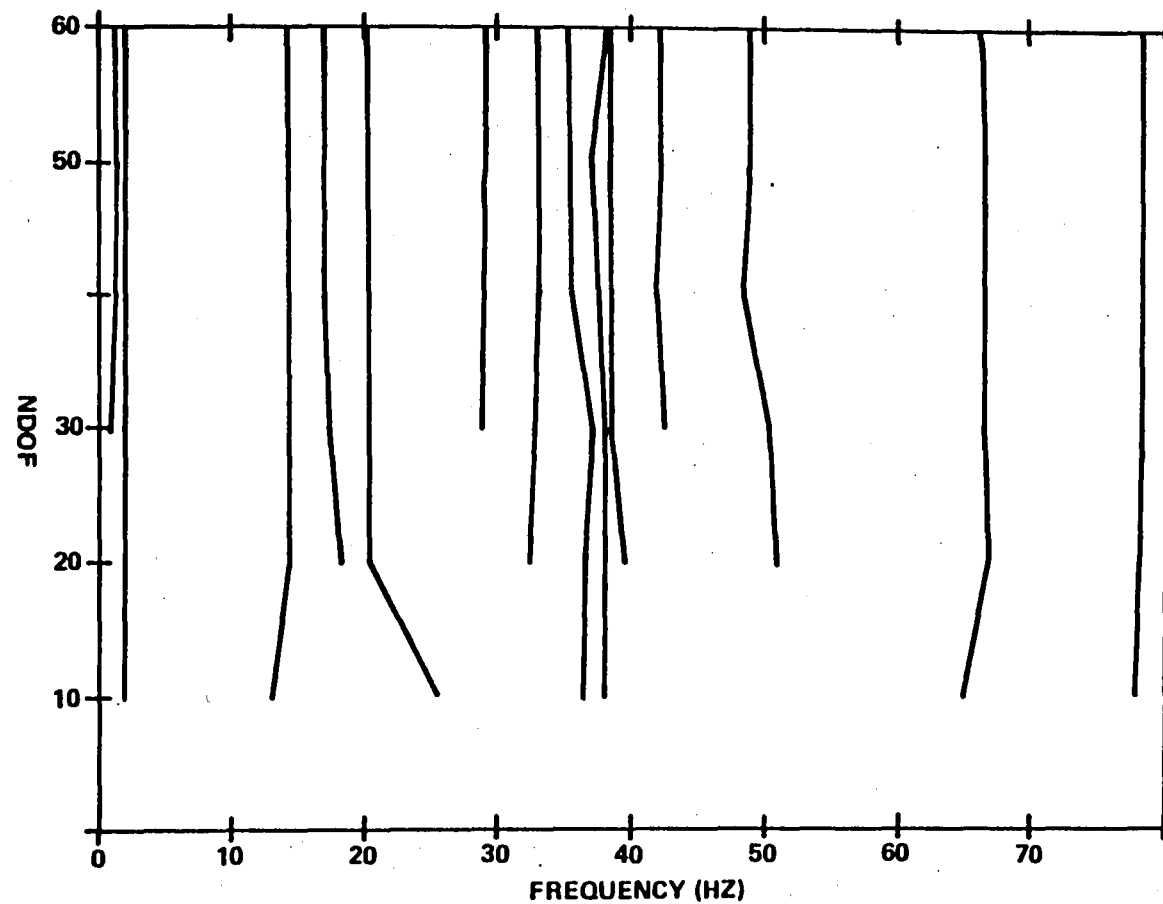
The responses to the various forcing functions were analyzed with a fast Fourier transform and the ITD algorithm. The modal characteristics that were calculated with the ITD algorithm were compared to the actual modal characteristics of the finite element model.

ORBITAL SIMULATION OF MSS SHUTDOWN



This chart displays a typical response of the orbital model at the Thematic Mapper to an Multi-Spectral Scanner shutdown event. Also shown is a plot of the fast Fourier transform of the time history data. A very small amount of noise was added to the time history data since this was required to avoid mathematical instabilities in the ITD algorithm that was employed. As can be seen, the time history is a lightly damped free decay. This is the form of data which is required by the algorithm for optimum results.

EFFECT OF NDOF PARAMETER ON MSS SHUTDOWN SIMULATION



This chart presents a typical example of the result of varying the statistical number of degrees of freedom in the ITD algorithm. As the value of this parameter is increased, the values of the modal parameters of the system are found more accurately. However, increasing the size of the parameter also leads to increased computer run time and cost. Therefore, the approach of running with a relatively small number of statistical degrees of freedom and slowly increasing the value until the solution converged was chosen.

**COMPARISON OF ACTUAL AND CALCULATED MODAL
PARAMETERS FOR MSS SHUTDOWN SIMULATION
(NDOF = 60)**

ACTUAL MODE NUMBER	ACTUAL FREQUENCY (Hz)	ACTUAL DAMPING (% C/C ₀)	ITD FREQUENCY (Hz)	% Δ	ITD DAMPING (% C/C ₀)	% Δ	MODE SHAPE DOT PRODUCT
11	1.615	1.0	1.336	-17.28	19.016	1801.60	-.993
12	2.145	1.0	2.166	.98	1.313	31.30	-.940
24	14.076	1.0	14.102	.18	.980	-2.00	-.918
27	16.771	1.0	16.758	-.08	.724	-27.60	1.000
30	20.066	1.0	20.081	.07	1.103	10.30	1.000
39	28.881	1.0	28.892	.04	1.104	10.40	.999
41	32.893	1.0	32.869	-.07	.981	-1.90	-.999
45	35.112	1.0	35.053	-.17	.941	-5.90	.999
49	38.186	1.0	37.959	-.59	2.238	123.80	.828
50	38.238	1.0	38.214	-.06	.779	-22.10	.996
58	42.144	1.0	41.964	-.43	1.177	-17.70	-.924
67	48.578	1.0	48.583	-.01	1.151	15.10	-1.000
92	65.967	1.0	65.949	-.03	.852	-14.80	-.997
108	78.513	1.0	78.407	-.14	1.163	16.30	1.000

This chart presents a comparison of the ITD derived modal characteristics to the actual characteristics of the analytical model. As can be seen, there is very good agreement between the model and ITD frequencies and mode shapes. The frequency is in error by less than one percent. The mode shapes are compared by a modal dot product. A magnitude of one corresponds to perfect agreement in the mode shapes. A negative sign indicates that the modes are out of phase. Magnitudes of greater than 0.9 indicate very good agreement in the shape of the modes between the ITD results and the finite element model.

The agreement in damping is somewhat worse, but still generally within twenty percent. In this case, only the Angular Displacement Sensor was employed, and therefore modes below about three Hz are suspect.

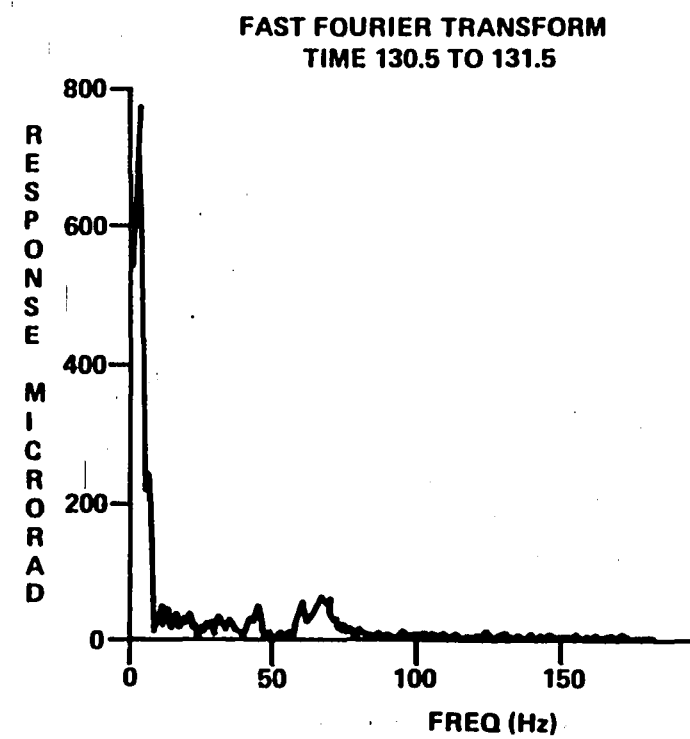
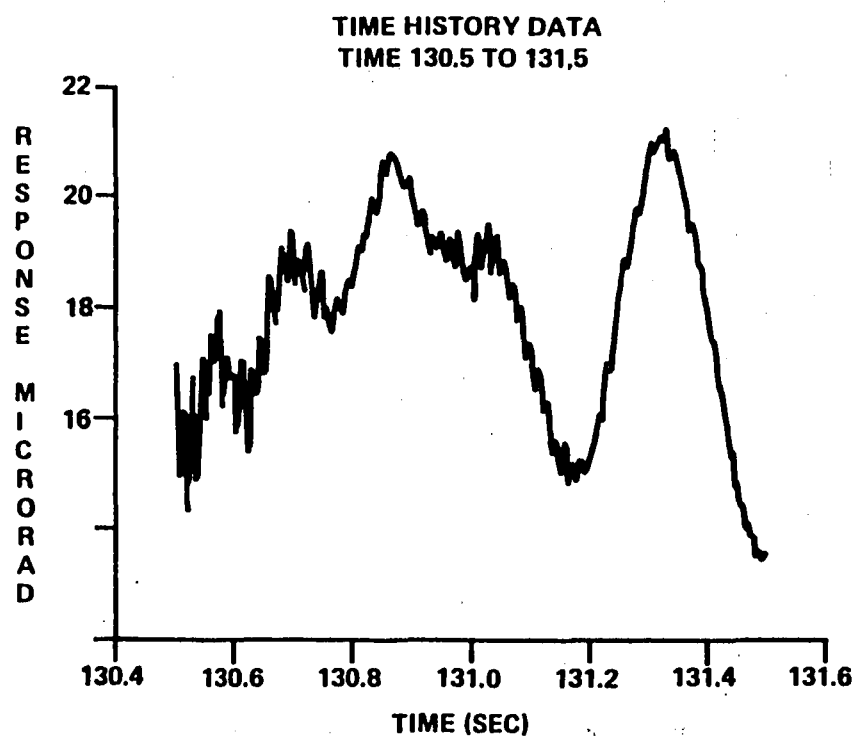
ORBITAL DATA ANALYSES

- USED PAYLOAD CORRECTION DATA COMPRISED OF:
 1. GYRO DATA (< 2.0 Hz)
 2. ANGULAR DISPLACEMENT SENSOR DATA (2.0 Hz < f < 125.0 Hz)
- ALL DATA WAS OBTAINED WITH THE ACS OPERATING
- ANALYSIS WAS DONE FOR FOLLOWING EVENTS
 1. LANDSAT 4 MULTISPECTRAL SCANNER SHUTDOWN
 2. LANDSAT 5 MULTISPECTRAL SCANNER SHUTDOWN
 3. LANDSAT 5 THEMATIC MAPPER SHUTDOWN

Next, the measured orbital data was analyzed. As was mentioned previously, the data that was employed was comprised of a combination of low frequency gyroscope data and high frequency Angular Displacement Sensor data. Note that this data measurement was not done under controlled conditions. Various disturbance sources (such as the Attitude Control System, the Gimballed Drive Antenna, and the Solar Array Drive) were operating during measurements made after the imaging instruments were shut down. Thus any data that was measured may have been contaminated by these disturbance sources.

The analysis was completed for three events. These were a Landsat 4 Multi-Spectral Scanner shutdown, a Landsat 5 Multi-Spectral Scanner shutdown, and a Landsat 5 Thematic Mapper shutdown. This allowed for comparisons of the results on two different satellites as well as at different different amplitudes (the Thematic Mapper disturbance is more severe than the Multi-Spectral Scanner disturbance).

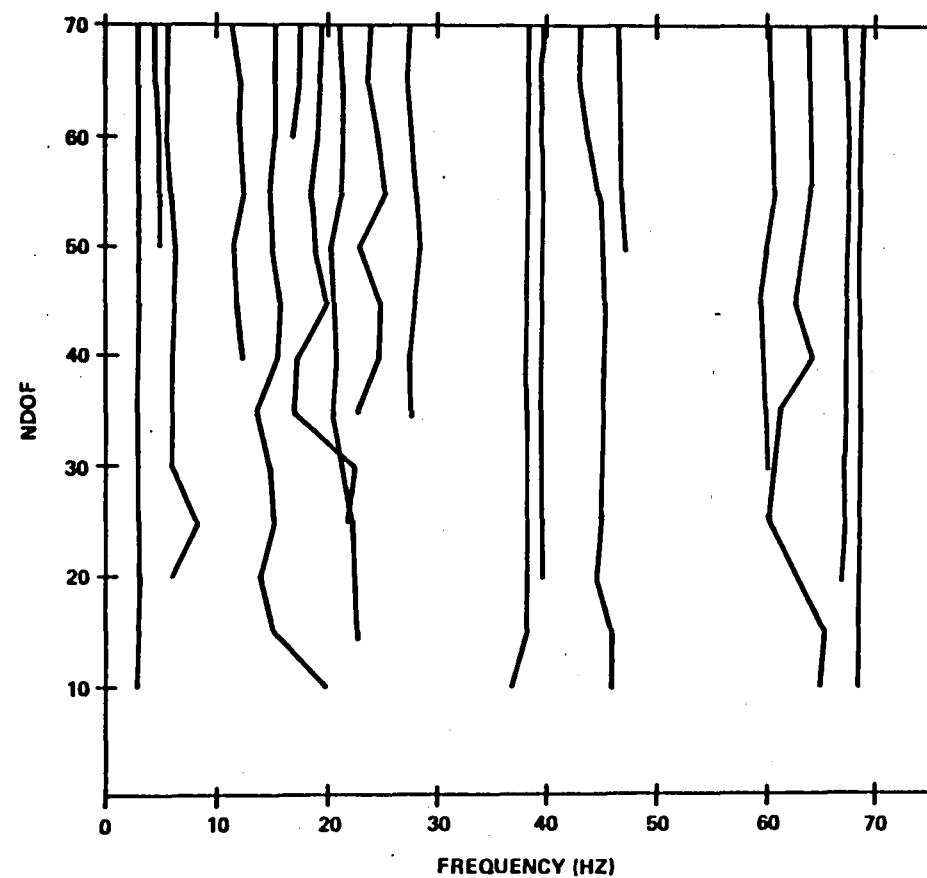
MEASURED MSS SHUTDOWN



494

This figure presents a typical channel of measured data for a Multi-Spectral Scanner shutdown event. As can be seen, higher frequency components die out quite rapidly, but the low frequency components do not appear to be a free decay. This is due to the fact that various disturbance sources were active during data measurement. Also shown is a fast Fourier transform of the data which displays a large low frequency response and many smaller high frequency peaks.

ORBITAL DATA ANALYSIS



In this chart the frequencies of various modes are plotted verses the number of statistical degrees of freedom. By the time the number of statistical degrees of freedom reaches seventy, it appears that the frequencies have stabilized. This data showed a great deal more variation in frequency than was evident in the analytical data that was presented earlier.

RESULTS OF ITD ANALYSES OF ORBITAL DATA

ANALYTIC MODEL		LANDSAT-4 MSS SHUTDOWN					LANDSAT-5 MSS SHUTDOWN					LANDSAT-5 TM SHUTDOWN				
MODE #	FREQ (HZ)	FREQ (HZ)	ΔFREQ (%)	DAMP (%C/CC)	DOT PRODUCT	FREQ (HZ)	ΔFREQ (%)	DAMP (%C/CC)	DOT PRODUCT	FREQ (HZ)	ΔFREQ (%)	DAMP (%C/CC)	DOT PRODUCT			
7	.428	.394	-7.9	.418	.783	.392	-8.4	.215	.931	.381	-11.0	1.307	.968			
8	.782	.859	12.7	1.007	.974	.790	3.7	-.102	.999	.789	3.5	.816	-.100			
9	1.209	1.174	-2.9	.525	.721	1.180	-10.7	.618	.952	1.409	16.5	3.198	-.722			
10	1.321					1.763	9.5	.237	.578	1.555	-3.7	.550	-.940			
11	1.615					2.754	28.4	-.036	.998	2.381	11.0	.493	-1.000			
12	2.145	2.794	30.3	-.004	.948	4.610	11.0	-.675	.935	5.410	30.3	-2.018	.941			
16	4.152	4.150	-.1	.203	-.888					6.161	-4.8	3.440	-1.00			
17	6.470					13.044	-7.3	2.66	.918							
18	8.916	5.394	-22.0	10.008	.852	16.814	-7.4	1.51	.734	17.126	2.1	1.922	-.464			
22	12.636	11.299	-10.6	9.941	-.731	19.655	1.3	-.329	.886	18.199	-5.3	.726	.976			
24	14.076					21.419	6.7	.527	-.982							
27	16.771	16.104	-9.9	2.236	-.912					21.121	-10.1	2.857	-.955			
28	18.163	17.463	-3.9	5.166	.951					28.096	-2.0	1.400	.691			
29	19.402									31.245	-5.0	1.497	.982			
30	20.068	20.922	4.3	1.680	.990											
33	23.508					37.021	-3.2	1.00	.991	37.955	-2.4	-2.312	.967			
35	26.017	23.617	-5.6	2.603	.894					39.489	-.2	-.685	.116			
38	28.665	27.135	-5.3	5.263	.841											
41	32.893									40.897	-4.1	.639	.699			
49	38.238									42.464	1.4	1.02	.999			
51	38.811	38.085	-1.9	1.423	.986					46.601	-4.1	1.30	-.996			
52	38.906									52.399	2.7	.809	.917			
54	39.549									59.204	.5	1.48	.983			
66	40.390	39.398	-2.5	1.104	.718					52.857	-3.4	1.835	.900			
67	41.887									64.769	-1.8	.478	-.939			
80	42.655	42.781	.3	2.795	-.889					66.088	1.68	-.928				
87	48.578	46.347	-4.6	1.285	-.957					68.741	-12.0	.852	.996			
71	50.568															
73	51.010									64.901	-2.0	1.682	-.515			
78	54.738															
83	58.905															
85	60.369	60.135	-.4	1.678	.983											
92	65.987	63.827	-3.6	1.218	-.485											
93	66.200															
94	67.140	67.143	.004	3.537	-.941											
99	70.838	68.497	-3.3	.985	.773											
106	76.993															

The results of the orbital data analysis are presented in this chart. Data from two events for Landsat 5 (a Multi-Spectral Scanner shutdown and a Thematic Mapper shutdown) as well as a Landsat 4 Multi-Spectral Scanner shutdown are compared to the analytical model of the orbital Landsat spacecraft. Note that analytical mode number seven is the first flexible mode of the model.

In general, the frequencies and mode shapes derived from the orbital data show good agreement with the analytical modes. One important exception to this is fundamental solar array bending mode which was predicted to occur at 0.428 Hz. When measured in orbit, this mode occurred at about 0.39 Hz, approximately ten percent lower than expected. This difference has since been traced to an assumption that was made in the calculation of the amount of virtual air mass that the solar array displaced during test. It was assumed that the virtual air mass was equal to the mass of air in a cylinder about the long axis of the solar array. Actually, the virtual air mass should be somewhat lower due to tip effects. When tip effects are corrected for, the analytical model agrees with the orbital data for the first mode.

The measured damping showed more variation. Some of the measured values were negative. It was concluded that the negative values were the result of the satellite being excited by other disturbance sources during the data measurement. It was concluded that for modes below three Hz a damping value of 0.2% was a reasonable lower value while for modes above three Hz the corresponding value was 0.5%.

Note that the use of the angular displacement data to extract low frequency data was very successful. Only one mode below three Hz was not extracted from the data. That mode was a KU band antenna elevation drive mode and had a shape that is not likely to be excited by the instrument shut down disturbances.

There was an anomaly found in the data at 0.2 Hz. It was concluded that this response was a subharmonic of the fundamental solar array mode at .39 Hz. Such responses sometimes occur in non-linear systems, although they usually have a much lower magnitude than the primary response.

RESULTS

- **DAMPING:**
 1. ON ORDER OF 0.2% FOR LOW FREQUENCY MODES (< 3 Hz)
 2. ON ORDER OF 0.5% FOR HIGH FREQUENCY MODES
- **THIRTY SEVEN MODES WERE RECOVERED IN AT LEAST ONE EVENT**
- **GYRO DATA ANALYSIS**
 1. ONLY ONE MODE BELOW 3 Hz NOT RECOVERED
 2. THAT MODE IS AN ELEVATION DRIVE MODE AT 2.869 Hz
- **FUNDAMENTAL SOLAR ARRAY MODE**
 1. FREQUENCY ~10% LOWER IN ORBIT THAN EXPECTED
 2. THIS MAY BE DUE TO "TIP EFFECTS" IN VIRTUAL MASS CALCULATION
- **90% OF MODES OCCURRING IN BOTH MSS CASES ARE WITHIN 10% IN FREQUENCY**

This chart summarizes the results of this study. It was found that the measured damping values were on the order of 0.2% for modes below three Hz and on the order of 0.5% for higher frequency modes.

Many modes were recovered from the data. Thirty seven modes were recovered in at least one event. Only one mode below three Hz was not recovered and that mode had a shape that is not likely to be excited by the instrument shutdown forcing forcing functions.

The fundamental solar array mode was approximately ten percent lower than predicted. It was concluded that this was due to tip effects in the virtual mass calculation.

Also, it was found that ninety percent of the modes in both MSS cases were within ten percent in frequency. This implies that the two vehicles were very similar dynamically.

CONCLUSIONS

- ITD AGLORITHM IS INSENSITIVE TO MODERATE NOISE LEVELS
- MULTIPLE MODES CAN BE CHARACTERIZED FROM A SINGLE CHANNEL OF DATA
- ITD ALGORITHM HAS DIFFICULTY DEALING WITH WIDE FREQUENCY RANGES
- MEASURED DAMPING VALUES ON ORDER OF .2% OR GREATER
- ITD ALGORITHM SHOULD BE APPLICABLE TO FUTURE LSS STUDIES

It was concluded that the ITD algorithm was insensitive to moderate amounts of noise (noise to signal ratio of less than five percent). This was evident from the five degree of freedom test case results.

Also, it was found that multiple modes could be characterized from a single channel of data. Indeed, thirty seven modes were recovered employing three channels of orbital data.

The algorithm did have difficulty dealing with wide frequency ranges. The narrow bandwidth low frequency data gave better results than were obtained from the wide bandwidth high frequency data.

The damping value was the least accurately recovered modal parameter. The measured damping values were on the order of 0.2% or greater.

The ITD algorithm should be applicable to future large space structure studies.

RECOMMENDATIONS

- **USE OF DIGITAL FILTERING TO SET BANDWIDTH OF DATA SHOULD BE INVESTIGATED**
- **IMPROVED ALGORITHMS OF THIS TYPE SHOULD BE DEVELOPED**
- **FUTURE STUDIES SHOULD USE IMPROVED INSTRUMENTATION**

It is recommended that digital filtering to set the bandwidth of the data should be investigated. This should result in more accurate recovery of the modal parameters.

Improved algorithms of this type should be developed. In particular, improved recovery of the damping values is needed.

Also, in future studies of this type, improved instrumentation and more controlled conditions should be employed.

N 93-72763

53-33
163813

Modal Identification Using Single-Mode Projection Filters
and Comparison with ERA and MLE Results

P-15

by

Jen-Kuang Huang, Ji-Yao Shen

Department of Mechanical Engineering and Mechanics
Old Dominion University
Norfolk, VA 23529-0247 Tel (804) 440-3734

Richard S. Pappa
NASA Langley Research Center
Structural Dynamics Branch
Hampton, VA 23665-5225

Presented at the USAF/NASA Workshop
on Model Determination for Large Space Systems
Pasadena, California, March 22-24, 1988

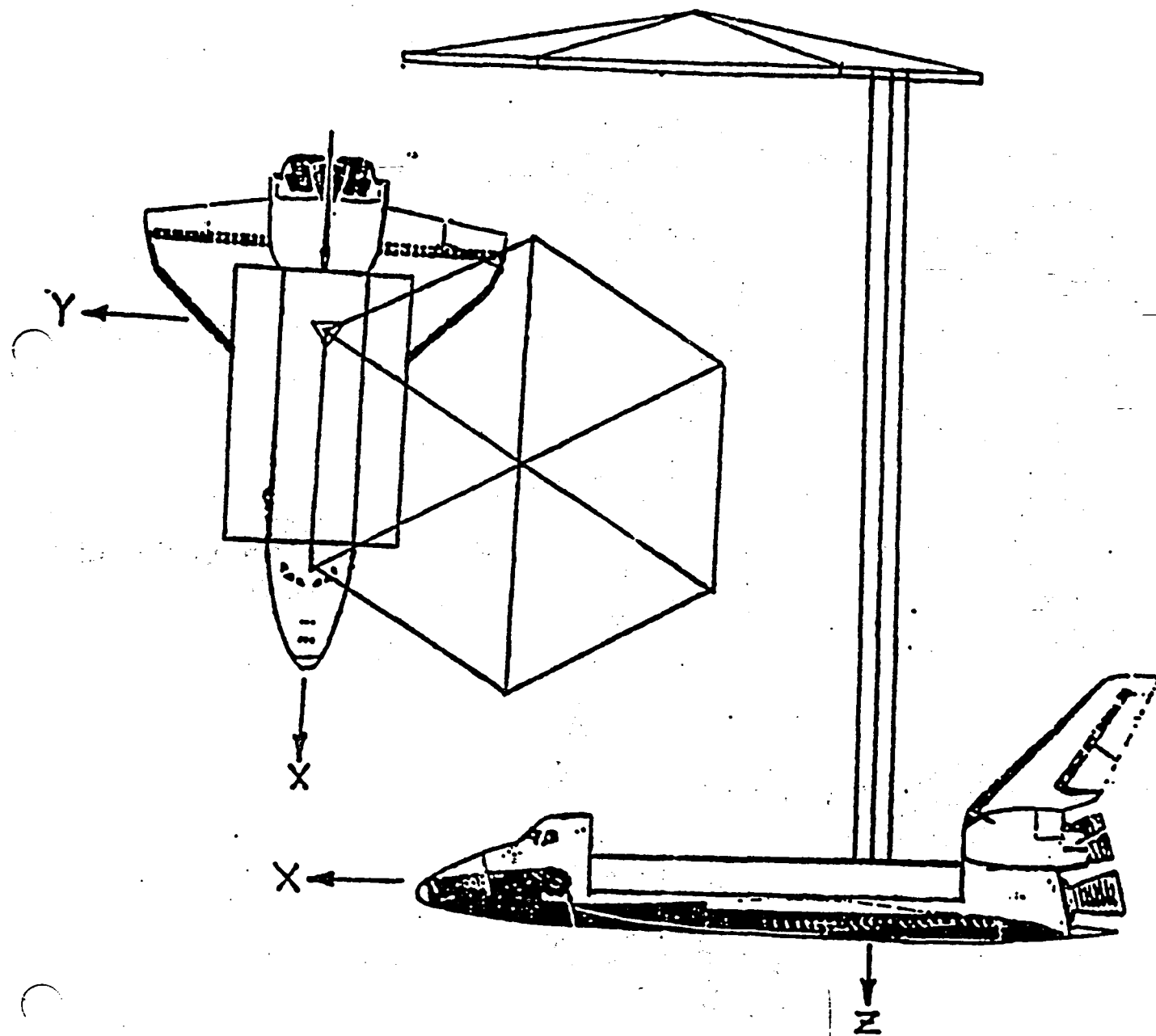
ABSTRACT

The Single-Mode Projection Filter (SPF) is a newly developed algorithm for eigensystem parameter identification from both analytical results and test data. The SPF is formulated with a single mode only and practical for parallel processing implementation. Explicit formulations of SPF are derived for the multi-input multi-output (MIMO) system by using the orthogonal matrices of the controllability and observability matrices in the general sense.

The modal parameters of SPF are initially obtained from an analytical model in modal space. The experimental data are then processed through SPF to update its modal parameters and to minimize a cost function defined by the norm of an error matrix. The updated modal parameters represent the characteristics of the test data. A two-dimensional global minimum optimization algorithm is developed and applied for the filter update by using the interval analysis method. The SPF is developed based on a single-mode subsystem and identifies only one modal frequency and one modal damping within a specified region. For an n modes structure, n SPF can be implemented for parallel processing to reduce the computational burden. The SPF is applied to analyze the simulated data for the MAST beam structure. The estimated modal parameters are comparable to those from the Eigensystem Realization Algorithm (ERA) and repeated modal frequencies are identified. The modal analysis of the Spacecraft Control Laboratory Experiment (SCOLE) data is also performed by using the ERA and the Maximum Likelihood Estimate (MLE). The result shows that the first five modal frequencies are very close from ERA and MLE. However, there are slight disparities in the damping rates and the computational burdens are quite different among these two algorithms.

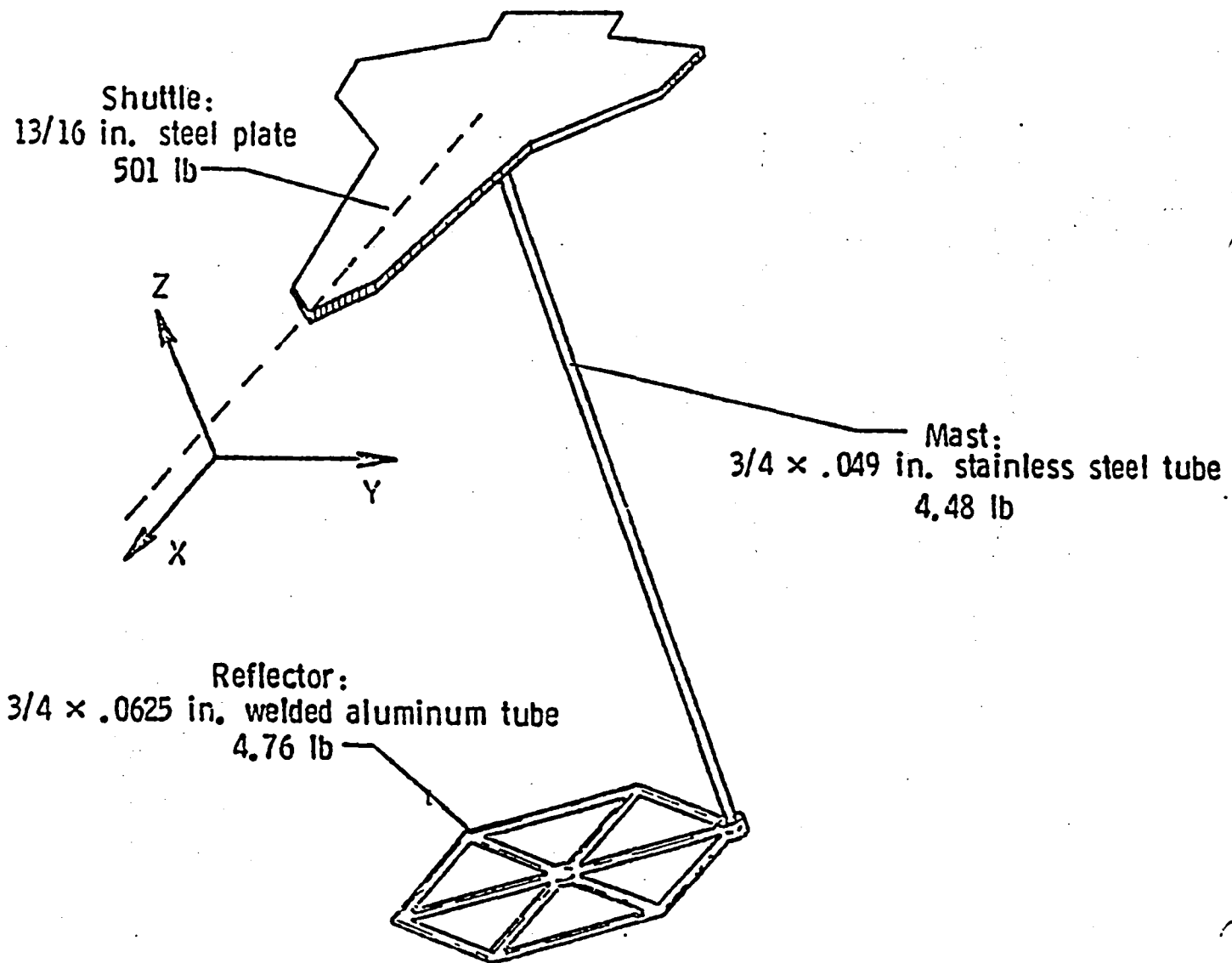
Spacecraft Control Experiment (SCOLE)

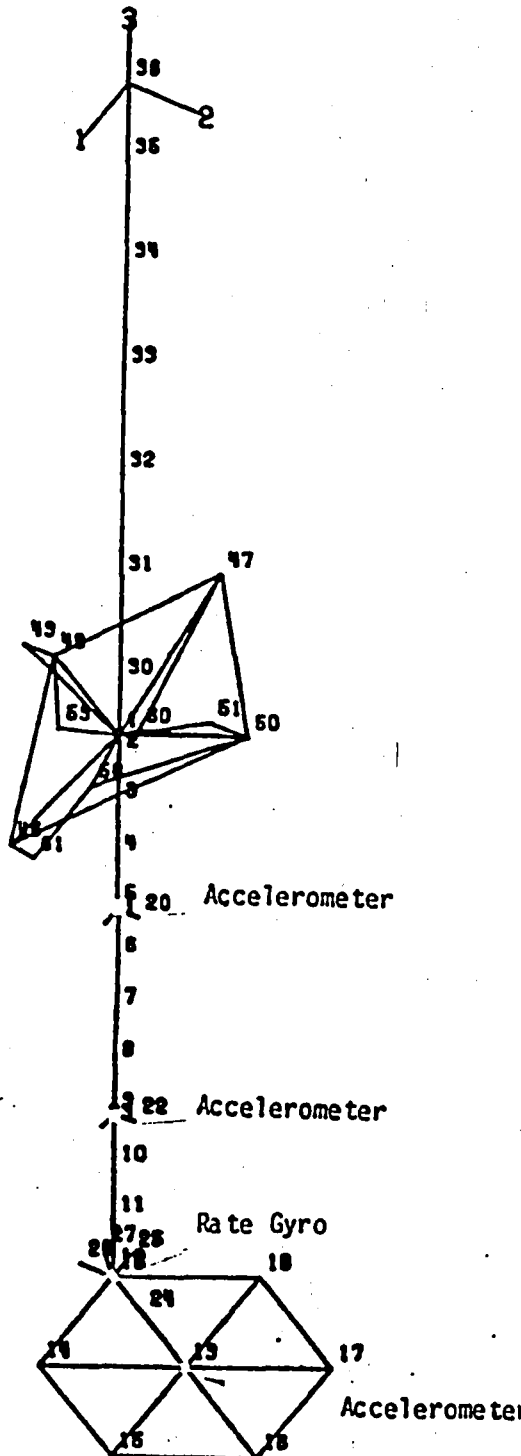
The Spacecraft Control Laboratory Experiment (SCOLE) was constructed to provide a physical test bed for the investigation of identification and control algorithm for large space structure. The control problems to be studied are slewing maneuver and pointing operations. The slew is defined as minimum time maneuver to bring the antenna line-of-sight (LOS) pointing to within an error limit of the pointing target. The second control objective is to rotate about the line of sight and stabilize about the new attitude while keeping the LOS error within a bound δ .



THE ASSEMBLY OF SCOLE AND THE GLOBAL REFERENCE FRAME

The following experiment facility exhibits the essential SCOLE characteristics of a large mass/inertia connected to a small mass/inertia by a flexible beam. The assembly shown is comprised of three basic structures, the shuttle, the mast, and the reflector panel. The assembly is suspended from a steel cable with the positive z-axis of the shuttle pointing up, thus minimizing the static bending of the antenna mast. The suspension point is a two-degree-of-freedom gimbal for pitch and roll with yaw freedom supplied by the suspension cable.





LOCATION OF SENSORS AND SENSED VARIABLES

The sensors for the experiment consist of 6 servo-accelerometers and a 3-axis rotational rate sensing units. An optical sensor will provide yaw attitude of the shuttle. Control sensors and actuators are typical of those which the control designer would have to deal with on an actual spacecraft. The sensors are aircraft quality rate sensors and servo-accelerometers.

Number of Sensor	Sensor Type	Sensed Variable	Number of Joint
2	Rate Gyro	r - roll r - pitch r - yaw	13
6	Accelerometer	m1 - x	5
7	Accelerometer	m1 - y	
8	Accelerometer	m2 - x	9
9	Accelerometer	m2 - y	
10	Accelerometer	r - x	
11	Accelerometer	r - y	19

r - reflector,

m1 - upper mast location

m2 - lower mast location

ETC

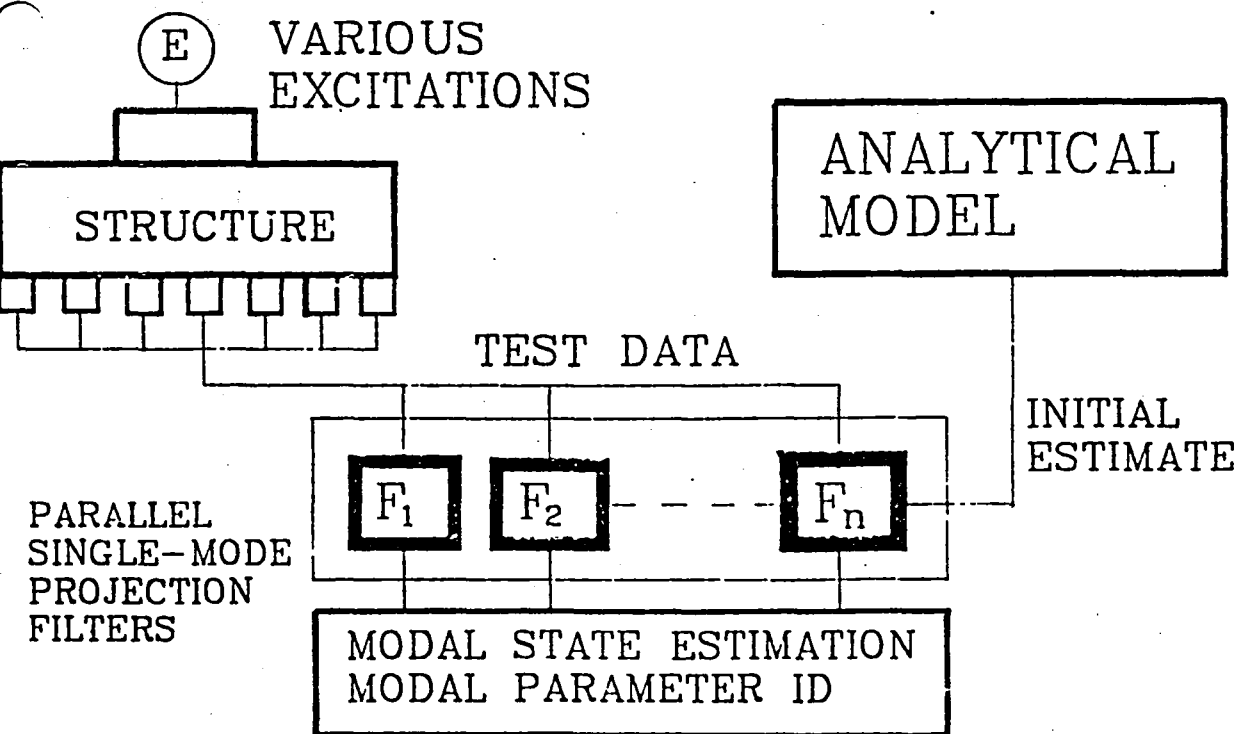
RESULTS OF MODAL ANALYSIS OF SCOLE

This table summarizes the model parameters of SCOLE system identified by Maximum Likelihood Estimate (MLE) and Eigensystem Realization Algorithm (ERA). The table shows that the first five modal frequencies identified by MLE and ERA are very close to those obtained from the finite element method (FEM). The MLE and ERA results are comparable and slight disparities are found in the damping rates.

Mode	Frequency (Hz)			Damping Rate (%)	
	FEM	MLE	ERA	MLE	ERA
2	0.447	0.440	0.446	0.128	0.156
3	1.504	1.540	1.547	0.0603	0.878
4	2.913	3.000	3.077	0.134	0.787
5	4.345	4.360	4.282	0.0841	0.359
6	6.821	6.080	6.765		0.328

FUNCTIONS OF SINGLE-MODE PROJECTION FILTERS

Single-mode projection filters are developed for eigensystem parameter identification from both analytical results and test data. The modal parameters (including modal frequency, modal damping and mode shapes) required for formulating the projection filters are initially obtained from an analytical model in modal space. The test data are then passed through the projection filters to determine whether there is a discrepancy between the analytical model and the experimental testing. Each projection filter is then updated by varying the corresponding modal parameters to minimize a cost function defined by the norm of a specified error matrix. The updated modal parameters represent the characteristics of the test data. Single-mode projection filters can be implemented for parallel processing to reduce the computational burden.



DATA STRUCTURE FOR PROJECTION FILTERS

The data used for projection filters are formulated by using a generalized Hankel matrix which contains discrete data $Y(k)$ in time domain. $Y(k)$ represents system free impulse response or initial state response.

Generalized Hankel matrix

$$H(0) = \begin{bmatrix} Y(1), & Y(1+t_1), & \dots, & Y(1+t_s) \\ Y(j_1+1), & Y(j_1+1+t_1), & \dots, & Y(j_1+1+t_s) \\ \vdots & \vdots & & \vdots \\ Y(j_r+1), & Y(j_r+1+t_1), & \dots, & Y(j_r+1+t_s) \end{bmatrix}$$

where j_i ($i=1, 2, \dots, r$) and t_i ($i=1, 2, \dots, s$) are arbitrary integers,

WHAT ARE THE SINGLE-MODE PROJECTION FILTERS?

Single-mode projection filters are developed based on a single-mode subsystem. Explicit formulations of single-mode projection filters are derived for the multi-input multi-output (MIMO) system by using the orthogonal matrices of the controllability and observability matrices in the general sense.

- **Projection filters**

$$H(0) = V_r W_s$$

where

$$V_r = \begin{bmatrix} C \\ CA^{11} \\ \vdots \\ CA^{1r} \end{bmatrix} \quad (r+1)pxn \quad \text{observability matrix}$$

$$W_s = [B, A^{t1}B, \dots, A^{ts}B]_{n \times m(s+1)} \quad \text{controllability matrix}$$

$$\rightarrow V_r^+ H(0) W_s^+ = I_n$$

V_r^+, W_s^+ : orthogonal matrix of V_r and W_s respectively

- **Single-mode projection filters**

Develop projection filters V^+ , W^+ based on a Single-Mode subsystem.

For an uncoupled distinct n-mode system $V^+ H(0) W^+ = I_2$

FILTERS UPDATE

The projection filters V^+ and W^+ are developed based on the analytical model. If the projection filters have the same modal characteristics as the test data (in $H(0)$), then the cost function J will go to a minimum value (ideally zero). Otherwise, the modal parameters in the projection filters are updated in order to minimize J . The updated modal parameters thus represent the characteristics of the test data.

• Projection Filters

$$V^+ H(0) W^+ \approx I_2 \quad V^+ H(0) W^+ - I_2 \approx 0_2$$

• Cost Function

$$J = (E_{11}^2 + E_{12}^2 + E_{21}^2 + E_{22}^2)/2,$$

$$\begin{bmatrix} E_{11} & E_{12} \\ & \\ E_{21} & E_{22} \end{bmatrix} = V^+ H(0) W^+ - I_2$$

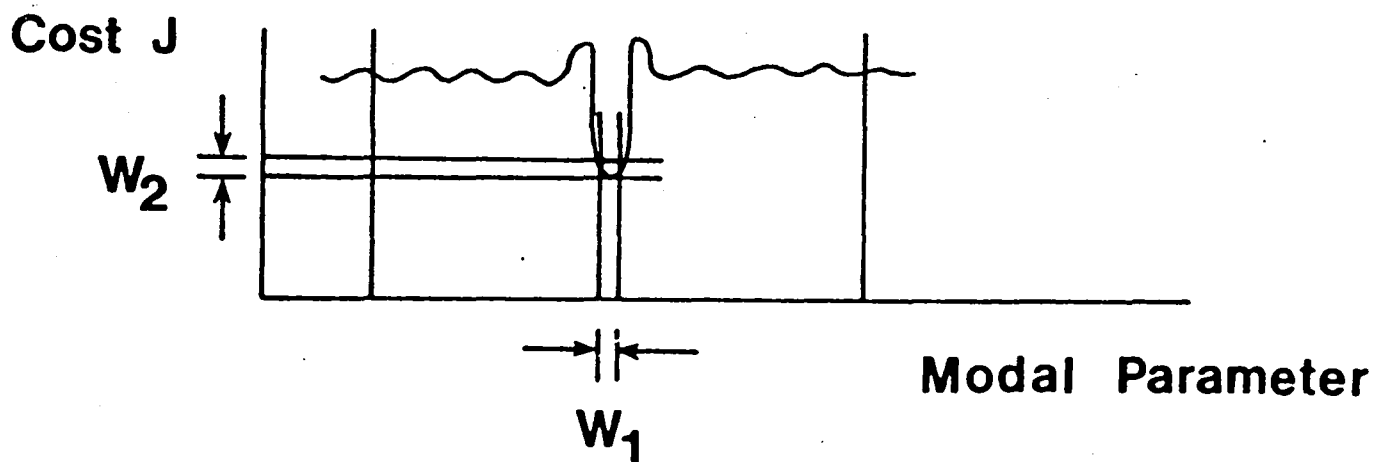
Update $V^+, W^+ \rightarrow$ Minimize $J \rightarrow$ Modal Parameters

GLOBAL MINIMUM OPTIMIZATION

A global minimum optimization algorithm is applied to update the filter parameters by using the interval analysis method. This method guarantees global minimum within a specified region of system parameters and can be applied to nonlinear multi-variable cases with inequality constraints. However, there are several requirements as shown below and the computational time is still considerable for the cost function J defined before.

• Requirements

1. Explicit expressions of J , J' , and J''
2. Specified closed intervals of system parameters
3. Specified windows for J and system parameters



NUMERICAL SIMULATION

- MAST Truss Beam Structure – 5 modes, MIMO
Analytic model

Frequencies: 1.422, 1.422, 8.554, 9.495, 9.495 Hz

Inputs: 4 impulses

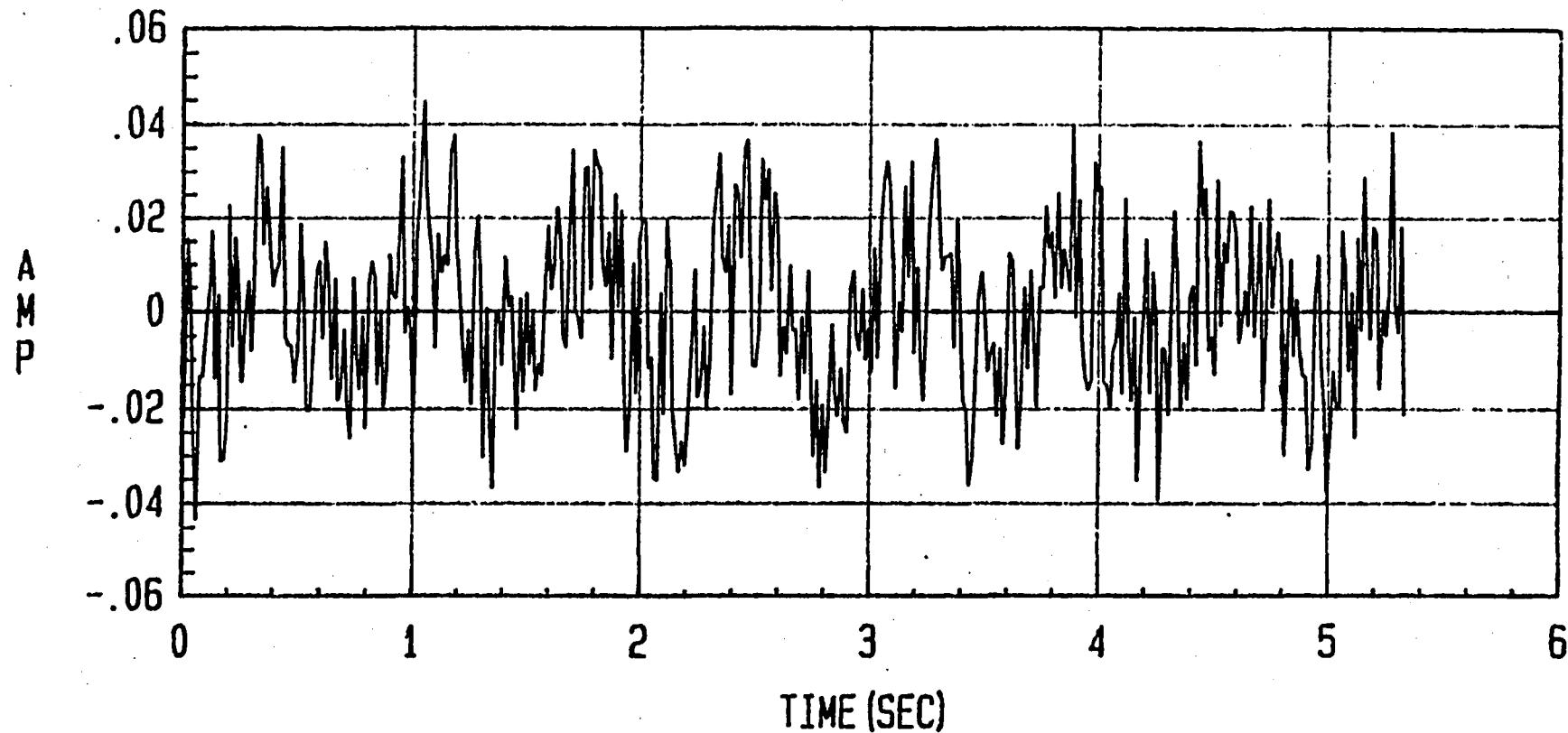
Outputs: 68 displacement sensors (four on each bay)

Sampling time: $T = 1/75$ sec

Measurements: 109 samples ($r=3$, $s=99$)

SIMULATED IMPULSE RESPONSE

This figure shows one of the simulated free impulse response data $Y(k)$ for the MAST truss beam structure with 10% measurement noise and zero damping.



SIMULATED IMPULSE RESPONSE

521

PERCENTAGE ERROR OF ESTIMATED FREQUENCY

This table shows the percentage error of estimated frequency from SPF for the simulated MAST beam structure with different damping ratios and noise levels. The SPF is effective to identify repeated modal frequencies and the errors fall within 1%. For a fixed noise level, the errors increase for most modes as the damping factor increases. This is caused by the fact that the signals decay faster for higher damping factors.

Damping ratio		0%			2%		
Freq (Hz)	Noise Level	0%	5%	10%	0%	5%	10%
1.4222	0.00#	0.01	0.02	0.00#	0.00#	0.01	
1.4222	0.02	0.06	0.16	0.03	0.09	0.18	
8.5545	0.21	0.21	0.20	0.38	0.40	0.42	
9.4954	0.82	0.80	0.78	0.97	0.95	0.90	
9.4954	0.29	0.30	0.30	0.43	0.43	0.42	

after numerical truncation

ERA AND SPF RESULTS FOR THE SIMULATED MAST BEAM STRUCTURE

This table shows the ERA and SPF results for the simulated MAST beam structure with 10% measurement noise and 2% damping ratio.

Both ERA and SPF can identify repeated modes and the results are comparable. There are slight disparities in the damping ratios and the computational burdens are considerably higher for the SPF because the global optimization algorithm are involved.

Mode	Frequency (Hz)			Damping(%)	
	FEM	ERA	SPF	ERA	SPF
1	1.422	1.422	1.422	1.860	2.020
2	1.422	1.423	1.420	2.050	2.020
3	8.555	8.565	8.519	2.940	1.160
4	9.495	9.489	9.581	1.930	0.430
5	9.495	9.494	9.535	3.040	1.120

RDA

LOGICON

ISE STRUCTURAL DYNAMIC EXPERIMENTS

M. H. LOCK

S. Y. CLARK

**R & D ASSOCIATES
2301 YALE BLVD. SE
ALBUQUERQUE, NM
(505) 842-8911**

N 93-122764

୮୭

RDA

DIRECTED ENERGY SYSTEMS: VIBRATION ISSUE

- **DEGRADATION OF SYSTEM PERFORMANCE**
 - REDUCED BEAM QUALITY
 - BEAM JITTER
- **DIFFICULTIES WITH PREDICTION CAPABILITY**
 - FIDELITY OF STRUCTURAL DYNAMIC MODELS
 - CHARACTERIZATION OF VIBRATION DISTURBANCES
- **DIFFICULTIES WITH GROUND VIBRATION/FIRING TESTS**
 - SIMULATION OF FREE-FREE CONDITIONS
 - EFFECT OF SPACE ENVIRONMENT (DAMPING, JOINT BEHAVIOR)
 - FACILITY DISTURBANCES

RDA

NPB-ISE OPPORTUNITY/STUDY OBJECTIVE

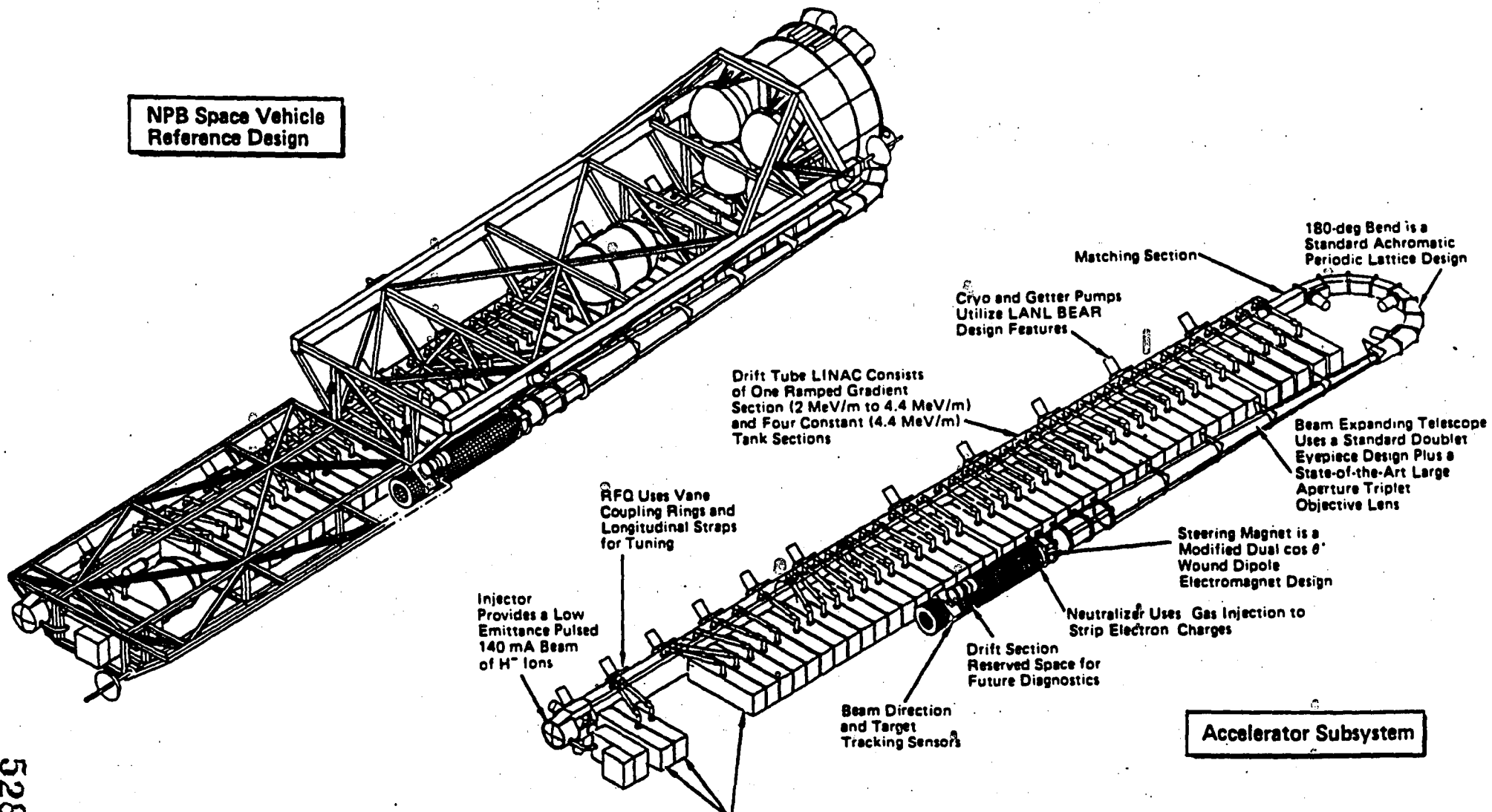
- **NPB-ISE: LARGE SPACE STRUCTURE (41K LBS, 75' DEPLOYED LENGTH)**
 - DEMONSTRATION OF ACCELERATOR OPERATION IN SPACE
- **POTENTIAL ON-ORBIT STRUCTURAL DYNAMIC EXPERIMENTS/DATA ACQUISITION**
 - SYSTEM IDENTIFICATION
 - RESPONSE TO OPERATIONAL DISTURBANCES: COOLING OF ACCELERATOR AND MAGNETIC OPTICS, DEVICE OPERATION
 - EMPHASIZE PERFORMANCE CRITICAL ITEMS - TPS, MAGNETS, DRIFT TUBES
- **PRESENT STUDY OBJECTIVE: IDENTIFY ADDITIONAL STRUCTURAL DYNAMIC EXPERIMENTS**
 - FOCUS ON REDUCTION OF INDUCED VIBRATION LEVELS

RDA

VIBRATION SOURCES/STUDY PLAN

- MAJORITY OF VIBRATION SOURCES ARE RANDOM AND DEPEND UPON SPECIFICS OF SYSTEM DESIGN
 - REACTANT COMBUSTION AND EXHAUST FLOWS
 - REACTANT TRANSFER AND HEX OPERATION
 - COOLING OF ACCELERATOR AND MAGNETIC OPTICS
 - COOLING OF BEAM TRANSFER AND RESONATOR MIRRORS
- ACS FORCES FOR SPACECRAFT SLEW ARE DETERMINISTIC
 - FORCES DEPEND UPON SLEW PARAMETERS AND OVERALL INERTIAL PROPERTIES OF SPACECRAFT
- STUDY PLAN: DEVELOP SLEW MANEUVER APPROACH THAT REDUCES INDUCED BEAM JITTER
 - DYNAMIC ANALYSIS OF SLEW MANEUVER
 - IDENTIFICATION OF PREFERRED APPROACH/EXPERIMENT

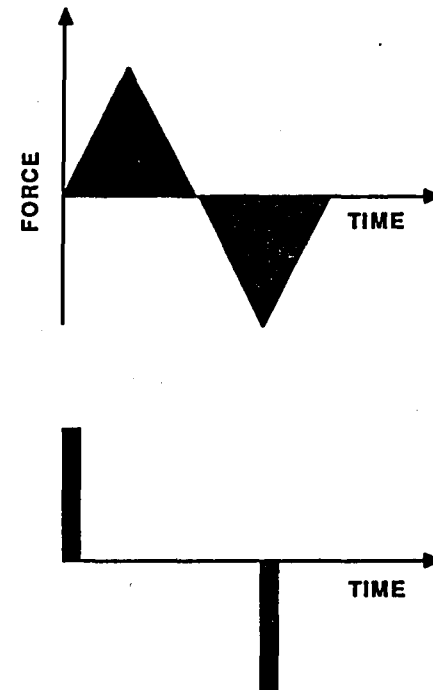
NPB-ISE SPACECRAFT CONFIGURATION



RDA

BASELINE SLEW ANALYSIS

- SLEW MANEUVER PARAMETERS
 - 20 DEGREE PITCH MANEUVER IN 8 SECONDS
- FORCE PULSE SHAPE
 - 8 SECOND FULL-CYCLE TRIANGULAR PULSE
 - TWO 0.5 SECOND PULSES
- ACS THRUSTER LOCATIONS
 - FORWARD AND AFT ENDS OF UNFOLDING SECTION
- MODAL INPUT TO ANALYSIS
 - THIRTY ELASTIC MODES (PROVIDED BY MDAC)
 - UNIFORM MODAL DAMPING OF 1.0 PERCENT



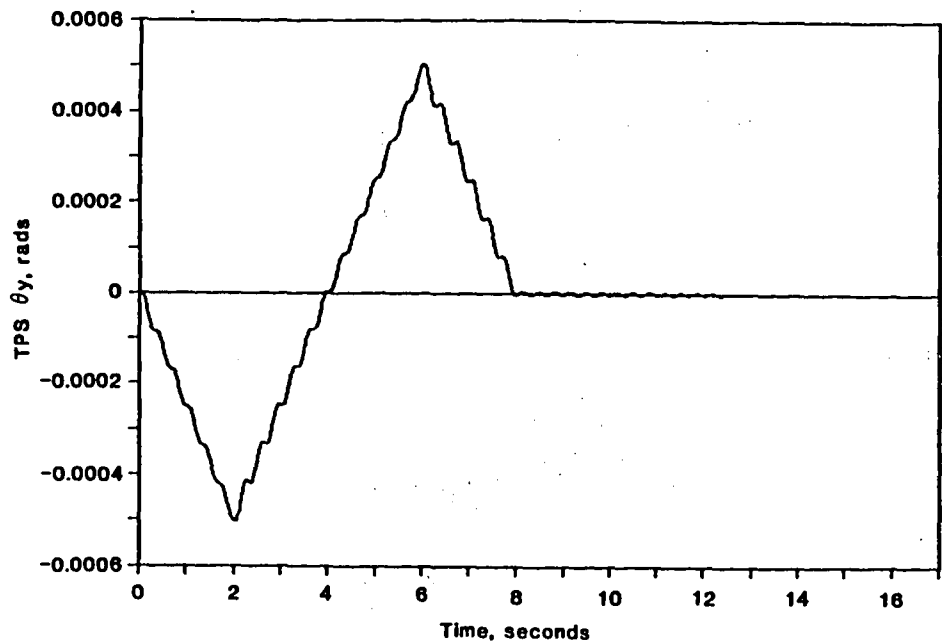
RDA

BASELINE ANALYSIS RESULTS

QUASI-STATIC RESPONSE DOMINANT DURING SLEW

- "STATIC" BENDING OF SPACECRAFT
- INSENSITIVE TO SYSTEM DYNAMICS

- LOWER AMPLITUDE VIBRATORY RESPONSE
- PEAK LEVEL $2.4 \cdot 10^{-5}$ RAD
- FUNDAMENTAL PITCH MODE (2.96 Hz)
MAIN CONTRIBUTOR

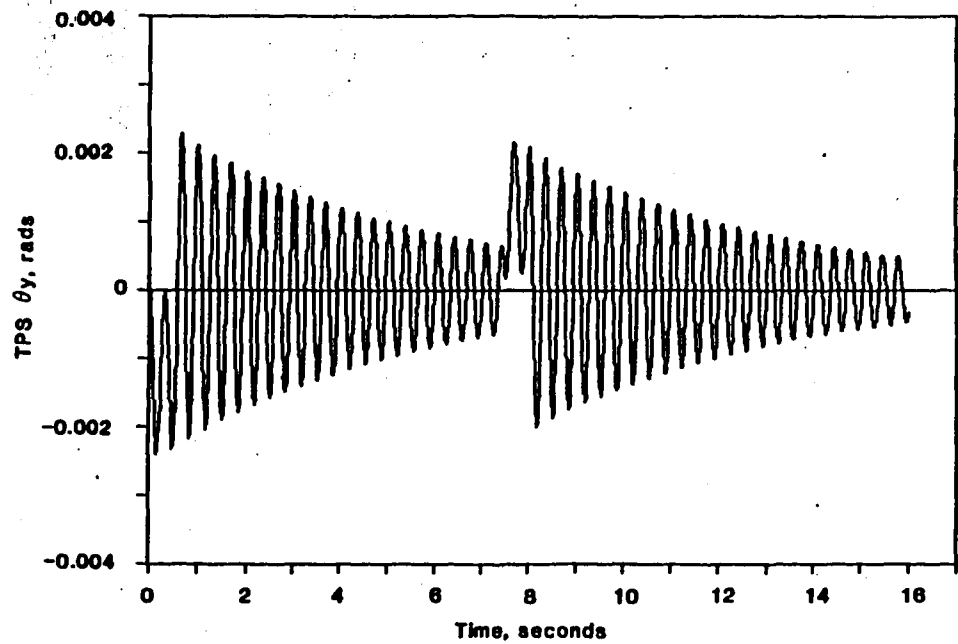


FULL-CYCLE TRIANGULAR PULSE

RDA

BASELINE ANALYSIS RESULTS (Cont)

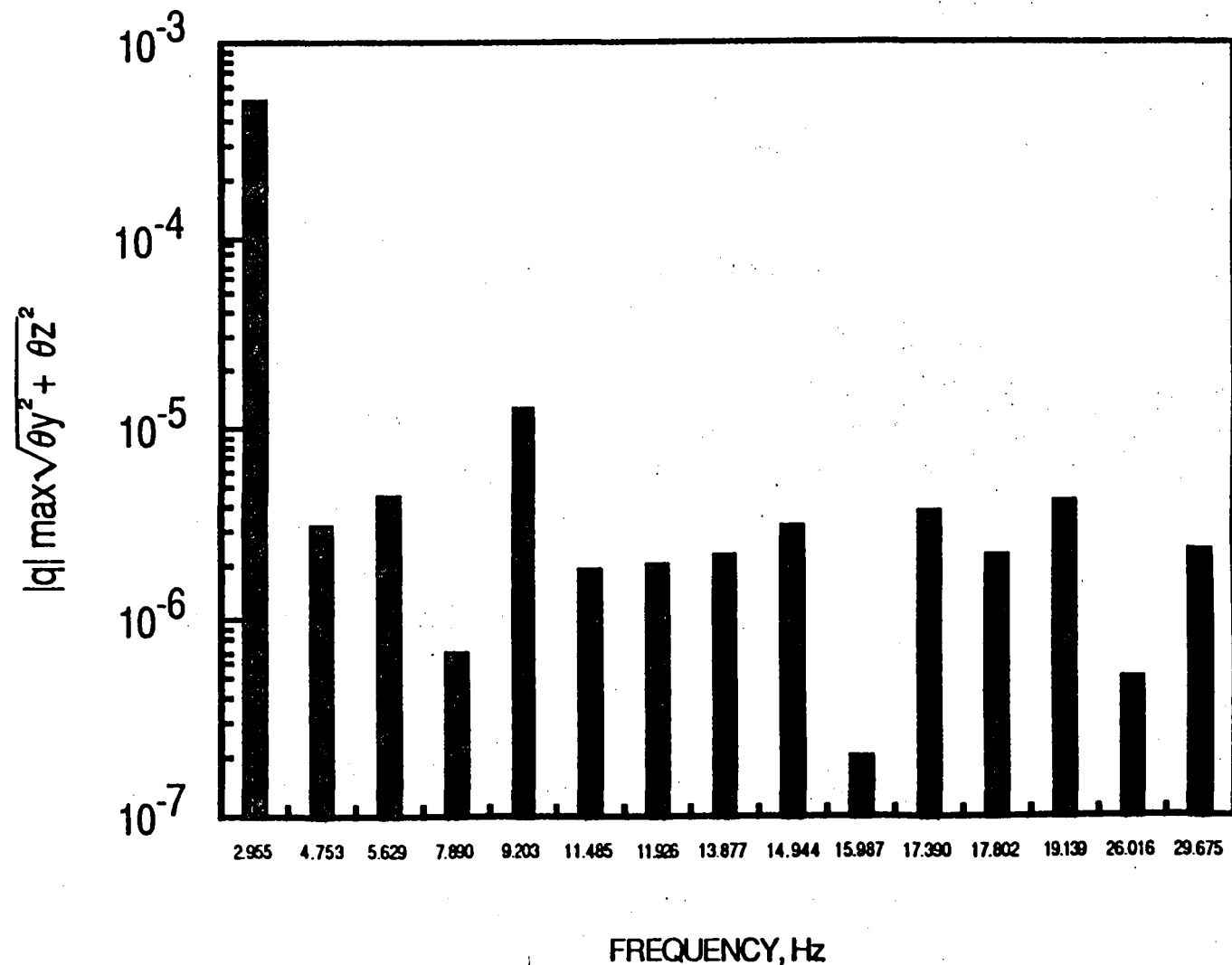
- PEAK VIBRATORY RESPONSE
ABOUT 5 TIMES HIGHER THAN
PEAK QUASI-STATIC RESPONSE
 - $2.3 \cdot 10^{-3}$ RADS VERSUS
 $5 \cdot 10^{-4}$ RADS
- FUNDAMENTAL PITCH MODE
DOMINANT CONTRIBUTOR



0.5 SECOND FORCE PULSES

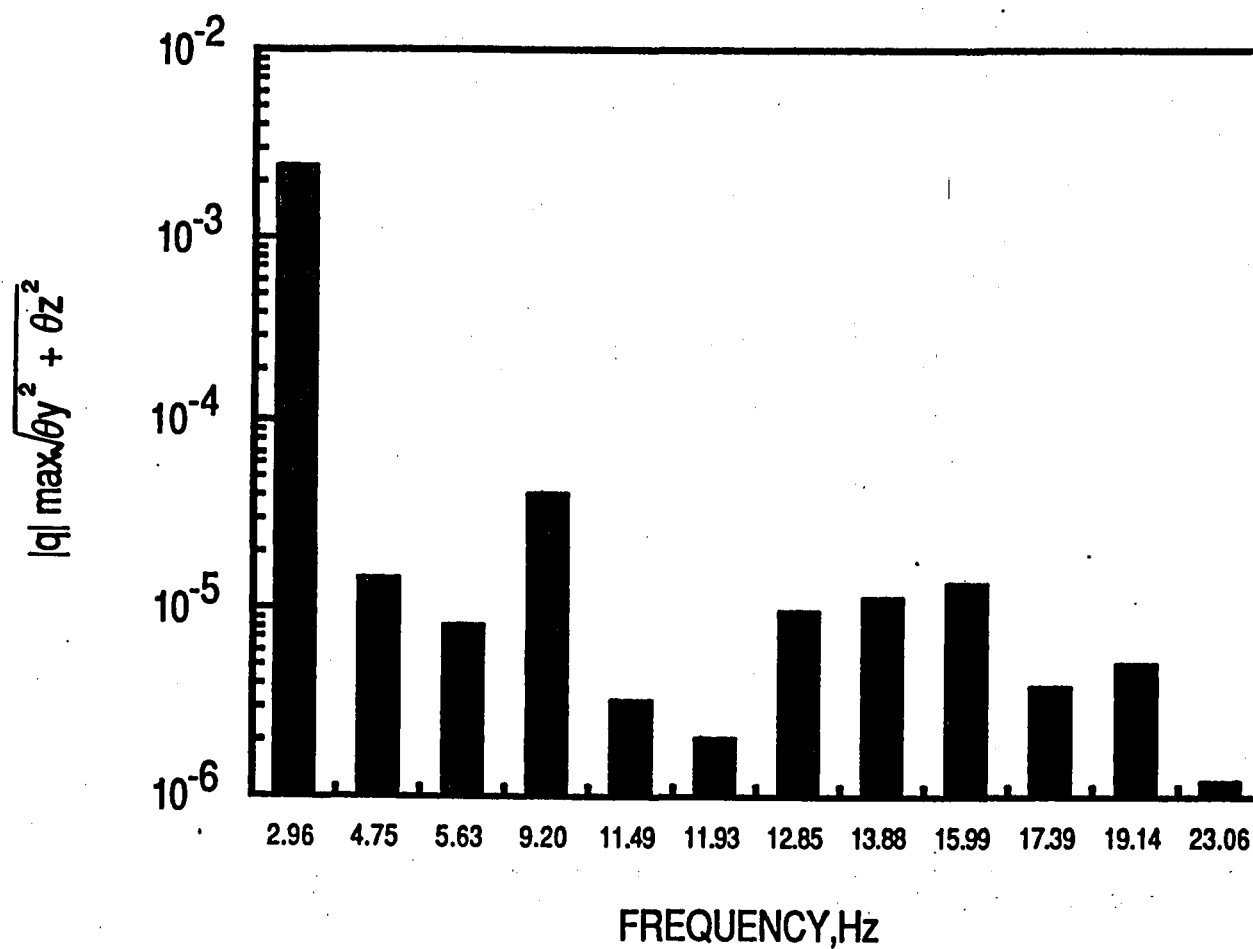
RDA

MODAL CONTRIBUTIONS: TRIANGULAR PULSE



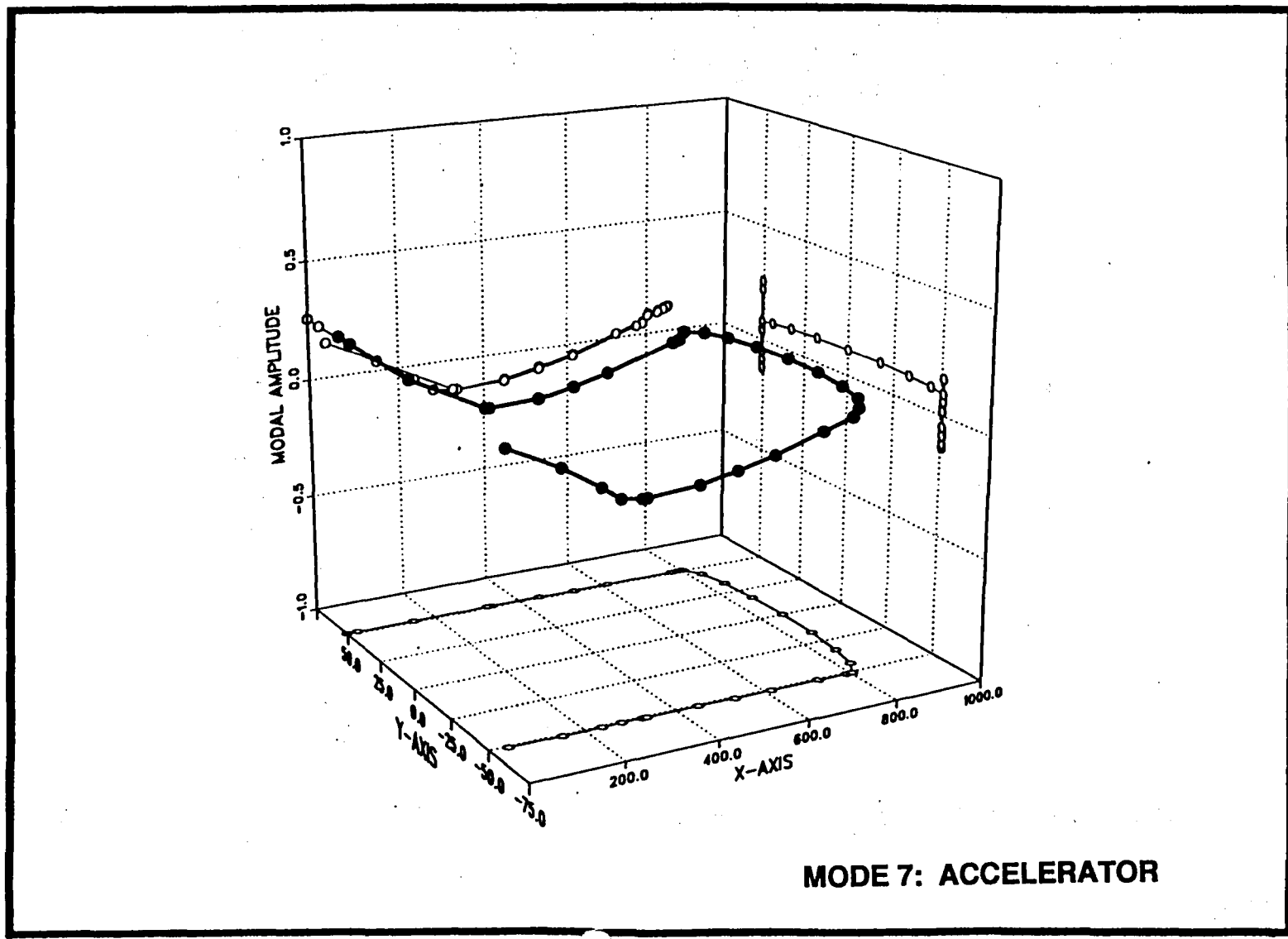
532

MODAL CONTRIBUTIONS: 0.5 SECOND PULSES



RDA

FUNDAMENTAL PITCH MODE



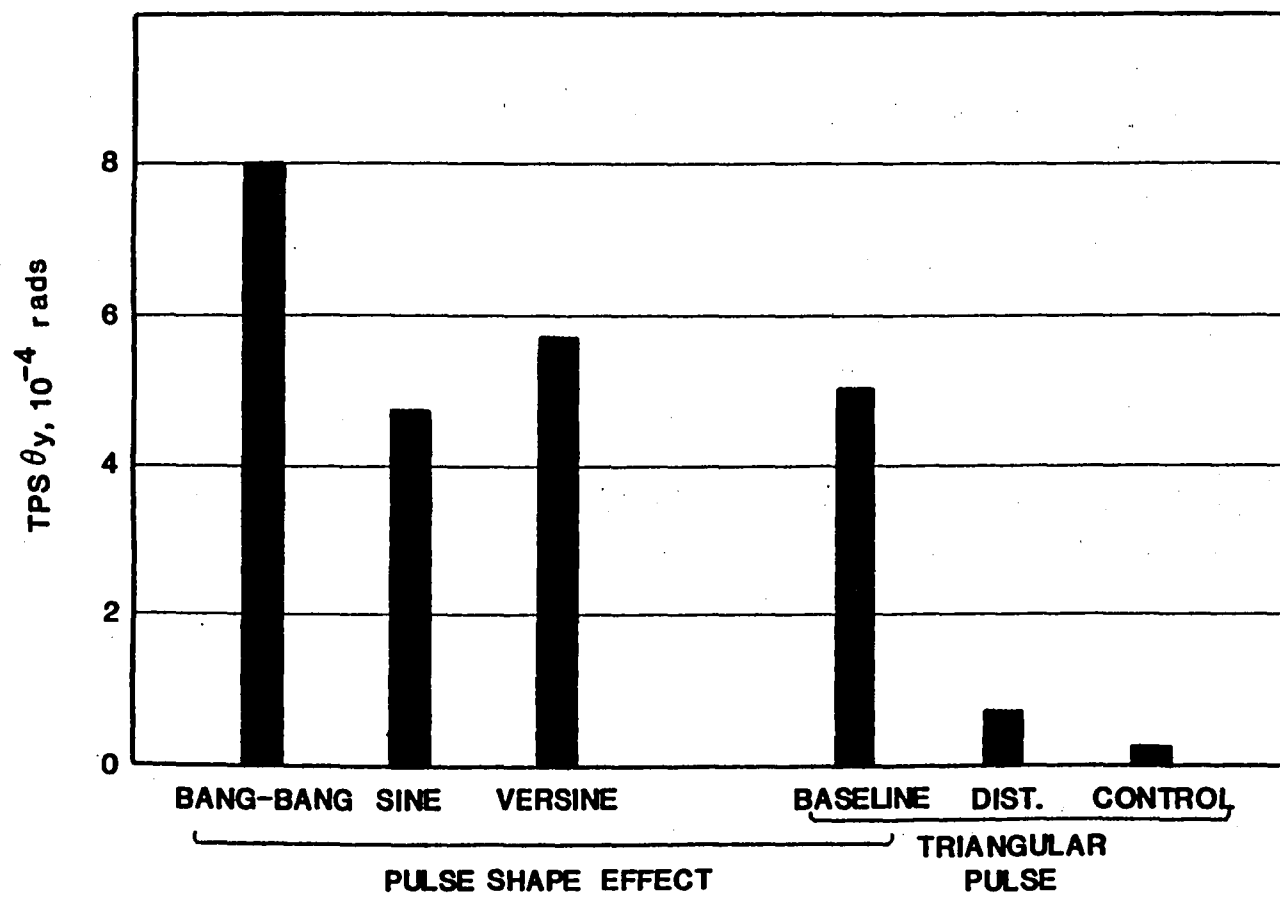
RDA

VIBRATION REDUCTION APPROACHES

- **MODIFY SPATIAL DISTRIBUTION OF THRUSTERS**
 - SELECT THRUSTER FORCE LEVELS TO ELIMINATE EXCITATION OF DOMINANT PITCH MODE
 - APPROACH REQUIRED ADDITION OF TWO THRUSTER CLUSTERS ON THE FORWARD END OF THE FOLDING SECTION
- **VARY THE DURATION OF THE FORCE PULSES**
- **VARY THE TEMPORAL FORM OF THE 8 SECOND FORCE PULSE (BANG-BANG, SINE, VERSINE)**
- **SIMULATE EFFECT OF BEAM CONTROL FOR QUASI-STATIC RESPONSE**

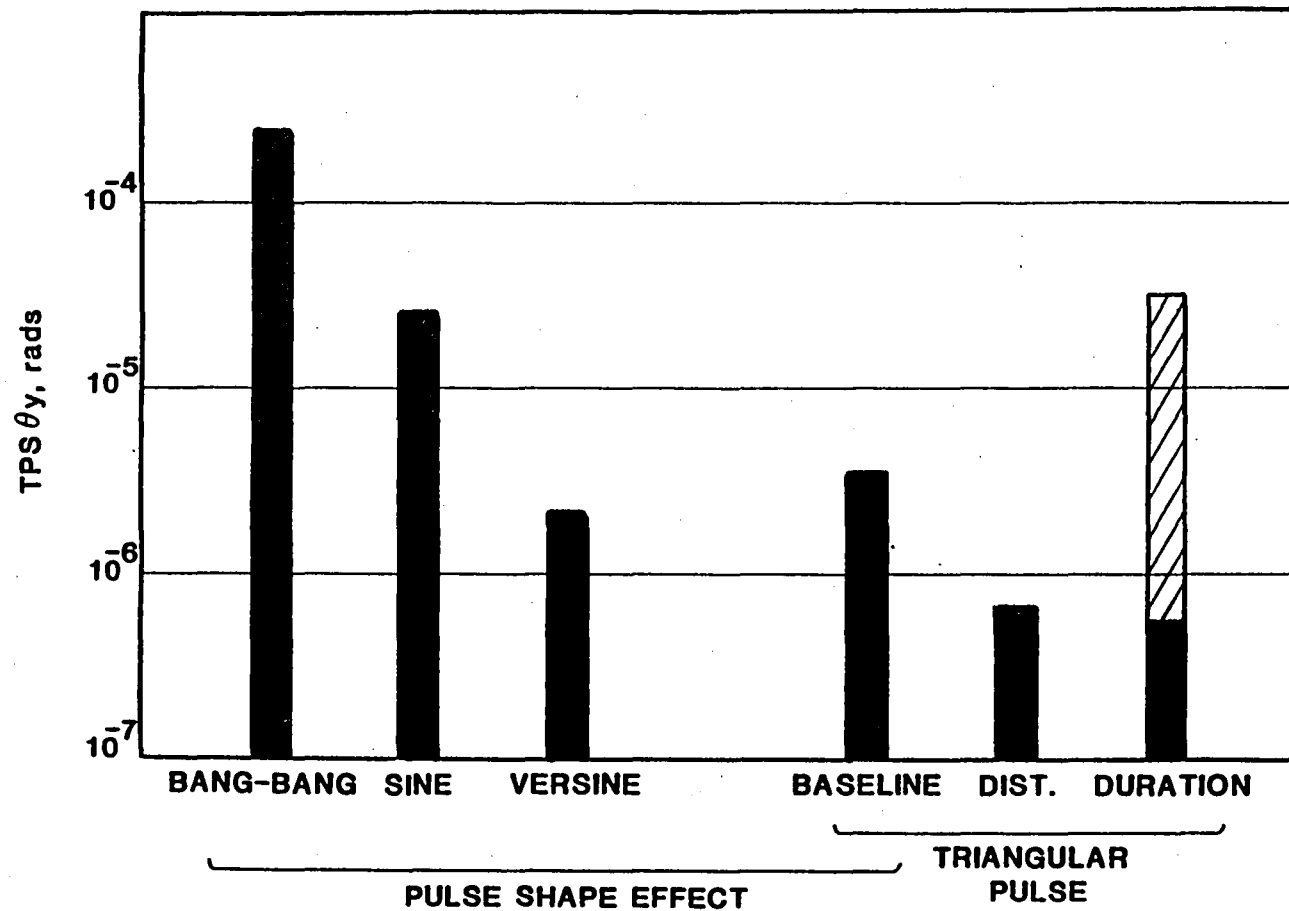
RDA

8 SECOND PULSE: RESPONSE DURING SLEW



RDA

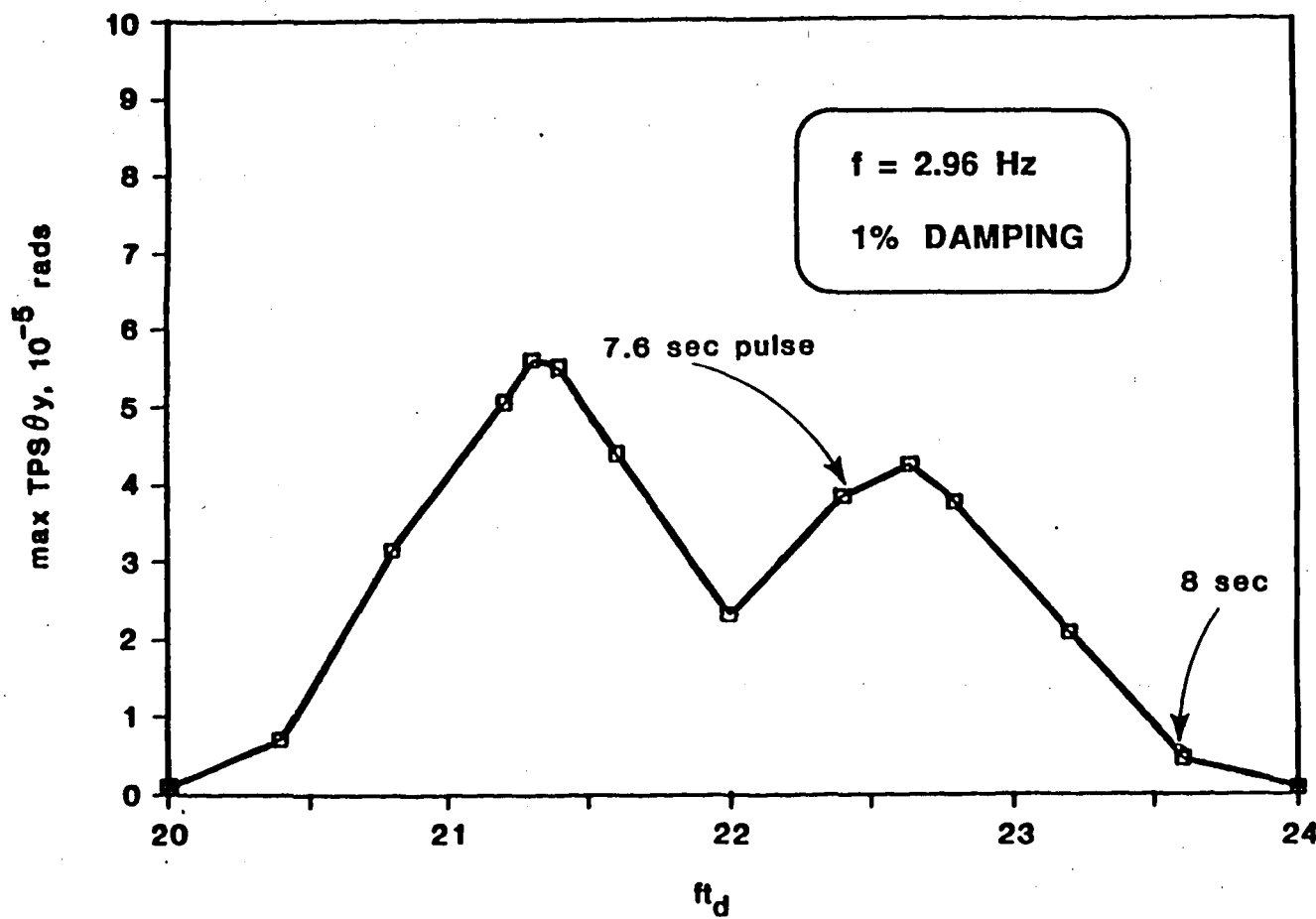
8 SECOND PULSE: RESIDUAL VIBRATION



435

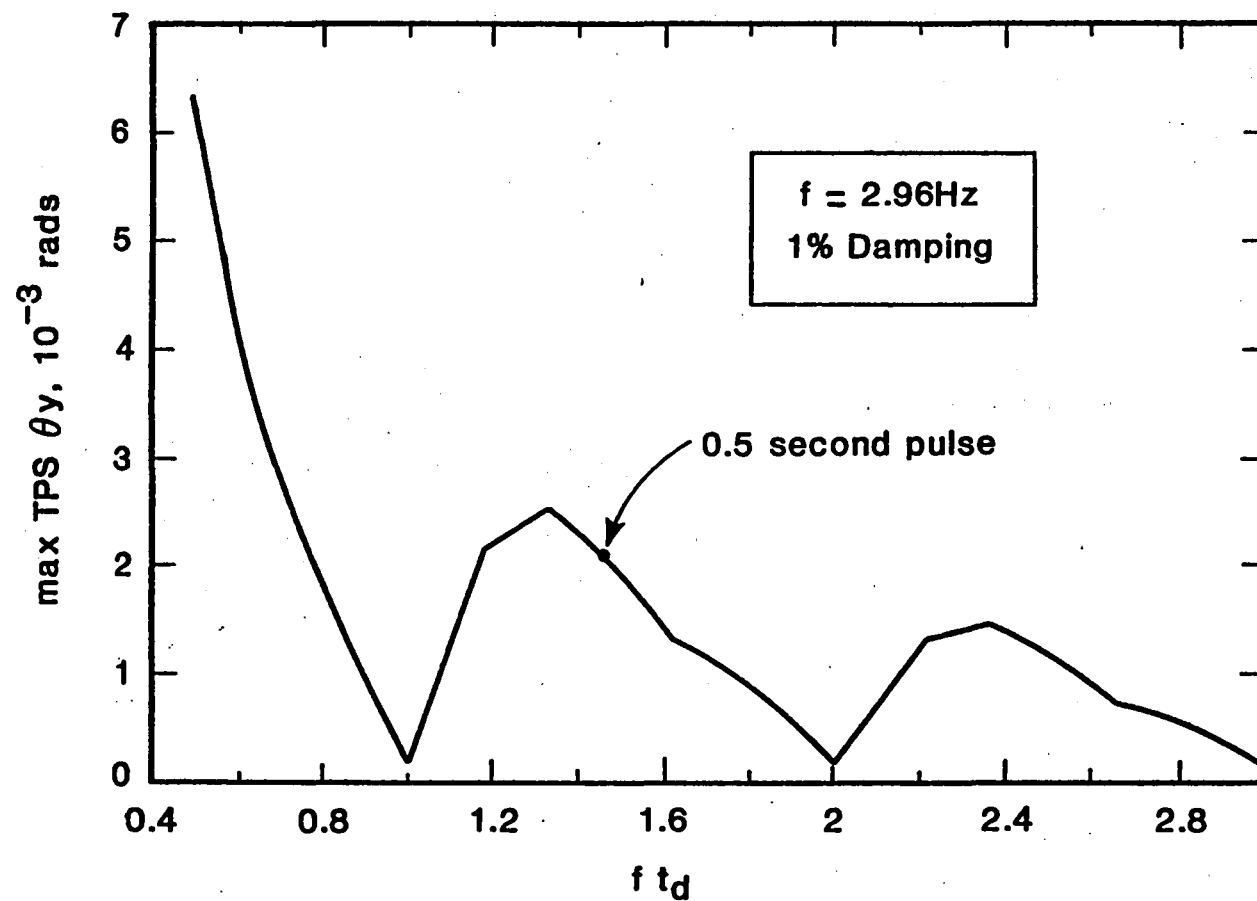
RDA

PEAK RESIDUAL VIBRATION: EFFECT OF PULSE DURATION



RDA

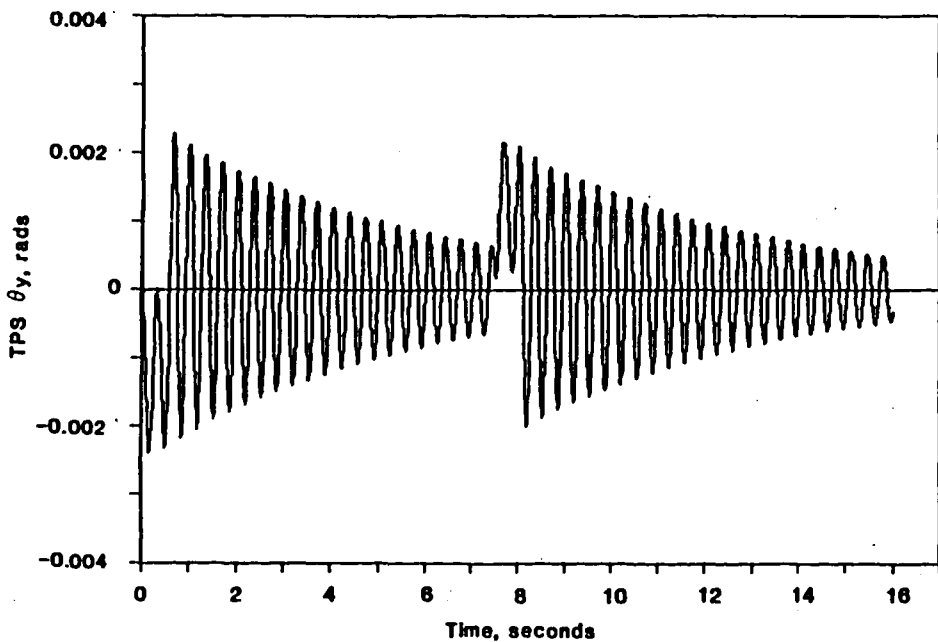
PEAK RESIDUAL VIBRATION: EFFECT OF PULSE DURATION



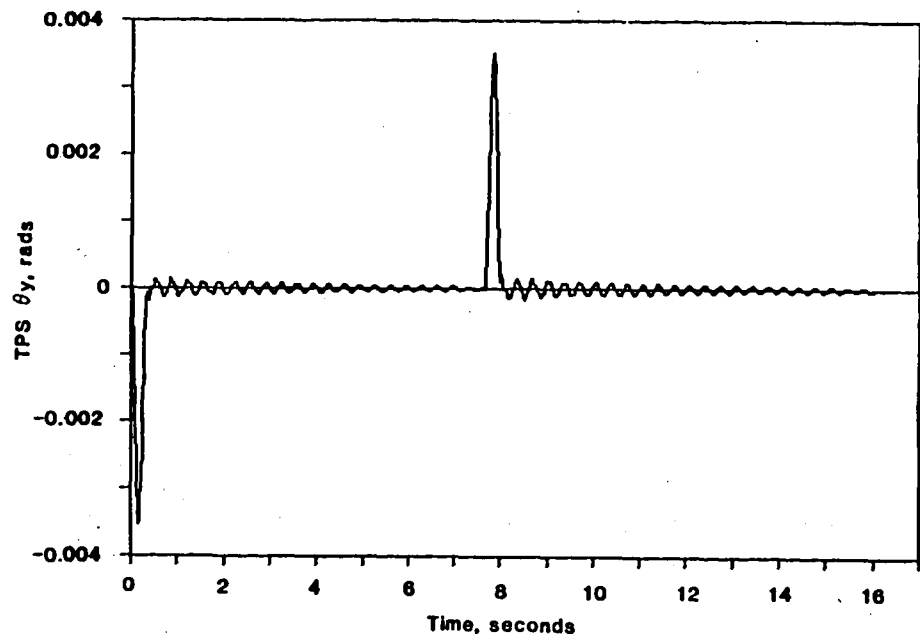
665

RDA

COMPARISON OF SLEW RESPONSES



0.5 SECOND FORCE PULSES



0.338 SECOND FORCE PULSES

045

RDA

NPB-ISE SPACECRAFT SLEW EXPERIMENT

- **IMPLEMENT SPACECRAFT SLEW EXPERIMENT TO INVESTIGATE EFFECT OF PULSE DURATION**
 - **SELECTED VARIATION OF ACS THRUST DURATION**
 - **MEASUREMENT OF INDUCED BEAM JITTER**
 - **MEASUREMENT OF RESPONSE OF INITIAL BEAM LINE ELEMENTS**
 - **CORRELATION WITH PREDICTIONS**

RDA

GOODBYE ISE - HELLO ZENITH STAR

- NPB-ISE PROJECT TERMINATED (JAN 1988)
- MMAG, LMSC, TRW TEAM WORKING ZENITH STAR PROJECT (SPACE-BASED LASER); PROGRAM OFFERS POTENTIAL FOR STRUCTURAL DYNAMIC EXPERIMENTS
 - PERFORMANCE RELATED EXPERIMENTS WITH LOW POWER LASER
 - EFFECT OF VIBRATION OF CRITICAL BEAM LINE ELEMENTS
 - SYSTEMATIC EXAMINATION OF INFLUENCE OF DISTURBANCE SOURCES
 - SYSTEM IDENTIFICATION
 - DEVELOPMENT OF SPACECRAFT SLEW EXPERIMENTS

CHART 1

The performance of directed energy systems such as space-based lasers (SBL's) and neutral particle beam (NPB) devices is very sensitive to structural vibration. The performance is effected by both degradation of beam quality and induced beam jitter. The prediction of the effect of vibration is hampered by uncertainties in the fidelity of the structural dynamic modeling (e.g., a reversal in the relative phase between two mirrors could change a performance estimate dramatically) and the difficulty in characterizing the vibration disturbances. Verification of the structural modeling and disturbance characterization by ground test is impeded by factors such as simulation of free-free conditions, the effect of the space environment (changes in damping and joint behavior) and the presence of test facility disturbances (e.g., the vibrations produced by operation of a pressure recovery system in a laser test).

CHART 2

The latter difficulties are avoided if the appropriate structural dynamic experiments can be carried out in space. An opportunity for such testing arose with the advent of the NPB Integrated Space Experiment (NPB-ISE). This project involved orbiting a large particle beam accelerator for the purpose of demonstrating operation of the device in space. The NPB-ISE spacecraft weighs some 41,000 lbs and is about 75' long in the deployed configuration. Obvious on-orbit structural dynamic experiments and data acquisition would involve system identification and the measurement of the response induced by the operational environment (e.g., cooling of the accelerator and the magnetic optics, operation of the device). The emphasis in such experiments should be upon elements that are critical to the performance of the system. Another area of major interest is reduction of the induced vibration environment. The present study investigates potential experiments in this particular area.

CHART 3

The majority of the vibration disturbances on a directed energy system are random in nature and are design specific. Examples of such vibration sources are reactant combustion, exhaust flows, reactant transfer, heat exchanger operations, accelerator and magnetic optics cooling, beam transfer mirror and resonator mirror cooling. In contrast to these disturbances, the spacecraft slew forces generated with the attitude control system (ACS) are deterministic. These forces only depend upon the slew maneuver parameters and the overall inertial properties of the spacecraft. In view of these factors the present study is directed to identification of approaches to slewing that reduce the induced structural vibration levels and the specification of a suitable experiment.

CHART 4

The NPB-ISE spacecraft designed by MDAC is illustrated in this chart. The overall features of the spacecraft are shown as well as details of the accelerator subsystem. The particular accelerator design shown in the chart was superceded by a version that extended to the forward end of the spacecraft. The modal data supplied by MDAC for use in this study reflected this later design. A key feature of the spacecraft is the hinge between the folding and unfolding sections. The forward part of the spacecraft is folded back over the remaining section of the vehicle during boost. This section is unfolded in the orbital configuration leading to a total spacecraft length of around 75'. The tracking and pointing system (TPS) is located at the end of the beam line.

CHART 5

The parameters of the selected slew maneuver, the type of ACS thruster pulses, the thruster locations and the modal input are described. The two types of force pulse reflect 1) the continuous application of a slowly varying force throughout the complete maneuver and 2) a pulse and drift approach to slewing the spacecraft. The first thirty elastic modes calculated by MDAC for the orbital configuration were used in the analysis. The first three elastic modes comprise a pitch mode at 2.96 Hz, a twist mode at 4.75 Hz and a yaw mode at 5.63 Hz; the highest elastic mode used in the analysis (mode 30) had a frequency of 31 Hz.

CHART 6

The response induced by the slew maneuver was calculated at several points along the beam line (bending magnet, eyepiece, objective, steering magnet, TPS). The overall character of the response was similar at all of these locations. The pitch response calculated for the TPS when the slew maneuver is implemented by means of the 8 second full-cycle triangular pulse is illustrated in this chart. During the period of force application the response is dominated by the quasi-static distortion of the spacecraft that is induced by the slowly varying thrust loads. The associated vibratory responses are about an order of magnitude lower than the peak quasi-static level. The dominant contributor to the motion of the spacecraft is the fundamental pitch mode.

CHART 7

The response induced at the TPS by the alternate approach to slewing - pulse and drift - is illustrated in this chart. The peak vibratory response is about 5 times higher than the peak quasi-static response induced by the 8 second loading. Again the fundamental pitch mode is the major contributor to the response.

CHARTS 8, 9, and 10

These charts illustrate the modal contributions to the response and the overall character of the dominant pitch mode.

CHART 11

The approaches taken to reduce the induced response of the spacecraft are specified. In the case of spatially distributed thrusters a pair of thruster clusters were added to the forward end of the folding section. The magnitude of the thrust levels at the three different thruster stations (forward end of folding section, forward end of unfolding section, aft end of unfolding section) were selected to eliminate the generalized force in the dominant pitch mode. Variation of pulse duration and the temporal form of the 8 second pulse were also examined. Simulation of beam control for the quasi-static response simply involved elimination of this response component. This approach was taken as a simple means of reflecting the effect of a beam control system used for this purpose.

CHARTS 12 and 13

These charts summarize the results obtained with the 8 second pulse. It is seen that the use of spatially distributed thrusters to eliminate the generalized force in the dominant response mode is very effective for both the quasi-static and vibratory responses. However, it should be noted that a possible drawback to implementation of this approach on a space-based laser would be the question of contamination of the primary and secondary mirrors on the beam expander. The vibratory response is also very sensitive to pulse duration (see cross-hatched area in Chart 13). Because of time constraints the remainder of the briefing will concentrate on the effect of pulse duration.

CHART 14

The effect of pulse duration on the peak residual vibration induced by the full-cycle triangular force loading is illustrated in this chart. The maximum vibration level is plotted against the parameter ft_d where f is the frequency of the fundamental pitch mode (2.96 Hz) and t_d is the duration of the loading pulse in seconds. It is seen that the 8 sec baseline pulse is close to ideal from the standpoint of induced vibratory response. It is also seen that relatively small changes in pulse duration produce major changes in the vibration level. For example a 4.5 percent reduction in pulse duration from the 8 second baseline produces an order of magnitude increase in the vibratory response. The variation of vibratory response with the parameter ft_d is related to the work done in exciting the dominant response mode. It might be noted that changes in either the frequency f or the pulse duration t_d would produce a similar effect.

CHART 15

This chart shows the variation of the peak vibratory response with the parameter ft_d for the case of the short load pulses. It is seen that the baseline 0.5 second pulse is not optimal from the standpoint of induced vibration. A pulse length of 0.338 seconds is predicted to be more suitable.

CHART 16

This chart provides a comparison of the TPS response induced by the baseline 0.5 second pulse and by the 0.338 second pulse. The dramatic reduction in vibratory response is apparent.

CHART 17

A slew experiment recommended for the NPB-ISE is described. The experiment would be directed at establishing the benefit of pulse duration control for the reduction of induced vibration levels. Ideally, both beam jitter and structural response measurements would be taken. The beam jitter measurements would be taken on the existing target vehicle and the structural response measurements would focus on the critical beam line elements. The test data would be subsequently correlated with analysis.

CHART 18

In January 1988 the NPB-ISE project was terminated. However, another large spacecraft program is currently being worked. This is the Zenith Star Program. This project involves orbiting a laser system. It offers considerable potential for meaningful on-orbit structural dynamic experiments.

12-3365
5/8/81

A Stereo Triangulation System for Structural Identification: Analytical and Experimental Results

J. L. Junkins
G. H. James III
T. C. Pollock
Z. H. Rahman

Department of Aerospace Engineering
Texas A&M University
College Station, Texas, USA 77843

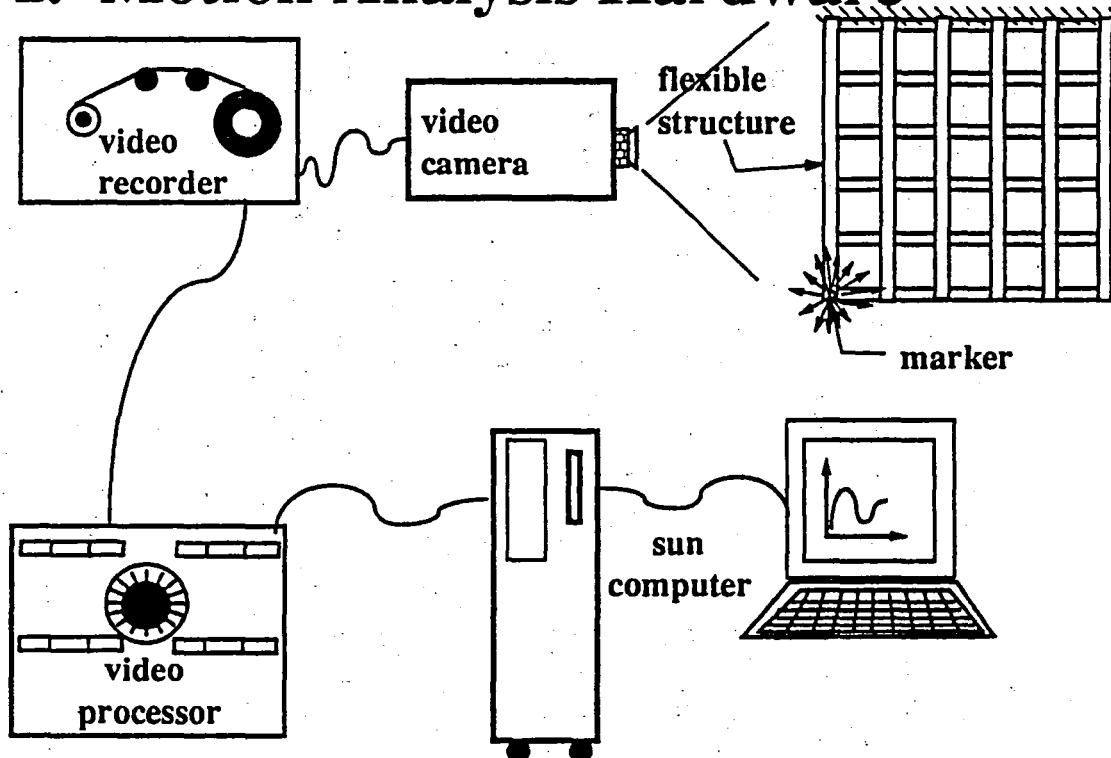
ABSTRACT

Identification of large space structures' distributed mass, stiffness, and energy dissipation characteristics poses formidable analytical, numerical, and implementation difficulties. Development of reliable on-orbit structural identification methods is important for implementing active vibration suppression concepts which are under widespread study in the large space structures community. Near the heart of the identification problem lies the necessity of making a large number of spatially distributed measurements of the structure's vibratory response and the associated force/moment inputs with sufficient spatial and frequency resolution. In the present paper, we discuss a method whereby tens of active or passive (retro-reflecting) targets on the structure are tracked simultaneously in the focal planes of two or more video cameras mounted on an adjacent platform. Triangulation (optical ray intersection) of the conjugate image centroids yield inertial trajectories of each target on the structure. Given the triangulated motion of the targets, we apply and extend methodology developed by Creamer, Junkins and Juang to identify the frequencies, mode shapes and updated estimates for the mass/stiffness/damping parameterization of the structure. The methodology is semi-automated, for example the post experiment analysis of the video imagery to determine the inertial trajectories of the targets typically requires less than thirty minutes of real time.

Using methodology discussed herein, the frequency response of a large number of points on the structure (where reflective targets are mounted) on the structure can be determined from optical measurements alone. For comparison purposes, we also utilize measurements from accelerometers and a calibrated impulse hammer. While our experimental work remains in a research stage of development, we have successfully tracked and stereo triangulated 20 targets (on a vibrating cantilevered grid structure) at a sample frequency of 200HZ, and have established conclusively the feasibility and desirability of this approach.

We discuss, in summary, recent advances in analog and digital video processing methodology, and actuation methods, and bring them to bear on the structural identification problem. We include a brief discussion of our experimental hardware and some recent experimental results which support the practical feasibility of this structural vibration sensing approach.

Figure 1. Motion Analysis Hardware



MAJOR HARDWARE ITEMS

ITEM	DESCRIPTION
Flexible Structure	monolithic 3003 H14 aluminum grid (5'x5') cantilevered in the vertical plane (clamped-free boundary conditions)
markers (targets)	3M Scotchlite Reflective Sheeting #3290
Video Cameras(2)	NAC model V-14B, 200/60 HZ, 2/3" MOS imaging CCD array with 320x244 pixels
Video Recorder(2)	NAC model VTR V-32, 200HZ, configured for VHS cassettes
Video Processor	Motion Analysis model VP-110 for threshold-based edge detection, hardware editing and filtering, digitizing image boundaries, and data transfer
Computer	SUN 1/120 with 42 megabyte hard disk and UNIX operating system

Measurement Geometry and Stereo Triangulation

The object-to image space transformation for a single lens camera is given by the *colinearity equations*

$$x = x_o - f \left[\frac{C_{11}(X-X_c) + C_{12}(Y-Y_c) + C_{13}(Z-Z_c)}{C_{31}(X-X_c) + C_{32}(Y-Y_c) + C_{33}(Z-Z_c)} \right] \equiv F(X, Y, Z; X_c, Y_c, Z_c; \phi, \theta, \psi; x_o, y_o, f)$$

$$y = y_o - f \left[\frac{C_{21}(X-X_c) + C_{22}(Y-Y_c) + C_{23}(Z-Z_c)}{C_{31}(X-X_c) + C_{32}(Y-Y_c) + C_{33}(Z-Z_c)} \right] \equiv G(X, Y, Z; X_c, Y_c, Z_c; \phi, \theta, \psi; x_o, y_o, f)$$

where

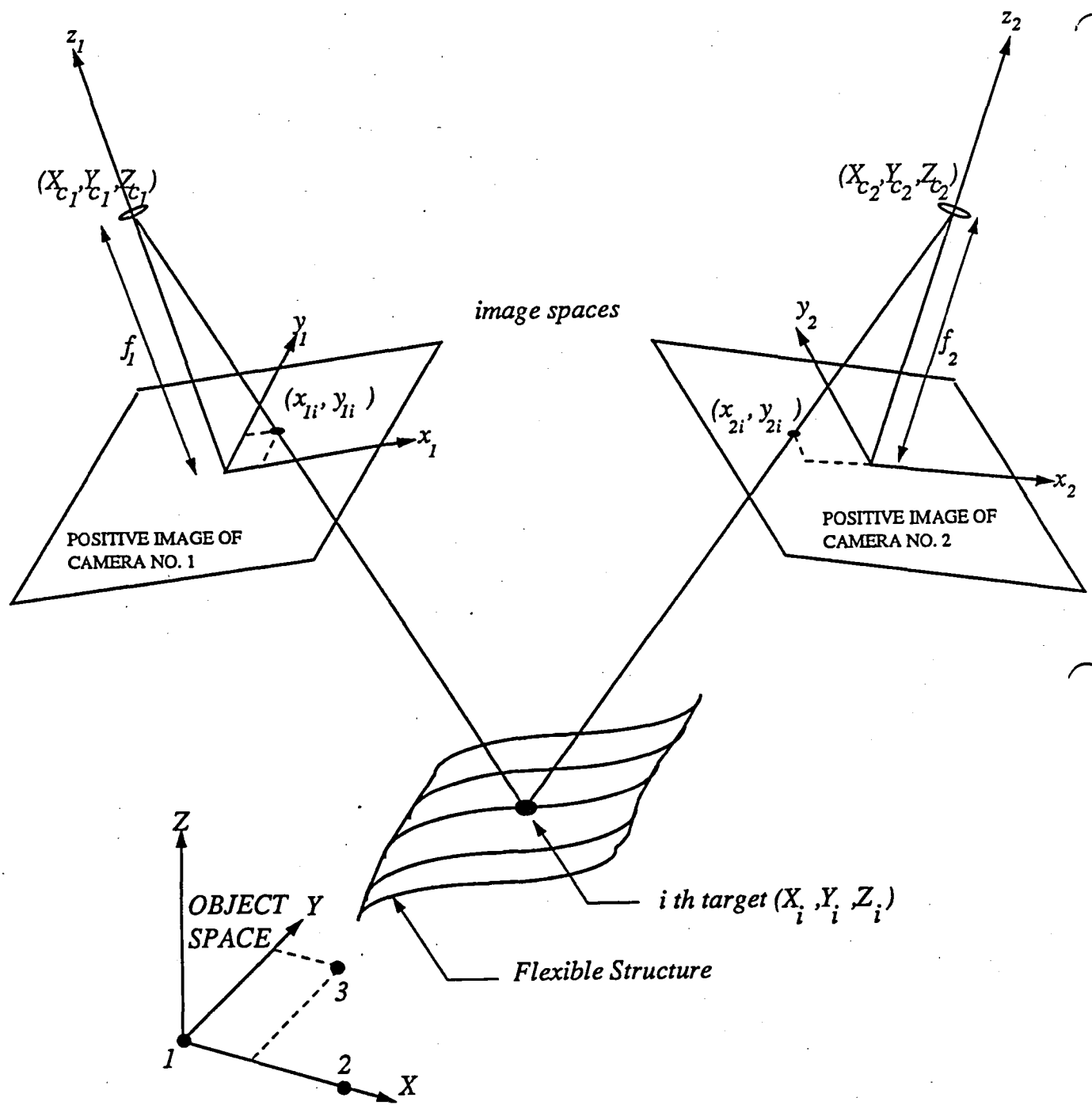
$$[C] = \begin{bmatrix} C_{11} & C_{12} & C_{13} \\ C_{21} & C_{22} & C_{23} \\ C_{31} & C_{32} & C_{33} \end{bmatrix} = \begin{bmatrix} 1 & 0 & 0 \\ 0 & \cos\psi & \sin\psi \\ 0 & -\sin\psi & \cos\psi \end{bmatrix} \begin{bmatrix} \cos\theta & 0 & -\sin\theta \\ 0 & 1 & 0 \\ \sin\theta & 0 & \cos\theta \end{bmatrix} \begin{bmatrix} \cos\phi & \sin\phi & 0 \\ -\sin\phi & \cos\phi & 0 \\ 0 & 0 & 1 \end{bmatrix}$$

For the case of two cameras simultaneously imaging the same structure, we adopt a subscript notation to denote the image coordinates of the i^{th} point measured in the j^{th} camera's image space as

$$x_{ij} = F(X_i, Y_i, Z_i; X_{c_j}, Y_{c_j}, Z_{c_j}; \phi_j, \theta_j, \psi_j; x_{o_j}, y_{o_j}, f_j), \quad j = 1, 2; \quad i = 1, 2, \dots, N$$

$$y_{ij} = G(X_i, Y_i, Z_i; X_{c_j}, Y_{c_j}, Z_{c_j}; \phi_j, \theta_j, \psi_j; x_{o_j}, y_{o_j}, f_j)$$

Figure 2. Stereo Triangulation Geometry



TWO PHOTOGRAMMETRIC ESTIMATION PROBLEMS

Problem One: *Static Calibration*

Each object space point imaged generates four measurements, these measurements can be combined with other a priori calibration information to determine the camera positions, orientation angles, focal lengths, and principle point offsets. Least square differential correction converges to yield estimates and associated covariance for camera geometric parameters.

Problem Two: *Dynamic Triangulation to Measure Deflections*

Given the results of the static calibration, the four equations for stereo images of each object space point can be solved for estimates of the object space coordinates; this can be done for each of several images, for each instant in time (e. g. at 200 HZ)

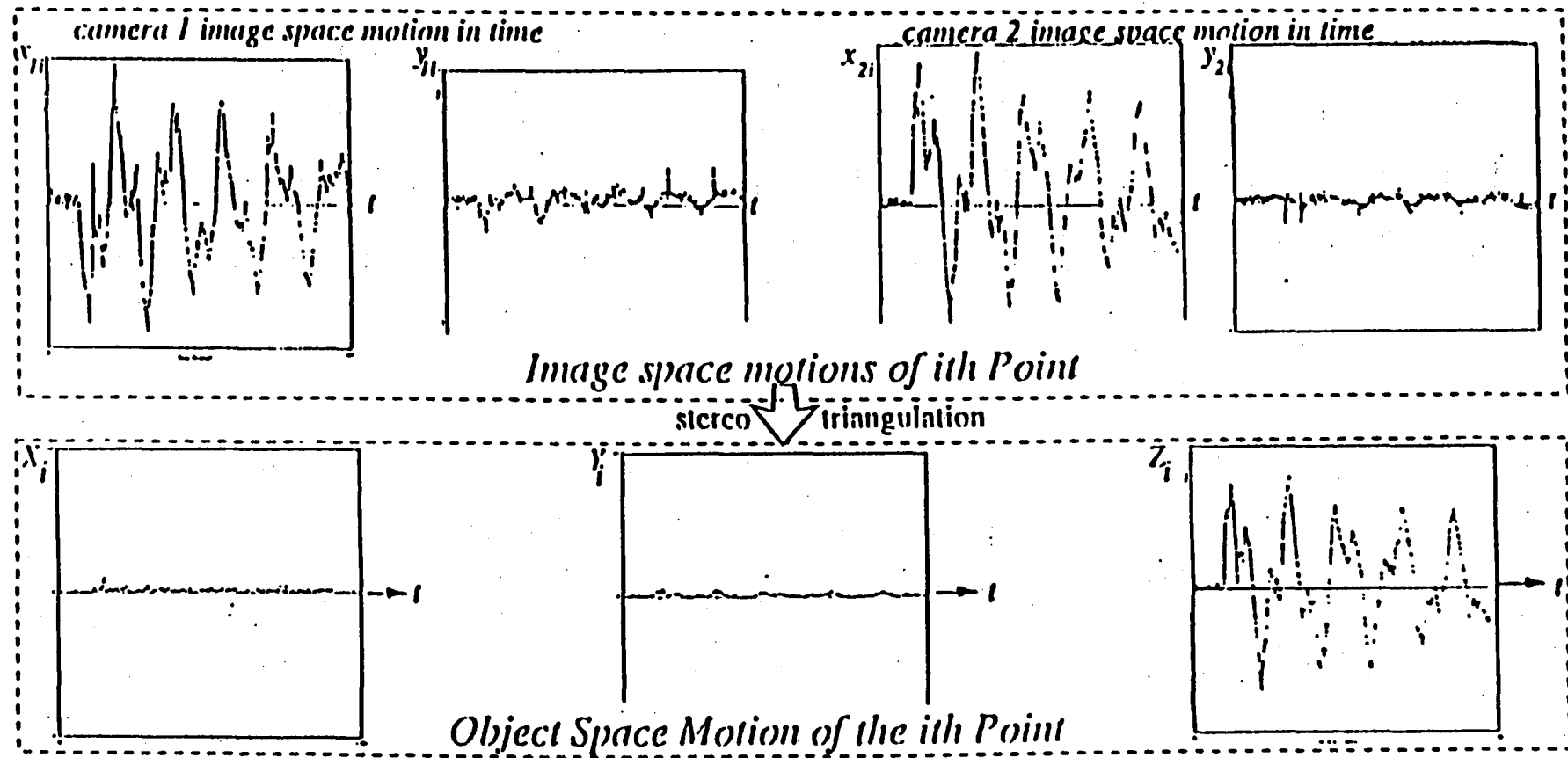
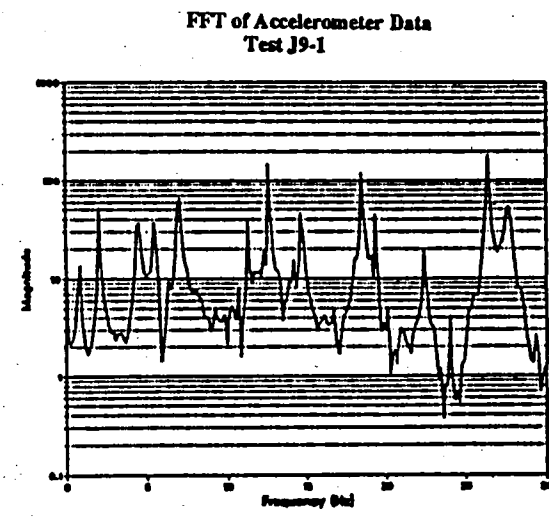
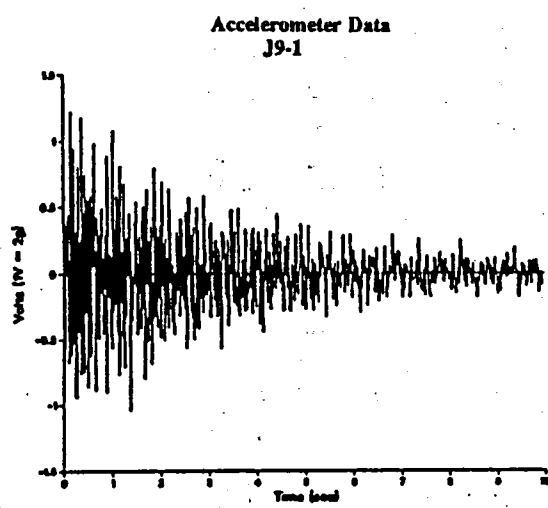
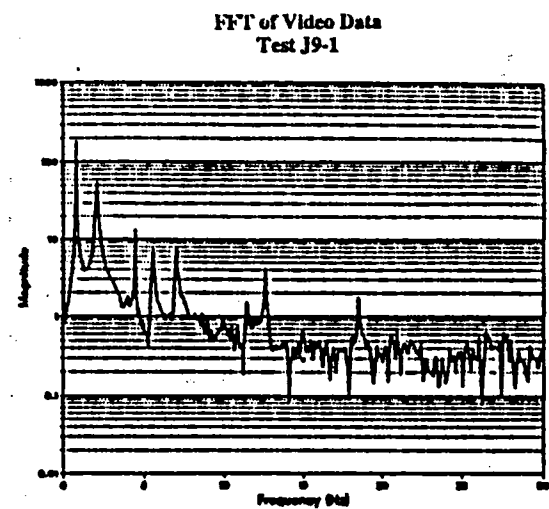
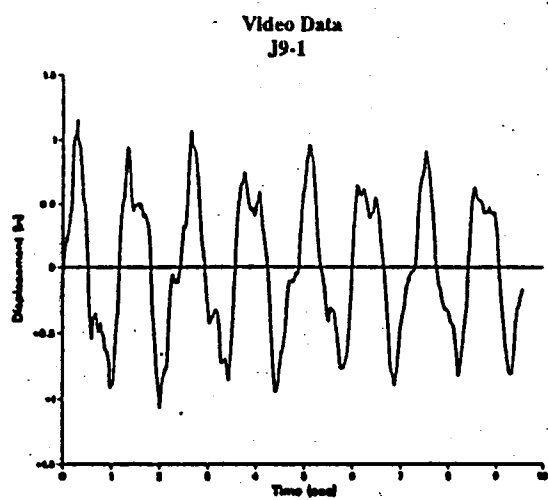


Figure 3. Typical Trajectory of Target Motion in Image Spaces and in Object Space

Figure 4. Comparison of Video-Derived Position Measurements with Accelerometer Measurements



STRUCTURAL IDENTIFICATION

We consider the class of linear elastic structures suitably modeled by

$$\mathbf{M}\ddot{\mathbf{x}} + \mathbf{C}\dot{\mathbf{x}} + \mathbf{K}\mathbf{x} = \mathbf{B}\mathbf{u}$$

To outline some of the details of our structural identification approach, we consider a special case. For harmonic excitation $\mathbf{u} = \mathbf{r} \exp(j\omega t)$, zero damping, and an identity \mathbf{B} matrix, the *frequency response* is given by taking the Fourier transform of the equations of motion to obtain

$$X(i\omega) = [-\omega^2 \mathbf{M} + \mathbf{K}]^{-1} \mathbf{r} = H(i\omega) \mathbf{r}, \quad H_{jk}(i\omega) \equiv \sum_{l=1}^n \frac{\phi_{jl} \phi_{kl}}{\omega_l^2 - \omega^2} \begin{pmatrix} \text{spectral} \\ \text{decomposition} \\ \text{theorem} \end{pmatrix}$$

where

$$\det [\mathbf{K} - \omega^2 \mathbf{M}] = 0, \Rightarrow \{\omega_1^2, \dots, \omega_n^2\}, \text{ and } [\mathbf{K} - \omega_i^2 \mathbf{M}] \phi_i = 0$$

$$\Phi^T \mathbf{M} \Phi = \mathbf{I}, \quad \Phi^T \mathbf{K} \Phi = \text{diag}(\omega_1^2, \dots, \omega_n^2), \quad \Phi = [\phi_1 \dots \phi_n]$$

Creamer and Junkins [3, 4] developed an identification process whereby linearly parameterized mass, stiffness and damping properties can be estimated; the structural parameterization adopted for the present discussion is of the form

$$\mathbf{M} = \mathbf{M}_0 + \sum_{r=1}^p \mu_r \mathbf{M}_r, \quad \mathbf{K} = \mathbf{K}_0 + \sum_{r=1}^q \kappa_r \mathbf{K}_r, \quad \mathbf{C} = \mathbf{C}_0 + \sum_{r=1}^s \chi_r \mathbf{C}_r$$

where μ_r, κ_r, χ_r are scalars determined to bring the calculated and measured eigenvalues, eigenvectors, and frequency response functions into least square agreement. Notice that the coupling pattern of the original structural model is preserved and that both the free vibration and forced vibration measurements are taken into account.

**Table 1. Modeled, Measured, and Identified
Natural Frequencies of the Grid Structure**

Mode No.	Modeled Value	Measured Value	Identified Value *	Identified Value **
1	.90 Hz	.92 Hz	.91 Hz	.92 Hz
2	2.34	2.32	2.32	2.32
3	4.85	4.93	4.93	4.93
4	6.05	6.38	6.38	6.38
5	7.78	7.27	7.26	7.27

*** - Element submatrices used**

**** - Modal submatrices used (coupling and sparsity may not be retained)**

CONCLUDING REMARKS

A Stereo Triangulation Approach has been developed for measuring vibratory structural deformation.

Measures many points simultaneously

Easy to calibrate

20 passive targets have been tracked @ 200HZ

Analog and digital processing is semi-automated

The Structural Identification Approach of Junkins and Creamer has been applied to match the natural frequencies, mode shapes and frequency response functions for a laboratory experiment.

The feasibility of the methodology has been established, main shortcoming is the moderate spatial resolution of the video cameras and edge detection methodology used.

REFERENCES

1. Manual of Photogrammetry (4th Edition), published by the American Society of Photogrammetry, Falls Church, VA(1980).
2. Junkins, J. L. Optimal Estimation of Dynamical Systems, Sijthoff-Noordhoff, Leyden, the Netherlands (1978).
3. Creamer, N. G., Identification of Flexible Structures., Ph. D. Dissertation, Engineering Mechanics, Virginia Tech, 1987.
4. Creamer, N. G., and J. L. Junkins, "An Identification Method for Flexible Structures", to appear, AIAA J. of Guidance , Control, and Dynamics, also presented at the AIAA/ASME/ASCE/AHS 28th Structures, Structural Dynamics, and Materials (SDM) Conference, Monterey, CA, April 6-8, 1987.
5. Deneman, E., Hasselman, T., Sun, C., Juang, J., Junkins, J., Udwadia, F., Venkayya, V., Kamat, M., "Identification of Large Space Structures on Orbit", Final report under Air Force Contract F04611-85-C-0092 with the American Society of Civil Engineering; Air Force Rocket Propulsion Laboratory Report No. AFRPL TR-86-054, 342 pp, August 1986.
6. White, C. W. and Maytum, B. D., "Eigensolution Sensitivity to Parametric Model Perturbations," Shock and Vibration Bulletin, Bulletin 46, Part 5, August 1976, pp123-133.
7. James, G. H., "An Optical Sensor System for Measuring Structural Dynamics with Applications to System Identification," final report under 1987 USAF-UES Summer Faculty/Graduate Student Research Program Contract No. F49620-85-C-0013, Texas A&M University, Department of Aerospace Engineering, August 28, 1987.
8. Das, A., Strange, W. T., Schlaegel, and Ward, J. M., "Experiment in Modeling and Parameter Estimation of Flexible Structures", Second NASA/DOD Control-Structure Iteration Conference, Colorado Springs, Co., November 17-19, 1987.
9. Paz, M., Structural Dynamics Theory and Computation, 2nd Ed., Van Nostrand Reinhold Co., New York, (1985).



GOVERNMENT AEROSPACE SYSTEMS DIVISION

Government Systems Sector

P-34
9/18/86
81-25

A Unified Process for Systems Identification based on Performance Assessment

C. Hyland and J. W. Shipley

(HARRIS CORPORATION)

Presented at the

**USAF/NASA WORKSHOP ON MODEL DETERMINATION FOR
LARGE SPACE SYSTEMS**

California Institute of Technology Pasadena, California
March 22-24, 1988

Many modern spacecraft are complex multi-body dynamic system where the bodies are connected by several active control systems for pointing and isolation. Mission requirements indicate that many structural modes and possibly some nonlinear effects will require characterization. Thus, even characterization at the subsystem level will become more difficult than usual. System level characterization difficulties will be compounded by the fact that only limited ground testing will be possible on the full up system and flight testing will be restricted by an extremely limited measurements set.

The object of the present discussion is the application of matrix majorant theory to the problem of assessing dynamic system performance when knowledge of the system is uncertain. We show how majorants provide an effective tool to relate required performance output to system identification test quality in terms of residual uncertainty in input-output relations, parameter values, nonlinearities and interactions.

The underlying machinery consists of the block-norm matrix which is a nonnegative matrix each of whose elements is the norm of a block of a suitably partitioned matrix. A matrix which bounds the block-norm matrix in the sense of nonnegative matrices, i.e., element by element is known as a majorant.

**A Unified Process for Systems Identification based on
Performance Assessment**

C. Hyland and J. W. Shipley

**Presented at the
USAF/NASA WORKSHOP ON MODEL DETERMINATION FOR
LARGE SPACE SYSTEMS**



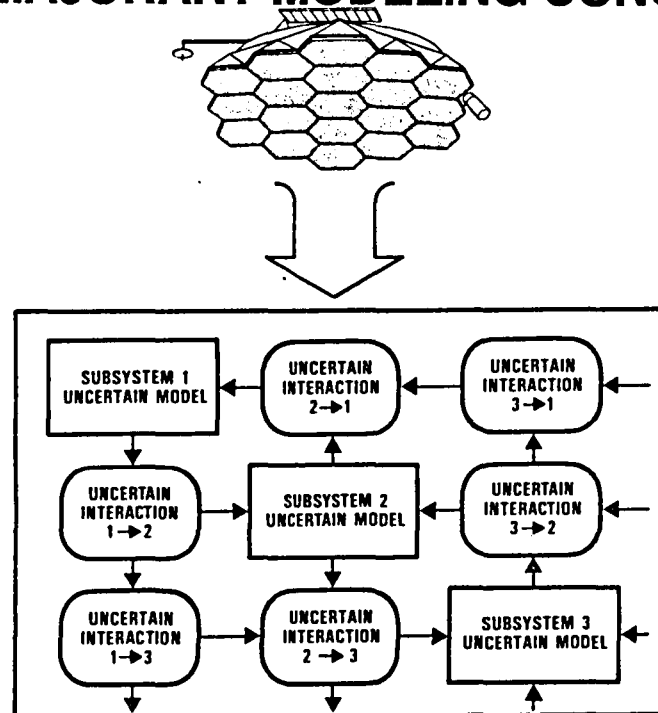
GOVERNMENT AEROSPACE SYSTEMS DIVISION

Government Systems Sector

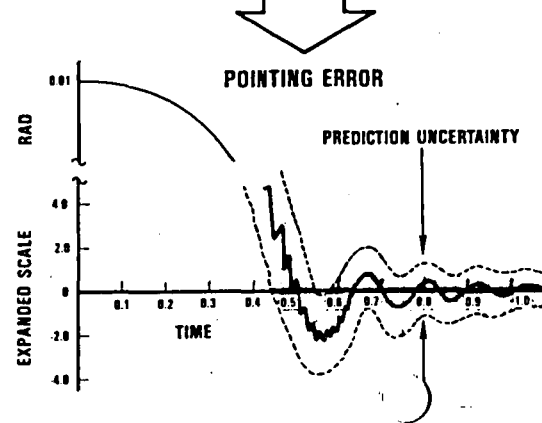
The system is broken up into subsystems which represent either physical boundaries within the system (e.g., joints in a multi-body dynamics model) or abstract partitions (e.g., modal regimes which are characterized by various levels of uncertainty for a linear state-space model). Bounds are developed for the uncertain interactions between subsystems and the uncertainties within a given subsystem.

ENG

MAJORANT MODELING CONCEPT



PERFORM MAJORANT ROBUSTNESS ANALYSIS



MAJORANT ANALYSIS - BASIC IDEA

PROBLEMS ADDRESSED:

- BOUND PERFORMANCE DEGRADATION DUE TO UNCERTAINTY
- BOUND PREDICTION ERROR DUE TO UNCERTAINTY

BASIC APPROACH:

- THINK OF THE SYSTEM AS KNOWN PIECES WITH UNCERTAIN INTERACTIONS
- MATRIX MAJORANT: A NONNEGATIVE MATRIX WHICH MEASURES THE "SIZE" OF A GIVEN MATRIX (GENERALIZATION OF SINGULAR VALUES)
- USE MAJORANT INEQUALITIES DEVELOPED BY DAHLQUIST [1]



GOVERNMENT AEROSPACE SYSTEMS DIVISION

Government Systems Sector

This paper is based on a number of key results which have been developed at Harris over the last several years. The idea of majorants was introduced by Ostrowski [2] and applied to stability analysis of integration algorithms for ODE's by Dahlquist in [1]. Work at Harris has resulted in majorant formulations for time domain, frequency domain and statistical response [3],[4] and [5].

576



GOVERNMENT AEROSPACE SYSTEMS DIVISION

Government Systems Sect.

This paper is based on a number of key results which have been developed at Harris over the last several years. The idea of majorants was introduced by Ostrowski [2] and applied to stability analysis of integration algorithms for ODE's by Dahlquist in [1]. Work at Harris has resulted in majorant formulations for time domain, frequency domain and statistical response [3],[4] and [5].

245

MAJORANT ANALYSIS - GENERAL RESULTS

- GIVES A SEQUENCE OF PROGRESSIVELY SHARPER BOUNDS (SINGULAR VALUE BOUNDS ARE THE CRUDEST SPECIAL CASE)
- EACH BOUND IN THE HIERARCHY IS EASY TO COMPUTE
- CAN BE APPLIED IN :
 1. GENERAL OPERATOR SETTING (BLURS DISTINCTION BETWEEN TIME AND FREQUENCY DOMAINS)
 2. FREQUENCY DOMAIN
 3. TIME DOMAIN
 4. STATISTICAL RESPONSE OF SYSTEM WITH RANDOM DISTURBANCES

The first majorant performance bound was developed for statistical response. In this case, when majorants are applied to a dynamical system, the model is written in the form shown below. The matrix A is block diagonal and is partitioned according to subsystem interfaces. The subsystem interactions represented by the matrix G are assumed to be uncertain. Computing the spectral norm of the individual blocks of G we generate a block-norm inequality (element-by-element) for the covariance of the system Q . Replacing the inequality by an equality we obtain the majorant Lyapunov equation. The solution may be interpreted as a majorant for the covariance.

References [3]-[5] describe the relationship between majorant analysis and robust stability. While robust stability is a requisite for our interest, it is not our primary interest and is not discussed further.

THE MAJORANT LYAPUNOV EQUATION

THE LSS MODEL INVOLVES KNOWN LOCAL DYNAMICS AND UNCERTAIN INTERACTIONS. THE DIMENSION (r) OF THE MATRIX LYAPUNOV EQUATION IS THE NUMBER OF SUBSYSTEMS IN WHICH THE SYSTEM IS PARTITIONED

$$\dot{x} = (A + G)x + w$$

$$J = E[x^T R x] = \text{tr } Q R$$

$$0 = (A + G)Q + Q(A + G)^T + V$$

$$H = \{Q(A_i \oplus A_j)\}$$

$$A = \begin{bmatrix} A_1 & 0 & \cdots \\ 0 & A_2 & \cdots \\ \vdots & \vdots & \ddots \end{bmatrix}$$

Known Subsystem Dynamics

$$G = \begin{bmatrix} 0 & G_{12} & \cdots \\ G_{21} & 0 & \cdots \\ \vdots & \vdots & \ddots \end{bmatrix}$$

Uncertain Subsystem Interactions

$$V = \begin{bmatrix} V_1 & V_{12} & \cdots \\ V_{21} & V_2 & \cdots \\ \vdots & \vdots & \ddots \end{bmatrix}$$

Noise Intensity

$$Q = \begin{bmatrix} Q_1 & Q_{12} & \cdots \\ Q_{21} & Q_2 & \cdots \\ \vdots & \vdots & \ddots \end{bmatrix}$$

State Covariance

$$V = \begin{bmatrix} \|v_1\|_F & \|v_{12}\|_F & \cdots \\ \|v_{21}\|_F & \|v_2\|_F & \cdots \\ \vdots & \vdots & \ddots \end{bmatrix}$$

$$Q = \begin{bmatrix} \|q_1\|_F & \|q_{12}\|_F & \cdots \\ \|q_{21}\|_F & \|q_2\|_F & \cdots \\ \vdots & \vdots & \ddots \end{bmatrix}$$

$$\begin{bmatrix} 0 & \bar{\sigma}(G_{12}) & \cdots \\ \bar{\sigma}(G_{21}) & 0 & \cdots \\ \vdots & \vdots & \ddots \end{bmatrix} \leq \leq G$$

$$A * Q \leq GQ + QG^T + V$$

FORMULATION OF A SIMPLE PROBLEM

CONSIDER A PAIR OF OSCILLATORS WHICH ARE COUPLED BY UNCERTAIN INTERACTIONS

PROBLEM PARAMETERS:

$$n=4, r=2, n_1=n_2=2$$

SYSTEM MATRIX:

$$\bar{A}_i = \begin{bmatrix} -\nu & \omega_i \\ -\omega_i & -\nu \end{bmatrix}, \quad i=1, 2$$

INPUT INTENSITY:

$$V = I_4 \text{ yields } \mathcal{V} = 2I_2.$$

SUBSYSTEM INTERACTION:

$$G = \begin{bmatrix} 0 & \gamma_{12} \\ \gamma_{21} & 0 \end{bmatrix}$$

$$\sigma_{\min}(\bar{A}_j \oplus \bar{A}_i) = [4\nu^2 + (\omega_j - \omega_i)^2]^{1/2}$$

$$Q = \begin{bmatrix} 2\nu & [4\nu^2 + (\omega_1 - \omega_2)^2]^{1/2} \\ [4\nu^2 + (\omega_1 - \omega_2)^2]^{1/2} & 2\nu \end{bmatrix}$$

$$\tilde{Q}_{(1,1)} = (2\nu^2\delta - \gamma_{12}\gamma_{21} + \gamma_{12}^2)/2\sqrt{2}\nu(\nu^2\delta - \gamma_{12}\gamma_{21}),$$

$$\tilde{Q}_{(1,2)} = (\gamma_{12} + \gamma_{21})/2\sqrt{2}(\nu^2\delta - \gamma_{12}\gamma_{21}),$$

$$\tilde{Q}_{(2,2)} = (2\nu^2\delta - \gamma_{12}\gamma_{21} + \gamma_{21}^2)/2\sqrt{2}\nu(\nu^2\delta - \gamma_{12}\gamma_{21})$$

$$\delta \triangleq [1 + \delta^2]^{1/2}, \quad \delta \triangleq (\omega_1 - \omega_2)/2\nu$$

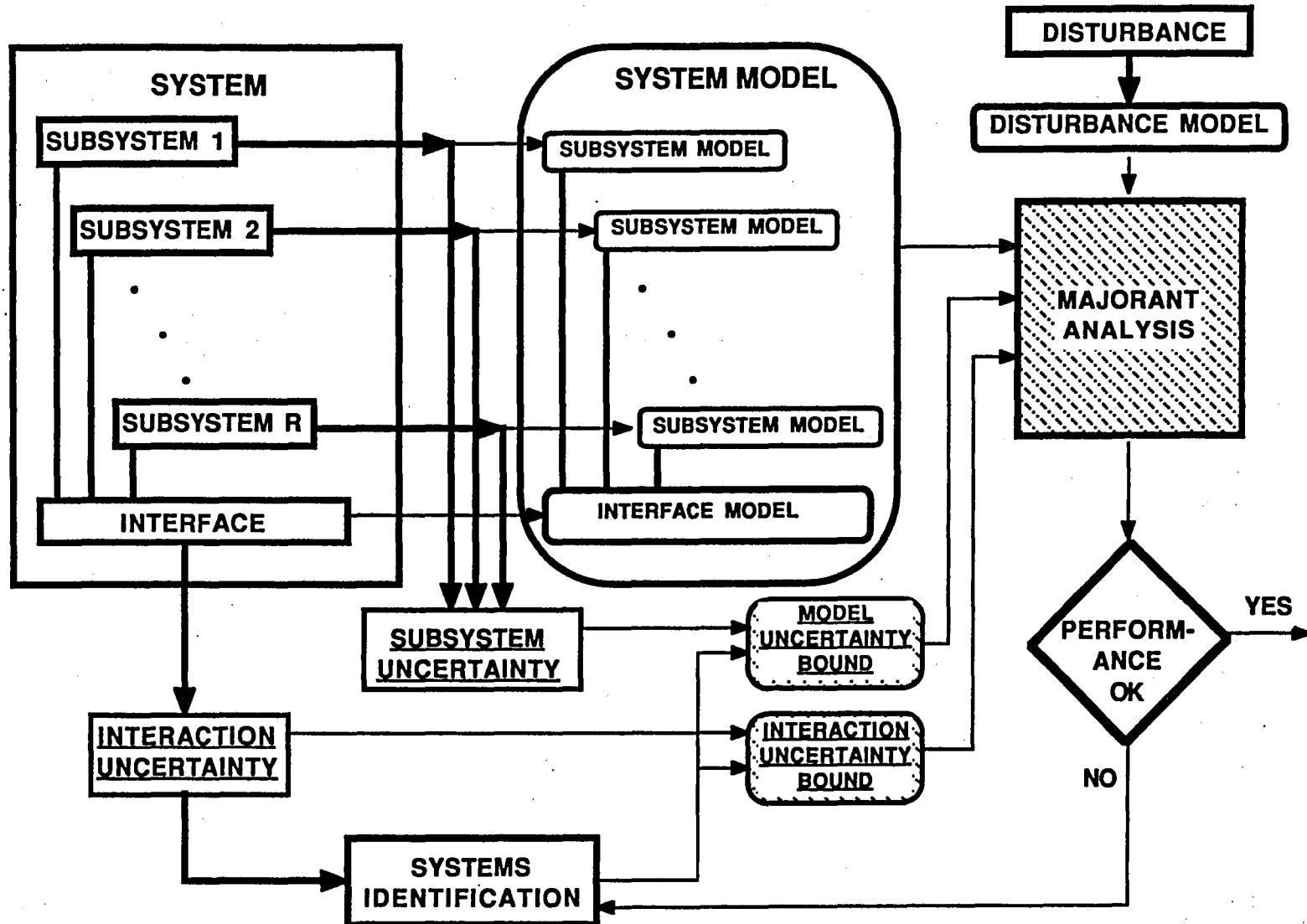


GOVERNMENT AEROSPACE SYSTEMS DIVISION

Government Systems Sector

The ideas discussed above fit logically into the test design data analysis as indicated in the enclosed diagram. Basically, majorant analysis is used to balance the requirements for the complementary test approaches and to define the overall test quality needs.

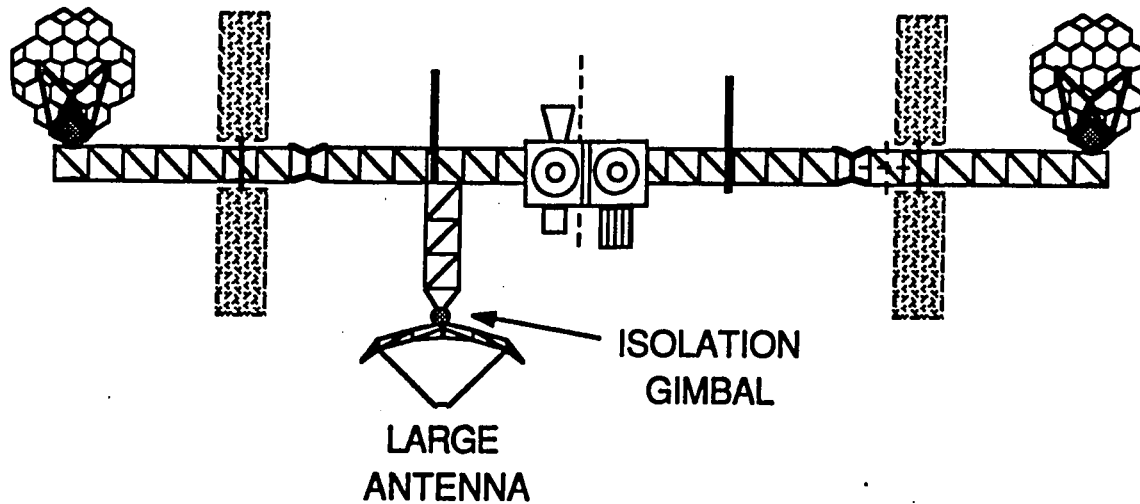
APPLICATION OF MAJORANT ANALYSIS IN SYSTEM ID PROCESS



The primary use of majorants is in the analysis of very large order systems. To illustrate the applications in test design, we formulate a problem which would involve both on-orbit systems identification and possible ground tests. Suppose we wish to qualify a large antenna system which would be used in a remote sensing experiment on the Space Station. We expect that at the time this application will be ready for flight some on orbit characterization of the Space Station is available which contains good information on the rigid body dynamics and the first few low frequency modes. We wish to define requirements for the system ID tests for the antenna system. We divided the system into three parts so that levels of uncertainty in the antenna elastic modes, the secondary modes of the Space Station, and the interactions between the three groups of modes can be varied separately.

SPACE STATION /ANTENNA INTERACTION EXAMPLE

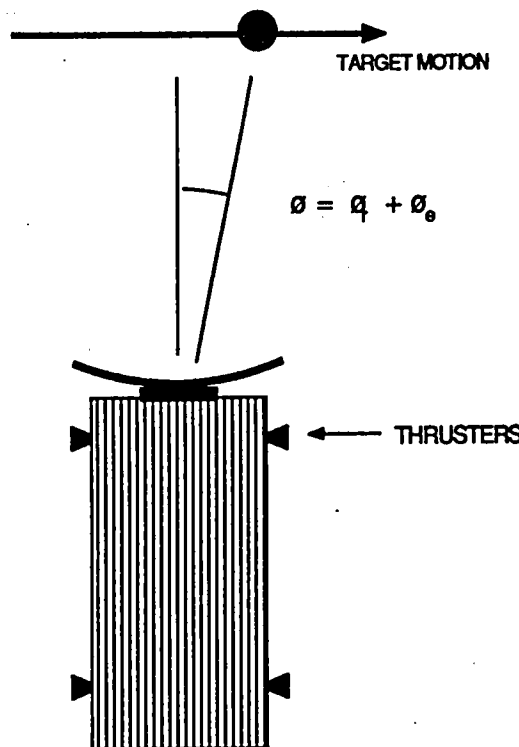
SPACE STATION



To illustrate application of time domain majorant analysis in systems ID consider a tracking problem where a flexible spacecraft with a rigidly mounted antenna must track a target through an encounter which takes 5.0 seconds and covers 180 degrees. In addition to the rigid body modes the spacecraft has elastic modes at 20.0 and 40.0 Hz. The objective is to determine the quality of the system identification testing necessary to support system certification for flight. Discrete time analysis is used in order to consider the effect of the controller sample rate.

TIME DOMAIN MAJORANT EXAMPLE SPACECRAFT TRACKING EXAMPLE

- ENCOUNTER DURATION : 5.0 SECONDS
- 180 DEGREES USING THRUSTERS.
- DYNAMIC MODEL: RIGID BODY MODES AND TWO ELASTIC MODES AT 20.0 AND 40.0 HZ
- CONTROLLER SAMPLE RATE: 50.0 HZ



TIME DOMAIN MAJORANT EXAMPLE SPACECRAFT TRACKING EXAMPLE (CONTINUED)

- **SYSTEM MODEL**
$$\begin{pmatrix} x_r \\ x_e \end{pmatrix}_{k+1} = \begin{bmatrix} A_r & 0 \\ 0 & A_e \end{bmatrix} \begin{pmatrix} x_r \\ x_e \end{pmatrix}_k + \begin{pmatrix} B_r \\ B_e \end{pmatrix} u_k$$

$$u_k = -[k_D, \quad k_V] \begin{pmatrix} \theta_T \\ \dot{\theta}_T \end{pmatrix}_k \quad (= -k \begin{pmatrix} \theta_T \\ \dot{\theta}_T \end{pmatrix}_k)$$

$$\begin{pmatrix} \theta_t \\ \dot{\theta}_T \end{pmatrix}_k = \begin{bmatrix} \tilde{C}_r & \tilde{C}_e \\ \tilde{\tilde{C}}_r & \tilde{\tilde{C}}_e \end{bmatrix} \begin{pmatrix} x_r \\ x_e \end{pmatrix}_k$$

$$\begin{pmatrix} x_r \\ x_e \end{pmatrix}_{k+1} = \begin{bmatrix} A_r - B_r K C_r & -B_r K C_e \\ -B_e K C_r & A_e - B_e K C_e \end{bmatrix} \begin{pmatrix} x_r \\ x_e \end{pmatrix}_k$$

$$\theta_r = [\tilde{C}_r, \quad \tilde{C}_e] \begin{pmatrix} x_r \\ x_e \end{pmatrix}_K$$

TIME DOMAIN MAJORANT EXAMPLE SPACECRAFT TRACKING EXAMPLE (CONTINUED)

- OBJECTIVE: DETERMINE THE QUALITY OF SYSTEMS ID TESTING NECESSARY TO SUPPORT THE SPACECRAFT DESIGNED
- TRANSFORM STATES SO THAT $A_r B_r K C_r$ IS DIAGONAL AND SEPARATE THE SYSTEM INTO ELASTIC AND THE RIGID BODY PARTS. THE MATRIX G CHARACTERIZES THE ELASTIC INTERACTION UNCERTAINTY; I.E., HOW WELL WE KNOW THE SYSTEM ELASTIC MODES.

$$\begin{pmatrix} \xi_r \\ x_e \end{pmatrix}_{k+1} = \begin{bmatrix} \Lambda_r & 0 \\ 0 & A_e - \{B_e K C_e\} \end{bmatrix} \begin{pmatrix} \xi_e \\ x_e \end{pmatrix}_k + G \begin{pmatrix} \xi_r \\ x_e \end{pmatrix}_k$$

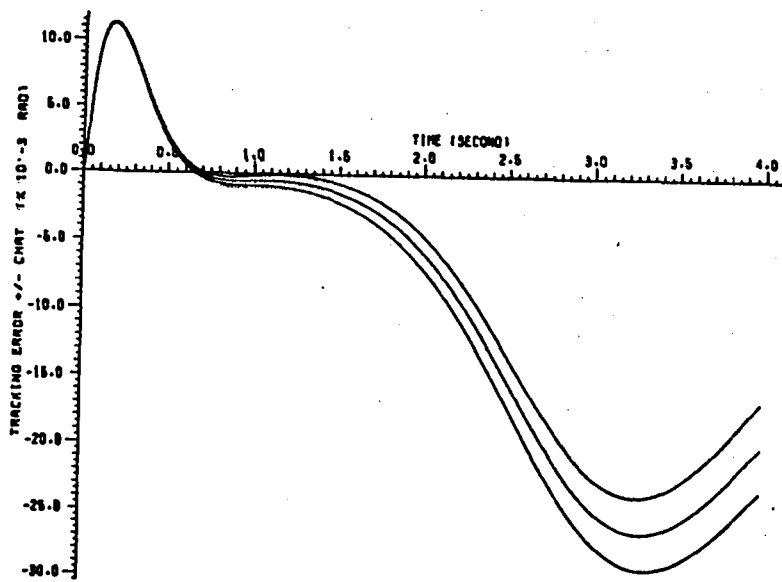
$$G = \begin{bmatrix} 0 & -B_r' K C_e \\ -B_e K C_r' & -\langle B_e K C_e \rangle \end{bmatrix}$$

$$\hat{G} = \begin{bmatrix} 0 & |B_r' \parallel K \parallel C_e| \\ |B_e \parallel K \parallel C_r'| & \langle |B_e \parallel K \parallel C_e| \rangle \end{bmatrix}, \quad \tilde{C}_e \equiv |\tilde{C}_e|$$

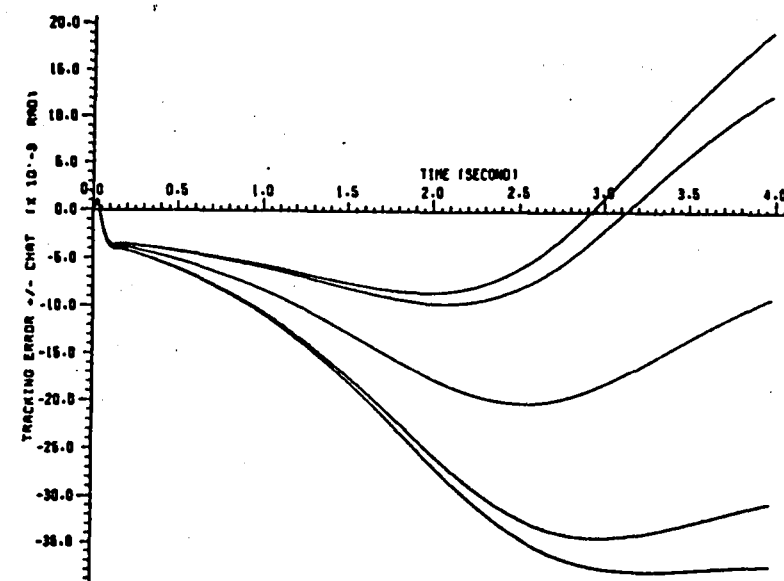
$$\theta_T = [\tilde{C}_r', \quad \tilde{C}_e] \begin{pmatrix} \xi_r \\ x_e \end{pmatrix}_k$$

The following plots show the nominal performance and various levels of off nominal performance. Case 1 and 2 show how increasing the controller bandwidth (from 1.0 Hz to 5.0 Hz reduces the nominal tracking error but increases the bound for a given amount of elastic mode uncertainty. Cases 2 through 4 show how decreasing the elastic mode uncertainty decreases the performance bounds. In going from case 2 to case 4 the uncertainty is reduced by an order of magnitude each time. To obtain 20 milli-radian performance would require a system ID test that reduces model uncertainty by an order of magnitude.

TIME DOMAIN MAJORANT EXAMPLE SPACECRAFT TRACKING EXAMPLE (CONTINUED)

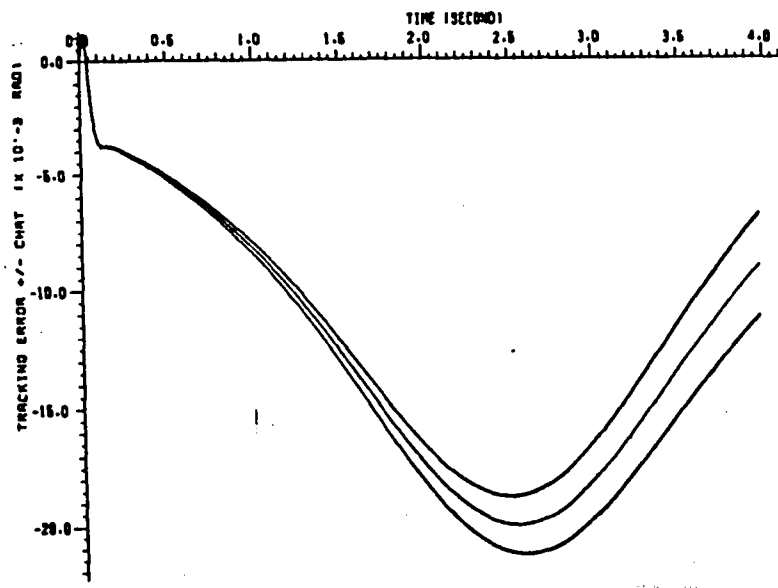


CASE 1: $f_c=1.0$ Hz, NOMINAL UNCERT.

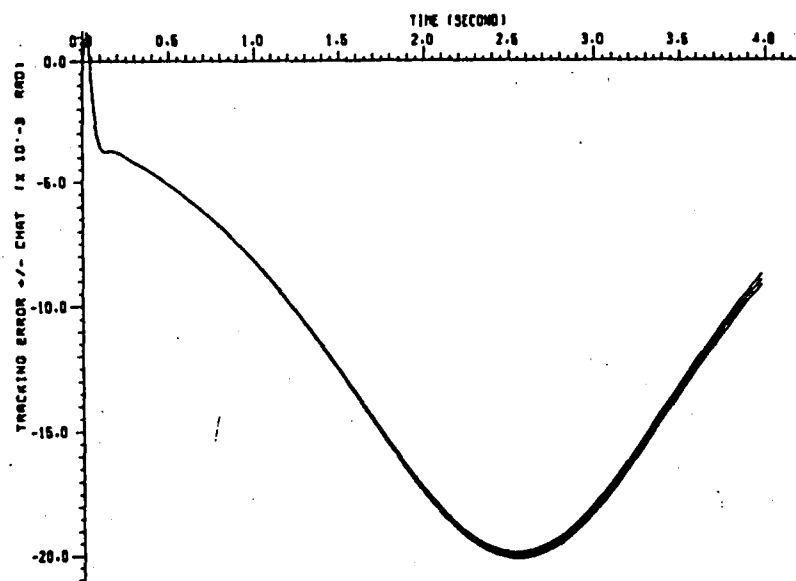


CASE 2: $f_c=5.0$ Hz, NOMINAL UNCERT.

TIME DOMAIN MAJORANT EXAMPLE SPACECRAFT TRACKING EXAMPLE (CONTINUED)



CASE 3: $f_c=5.0$ Hz, $0.1 \times$ UNCERT.



CASE 4: $f_c=5.0$ Hz, $0.01 \times$ UNCERT.

TIME DOMAIN MAJORANT

ACTUAL SYSTEM $\left\{ \begin{array}{l} x_{k+1} = Ax_k + Gx_k + \nu_k; \quad x_0 = 0 \\ A = \text{diag } \{A_k\}; \quad A_k \text{ stable} \\ G = \langle G \rangle; \quad |G| \leq \hat{G} \in \mathbb{R}_+^{n \times n} \end{array} \right.$

NOMINAL SYSTEM $\left\{ \bar{x}_{k+1} = A\bar{x}_k + \nu_k, \quad \bar{x}_0 = 0 \right.$

GIVEN THAT $|G| \leq \hat{G}$, WHAT IS THE WORST CASE BOUND ON $x_k - \bar{x}_k \equiv E_k$?

MORE SPECIFICALLY, FIND A NOT-TOO-CONSERVATIVE $\hat{E}(k) \in \mathbb{R}_+^n$ SUCH THAT:

$$|x_\ell(k) - \bar{x}_\ell(k)| \leq \hat{E}_\ell(k)$$

$$\forall G : |G| \leq \hat{G}$$

TIME DOMAIN MAJORANT

ZEROth ORDER BOUND: $\hat{E}(k)$

OBTAINED BY DIRECTLY MAJORIZING THE ERROR PROPORATION EQUATION

$$\hat{E}(k) = \sum_{\ell=0}^{k-1} \hat{G} [\hat{E}(\ell) + |\bar{x}(\ell)|]$$

HIGHER ORDER BOUND: $\hat{E}(k)$ (UPPER)

GIVEN

$$\hat{E}_n(k) = \sum_{\ell=0}^{k-1} \sum_{\substack{m=1 \\ r=1}}^n \hat{G}_{nm} |P_{nm}(k-\ell-1)| \hat{G}_{mr} \hat{E}_r(\ell)$$

$$+ \sum_{r=1}^n \hat{G}_{nr} \hat{F}(k-1) + \sum_{\substack{m=1 \\ r=1}}^n \hat{G}_{nm} \hat{G}_{mr} \hat{g}_{nmr}(k-1)$$

WHERE

$$P_{nm}(\ell) \triangleq \begin{cases} \frac{A_n^\ell - A_m^\ell}{A_n - A_m} & n \neq m \\ \ell A_n^{\ell-1} & n = m \end{cases}$$

REFERENCES

1. G. Dahlquist, "On Matrix Majorants and Minorants with Applications to Differential Equations," *Lin. Alg. Appl.*, Vol. 52/53, pp. 199-216, 1983.
2. A. M. Ostrowski, "On Some Metrical Properties of Operator Matrices and Matrices Partitioned Into Blocks," *J. Math Anal. Appl.*, Vol. 2, pp. 161-209, 1961.
3. D. C. Hyland and D. S. Bernstein, "The Majorant Lyapunov Equation: A Nonnegative Matrix Equation for Robust Stability and Performance of Large Scale Systems," *IEEE Trans. Autom. Control*, Vol. AC-32, pp. 1005-1013, 1987.
4. E. G. Collins, Jr. and D. C. Hyland, "Improved Robust Performance Bounds in Covariance Majorant Analysis," submitted for publications.
5. D. C. Hyland and E. G. Collins, Jr, "An M-Matrix and Majorant Approach to Robust Stability and Performance Analysis for Systems with Structured Uncertainty," submitted for publication.

SP-18361
JAN 5 1981
oe-8

ON-ORBIT SYSTEM IDENTIFICATION OVERVIEW

EDWARD METTLER

29222-36N
USAF/NASA WORKSHOP ON MODEL
DETERMINATION FOR LARGE
SPACE SYSTEMS

JET PROPULSION LABORATORY
CALIFORNIA INSTITUTE OF TECHNOLOGY

MARCH 23, 1988

SYSTEM IDENTIFICATION FOR SPACECRAFT CONTROL

OVERVIEW

- PARAMETER IDENTIFICATION AND MODELING ARE KEY ELEMENTS OF A DESIGN AND OPERATIONAL FLIGHT STRATEGY FOR CONTROL OF FLEXIBLE SPACE STRUCTURES
- EMPHASIS OF IDENTIFICATION PROGRAM IS ON-ORBIT APPLICATIONS TO SPACECRAFT CONTROL
- HIGH PERFORMANCE ROBUST CONTROLLERS FROM ADVANCED DESIGN SYNTHESIS TECHNIQUES AND ON-ORBIT IDENTIFICATION/SYSTEM TUNING
- AUTONOMOUS PERFORMANCE MAINTENANCE FUNCTIONS ENABLED UTILIZING IDENTIFICATION INFORMATION
- NEAR TERM GOALS FOR THE PROGRAM INCLUDE DEVELOPMENT OF:
 - AN INTEGRATED ON-LINE PROCESSING CAPABILITY FOR FLEXIBLE BODY PARAMETER IDENTIFICATION
 - VALIDATION WITH PHYSICAL STRUCTURE EXPERIMENTS

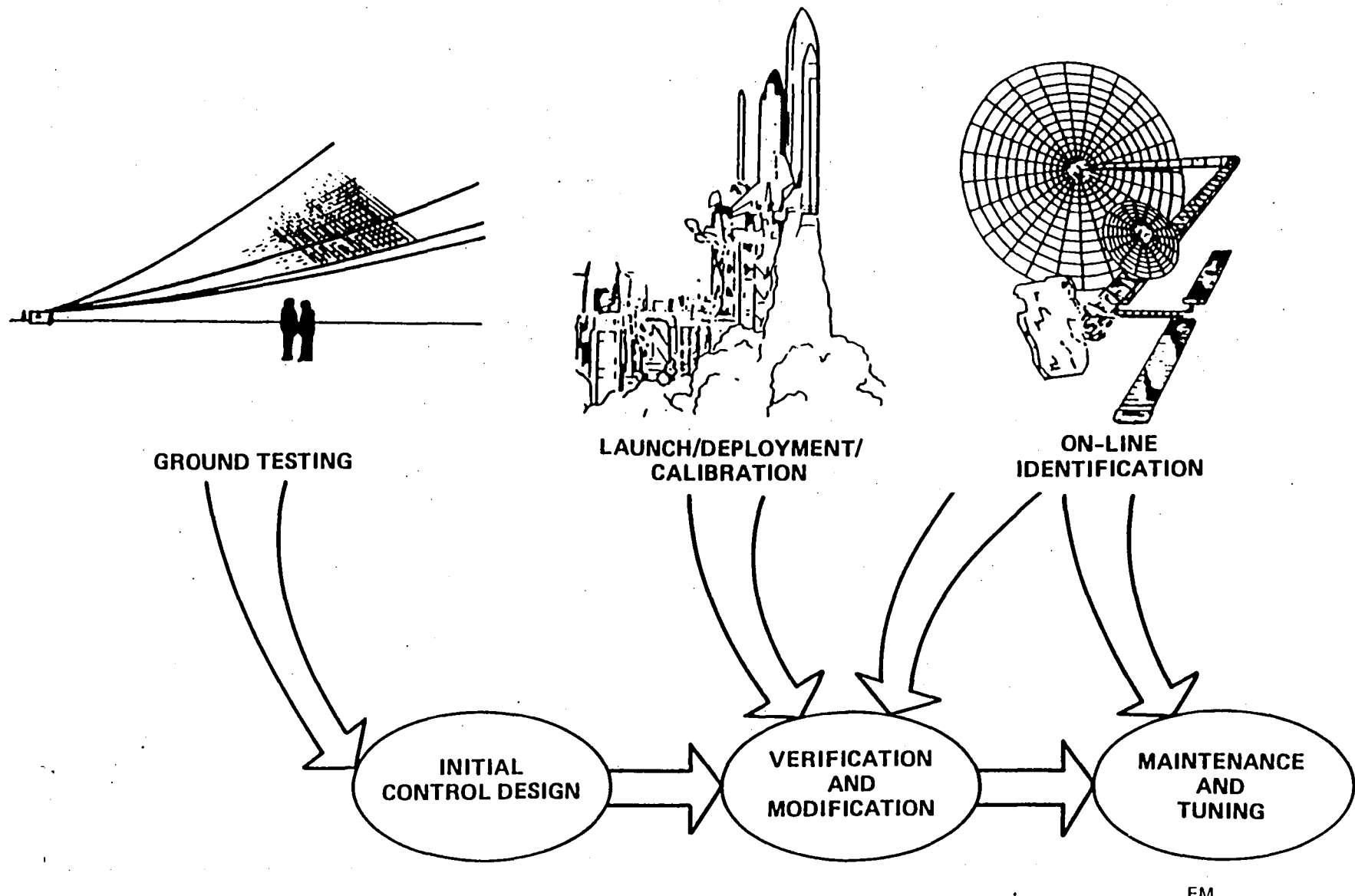
ON-ORBIT IDENTIFICATION FOR SPACECRAFT CONTROL

In recent years considerable effort has been made to find solutions to dynamics and control problems presented by large space structures (LSS). In the past and present generations of spacecraft, the control systems designers specified structural response constraints so that the control system and structure dynamics did not interact to degrade performance or destabilize the vehicle. With the future LSS concepts, this straight-forward avoidance solution is no longer an option. Examples of LSS characteristics that affect the control systems are low frequency fundamental modes that are densely packed and strongly coupled, joint dominated space assembled/deployed structures, low structural damping, and significant uncertainties in the dynamic models.

In general, the order of the LSS dynamics will be too large to design an effective wideband control system. New methods are required to control the low frequency modes without exciting the higher frequency dynamics inherent in the structure, and to constrain the control gains from spill-over into the higher modes causing instabilities or performance loss. This area is a major thrust in the extension of modern control theory and the cross-discipline technology of active structural control covers a wide range of interrelated design and system issues.

An on-orbit identification function would provide the near real-time knowledge of modal parameters, transfer functions, disturbances, surface distortions, and static mass and stiffness properties. This information would then be available for updating the controller plant model, and could serve as the data base from which an autonomous control function makes adjustments to tune the system performance and stability margins.

SYSTEM IDENTIFICATION FOR SPACECRAFT CONTROL



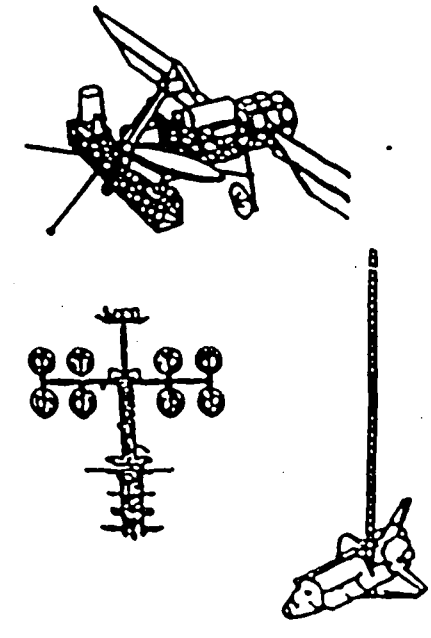
ON-ORBIT IDENTIFICATION MOTIVATIONS

Control performance of spacecraft with extended structures and on-orbit assembly/deployment operations, such as manned and unmanned space platforms and large antennas, will be very sensitive to inevitable uncertainties in predicted dynamics. Past experience indicates that in-flight instabilities may occur because of deficiencies in the pre-flight dynamical model embedded in the on-board control system design. In recognition of this need, the activity at JPL seeks to develop the technology to a level of readiness to support advanced spacecraft control subsystem designs and autonomous tuning of plant models and controller performance.

MOTIVATIONS FOR ON-ORBIT IDENTIFICATION TECHNOLOGY

CONTROL STRUCTURE INTERACTION:

SPACE STRUCTURES ASSEMBLED, DEPLOYED, RECONFIGURED ON ORBIT
EXTENDED CONNECTED BODIES WITH MODES DOWN TO 0.1 Hz
OPERATIONS PRODUCE COMPLEX DISTURBANCES WITHIN CONTROL BANDWIDTH
LARGE FLEXIBLE ATTACHED PAYLOADS WITH STRINGENT STABILITY REQ.



ADVANCED CONTROL SYSTEMS NEED:

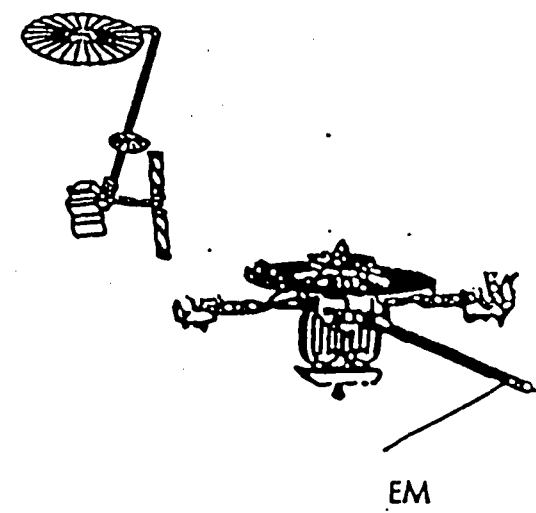
CORRECT FLEXBODY EMBEDDED MODELS
ON-ORBIT TUNING FOR STABILITY AND PERFORMANCE
TO PROVIDE PRECISE PHASE STABILIZATION OF IN-BAND MODES

HOWEVER:

NO ENVIRONMENTALLY VALID DYNAMIC GROUND TESTING OF COMPLETE SYSTEM IS POSSIBLE
RELIABLE STRUCTURE CONTROL REQUIRES DATA IN ACTUAL FLIGHT OPERATIONS

ON-ORBIT IDENTIFICATION WILL SUPPORT:

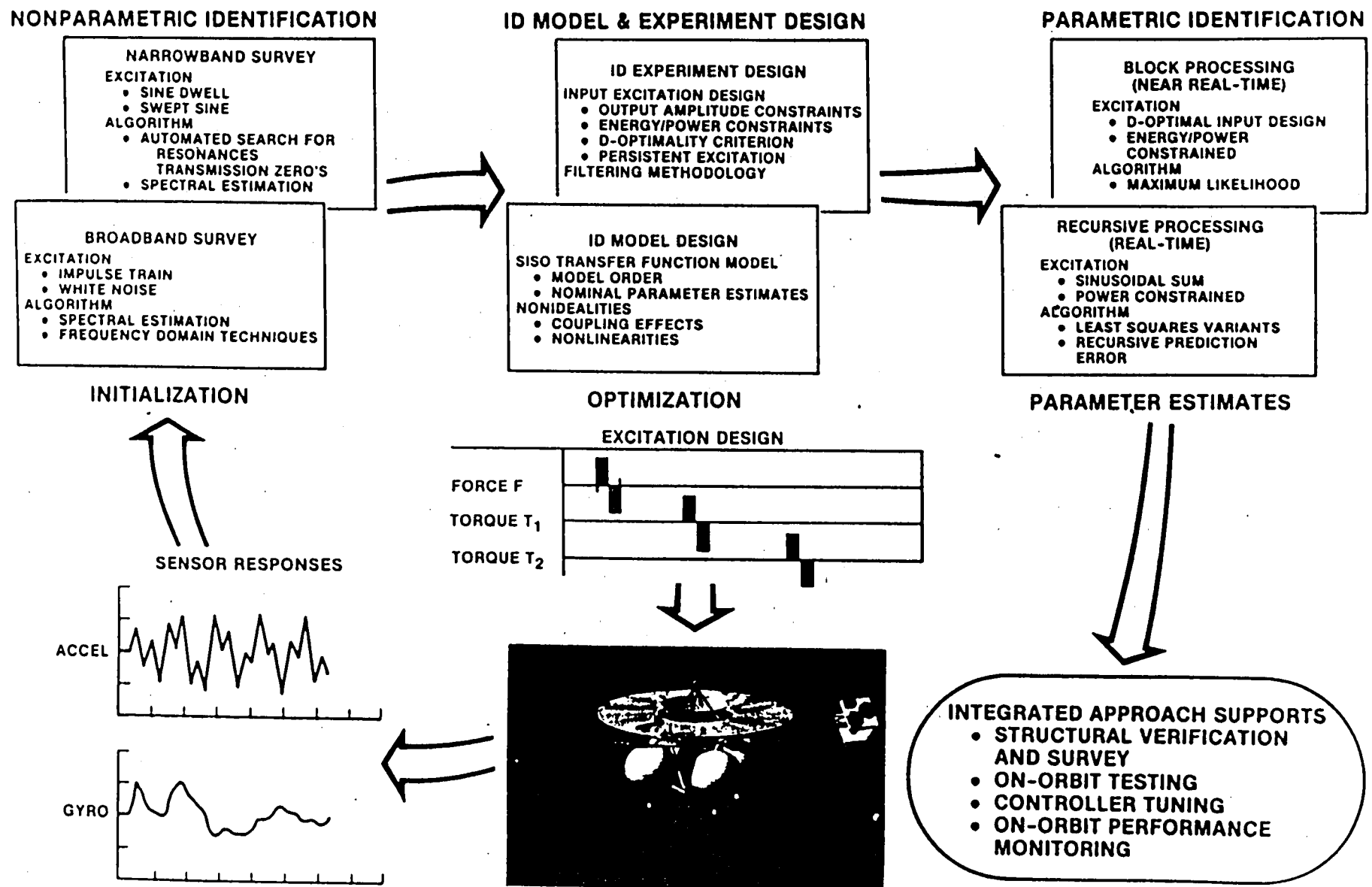
BUILD-UP VALIDATION OF SPACE STRUCTURES
CONTROL STABILIZATION DURING SPACE ASSEMBLY OPERATIONS
MONITORING OF REAL-TIME CONTROL SYSTEM PERFORMANCE
ON-LINE TUNING OF CONTROLLER STABILITY AND PERFORMANCE
AUTOMATING CONTROL SYSTEMS OPERATION
REDUCTION OF GROUND OPERATIONS COST



SYSTEM IDENTIFICATION APPROACH

The objective of this research is to develop a system of methods, algorithms and software for the on-orbit identification of control/structure interaction parameters and dynamical system characterization for large space platforms and payloads. Specific development approach includes integration of non-parametric frequency domain and parametric time domain techniques and algorithms, methods for optimization of sensing and excitation, progressive model refinement, and initialization of both recursive and data block algorithms.

INTEGRATED SYSTEM IDENTIFICATION APPROACH



MULTISTAGE IDENTIFICATION PROCESS

The problem of on-orbit identification differs significantly from the problem of identification performed on the ground. In particular, the actuators and sensors are severely restricted in number, type and placement; the time allocated for experimentation is relatively short, and the data which is required must often be processed quickly for use in controller tuning. These requirements are quite challenging and require a significant advance over techniques presently used for ground structural testing. An integrated systems approach emphasizing on-line processing is being developed through our research and development efforts.

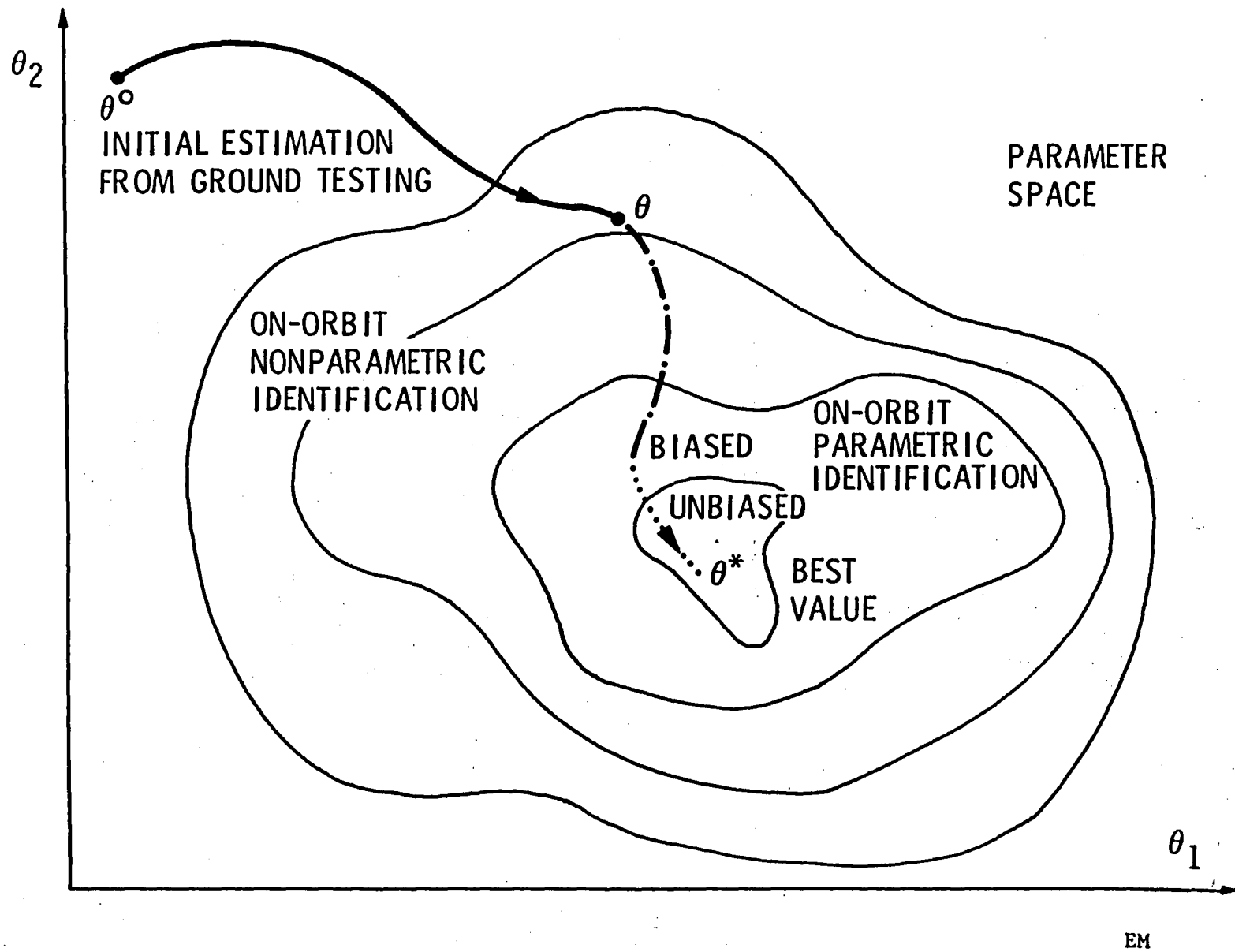
This methodology involves a multi-stage sequence of identification techniques that incrementally improves parameter identification fidelity while maintaining robustness, as each step serves to initialize the method that follows.

This convergence process (see Figure) begins with nonparametric survey-type methods and progresses to recursive parametric identification and non-recursive or data-block parametric methods, supported by experiment design (sensing and excitation) optimization and model refinement, which become increasingly effective as the sequence evolves.

Development of this end-to-end integrated methodology is taking place with a focus on physical experimentation using the JPL ground antenna test facility. Experiment design, algorithm development, software design, and computer simulation activities are ongoing for these identification technologies.

JPL

MULTISTAGE IDENTIFICATION PROCESS



DYNAMIC IDENTIFICATION LABORATORY EXPERIMENTS

The physical characteristics of the JPL ground test facility impose restrictions similar to the operational constraints encountered in on-orbit applications. Hence, the facility offers a unique opportunity to investigate identification methods applicable to the on-orbit testing environment. This methodology involves a multi-stage process or sequence of identification techniques that incrementally improves parameter identification fidelity while maintaining robustness, as each step serves to initialize the method that follows.

Dynamic identification experiments to be performed on the ground facility are being designed to apply the above approach. Emphasis will be toward on-line processing, with the initial experiments focusing on non-parametric identification methods. Presently, the following techniques have been developed and integrated in the first experiment which will operate as a menu-driven automated process with the investigator in an interactive/executive role:

- Wideband Excitation
- Narrowband Excitation
- Digital Filter Design for Stochastic Narrowband Excitation
- Sine-Dwell
- Resonance Tuning
- Spectral Estimation
- Product Moment Matrix/Model Order Determination
- Transfer Function Curve Fit
- Output Error Analysis

RECURSIVE PARAMETRIC IDENTIFICATION EXPERIMENTS

The recursive identification objective is to process data on-line and to generate estimates of SISO transfer function (TF) coefficients in real-time. A priori estimates of TF coefficients and model order are used, as determined from nonparametric methods derived earlier, and power constrained input excitation is determined from the experiment design procedure.

The recursive identification algorithm options include recursive least squares, and recursive maximum likelihood. Each algorithm has variants to be considered during the development stage involving the appropriate choice of data windowing, covariance update, regressor filtering, output error versus equation error tradeoffs, convergence conditions, and bias elimination techniques.

The final algorithm will be coded with emphasis on efficient implementation, speed, and numerically robust performance. The operational sequence will be to 1) initialize parameter estimates, model order, algorithm design parameters and experiment design parameters, 2) run the recursive subroutine which simultaneously controls the actuators, processes measurements and generates parameter estimates on the monitor in real-time. Measurements are processed as they are taken, and hence, no storage of sensor data is required.

MAXIMUM LIKELIHOOD PARAMETRIC IDENTIFICATION EXPERIMENT

Maximum Likelihood Estimation (MLE) is a nonlinear optimization technique that is used as the primary means of block processing of the experimental data. With a continuous time state space model, the time domain MLE algorithm finds the unknown parameter vector by minimizing the likelihood function constructed from the associated prediction errors. The initial values for the model will be determined by the model development stage, and the system response to different actuation signals will be processed in blocks of data as a near real-time analysis function.

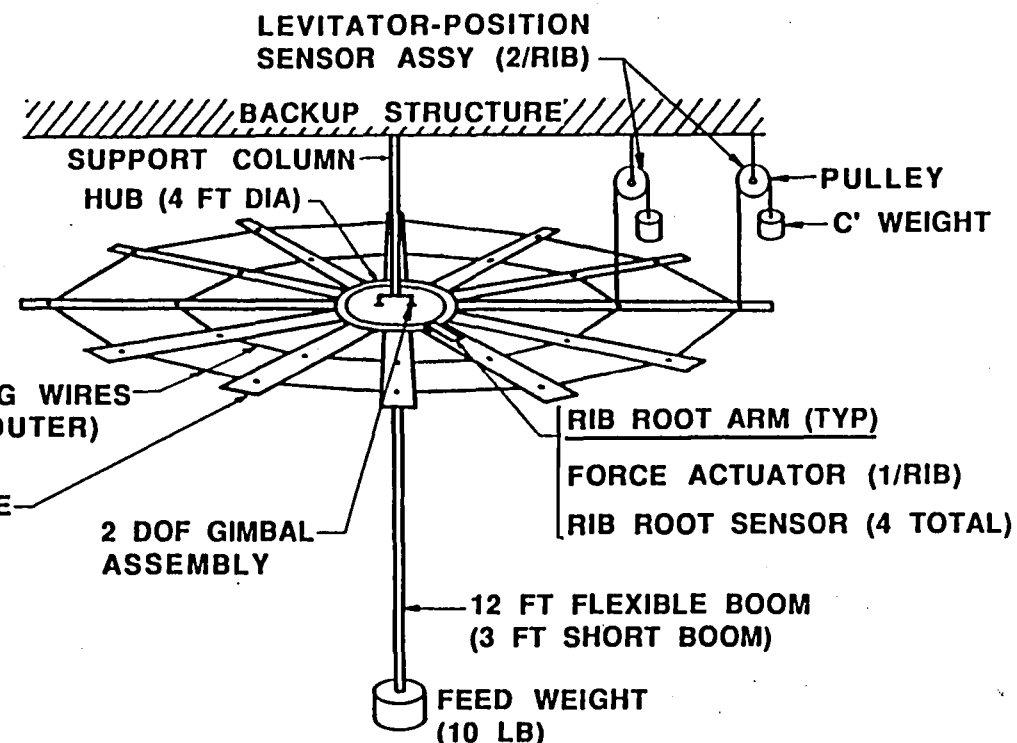
DYNAMIC IDENTIFICATION LABORATORY EXPERIMENTS

- OVERALL OBJECTIVES

- INTEGRATED IDENTIFICATION METHODOLOGY
- REAL-TIME PARAMETER ESTIMATION
- ON-LINE CONTROL-TUNING

- NEAR-TERM OBJECTIVES

- NONPARAMETRIC IDENTIFICATION AND MODEL BUILDING
 - MODEL ORDER ESTIMATION
 - ARX PARAMETERS L.S. FIT TO $G(j\omega)$ ESTIMATE
 - OUTPUT ERROR SPECTRUM AND BOUNDS
- ID OF 20-30 ARMAX PARAMETERS IN REAL-TIME
 - RECURSIVE LEAST SQUARES VARIANTS
 - RECURSIVE PREDICTION ERROR METHODS
- ID OF ~20 STATE-SPACE PARAMETERS IN NEAR REAL-TIME
 - BLOCK PROCESSING MLE



EXPERIMENT STRUCTURE

NONPARAMETRIC IDENTIFICATION (ID)

Nonparametric ID is directed at identifying key transfer function characteristics of structures in support of control related objectives and as an initialization hand-off to parametric identification.

Nonparametric ID utilizes spectral estimation techniques in concert with broadband and narrowband excitation experiments. These identification procedures provide an initial assessment of the structure, and the data needed to perform model design and parametric ID experiment design.

Broadband Excitation

The first identification process consists of a broadband excitation of the structure with the objective of extracting preliminary information about the plant's pole and zero locations. Admissible input signals may be either stochastic or deterministic and must be sufficiently rich to excite the full range of structural modes. Excitation of the structure in this form will yield spectral estimates indicating frequency windows within which the plant's poles and zeros to lie. Spectral estimation techniques based on auto and cross correlation of input and output data will be used in the data processing.

Narrowband Excitation

Once the broadband excitation techniques have identified windows in which the poles and zeros lie, narrowband methods will be used to yield a better resolution of these locations. The narrowband method will also furnish a model order of the system, a baseline transfer function, and a range of input frequencies and amplitudes in which the structure behaves linearly.

NONPARAMETRIC ID SIGNAL PROCESSING

Spectral Estimation (SE) produces correlation functions and spectral estimates for determining the plant phase and amplitude characteristics. The outputs of the SE techniques are the correlation functions R_{uu} , R_{yy} , R_{uy} , the spectral estimates P_{uu} , P_{yy} , P_{uy} , and the transfer function estimate $G_{se}(jw) = P_{uu}^{-1}P_{uy}$. These quantities are used as inputs to the PMM and TFCF algorithms described below.

Product Moment Matrix (PMM) provides an estimate of the plant order in a given frequency band by using a determinant ratio test on the product moment matrix. The product moment matrix is constructed from the correlation functions R_{uu} , R_{yy} and R_{uy} generated from the SE task described above. The model order estimated in this manner is used for initializing the TFCF algorithm described below, as well as for general model building purposes.

Transfer Function Curve Fit (TFCF) fits ARMA parameters in a least squares sense to the frequency response data. The frequency response data used for the fit is of two types:

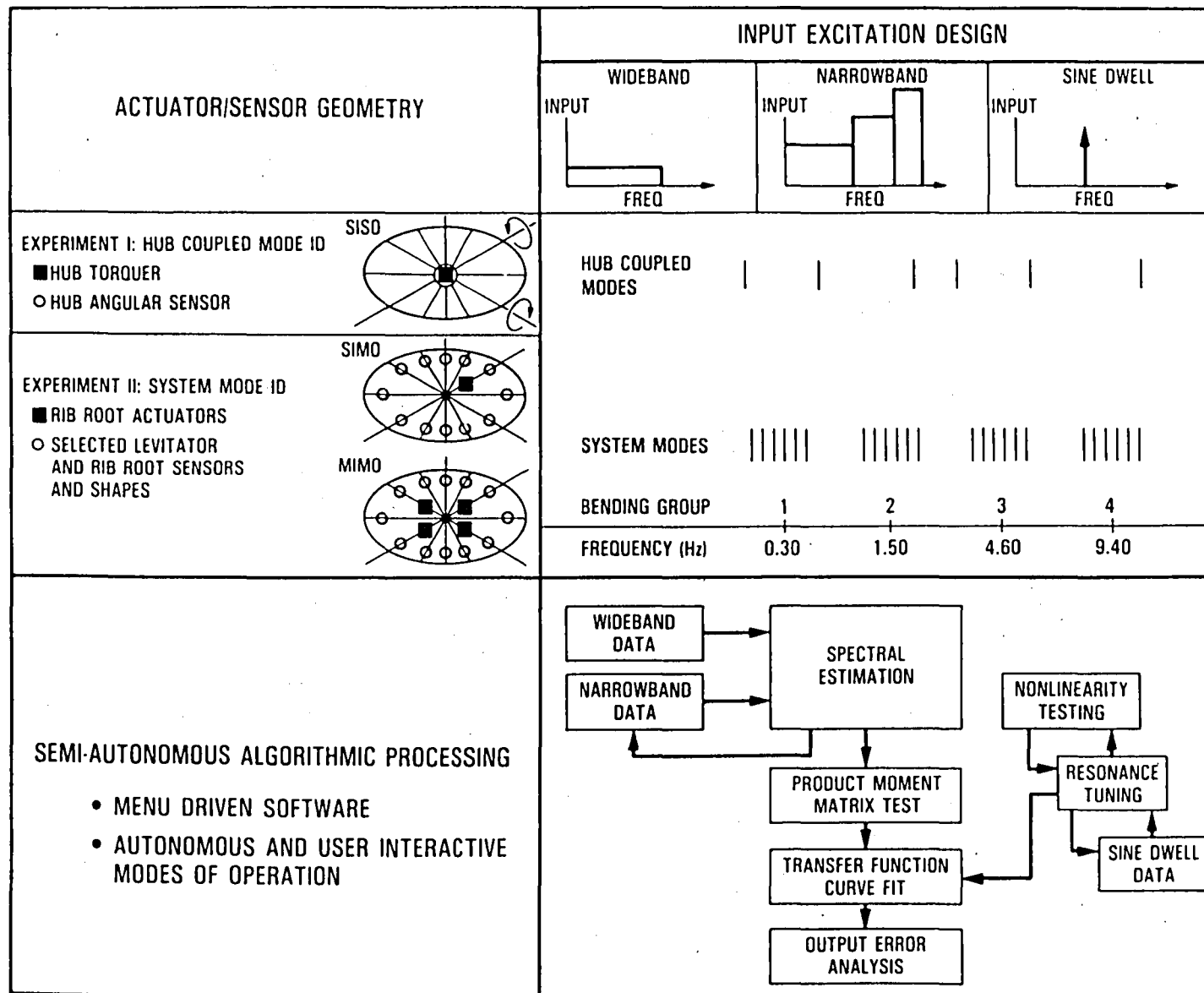
1. SE generated transfer function estimate $G_{se}(jw_i) = P_{uu}^{-1}P_{uy}(jw_i)$ at selected frequencies w_i $i=1, \dots, m$
2. Sine-Dwell data $G(jw_i)$ at frequencies w_i $i=1, \dots, n$

In general, the number of frequencies m in (1) will be larger than n in (2). However, the data from (2) will be more reliable than from (1). The TFCF algorithm is designed to handle either type of data, or incorporate both in a statistically weighted fashion. The model order used for the fit is based on the PMM test above.

Output Error Spectrum & Bounds

This technique characterizes the unstructured additive uncertainty $(D(jw) = G(jw) - G_f(jw))$ where $G_f(jw)$ is the curve fitted estimate of the true plant $G(jw)$. This is done by first forming the difference $e = (G(jw) - G_f(jw)) * u$ between the empirical data $y = G(jw) * u$ and the artificially generated data $y_f = G_f(jw) * u$ for a typical wideband excitation u , and then forming the output error transfer function estimate $D_f(jw) = P_{uu}^{-1}P_{eu}$. The quantity $D_f(jw)$ is then an estimate of $D(jw)$. This effort quantifies the accuracy of $G_f(jw)$ and provides information on the unstructured additive uncertainty required for robust control design efforts.

INTEGRATED NONPARAMETRIC ID EXPERIMENTS



ISSUES FOR FUTURE RESEARCH

The subjects outlined in the opposite page serve to highlight the wide range of the application issues that are important in the development of an on-orbit identification capability. As discussed earlier in this paper, the in-situ constraints of an operational system require an integrative approach to developing, embedding and utilizing identification technology.

A key facet of this approach is the role played by identification in directly enabling advanced control methodologies to become practical and reliable in an overall strategy of control systems on-orbit adaptation and self-tuning. The development of techniques for parameterization of both structured and unstructured uncertainty for robust control; recursive identification with and without persistent excitation for indirect adaptive control; and concurrent algorithms to support multi-input, multi-output identification and multi-variable control are prime examples of these advanced technologies.

These methods will in turn, be basic to the automation of future space systems that must deal with a wide range of mission uncertainty and time-critical operations that are also performance driven.

ON-ORBIT SYSTEM IDENTIFICATION ISSUES FOR FUTURE RESEARCH

- OPERATIONAL TIME DEMANDS

- SPECTRAL ESTIMATION TIME REQUIRED TO FULLY DEVELOP BROADBAND OR NARROWBAND INPUT SPECTRUM, AND DATA WINDOW SIZE NEEDED FOR SUFFICIENT STATISTICS
- SINE-DWELL WITH BINARY SEARCH FOR RESONANCE TUNING IS TIME CONSUMING
- INVESTIGATE USE OF SINE-SWEEP WITH FREQUENCY-LOCKED-LOOP AROUND PLANT FOR RESONANCE TUNING, AND FOR RECURSIVE REAL-TIME IDENTIFICATION
- TAILOR IDENTIFICATION STRATEGIES TO MISSION AND CONTROL SYSTEM OPERATIONS

- MODE SHAPE IDENTIFICATION

- USE OF SINE-SWEEP VS SPATIAL WHITE NOISE FOR TUNING MODE SHAPES AND SUPPORTING MULTI-VARIABLE CONTROL PARAMETERIZATION
- DESIGN OF DISTRIBUTED SENSING SYSTEM

ON-ORBIT SYSTEM IDENTIFICATION ISSUES FOR FUTURE RESEARCH (Cont'd)

- HIGHLY ROBUST PARAMETRIC IDENTIFICATION
 - INPUT DESIGN SENSITIVITY, PARTICULARLY AT HIGHER FREQUENCIES
 - METHODS FOR RESOLUTION OF MULTIPLE LOCAL MAXIMA WITH MLE
- COMPUTATIONAL DEMANDS
 - CONCURRENT ARCHITECTURES OF MACHINES AND ALGORITHMS TO SUPPORT SIMO AND MIMO IDENTIFICATION, AND MULTI-VARIABLE CONTROL
 - CONCURRENT METHODOLOGIES FOR ROBUST MLE
- INTEGRATED IDENTIFICATION AND CONTROL ARCHITECTURES
 - DEVELOP CLOSED LOOP IDENTIFICATION METHODOLOGIES
 - DESIGN OF DISTRIBUTED ACTUATION FOR LOCAL IDENTIFICATION AND CONTROL
 - UNCERTAINTY PARAMETERIZATIONS FOR ROBUST CONTROL
 - ROBUST RECURSIVE IDENTIFICATION FOR INDIRECT ADAPTIVE CONTROL

163818
8/1-85

616

OPTIMAL EXPERIMENT DESIGN FOR ON-ORBIT IDENTIFICATION

David S. Bayard

89222-36N
USAF/NASA WORKSHOP ON MODEL
DETERMINATION FOR LARGE SPACE SYSTEMS



Jet Propulsion Laboratory
California Institute of Technology
March 23, 1988

An optimal on-orbit experiment is designed to extract the most information from an on-orbit test, subject to the constraints of the testing environment. However, simply jumping in and optimizing standard measures of information with respect to the experiment design can cause severe problems if attention is not paid to the specific needs and properties of the problem at hand. The actual criteria to be optimized depends on (among other things), the particular ID algorithm and parametrization being used.

OPTIMAL EXPERIMENT DESIGN FOR ON-ORBIT IDENTIFICATION

- MAXIMALLY INFORMATIVE EXPERIMENTS WITH RESPECT TO
ON-ORBIT CONSTRAINTS
 - SENSOR TYPE AND PLACEMENT
 - ACTUATOR TYPE AND PLACEMENT
 - INPUT EXCITATION DESIGN
 - SAMPLING PERIOD T
 - HORIZON LENGTH
- OTHER IMPORTANT ISSUES
 - CHOICE OF PARAMETRIZATION
 - ID ALGORITHM
 - MODEL SET AND STRUCTURE
 - BLOCK DATA VS. RECURSIVE PROCESSING
 - ETC.

In order to best support control related objectives, two parametric techniques will be the focus of this discussion: RPEM and MLE. The RPEM and MLE algorithms outlined below, produce parametric models which characterize the dynamics between actuator and sensor outputs of interest and over a bandwidth of interest. It is emphasized that these models directly support the multivariable control design objectives while requiring a minimal amount of information to be identified on-orbit. On the other hand, the RPEM and MLE techniques are complementary in their relative advantages and disadvantages. These properties are contrasted below. The two techniques have different requirements as far as the experiment design is concerned.

PARAMETRIC ID USING COMPLEMENTARY TECHNIQUES

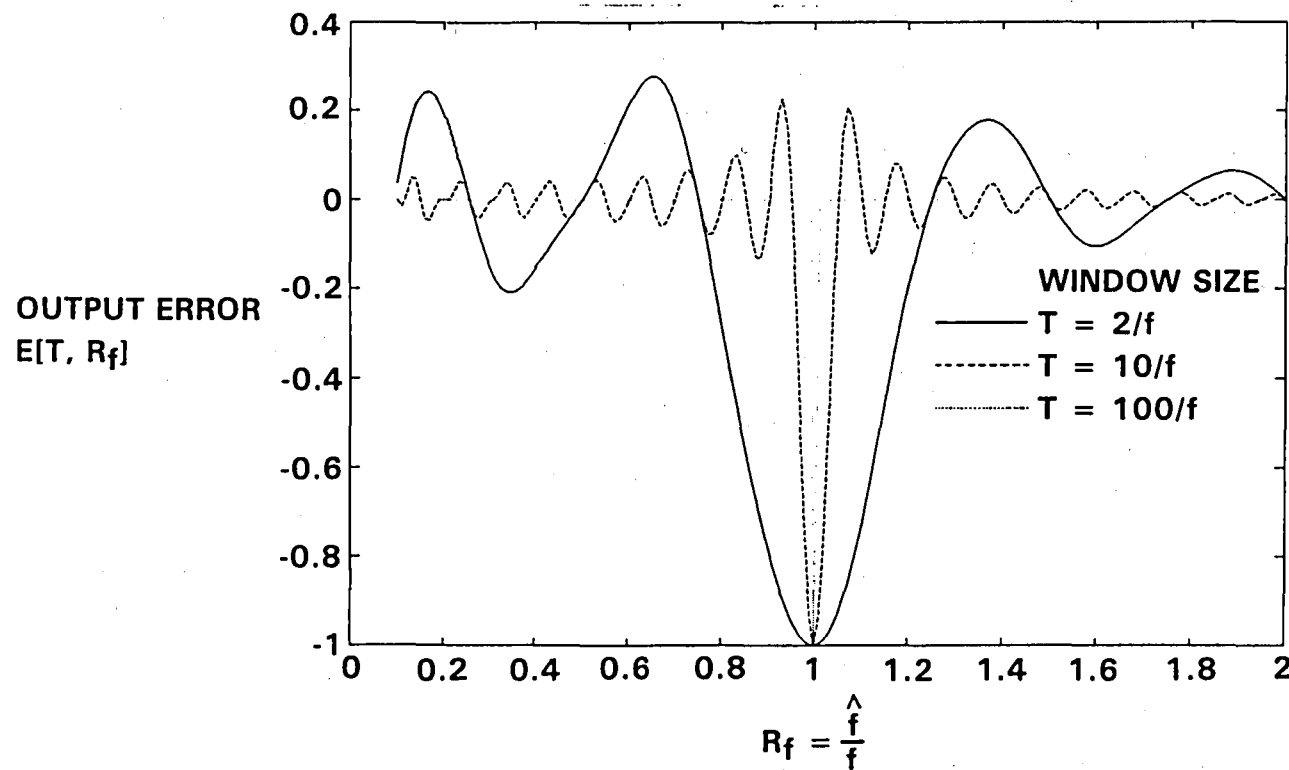
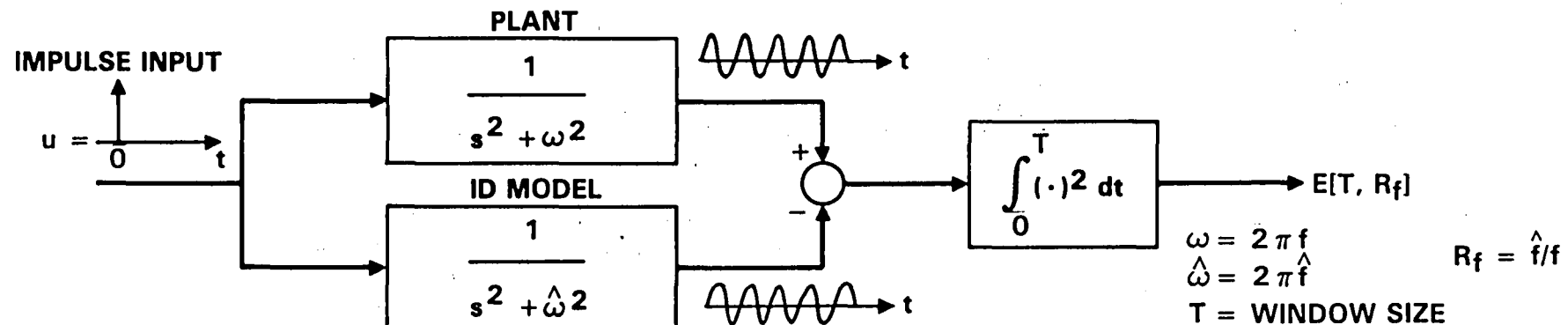
	RECURSIVE/REAL-TIME	BLOCK PROCESSING/NEAR REAL-TIME
	RECURSIVE PREDICTION ERROR METHOD (RPEM) ARMAX $Ay = Bu + Ce$ DISCRETE-TIME FORMULATION	MAXIMUM LIKELIHOOD ESTIMATION (MLE) STATE-SPACE/MODAL PARAMETRIZATION CONTINUOUS-TIME FORMULATION
ADVANTAGES	<ul style="list-style-type: none"> • NO FALSE MINIMA FOR LARGE S/N RATIO • TIME-RECURSIVE COMPUTATION 	<ul style="list-style-type: none"> • MIMO FORMULATIONS EASIER • PHYSICAL INTERPRETATION FOR PARAMETERS
DISADVANTAGES	<ul style="list-style-type: none"> • ROOT-SENSITIVITY PROBLEM • MIMO REQUIRES MANY PARAMETERS • PARAMETERS ARE NONPHYSICAL • PERSISTENT EXCITATION CONDITIONS 	<ul style="list-style-type: none"> • FALSE MINIMA IN LIKELIHOOD SURFACE

The predominant difficulty associated with MLE for identification of structures, lies in the existence of many false minima in the likelihood surface. This difficulty is essentially a deterministic one, and is due primarily to the estimation of the modal frequency parameter. This is seen from the output error surface depicted for a finite-time experiment (note that this would be the likelihood surface if white sensor noise were the only disturbance). The output error curves are given for three different values of experiment horizon length, corresponding to 2, 10 and 100 cycles of the modal response to an impulse input. These curves are very revealing. It is noted that there exist many false minima in the error surface due to the effect of finite-time windowing. Furthermore, for a system with multiple modes, the high frequency modes would have more cycles than the low frequency modes in any finite-time horizon of fixed length. Hence, we can conclude the following,

1. The surface near the global minimum is sharper for high frequency modes than low-frequency modes. Since the Cramer-Rao bound is directly related to the curvature of the surface about the global minimum, high modal frequencies can be found with better accuracy than low modal frequencies. On the other hand, the high modal frequencies must be initialized more accurately to ensure global convergence.
2. An experiment design based on optimizing local criteria (e.g., measures of the Cramer-Rao bound or inverse Fisher matrix), may generate a very sharp valley about the global minimum, making global optimization more difficult. This disadvantage may offset any benefits from using optimal experiment designs.
3. In a broad sense, the experiment design to support MLE should pay special attention to the modal frequency estimation problem to ensure both global and local properties of the optimal solution.

JPL

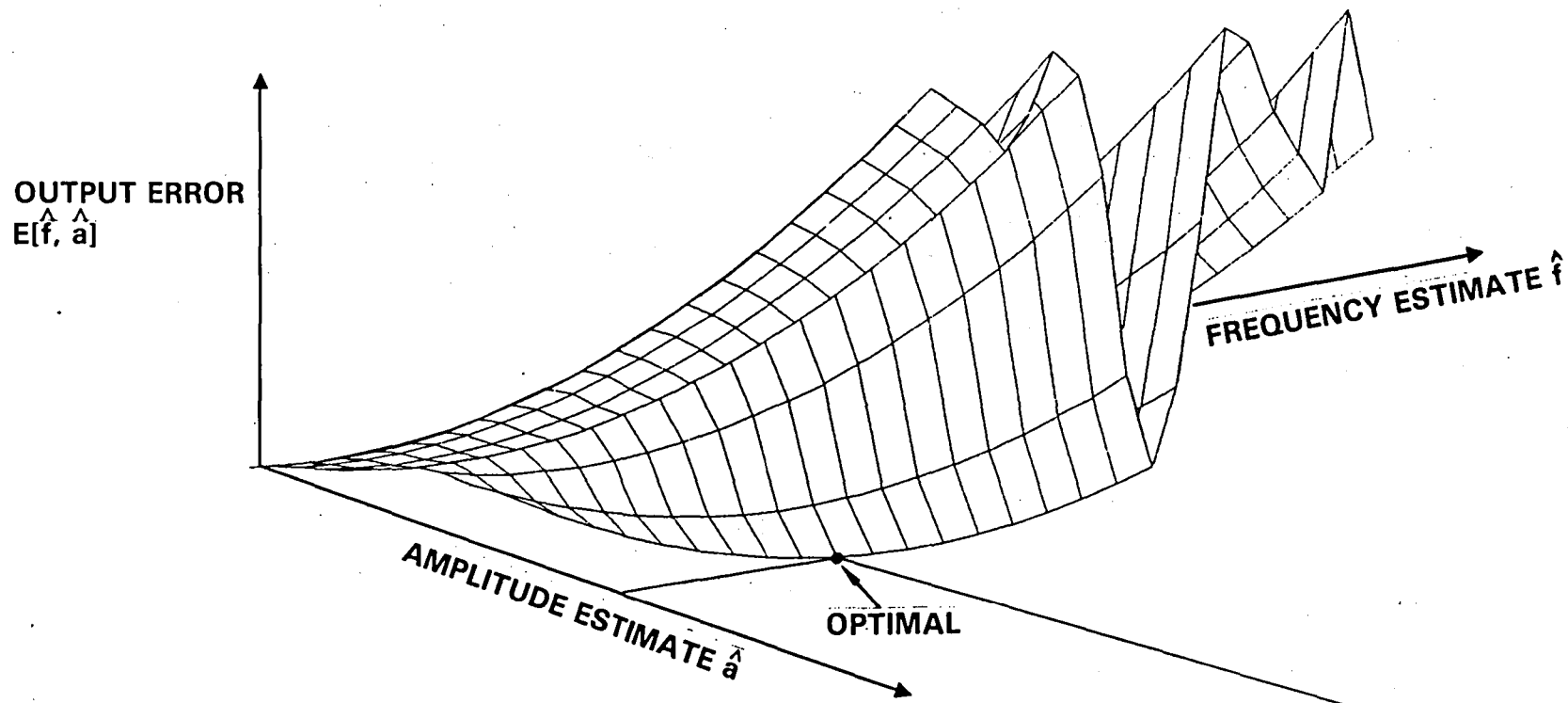
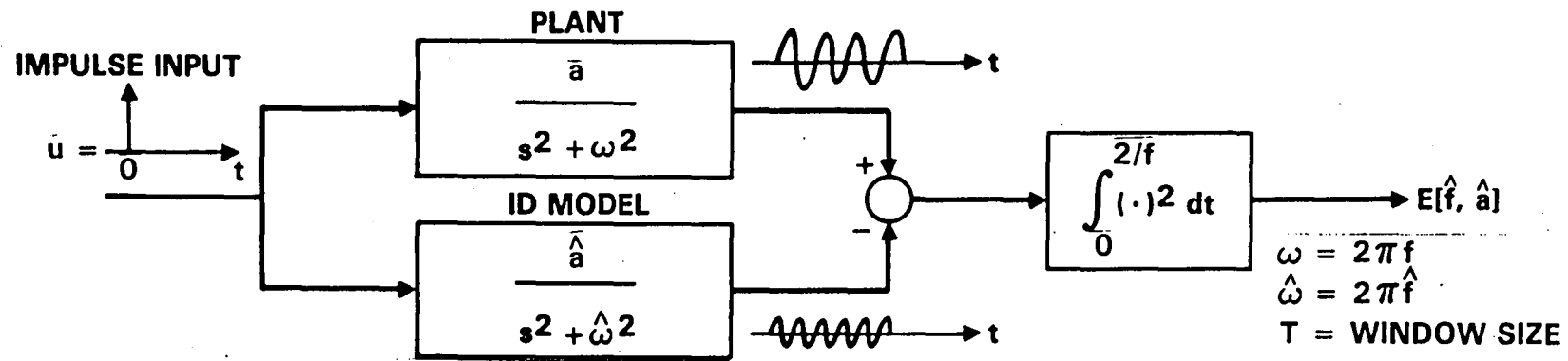
OUTPUT ERROR SURFACE FOR FREQUENCY ESTIMATION



622

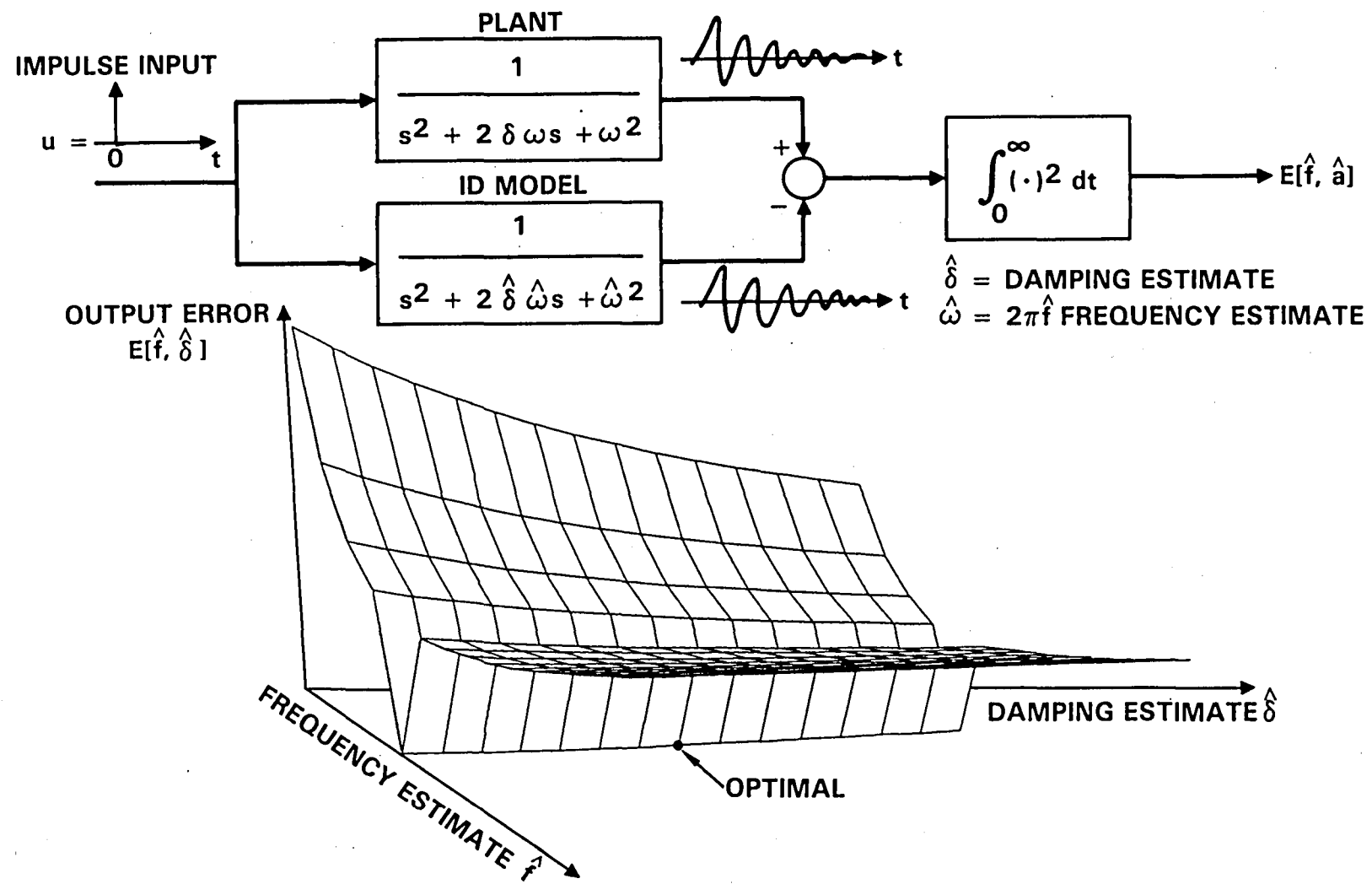
It is of interest to see if the output error surface is better behaved with respect to parameters other than the modal frequencies. The surface is plotted with respect to an additional modal amplitude parameter below. The surface has a smooth broad valley with respect to the modal amplitude parameter, and hence, is better behaved in this direction with respect to the false minima problem. However, it is seen that the modal amplitude can only be identified correctly if one is in the correct cusp of the surface with respect to the modal frequency estimate. This emphasizes the need for good initial frequency estimates.

JPL OUTPUT ERROR SURFACE FOR AMPLITUDE AND FREQUENCY ESTIMATION



The output error surface is plotted with respect to an additional modal damping parameter below. Since an infinite-time horizon is used in this plot, and nonzero damping is assumed in the system response, there is additional smoothing in the surface in the direction of the frequency estimate. The surface has a smooth broad valley with respect to the damping parameter, and hence, is well behaved in this direction with respect to the false minima problem. However, the surface is very flat in this direction, which indicates that the damping will not be estimated very accurately in a statistical setting. Since the damping is small to begin with, it is not uncommon for the damping parameter estimate to become negative. This poses numerical problems for MLE since one is forced to propagate unstable sensitivity equations conditioned on the estimated parameters. This is also a cause of major difficulties when applying general purpose identification software to this problem.

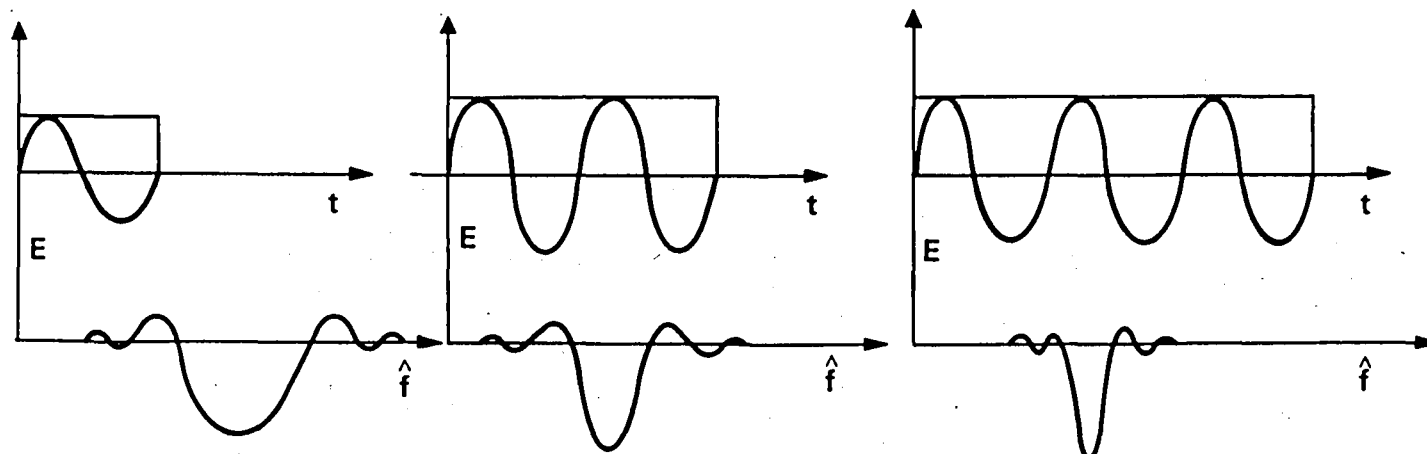
JPL OUTPUT ERROR SURFACE FOR FREQUENCY AND DAMPING ESTIMATION



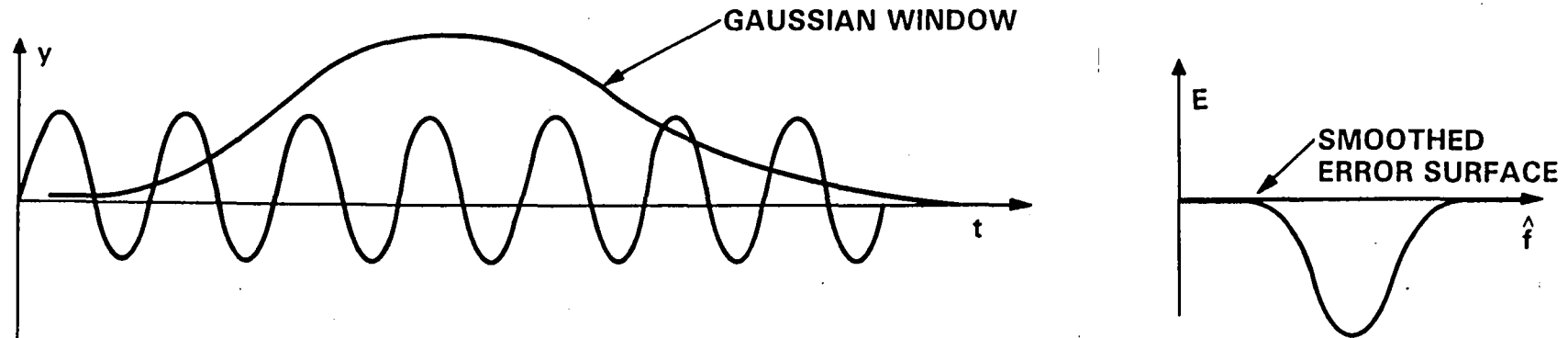
The lesson to be learned from the previous slides, is that the output error surface has many false minima due primarily to the frequency estimation parameter. With this understanding, several remedies can be posed. The most basic approach is to initialize the MLE with accurate frequency estimates from a nonparametric precursor experiment (e.g., an FFT). Other methods include numerical methods for global optimization, surface regularization, surface switching, and surface smoothing.

SOME AD-HOC SOLUTIONS TO THE FALSE MINIMA PROBLEM

- INITIALIZE FREQUENCY ESTIMATES FROM NONPARAMETRIC ID PRECURSOR
- GLOBAL OPTIMIZATION TECHNIQUES (TUNNELING, SIMULATED ANNEALING, ETC.)
- START WITH EQUATION ERROR METHODS AND SWITCH TO MLE
- SOLVE WITH A SEQUENCE OF INCREASING WINDOW SIZES



- SMOOTH ERROR SURFACE BY WINDOWING TIME SIGNALS



If one is confident that the likelihood surface can be minimized globally, then one has license to use local criteria for determining the optimal experiment design. Several such criteria are given below in terms of the Fisher information matrix (i.e., the inverse of the Cramer-Rao bound). Optimization of the D, E or A optimal criteria will insure a design which renders the Fisher matrix nonsingular (assuming such a design exists) which guarantees parameter identifiability. These criteria, however, are nonlinear functions of the entries of the Fisher matrix, and are difficult to optimize in practice (some results on this will be given on the next slide). The trace criteria is generally much simpler to optimize but generally leads to a design that does not guarantee identifiability (i.e., modes which are not excited and/or sensed). A criteria which lies somewhere in between, is the product of diagonals criteria of Nahi and Napjus which can be solved by an iterative sequence of weighted trace optimizations.

DESIGN BY OPTIMIZATION OF INFORMATION MATRIX

- CRITERIA WHICH ENSURE IDENTIFIABILITY (EFFICIENT ESTIMATORS)

D-OPTIMAL: $\max_{\beta, u} \det \{F\}$ β — SENSOR PLACEMENT
 β, u — INPUT DESIGN

E-OPTIMAL: $\max_{\beta, u} \lambda_{\min} \{F\}$ F — FISHER INFORMATION MATRIX
 β, u W — WEIGHTING MATRIX

A-OPTIMAL: $\min_{\beta, u} \text{TR} \{F^{-1} W\}$ f_{ii} — i^{TH} DIAGONAL
 β, u f_{ii} — ENTRY OF F

- $\max_{\beta, u} \text{TR} \{F W\}$ CRITERIA IS SOMETIMES USED BUT CAN LEAD TO IDENTIFIABILITY PROBLEMS (GOODWIN AND PAYNE 1977)

- PRODUCT DIAGONALS CRITERIA $\max_{\beta, u} \prod_{i=1}^n f_{ii}$ (NAHI AND NAPJUS 1971)

$$\cdot \left[\frac{1}{n} \text{TR} \{F\} \right]^n \geq \prod_{i=1}^n f_{ii} \geq \det \{F\}$$

• CAN SOLVE BY SEQUENCE OF $\text{TR} \{F W\}$ OPTIMIZATIONS

• INVARIANT UNDER CHANGE IN UNITS

Certain simplifications occur in the determination of D-optimal experiments for identifying modal frequency and damping parameters in LSS. In particular, the D-optimal cost separates into two components such that the sensor placement problem is decoupled from the input design problem. This decoupling effect significantly simplifies the overall optimal experiment design determination. The error from using the uncoupled design is on the order of the damping squared, and hence is a meaningful approximation for lightly damped structures.

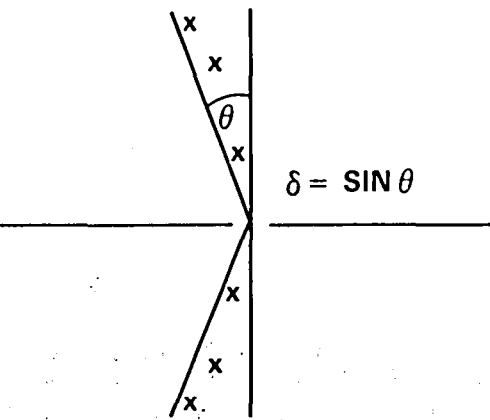
JPL

OPTIMAL EXPERIMENT DESIGN FOR MODAL FREQUENCY AND DAMPING IDENTIFICATION

- D-OPTIMAL CRITERIA: $\max_{\beta, u} \det \{ \mathcal{F} \}$

β - SENSOR PLACEMENT VARIABLE
 u - INPUT DESIGN
 \mathcal{F} - FISHER INFORMATION MATRIX

- STRUCTURAL DAMPING δ :



- SEPARATION PRINCIPLE FOR LIGHTLY DAMPED STRUCTURES

$$\max_{\beta, u} \det \{ \mathcal{F} \} = \max_{\beta} \det \{ R(\beta) \} \max_u \det \{ J(u) \} + \sigma(\delta^2)$$

- OPTIMAL SENSOR PLACEMENT β AND OPTIMAL INPUT u CAN BE SOLVED INDEPENDENTLY
- $R(\beta)$ IS INDEPENDENT OF MODAL FREQUENCIES AND DAMPINGS i.e., UNCONDITIONAL OPTIMAL SENSOR PLACEMENT

A fundamental problem associated with identifying the transfer function coefficients of a discretized modal system is the root sensitivity problem. For example, the denominator coefficients corresponding to a discretized system having eight specified modal frequencies is computed to 16 significant digits. These coefficients are rounded to 10 significant digits. A somewhat startling fact is that the roots of the resulting polynomial do not agree with those of the original polynomial to even the first significant digit.

ROOT SENSITIVITY PROBLEM

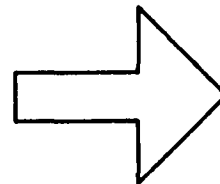
TYPICAL EXAMPLE

STRUCTURAL PARAMETERS (8 MODES)

FREQ (Hz)	DAMPING
0.349991E+01	0.700114E-02
0.320000E+01	0.697706E-02
0.299973E+01	0.708050E-02
0.280008E+01	0.686493E-02
0.265676E+01	0.709098E-02
0.731315E+00	0.656019E-02
0.549268E+00	0.804721E-02
0.612079E-01	0.378008E-02

SAMPLING PERIOD

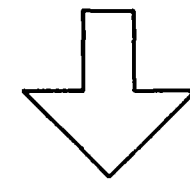
$T = 0.03$ sec



DISCRETE TRANSFER FUNCTION

$$G(z) = \frac{B(z)}{A(z)}$$

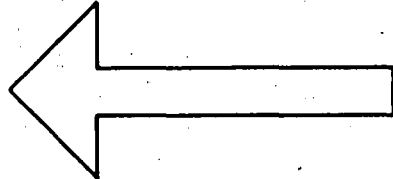
$$A(z) = z^{16} + a_1 z^{15} + \dots + a_{16}$$



$A_T(z)$ COEFFICIENTS

-.1433157024D02
 .9771317541D02
 -.4206232201D03
 .1279287523D04
 -.2914512176D04
 .5144460501D04
 -.7176063793D04
 .7994218683D04
 -.7135905162D04
 .5087115810D04
 -.2866020586D04
 .1251072968D04
 -.4091056752D03
 .9452747852D02
 -.1379131258D02
 .9573564793D0

ROUND-OFF FROM 16 TO 10 SIGNIFICANT DIGITS



$A(z)$ COEFFICIENTS

-.1433157023880846D02
 .9771317541274720D02
 -.4206232200907015D03
 .1279287523027041D04
 -.2914512176210783D04
 .5144460500626343D04
 -.7176063793295143D04
 .7994218683170717D04
 -.7135905162079569D04
 .5087115810204192D04
 -.2866020585540510D04
 .1251072967803763D04
 -.4091056752151899D03
 .9452747852297180D02
 -.1379131257627273D02
 .9573564792851850D0

- COEFFICIENTS OF $A(z)$ AND $A_T(z)$ AGREE TO 10 SIGNIFICANT DIGITS
- ROOTS OF $A(z)$ AND $A_T(z)$ DIFFER IN 1ST SIGNIFICANT DIGIT

Fortunately the root sensitivity problem has been well-studied in the numerical analysis literature. Assuming that the roots are on the unit circle, the root perturbation corresponding to a specified coefficient perturbation is given below. In particular, the sensitivity of the j th root is inversely proportional to the "product of the secants" from roots i (i not equal to j) directed towards root j . This relation immediately gives criteria for choosing the sampling time to minimize the root sensitivity.

ROOT SENSITIVITY PROBLEM

- DISCRETE TRANSFER FUNCTION: $G(z) = \frac{B(z)}{A(z)}$

$$A(z) = z^n + a_1 z^{n-1} + \dots + a_n$$

ROOTS ON UNIT CIRCLE: $z_i = e^{j\omega_i T}$ $i = 1, \dots, n$

$T \triangleq$ SAMPLING PERIOD

z_i COMPLEX CONJUGATE PAIRS

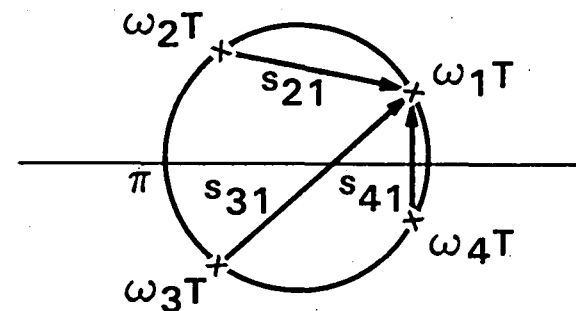
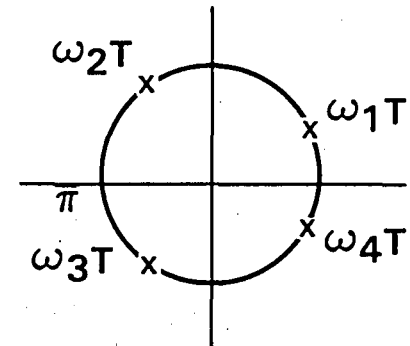
ASSUME RELATIVE PERTURBATION:

$$\left| \frac{\delta a_i}{a_i} \right| \leq \epsilon \text{ FOR } i = 1, \dots, n$$

THEN

$$\left| \frac{\delta z_j}{z_j} \right| \leq \frac{\sum_{k=1}^n |a_k| \epsilon}{\prod_{i \neq j} s_{ij}}$$

s_{ij} IS SECANT FROM ω_i TO ω_j



Simply stated, the sampling time and bandwidth of interest should be chosen so that there are no "short secants". Several rules of thumb are to 1) avoid estimating a large number of modes at one time 2) avoid oversampling the lowest frequency mode in the bandwidth under consideration 3) avoid modes near the Nyquist fold-over frequency and 4) avoid oversampling the "difference frequencies" between closely spaced modes.

RULES OF THUMB FOR CHOICE OF SAMPLING PERIOD

$$\left| \frac{\delta z_j}{z_j} \right| \leq \frac{\sum_{k=1}^n |a_k| \epsilon}{\prod_{i \neq j} s_{ij}} \} \text{ ROOT SENSITIVITY}$$

- AVOID ESTIMATING TOO MANY MODES AT ONE TIME
- OPTIMAL T FOR ONE MODE IS GIVEN BY $\omega T = \frac{\pi}{2}$
i.e., 4 SAMPLES/CYCLE



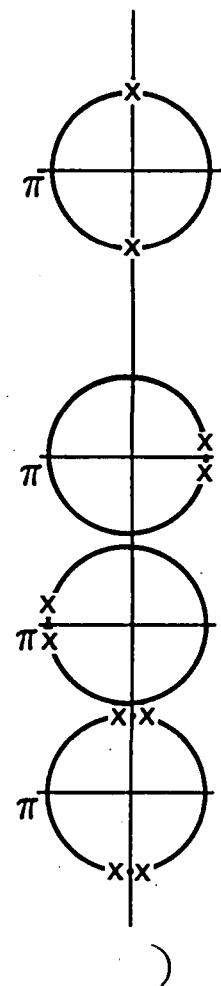
- AVOID OVERSAMPLING LOW FREQUENCY MODES

$$\frac{b_1 z + b_0}{z^2 - 2 \cos \omega T z + 1} \approx \frac{b_1 z + b_0}{z^2 - 2(1 - \omega^2 T^2) z + 1}$$

- AVOID MODES NEAR FOLD-OVER FREQUENCY
- AVOID MODES CLOSE TO EACH OTHER

IN GENERAL, CHOOSE T TO KEEP ROOTS AWAY FROM
 ± 1 AND AWAY FROM EACH OTHER

$$\begin{aligned} \omega &= (2\pi)(.01) \\ T &= 0.1 \\ \omega^2 T^2 &= 0.00004 \end{aligned}$$



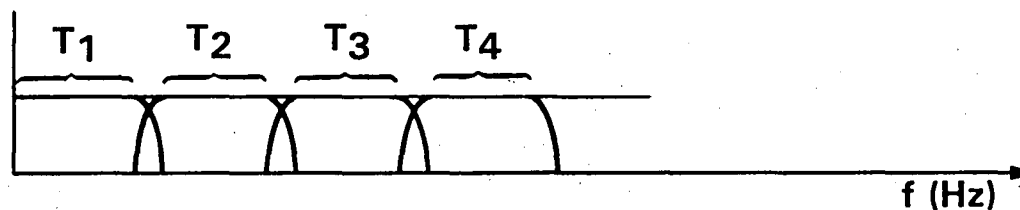
If nominal frequency estimates are available, a formal criteria for choosing the sampling time can be written directly in terms of the size of the induced secants. The best results can of course be obtained if one is further allowed to break up the frequency axis into separate bands, and to perform the identification in each band with a different choice of sampling time (i.e., multirate bandpass reconstruction). A somewhat novel alternative which may work in certain circumstances, is to undersample and let the higher frequency modes alias down.

OPTIMAL CHOICE OF SAMPLING PERIOD

- IF NOMINAL ESTIMATES OF ω_i $i = 1, \dots, n$ ARE AVAILABLE, USE

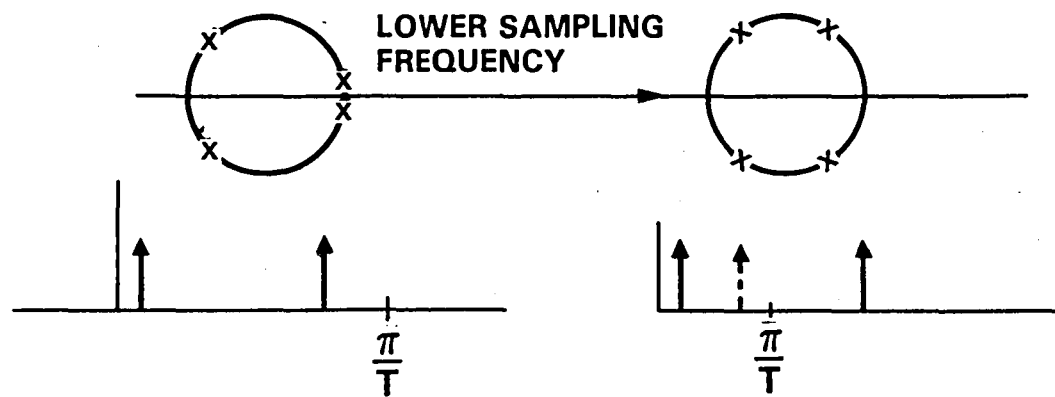
$$T^* = \operatorname{ARG} \max_T \min_j \prod_{i \neq j} \sin \left(\frac{|\omega_i + \omega_j| T}{2} \right)$$

- MULTIRATE BANDPASS RECONSTRUCTIONS



OPTIMAL FREQUENCY PARTITION AND CHOICE OF T_i

- UNDERSAMPLING



In summary, before one can talk about optimal experiment design it is important to know exactly what is to be optimized. This of course, depends on the ID algorithm and parametrization under consideration. In order to best support control design two specific parameteric methods are focused on here: the MLE block data processing algorithm with state-space/modal parametrization, and the RPEM with ARMAX parametrization.

The major problem associated with MLE is the false minima in the likelihood surface. This motivates an experiment design strategy for effectively dealing with the frequency estimation problem (e.g., nonparametric precursor experiments) and/or numerical techniques aimed at global optimization of the likelihood surface. If global optimization can be reliably performed, then the use of local optimization criteria (i.e., measures of the Fisher information matrix) is warranted. For this purpose, several simplifications in the D-optimal criteria occur for lightly damped structures which can be used to advantage.

A fundamental problem associated with the identification of a structure using transfer function coefficients (i.e., the ARMAX parametrization), is due to the classical root sensitivity problem. Some insight into this problem is given by looking at the numerical analysis literature. This provides criteria and rules of thumb for choosing the sampling time and frequency partitions for the identification problem. It must be mentioned, however, that these results are purely numerical and deterministic. The same sensitivity which hinders the numerics, tends to help the estimation problem (i.e., the Cramer-Rao bounds on the transfer function coefficients are related to the reciprocal of the root sensitivities). A complete understanding of these relationships is required before the correct criteria can be established.

SUMMARY

- EXPERIMENT DESIGN DEPENDS ON PARAMETRIZATION AND ID ALGORITHM
- MLE/BLOCK PROCESSING
 - MANY FALSE MINIMA IN OUTPUT ERROR SURFACE -- DUE PRIMARILY TO FITTING MODAL FREQUENCIES
 - REQUIRES STRATEGY FOR "SNEAKING UP" ON FREQUENCY ESTIMATES OR SMOOTHING ERROR SURFACE
 - OPTIMAL EXPERIMENT DESIGNS MAY MAKE FINDING GLOBAL OPTIMAL MORE DIFFICULT
 - SEPARATION RESULTS FOR EXPERIMENT DESIGNS WITH LIGHTLY DAMPED SYSTEMS
- RECURSIVE PREDICTION ERROR METHOD/ARMAX PARAMETRIZATION
 - ERROR SURFACE WELL-BEHAVED FOR LARGE S/N RATIO
 - ROOT SENSITIVITY PROBLEM -- OPTIMAL CHOICE AT SAMPLING PERIOD
 - 2 SINUSOID/MODE PERSISTENT EXCITATION REQUIREMENT

IN-FLIGHT IDENTIFICATION OF THE
GALILEO SPACECRAFT
FLEXIBLE MODE CHARACTERISTICS

EDWARD C. WONG

USAF/NASA WORKSHOP ON
MODEL DETERMINATION
FOR
LARGE SPACE SYSTEMS

JET PROPULSION LABORATORY
CALIFORNIA INSTITUTE OF TECHNOLOGY

MARCH 22-24, 1988

643

61-19

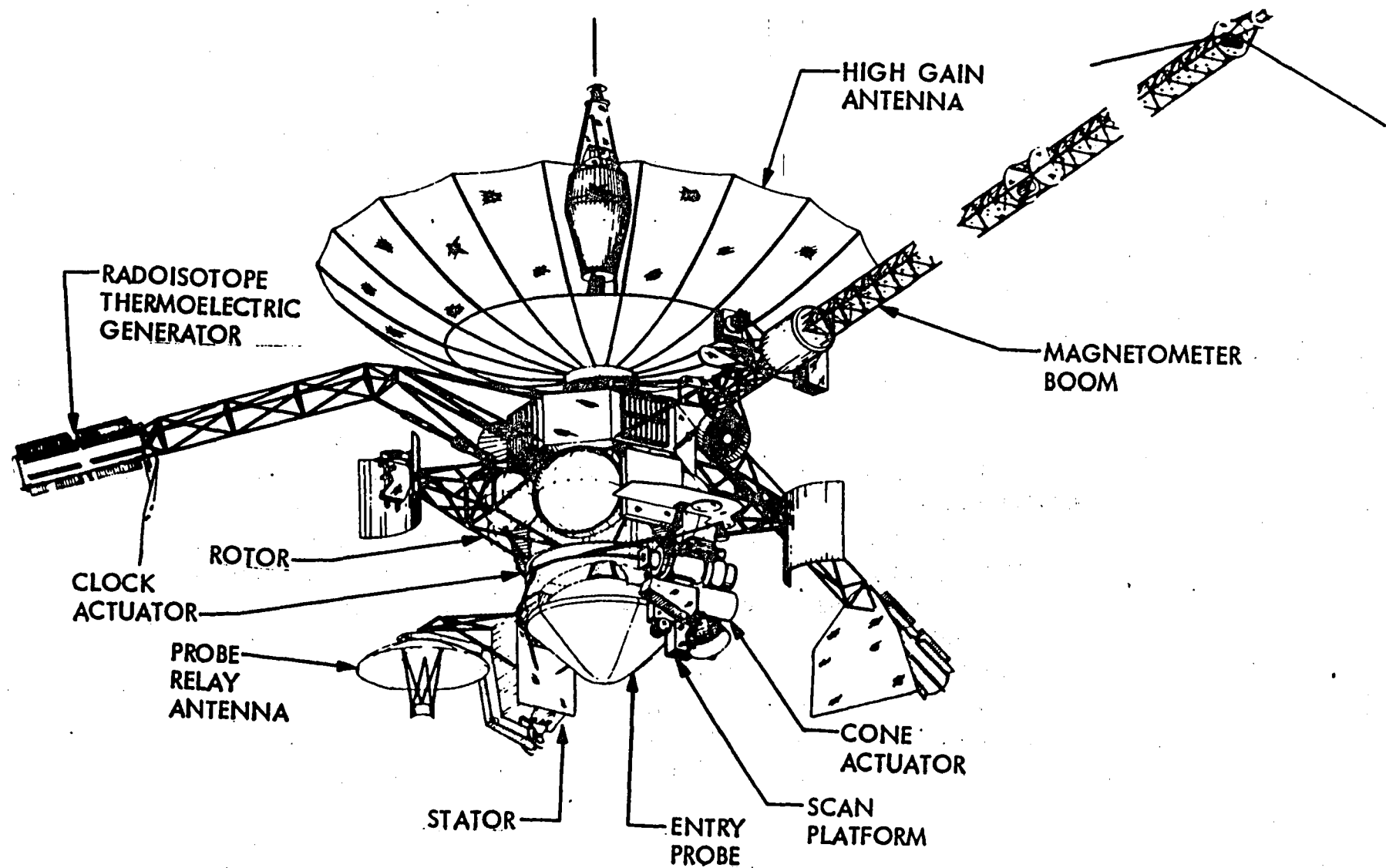
618391
81-65

69222-36N

The Galileo project is a planetary mission to Jupiter. The dual-spin spacecraft will orbit Jupiter and release a probe to penetrate the Jovian atmosphere. It will also conduct an asteroid flyby and new observations of Venus, Earth and the Moon. The launch date is set for October 1989, and will arrive at Jupiter in December 1995.

The scan platform is controlled in two degrees of freedom. A clock (Spin Bearing) actuator controls the relative position between the rotor and stator, and a cone actuator controls the position between the stator and the platform. Instruments on the platform are required to point to 140 micro-rad accuracy and 50 micro-rad per second stability.

THE GALILEO SPACECRAFT



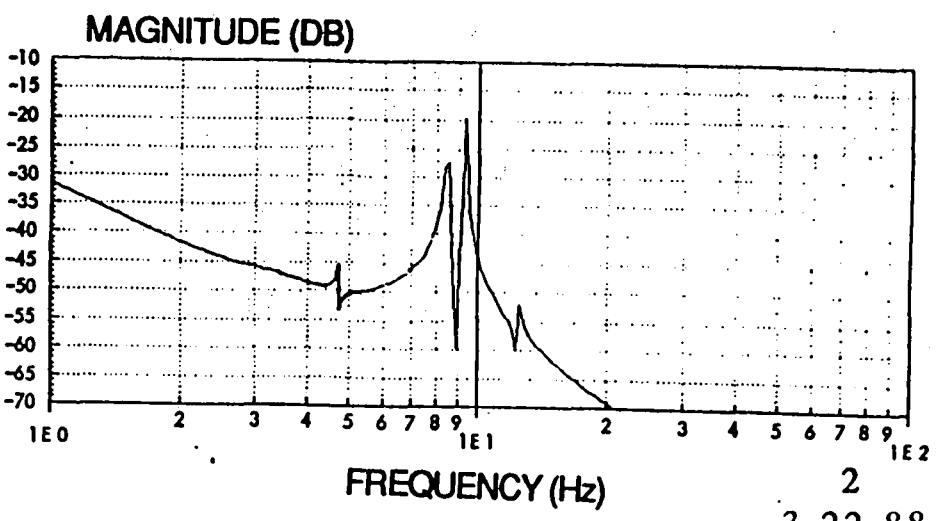
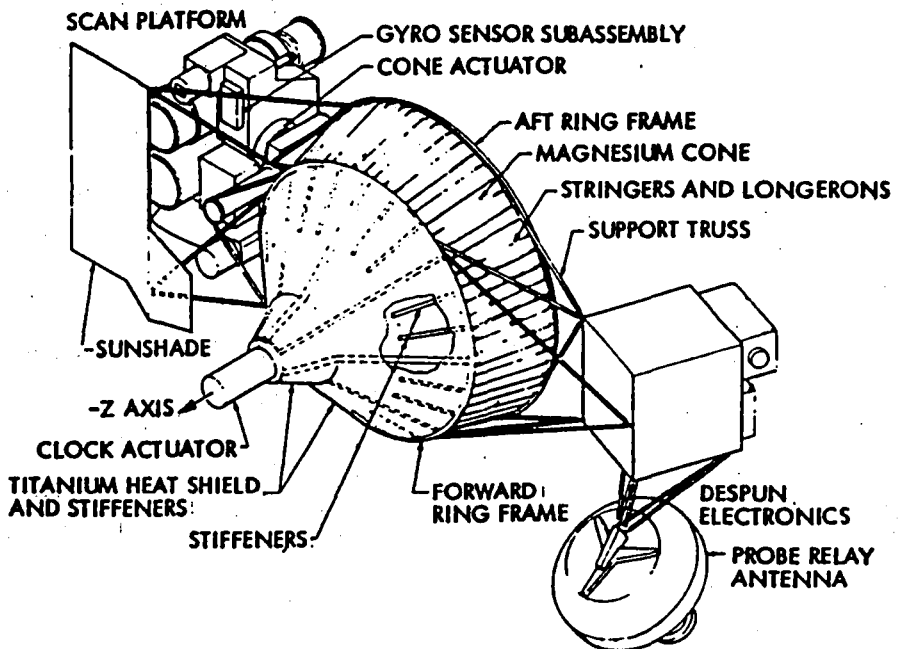
The stator structure, to which the platform is attached, is quite flexible. It has six very lightly damped natural frequencies below 15 Hz. The clock actuator, which controls the platform about the rotor spin axis, is separated from the gyros by the flexible stator. Structural data evaluation indicates possible dominant modes between 2.5 to 15 Hz, which are near the controller bandwidth (around 1 Hz). In order to prevent the flexible motion from feeding back into the stator structure through the clock actuator, these critical frequencies need to be identified in flight, and the parameters of a notch filter will be adjusted to attenuate the control gains at these frequencies.

SYSTEM IDENTIFICATION OBJECTIVES

- o IDENTIFY DOMINANT STRUCTURAL RESONANCE FREQUENCIES, MODE SHAPES, AND DAMPING RATIO WHICH EXIST IN THE TRANSFER FUNCTION BETWEEN CLOCK ACTUATOR AND GYRO SENSOR
- o POSITION NOTCH FILTER TO LIMIT UNDESIRABLE ACTUATOR TORQUE OUTPUT TO ENSURE STABILITY AND PERFORMANCE

PRE-FLIGHT MODAL UNCERTAINTY

MODAL FREQUENCY	+/- 20 %
MODE SHAPE	+/- 50 %
DAMPING	LOWER BOUND



The Clock Controller is a proportional-integral-derivative controller. To prevent the torque signal generated by this controller from exciting the stator structure, the control signal is passed through a double notch filter. When the structural frequency has a large resonance peak, the notch frequency can be set at that frequency to achieve maximum attenuation. When the structure has a number of modal frequencies with large resonance peaks, the notch filter will be used as a low pass filter, attenuating frequencies higher than the notch frequency.

A special mode for telemetry, has been created for the purpose of in-flight identification. Such a telemetry buffer provides up to six measurements of variables at a rate of 66 2/3 msec. Each memory readout from the bulk memory contains a maximum of 28 seconds of sampling at 15 samples per second, or a total of 420 samples per telemetry variable.

One of the challenges of the Galileo identification design is to obtain an open-loop response of the stator/platform structure while maintaining a "closed-loop" fault protection capability in the event of an anomaly during the identification process. The structure should be excited to a level within the fault limit. The control system should ensure an automatic and immediate abort of the process in the event that a fault is detected.

IDENTIFICATION DESIGN CONSIDERATIONS

SCAN PLATFORM CONTROLLER DESIGN:

- CONTROL TORQUE FOLLOWS SMOOTH TORQUE PROFILE FOR PLATFORM SLEWS
- NOTCH FILTER TO ATTENUATE CONTROL SYSTEM GAIN AT RESONANCE FREQUENCIES

IDENTIFICATION DESIGN CONSTRAINTS:

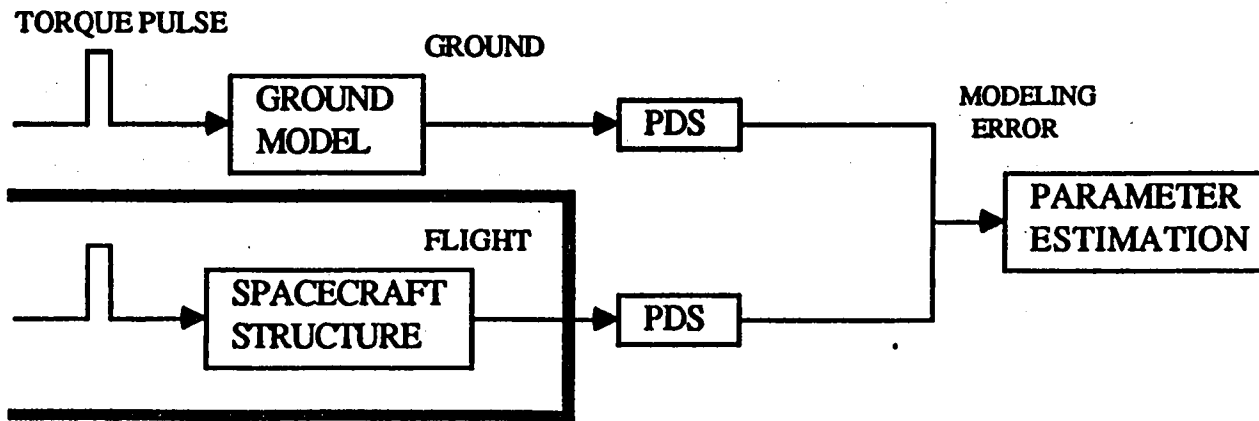
- ACTUATOR:
TORQUE SATURATION AT 4 NM
- SENSOR (GYROS):
SAMPLING RATE AT 15 HZ (66 2/3 MSEC), CAPTURE RATE 3 DEG/SEC
INTEGRATED RATE MEASUREMENT QUANTIZED AT 6 MICRO-RAD
LIMIT OF 28 SEC TELEMETRY PER BUFFER READOUT
- FLIGHT SOFTWARE:
32 K FOR ATTITUDE CONTROL, LOW MEMORY MARGIN
REQUIRED MINIMAL IMPACT TO EXISTING S/W DESIGN
- FAULT PROTECTION:
"OPEN-LOOP" FOR SCAN CONTROL
"CLOSED-LOOP" FOR FAULT PROTECTION

The identification scheme takes the approach of model matching by means of comparing the power density spectra from both ground model output and flight data. A torque pulse from the clock (spin bearing) actuator is used as the input excitation due to its rich frequency harmonics content and simplicity of implementation. Gyros on the platform are used for position sensor.

IDENTIFICATION METHOD

- o A TORQUE PULSE IS USED AS THE SYSTEM STIMULUS
- o OBTAIN OPEN-LOOP STRUCTURAL RESPONSE ABOUT CLOCK (SPIN) AXIS AND MATCH POWER DENSITY SPECTRA GENERATED BY MODEL AND FLIGHT DATA
- o UPDATE MODEL PARAMETERS: FREQUENCY λ_i , MODAL DAMPING ζ_i , AND COEFFICIENT C_i

$$F(s) = \sum_{i=1}^N \frac{C_i^2}{s^2 + 2\zeta_i\lambda_i s + \lambda_i^2}$$



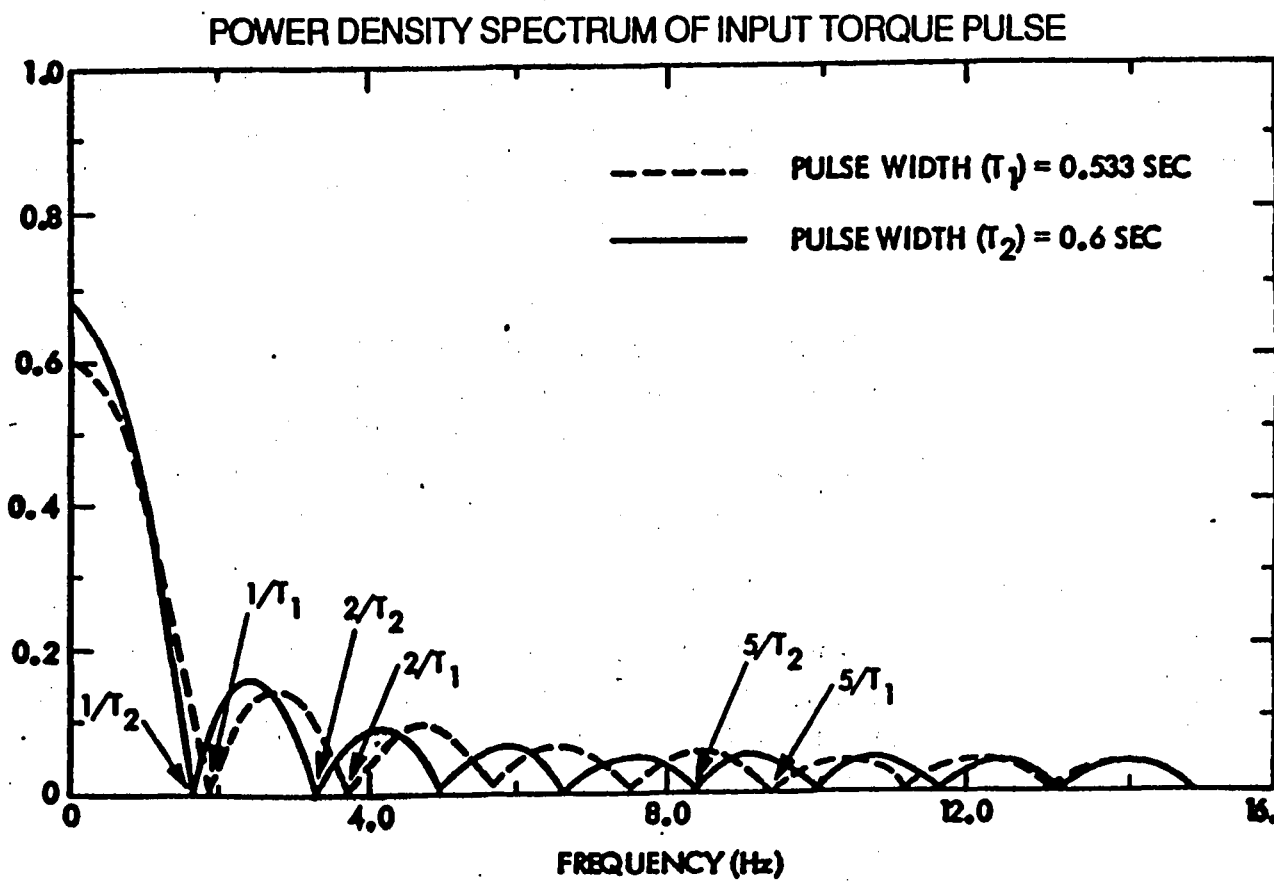
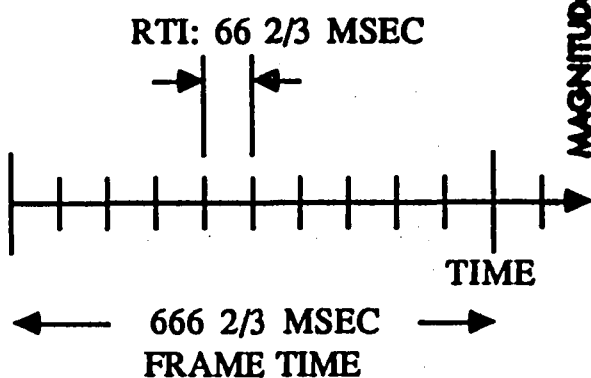
A square torque pulse exhibits various frequency harmonics whose nodes are a function of pulse width T , located at n/T Hz, $n=1,2,3,\dots$. Variable pulse widths should be used to adequately excite the structural modes.

The torque input PDS (Power Density Spectrum) shows nodes at various frequencies. No modal response should occur at around a node as indicated by the input PDS. This can be used to determine whether an identified frequency from the structural response PDS is actual or aliased. If necessary, a torque pulse of a specified width can be sent in flight such that a node falls in one of the two possible resonance frequencies.

Two commands are needed to generate the torque pulse. The first command is to slew at high rate to instantly saturate the spin bearing actuator software limiter. The next command is to lower the saturation level T seconds later to a level just enough to cancel the steady-state friction of the Spin Bearing Assembly.

INPUT TORQUE PULSE

- FLIGHT SOFTWARE CONSTRAINS TORQUE PULSE WIDTH TO BE MULTIPLES OF $66 \frac{2}{3}$ MSEC REAL-TIME INTERRUPTS
- FREQUENCY HARMONICS: NODES AT n/T , $n = 1, 2, 3, \dots$
- PULSE WIDTH VARIABILITY: AT LEAST THREE TORQUE PULSES OF VARYING WIDTH REQUIRED



DISCOS program was used to simulate flight data using NASTRAN generated modal data for the transfer function between the Spin Bearing Actuating point and the sensor point at the scan platform. Only the flexible modes below 15 Hz with dominant mode shapes were selected and used in the simulations.

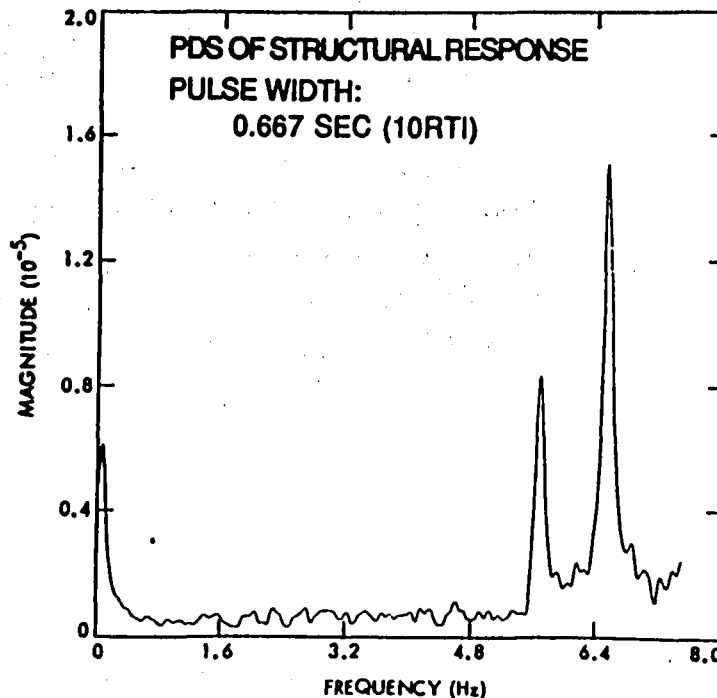
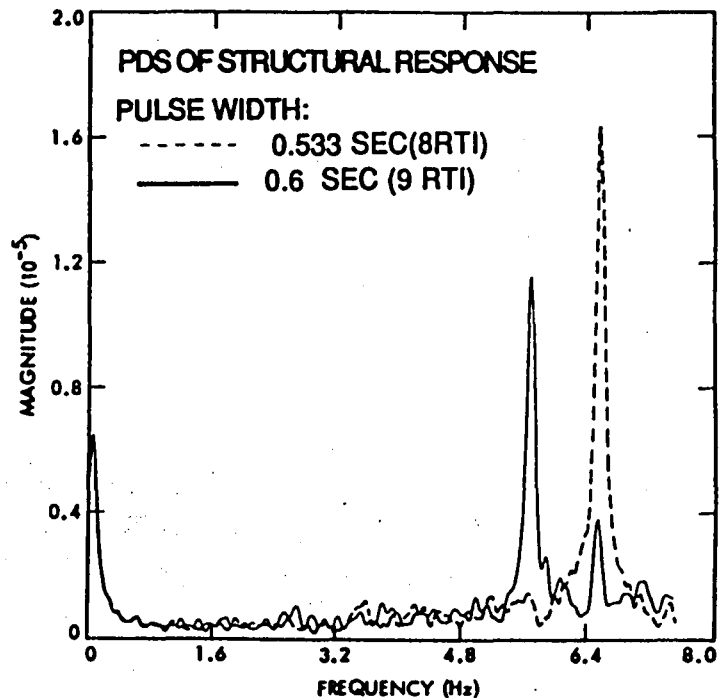
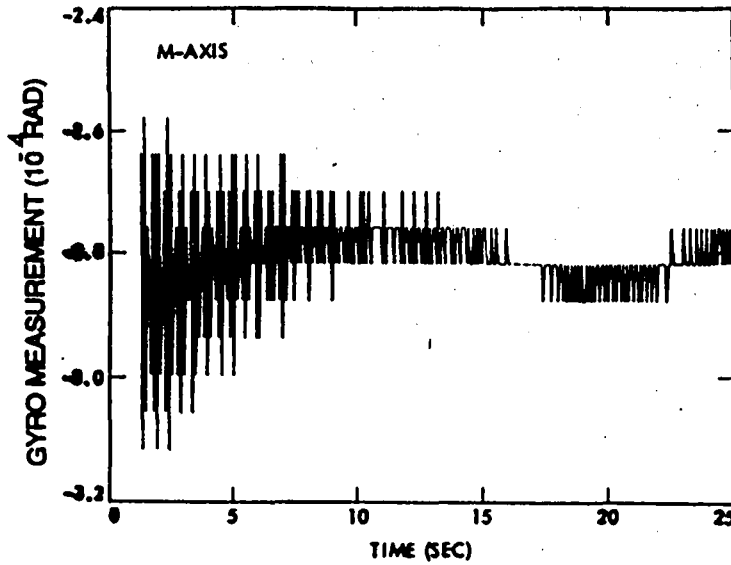
Two dominant modes were observed at cone angle of 90 degrees. The aliasing phenomenon is an effect of gyro sampling rate at 15 Hz. Modal frequency above the Nyquist sampling frequency of 7.5 Hz will be aliased. Both true and aliased frequencies of dominant modes will be notched out because they are the ones that will actually be observed by the gyros and scan controller.

A structural mode would be excited differently by torque pulses of different widths, since they contain different frequency harmonics and power spectra. For example, pulse width of 0.533 sec (8 RTI) is selected for the 8.43 Hz mode (aliased at 6.57 Hz) for its maximum excitation.

SIMULATION OF STATOR STRUCTURAL RESPONSE

FLIGHT DATA SIMULATIONS:

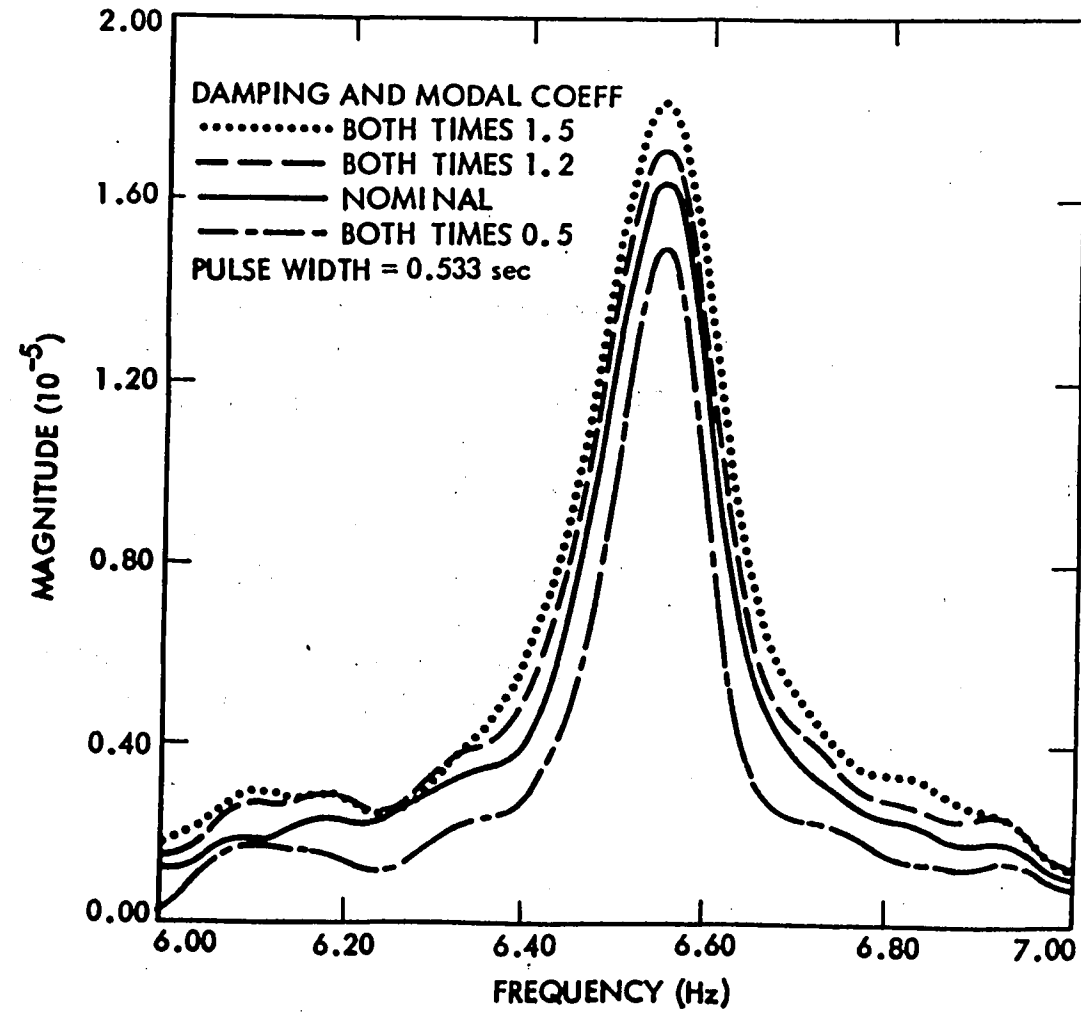
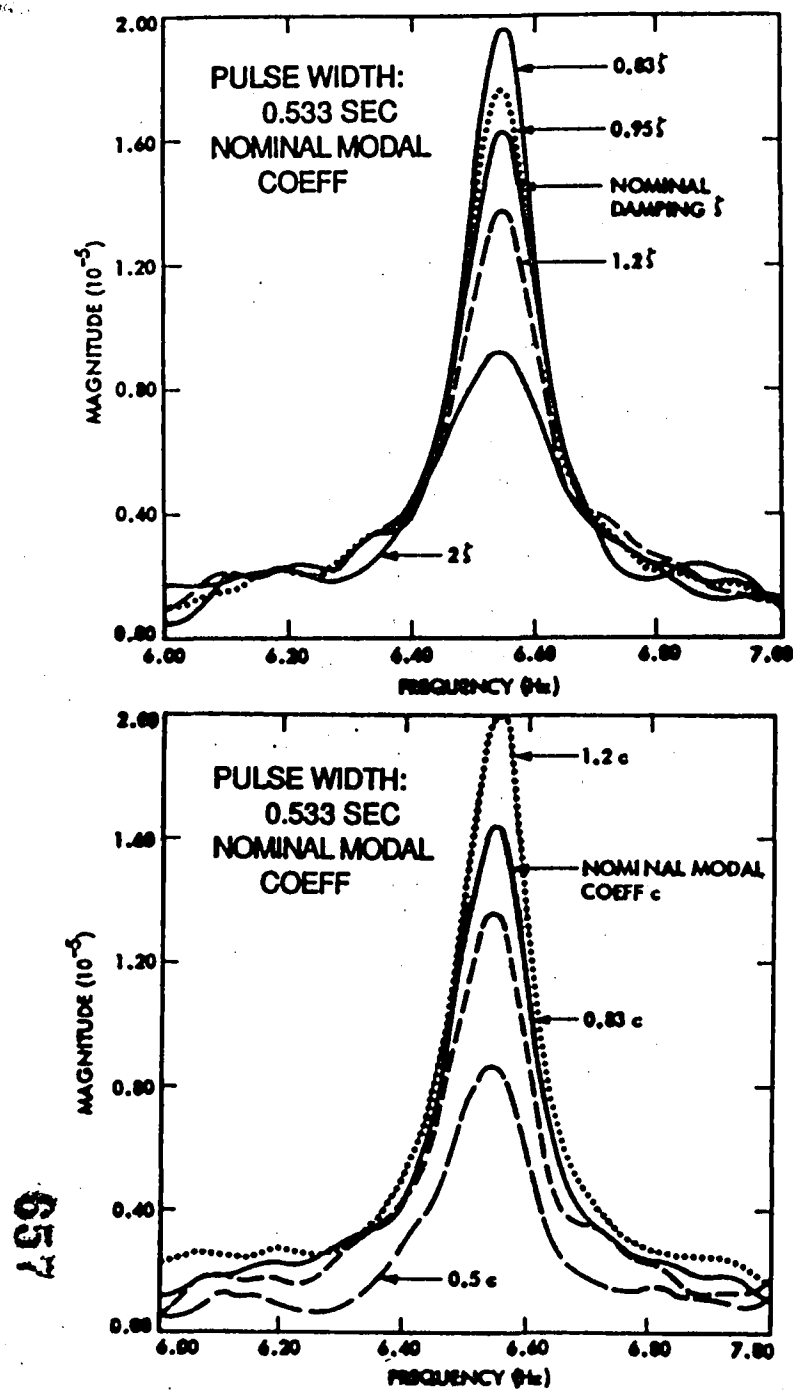
- o DISCOS PROGRAM CONTAINS DOMINANT FLEX MODES BELOW 15 Hz
- o GYRO MEASUREMENT CONTAINS QUANTIZATION NOISE (6 MICRO-RAD)
- o ACTUATOR TORQUE CONTAINS SPIN BEARING NOISE, FRICTION, AND SATURATION LIMIT
- o TELEMETRY PROVIDES 15 Hz DATA RATE AND 28 SEC DATA LENGTH



These figures show the sensitivity of the PDS amplitude with respect to dampings and modal coefficients. PDS profile is quite sensitive to even a 5% change in damping. For a constant modal coefficient, the base width of the amplitude remains constant while the height varies with damping. For a constant damping value, the area under the curve varies with the modal coefficient. These characteristics indicate the direction of adjusting the modal parameters in the model. Parameters adjustment is done by a least-square estimator for fitting the model PDS profile to the "flight" data.

The shape of the PDS has demonstrated sufficient sensitivity to the variation of modal parameters to satisfy the accuracy requirement of the Galileo project. When the profiles are reasonably matched, accuracy of the modal damping and coefficients falls within 5-20%.

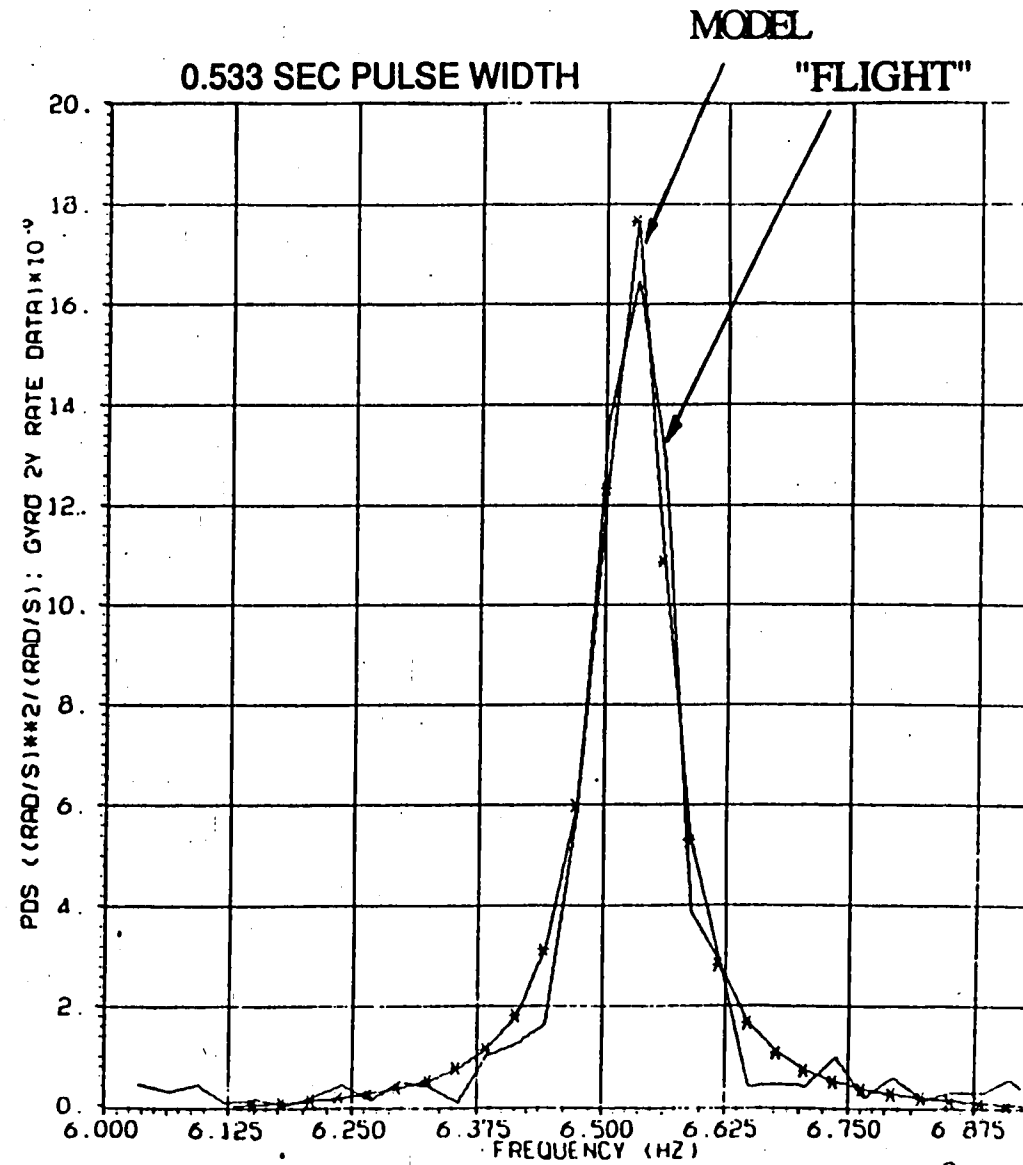
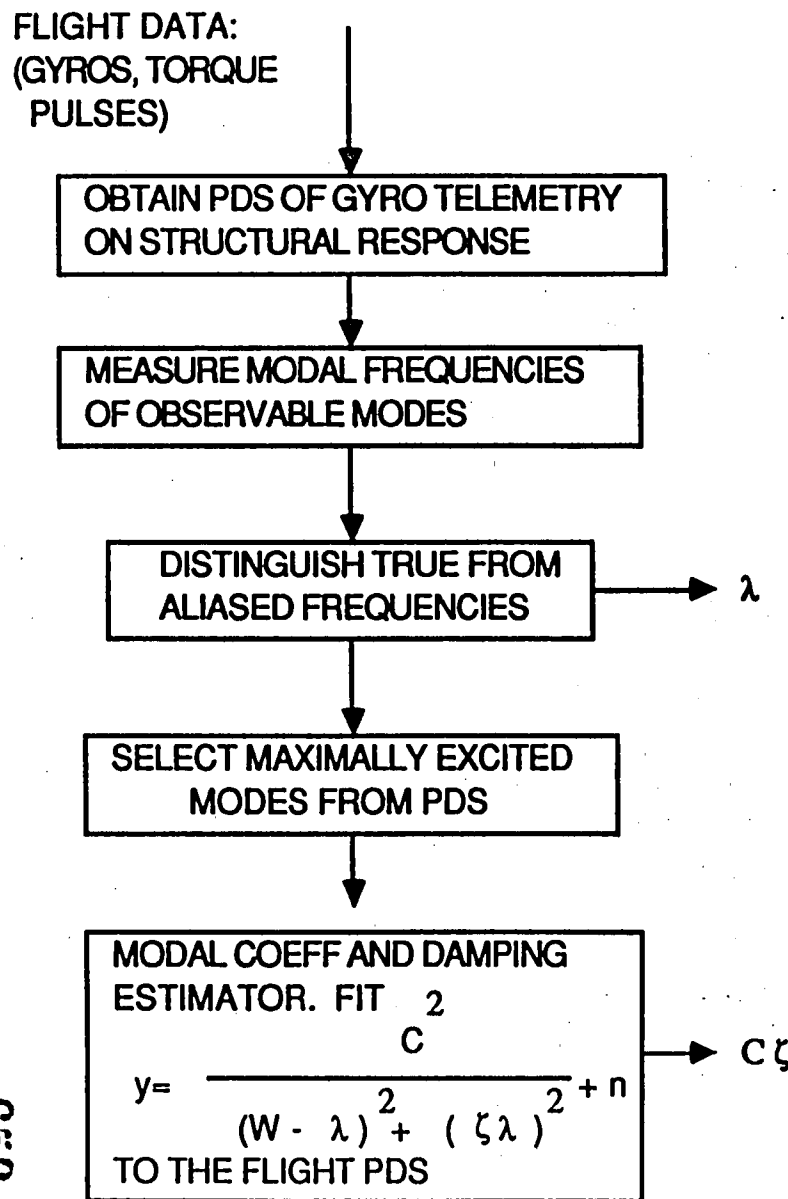
PDS VS DAMPING AND MODAL COEFFICIENTS



The steps for identification are as follows:

1. Process gyro data of structural response from five different pulse widths (7-11 RTI) for each platform (cone) orientation, and obtain their respective PDS.
2. Measure modal frequencies of the observable modes from the PDS plots.
3. Distinguish true from aliased frequencies. (New telemetry data corresponding to a different pulse width may be required).
4. Select the PDS of modes that were maximally excited by the input torque pulse for the purpose of model matching.
5. Obtain an initial estimate of coefficient and damping , and start the parameter iterations using a least-square estimator.

IDENTIFICATION FLOW DIAGRAM



660

LESSONS LEARNED FROM GALILEO FOR FUTURE IDENTIFICATION DESIGN

PROBLEMS EXPERIENCED

- o NON-COLOCATION OF ACTUATOR AND SENSOR
COMPLICATED CONTROL DESIGN AND
NECESSITATED SYSTEM ID
- o IDENTIFICATION DESIGN STARTED AFTER
SYSTEM AND S/W DESIGN:
 - o ID SUBJECTED TO MANY CONTROL DESIGN
AND OPERATIONAL CONSTRAINTS
 - o FLIGHT S/W NOT ABLE TO GENERATE
REQUIRED TIMING FOR PULSE WIDTH
WITHOUT MODIFICATION. TELEMETRY DATA
RATE NOT ADEQUATE
- o UNCERTAINTY OF ACTUATOR/SENSOR HARDWARE
CHARACTERISTICS (E.G. BEARING FRICTION)
- o DYNAMICS MODEL/SIMULATION TOOLS
INADEQUATE FOR CONTROL AND SYSTEM ID
VERIFICATIONS (LONG TURNAROUND TIME FOR
SIMULATION RUNS, LIMITED CONFIGURATION
TRADES)

FUTURE REMEDY/WORKAROUND

- AVOID ACTUATOR/SENSOR NON-COLOCATION.
ANALYSE STRUCTURAL MODEL EARLY IN
PROJECT PHASE TO INFLUENCE REQUIREMENTS
DEFINITION ON CONFIGURATION AND
STIFFNESS
- INCLUDE SYSTEM ID IN DESIGN BASELINE
- INCLUDE ID REQUIREMENTS IN FLIGHT S/W
AND FLIGHT DATA SYSTEM PLANNING
- PROVIDE CONSERVATIVE DESIGN MARGIN.
INCLUDE ID OF H/W CHARACTERISTICS IN
DESIGN BASELINE
- DEVELOP HIGH EFFICIENCY "NEXT GENERATION"
SIMULATION TOOLS NOW

662

CONCLUSIONS

- o DEVELOPED AN IDENTIFICATION METHOD FOR GALILEO SPACECRAFT FLEXIBLE MODE CHARACTERISTICS, AND VERIFIED WITH DISCOS SIMULATED FLIGHT DATA
- o OBJECTIVE OF MODAL FREQUENCY IDENTIFICATION TO WITHIN 2 -4 %, AND MODAL DAMPING AND COEFFICIENT TO WITHIN 5-20 % IS FEASIBLE
- o VARIABLE TORQUE PULSE WIDTHS AND SEVERAL ITERATIONS OF REAL-TIME COMMANDS TO EXCITE STATOR STRUCTURE ARE NECESSARY

499

**EVALUATION OF A METHODOLOGY
FOR MODEL IDENTIFICATION
IN THE TIME DOMAIN**

163820

P-25

R. T. Beck and J. L. Beck
Division of Engineering and Applied Science
California Institute of Technology

Summary

A model identification methodology for structural dynamics has been applied to simulated vibrational data as a first step in evaluating its accuracy. The evaluation has taken into account a wide variety of factors which affect the accuracy of the procedure. The effects of each of these factors were observed in both the response time histories and the estimates of the parameters of the model by comparing them with the exact values of the system. Each factor was varied independently but combinations of these have also been considered in an effort to simulate real situations.

The results of the tests have shown that for the "chain" model, the procedure yields robust estimates of the stiffness parameters under the conditions studied whenever uniqueness is ensured. When inaccuracies occur in the results, they are intimately related to non-uniqueness conditions inherent in the inverse problem and not to shortcomings in the methodology.

Description of Methodology

Mechanical Model

The mechanical model on which the methodology is based was motivated by the problem of detection of damage in offshore and aerospace structures by monitoring their vibrational response. Assuming that the structures are excited by low-amplitude forces, they will remain in the linear elastic range. In this case, the governing equations are the well-known equations of motion,

$$M\ddot{\mathbf{u}} + C\dot{\mathbf{u}} + K\mathbf{u} = \mathbf{f} \quad (1)$$

where M , C and K are the mass, damping and stiffness matrices, respectively, \mathbf{u} is the generalized displacement vector and \mathbf{f} is the corresponding forcing vector. Dots denote time derivatives.

PAGE 664 INTENTIONALLY BLANK

665

Damage occurring in a particular member of a structure with a large amount of redundancy is likely to have little effect on the response at any of the monitored degrees of freedom. As a result, if vibrational response is used to detect damage through identification of changes in the stiffness parameters of the members, the approach will be rendered ineffective by the ill-conditioned nature of the inverse problem. If the structure has been adequately partitioned into modules (or substructures), however, damage can be detected and located to within a module. For this purpose, damage is modeled as producing a uniform reduction in the module stiffness. Thus, if the initial stiffness matrix corresponding to module i is K_i , the "damage" stiffness matrix K_i^d is given by

$$K_i^d = \theta_i K_i$$

where $0 \leq \theta_i \leq 1$. The parameter θ_i is called the stiffness factor for module i . The global stiffness matrix K can be written as

$$K = \sum_{i=1}^N \theta_i K_i \quad (2)$$

where K_i now denotes the contribution of module i to the global stiffness, θ_i is unity unless damage occurs in module i , and N is the number of modules in the structure. The choice of N involves a compromise between the desire for high spatial resolution in localizing any damage and the need to avoid ill-conditioning or non-uniqueness in the identification of the θ_i . In general, a more dense distribution of sensors over the structure will allow a larger value of N .

Figure 1 shows an offshore structure and a building. For these systems, a module could correspond to a level or story, or even to a bay within a story. The third diagram in Figure 1 shows a mechanical model, the "chain" model, used as the system in this feasibility study because of its simplicity. Each story represents a module.

The aim of the identification methodology is to determine the parameters θ_i . Values of θ_i close to zero may indicate a significant loss in the stiffness of module i and therefore close inspection of the structure or other measures must be taken. It should be noted from (2) that the introduction of the θ parameters into the formulation does not change the structural topology or connectivity specified by the model, that is, if there is initially no stiffness linking two degrees of freedom, then this condition is maintained. Also, due to the uncertainty in the initial modeling of the stiffness of the structure, it is appropriate to constrain the parameters in the following way: $0 \leq \theta_i \leq Q$ where $Q = 1.5$, for example, rather than taking $Q = 1$.

The first step in the methodology is to establish the initial matrices K_i . This can be done, once the degrees of freedom of the structure have been specified, by using a suitable analytical

model. The Finite Element Method (FEM) is the most general analytical modeling approach that can be used, although other models such as the chain system, beam model or shear-wall model may be useful for certain systems.

Extension of the idea of a stiffness factor can be applied to the other dynamic matrices, i.e.,

$$M = \sum_{i=1}^N \gamma_i M_i \quad (3)$$

and

$$C = \sum_{i=1}^N \mu_i C_i \quad (4)$$

where M , γ_i and M_i are the global mass matrix, the mass factor and the module mass matrix, respectively. Similarly, C , μ_i and C_i are the global damping matrix, the damping factor and the module damping matrix, respectively. The M_i can be estimated with an appropriate choice of inertial model and from data obtained from the structural plans. In the case of the module damping matrix, C_i , the mathematical structure can be based on Rayleigh damping at the module level, i.e.,

$$C_i = \alpha_i M_i + \beta_i K_i \quad (5)$$

and so

$$C = \sum_{i=1}^N \mu_i (\alpha_i M_i + \beta_i K_i)$$

although this formulation does not, in general, yield classical modes. With an appropriate choice of α_i , β_i and μ_i , namely,

$$\begin{aligned} \alpha_i &= \tilde{\alpha} \gamma_i \\ \beta_i &= \tilde{\beta} \theta_i \\ \mu_i &= 1 \end{aligned} \quad (6)$$

the global damping matrix takes the global Rayleigh damping form:

$$C = \tilde{\alpha} M + \tilde{\beta} K \quad (7)$$

where $\tilde{\alpha}$ and $\tilde{\beta}$ are the global Rayleigh damping factors to be determined. In this case, classical modes are ensured.

Damping models other than Rayleigh damping can be used. For example, modal damping could be employed, which is introduced via damping factors in the modal equations, and which independently control the damping in each of the modes. Modal damping would be appropriate to

use if the model response was computed via the modal equations rather than by direct integration of the equations of motion (1).

Estimation of Parameters

The second stage of the methodology corresponds to the estimation of the parameters $\tilde{\alpha}$, $\tilde{\beta}$ and θ_i . The parameters γ_i are all set to 1 since the mass matrix predicted by the inertial model is assumed to be sufficiently accurate.

The output-error method [1] is used to determine the parameters. For this method, an error vector e is defined as the difference between the system (observed) response and the model (calculated) response. The components of the error vector are given by

$$e_j(t; \tilde{\alpha}, \tilde{\beta}, \theta) = r_j^s(t) - r_j^m(t; \tilde{\alpha}, \tilde{\beta}, \theta) \quad (8)$$

where $r_j^s(t)$ is the system response and $r_j^m(t; \tilde{\alpha}, \tilde{\beta}, \theta)$ is the model response, and where $1 \leq j \leq M$ and M is the number of monitored degrees of freedom.

The least-squares method is used to determine the optimal values of these parameters. This can be interpreted as giving the most probable values of the parameters based on the data [1]. A measure of error $J = J(\tilde{\alpha}, \tilde{\beta}, \theta)$ is defined as

$$J = \int_0^{T_f} e^T(t) W e(t) dt \quad (9)$$

where the weighting matrix W is diagonal under the assumption that the components of e are statistically independent. Furthermore, if the errors at all degrees of freedom are assumed to have the same variance, σ^2 , then $W = 1/\sigma^2 I$ where I is the identity matrix. Least squares corresponds to minimizing the measure of error J . Since $J(\tilde{\alpha}, \tilde{\beta}, \theta)$ is not quadratic in $\tilde{\alpha}$, $\tilde{\beta}$ or θ_i , the equations associated with the minimization problem are nonlinear in the parameters. The values of these parameters are estimated using the conjugate-gradient method. The Polak-Ribiere algorithm was used in this study [2]. The calculation of the model responses was done by direct integration using Newmark's method [3] for the matrix equations with $\beta = 1/4$ and $\gamma = 1/2$.

Evaluation Stage

The evaluation stage of the methodology consists in observing how well the model data compares with the system data. Both the time history matching and the parameter estimates should be in agreement with the expected mechanical behavior of the system under study. It is conceivable that good response matching occurs even though the values of the parameters are not physically

meaningful. Alternatively, the methodology can yield an acceptable parameter set while the time domain matching of signals is poor (because of nonlinearities, for example). In most cases, the matching of response signals is straightforward but the interpretation of the parameter set is more difficult.

Test of Methodology

A useful first step in testing an identification methodology is to make use of simulated data. In this approach, parameter values are prescribed for a specified model and the necessary time domain signals are then calculated and made available as "measured" signals. One advantage of doing this is that the exact values for the parameters are known. Another advantage of simulated data is the fact that it can be contaminated with a controlled amount of noise and other similar effects. Furthermore, each of these effects can be examined independently.

The factors considered in this study that may cause inaccuracies in the determination of the parameters are the following:

Excitation related—

1. Location of the excitation
2. Frequency content of the signal

Response related—

1. Number of monitored degrees of freedom
and their location within the structure
2. Mechanical quantity to monitor

Noise in the measured signals

Number of parameters θ considered

Type of damage present in the structure

Model errors arising from discrepancies between the system and the mathematical form of the model are not considered in this study, but results will be reported at a later date.

Various numerical tests were performed in order to evaluate the robustness of the methodology. For these tests, a ten-story structure was chosen modeled as a chain system (the right-hand model in Figure 1). The structure was excited either at the base or at the roof with a broad-band, time-decaying signal depicted in Figure 2. Acceleration "measurements" were taken at each of the ten degrees-of-freedom. Damage was simulated by a 30% reduction of interstory stiffness at the 2nd and 3rd stories and a 10% reduction at the 4th level. This stiffness distribution can be seen in Figure 3. The values for $\tilde{\alpha}$ and $\tilde{\beta}$ were 0.471 and 0.0008, respectively, corresponding to 2% to 4%

damping for the four lower modes (and higher damping for the higher modes). The initial estimates of the parameter values corresponded to the undamaged system and were $\theta_i = 1$, $\tilde{\alpha} = 1.00$ and $\tilde{\beta} = 0.0001$. The difference between the true response and that due to the initial estimates can be seen in Figure 4. No noise was present in any of the signals, except when mentioned otherwise. The time step used in the numerical integrations was .02 sec and the number of time steps was 1024, producing signals 20.48 sec long. The fundamental period of the "damaged" structure was close to 1.1 sec, while the highest modal period was close to .07 sec.

Results and Discussion

1. Location of the Excitation

The structure was excited at two different locations: at the base and at the topmost degree of freedom, also referred to as the "roof." Figure 5 shows the stiffness distribution for the system ("true" or "exact" distribution) and as predicted by the two tests. The results for both cases were indistinguishable from the exact distribution. The roof case exhibited a "faster" convergence rate. This may be due to the fact that dynamic loading at the roof excites the higher modes more strongly than when exciting the structure through the base, thereby providing more "information" or "resolution." This can be seen more clearly in Figure 6 where the amplitude of the empirical transfer function for the base-excitation case decays with modal frequency while the one for the roof excitation peaks at the fourth mode.

2. Frequency Content of the Excitation

Two frequency bands were chosen in order to observe the influence of frequency content on the parameter estimates. The "low" frequency signal contained frequencies in the range 0 to 2 Hz. From the transfer function plots presented in Figure 6, it can be seen that only the first mode could have been significantly excited. The "high" frequency signal contained frequencies in the range 0 to 25 Hz as shown previously in Figure 2. The results for both the roof and the base-excitation are shown in Figures 7(a) and (b). The parameter matches were very good in all cases. The worst case corresponded to the low-frequency base-excitation signal (within 3% from the exact) and the best to the high-frequency roof excitation (indistinguishable from the exact). As expected, the smaller the high frequency content in the output signal, the lower the resolution and, thus, the slower the rate of convergence. This conclusion is similar to that drawn from the results in the previous section.

3. Number of Monitored Degrees of Freedom and their Location within the Structure

Three sets of signals were considered. In set 1, all degrees of freedom were monitored; in set 2, only the topmost degree of freedom was monitored, and in set 3, only the first degree of freedom was monitored (i.e., degree of freedom 1).

Figure 8(a) shows the results for the roof-excitation case. The results for sets 1 and 2 were almost exact, while for set 3 the results were poor. Figure 8(b) shows the results for the base-excitation case. Here, the results for sets 1 and 3 were accurate while for set 2 the results were poor. The poor results were expected in both situations because of non-uniqueness. Udwadia [4] has presented a discussion on output configurations for a chain system from which unique stiffness parameter values can be obtained in the base-excitation case and this can be extended to the roof-excitation case. The output configurations that produced the poor results are input-output configurations that lead to non-unique stiffness determinations. In the other situations, however, uniqueness is only guaranteed as long as "clean" information from all modes is present in the output signals as in this "noise-free" case. In the presence of noise, uniqueness is no longer guaranteed, but the more higher-mode-information there is, the better the accuracy that can be expected.

4. Mechanical Quantity to Monitor

Different quantities such as strains, displacements, stresses and accelerations can be monitored during actual tests. In this section, only two quantities are considered: displacements and accelerations.

Figure 9(a) shows the identified stiffness distribution for the roof-excited case. In this diagram, the values are only slightly off from the true distribution. In Figure 9(b), the results for base excitation are presented. When displacements were used as response signals, the estimates showed some error (up to 2%) but the estimates from the acceleration signals were very good.

The frequency content of the displacement signals involves only the lower frequencies. In the frequency domain, the acceleration amplitudes differ from the displacement amplitudes by a factor ω^2 where ω is the frequency. As the frequency increases, this factor becomes large. Thus, the acceleration signals have much larger components at higher frequencies than the displacement signals. This higher-frequency content leads to faster convergence rates in the parameter estimates when using acceleration signals.

5. Noise in the Measured Signals

Noise in the form of a Gaussian white-noise signal was added to both the input and the output of the system. The noise signal added to the input had an r.m.s. value equal to a specified fraction

of the r.m.s. value of the input signal. Similarly, the noise signals added to the output had an r.m.s. value equal to a specified fraction of the r.m.s. value of the response at the topmost degree of freedom. An illustration of how one of these signals was constructed is presented in Figure 10. The first level of noise considered corresponded to the case where the r.m.s. ratios were 0.5 (or 50% r.m.s. noise). The second level of noise corresponded to the extreme case of adding 100% noise. It is important to note that since the r.m.s. for the signal at the topmost degree of freedom is normally the largest, the ratios between the r.m.s. of the noise and the r.m.s. of the signals from the lower levels of the system were larger than the prescribed ratio.

Figure 11 shows the results for the noise-free case and for the 50% and 100% noise-added cases. Even though the stiffness values for the 100% case vary considerably, they remain within 30% of the exact results for the base-excitation case and within 10% for roof excitation. For the 50% noise case, the results remain very close to the exact distribution, within 14% for base excitation and within 5% for roof excitation.

6. Number of Parameters

The number of parameters used in the model may alter the accuracy of the results if the number becomes large. Three base-excited structures, with 10, 20 and 40 parameters (one for each module), were tested. For the 10 and 20 parameter cases, the accelerations at all degrees of freedom were monitored. For the 40 parameter case, only the accelerations at the even numbered degrees of freedom were monitored. The results were excellent in all three cases, as can be seen in Figure 12.

7. Type of Damage Present in the Structure

The sensitivity of the results to the "damage" pattern in the structure was considered. The first pattern consisted of a reduction of module stiffness at the 2nd, 3rd and 4th levels, as used in previous sections. The second pattern consisted of a similar stiffness reduction at the 7th, 8th and 9th levels. The third pattern was a combination of the two former patterns. Figure 13 shows that the estimates in all three cases were in excellent agreement with the true values.

8. Combination of Effects

Various effects were combined simultaneously in order to simulate a real situation more closely. The building was assumed to be 20 stories high and the accelerations were monitored at the base, at the second and 11th floors, and at the roof. The damage in the structure was as described in previous sections, that is, a reduction of stiffness of 30% was present at the second and third

stories and a reduction of stiffness of 10% at the fourth story. Noise was modeled by a Gaussian white-noise signal with an r.m.s. value 20% of the r.m.s. roof response for the output signals and an r.m.s. value 20% of the r.m.s. base acceleration for the input signal. Figure 14 shows the results corresponding to this more realistic situation. A maximum error of 7% in the estimates occurred at the roof. Significant damage could easily be detected and located to within the first few stories of the structure.

Conclusions

The cases where poor estimates were obtained are the following:

1. Roof excitation, acceleration at 1st degree of freedom monitored.
2. Base excitation, acceleration at top degree of freedom monitored.
3. 100% r.m.s. noise-to-signal ratio.

In the first two cases, the matching of the time responses was good, showing that this does not necessarily mean that the correct stiffness distribution is ensured. This can be seen clearly in Figure 15, where the signal matching corresponds to the problem described in Case 2 above. The problem in Cases 1 and 2 was that the conditions for uniqueness were violated, that is, the output was monitored at the wrong locations for uniqueness. Case 3 corresponds to an extreme case of noise and therefore it is not surprising that the errors were large. What was surprising in Case 3 was the fact that the estimates "distorted" gracefully as the noise level was increased and they remained well bounded.

In conclusion, the methodology for model identification provides accurate estimates if the following conditions are satisfied:

1. The input and output signals correspond to a configuration which, theoretically, provides unique results for the inverse (parameter estimation) problem.
2. The noise is small enough such that the information in the output from the higher modes is still significant.

If these conditions are satisfied, the results are expected to be reliable. Since uniqueness plays such an important role in the determination of the parameters, attention should be focused on establishing sufficient conditions for uniqueness in the inverse problem for an arbitrary analytical model of a structure.

References

- [1] J. L. Beck, "Probabilistic System Identification in the Time Domain," *Proceedings of the USAF/NASA Workshop on Model Determination for Large Space Systems*, Caltech, Pasadena, March 1988.
- [2] W. H. Press, et al., **Numerical Recipes**, Cambridge University Press, New York, 1986.
- [3] N. M. Newmark and E. Rosenblueth, **Fundamentals of Earthquake Engineering**, Prentice-Hall, New Jersey, 1971.
- [4] F. E. Udwadia, D. K. Sharma and P. C. Shah, "Uniqueness of Damping and Stiffness Distributions in the Identification of Soil and Structural Systems," *Journal of Applied Mechanics*, ASME, 45, pp. 181-187, 1978.

MOTIVATION

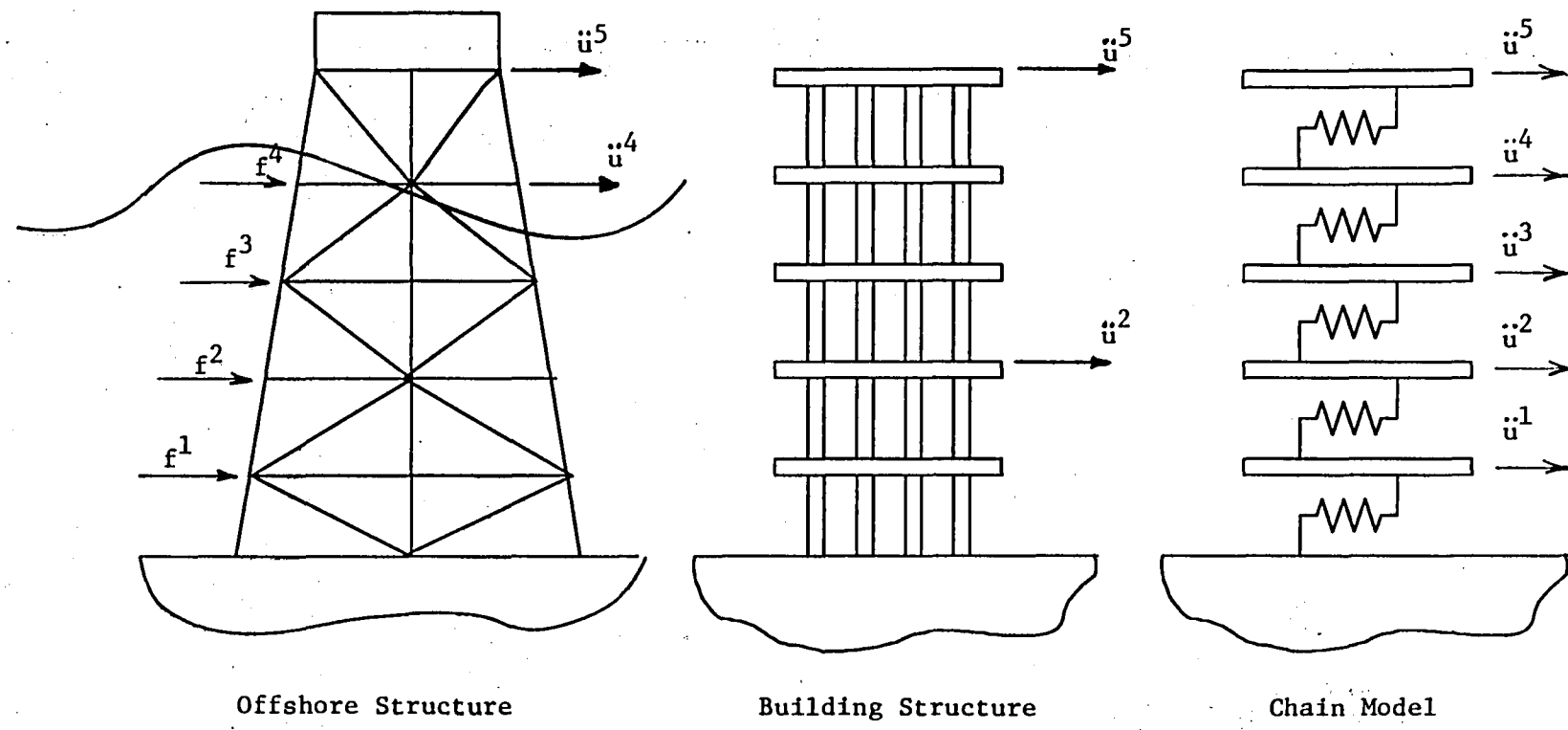


Figure 1.

EXCITATION SIGNAL

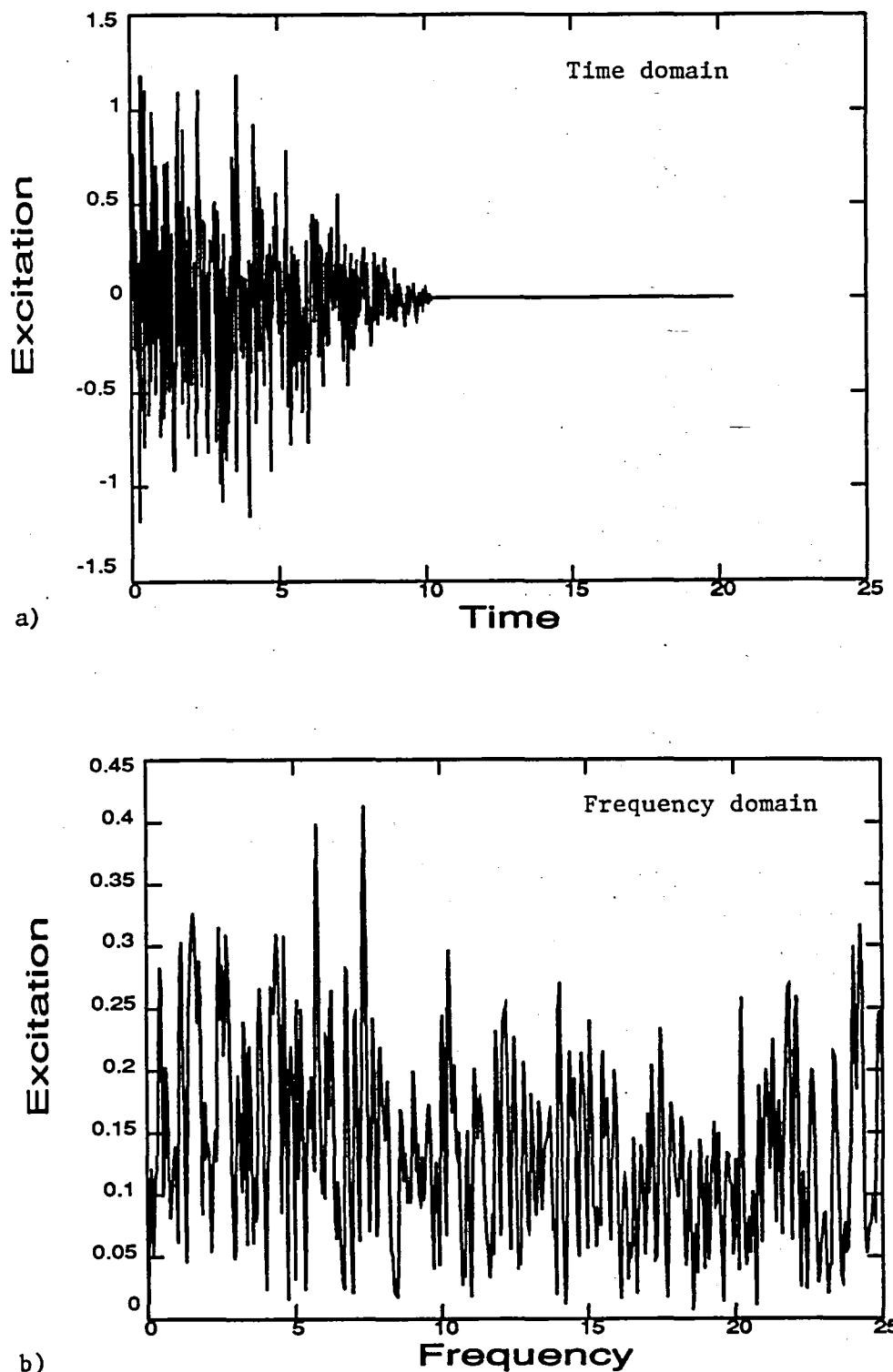


Figure 2.
Excitation signal used in the numerical tests. When used at the base, it is interpreted as acceleration. When used at any story, it is interpreted as a force. a) Time domain, b) amplitude of frequency spectrum.

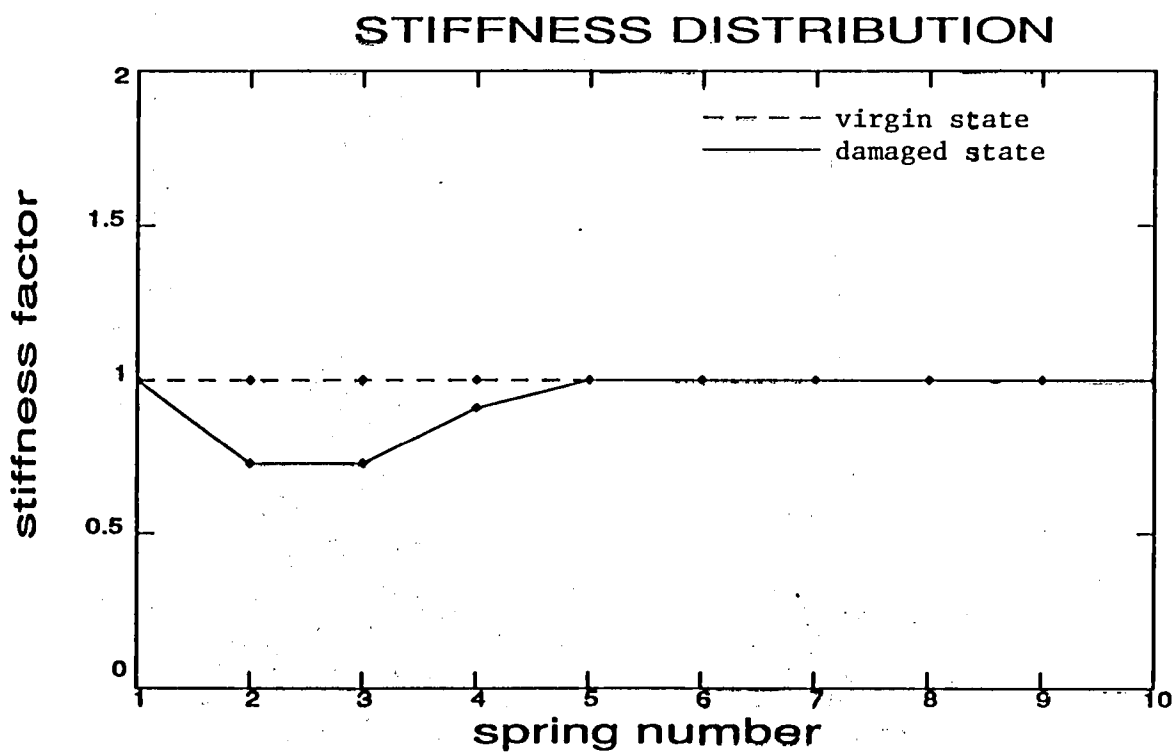


Figure 3.

Damage pattern within the chain system. Damage was modeled by a reduction in the lateral stiffness at the 2nd, 3rd, and 4th levels as depicted above. Damage was not present in the initial virgin state.

INITIAL AND SYSTEM RESPONSES

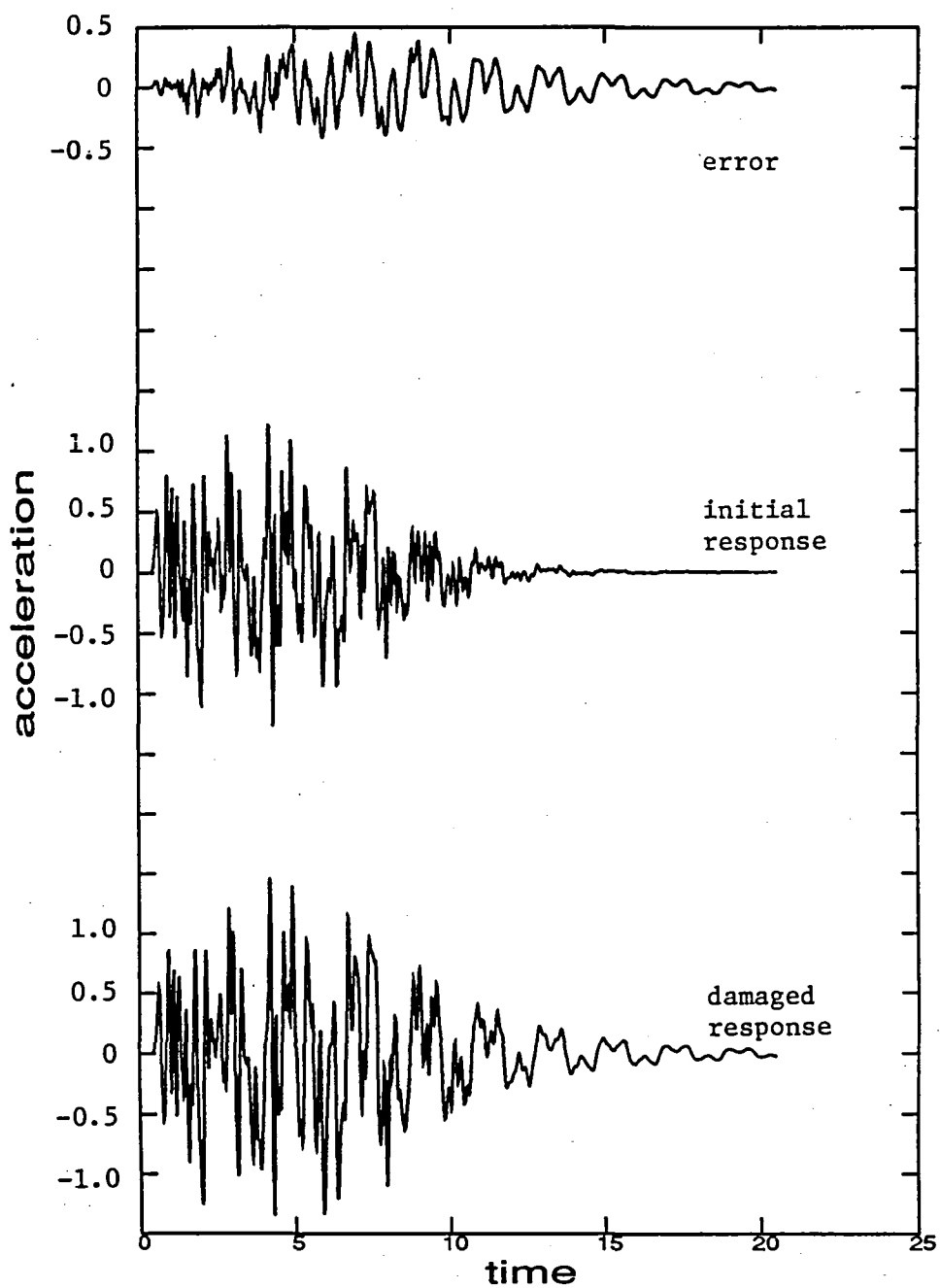


Figure 4.

Difference between the virgin and the damaged system responses. The difference or "error" is shown as the top signal.

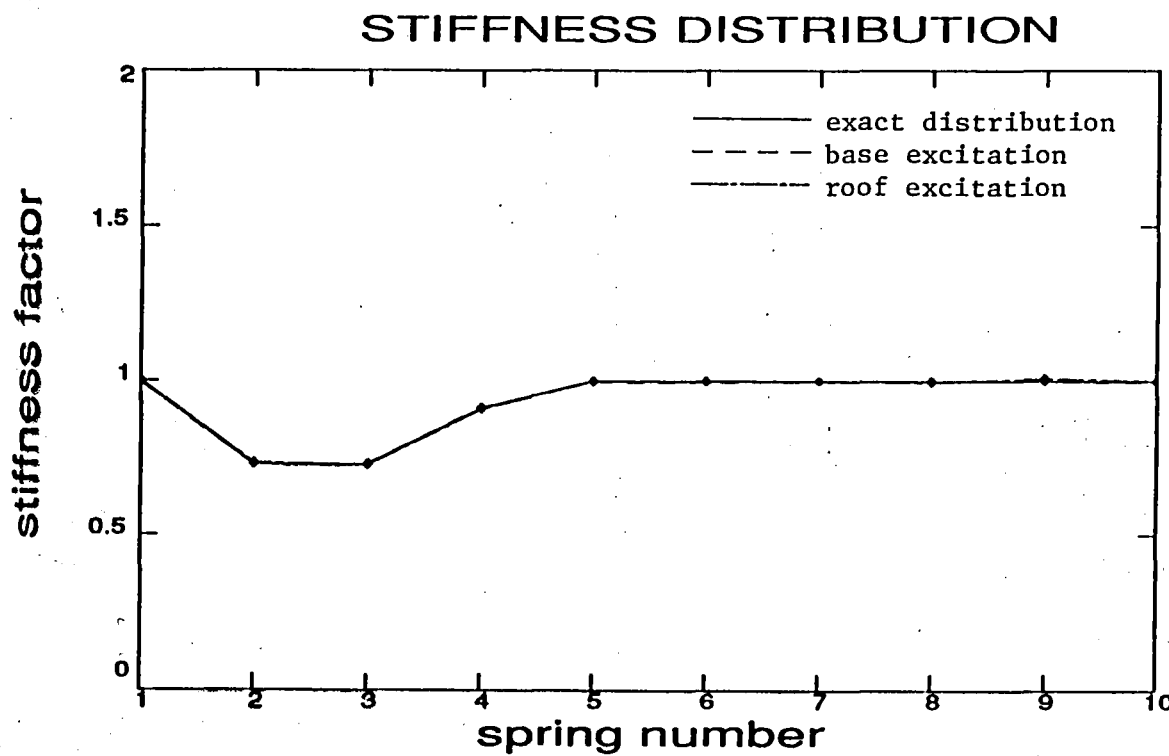
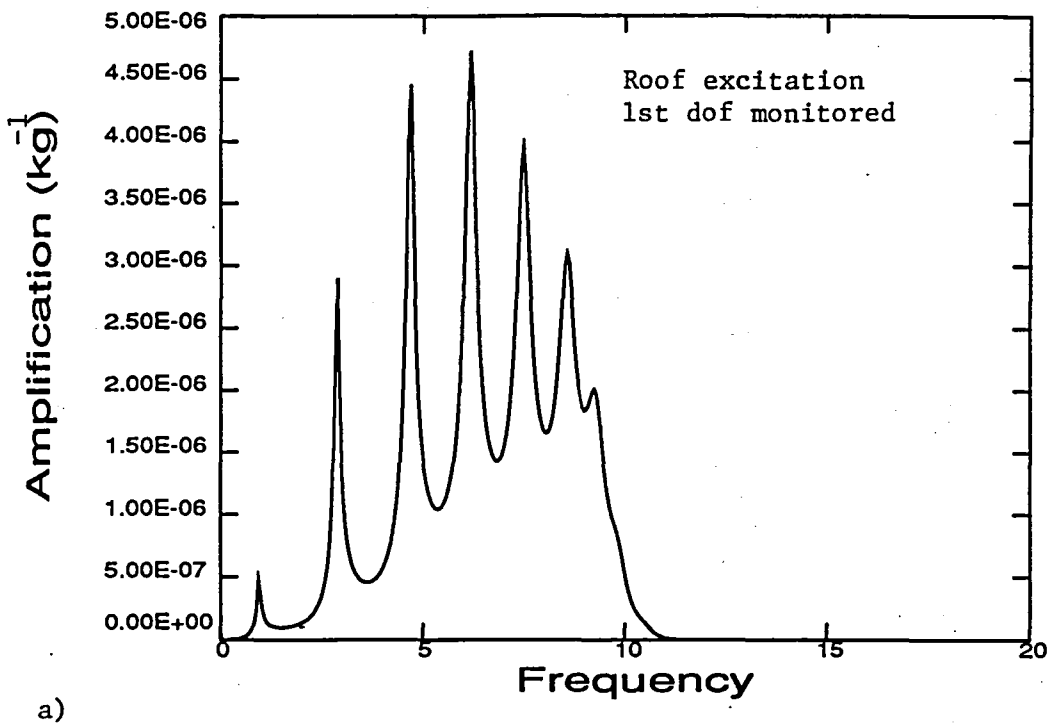


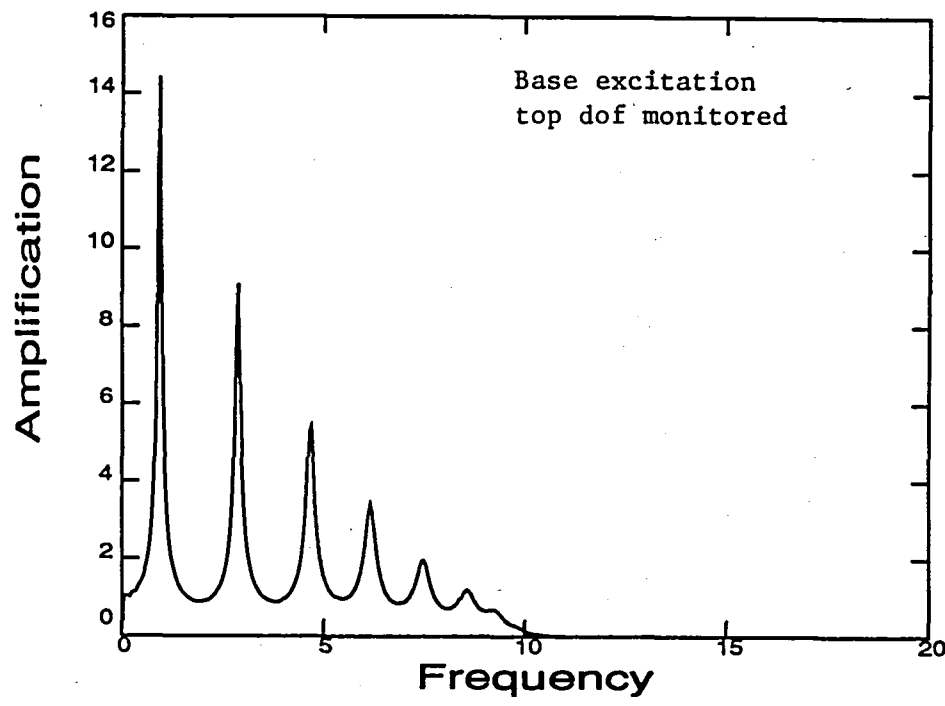
Figure 5.

Stiffness distributions for the chain system. The base-excitation estimates are not more than 0.5% off from the true distribution while the roof-excitation estimates are within 0.3% from the exact.

EMPIRICAL TRANSFER FUNCTIONS



a)



b)

Figure 6.
Amplitude diagrams for two empirical transfer functions. a) Transfer function between the acceleration at the first degree of freedom and the excitation at the roof; b) transfer function between the acceleration at the roof and the acceleration at the base.

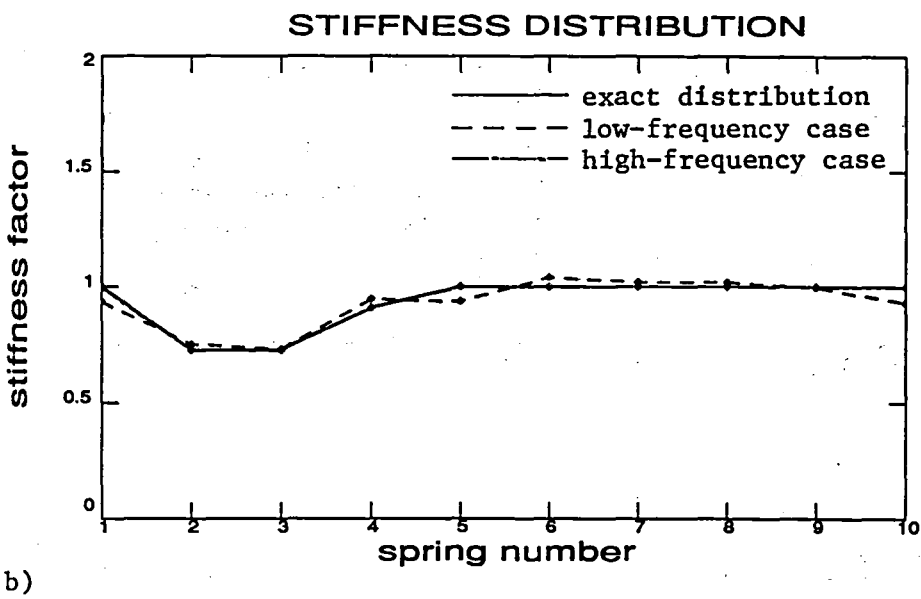
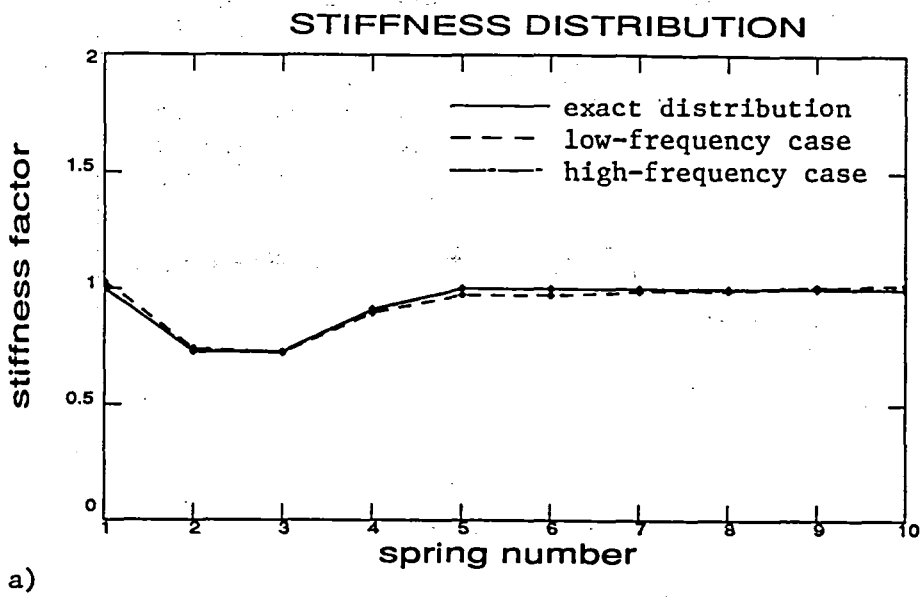


Figure 7.
 Estimation of the stiffness distribution from tests with excitation signals containing different frequency contents. a) Roof-excitation results. The high-frequency results are closer to the exact distribution than the low-frequency results. The latter are within 3% from the exact. b) Base-excitation results. The same features are presented here except the the low-frequency results are not as close to the exact distribution (only within 5% from the exact).

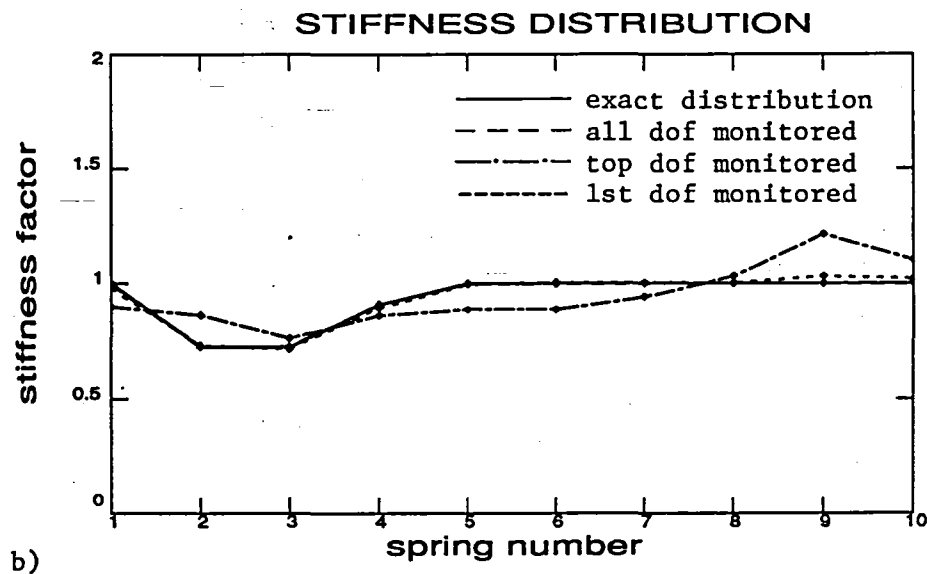
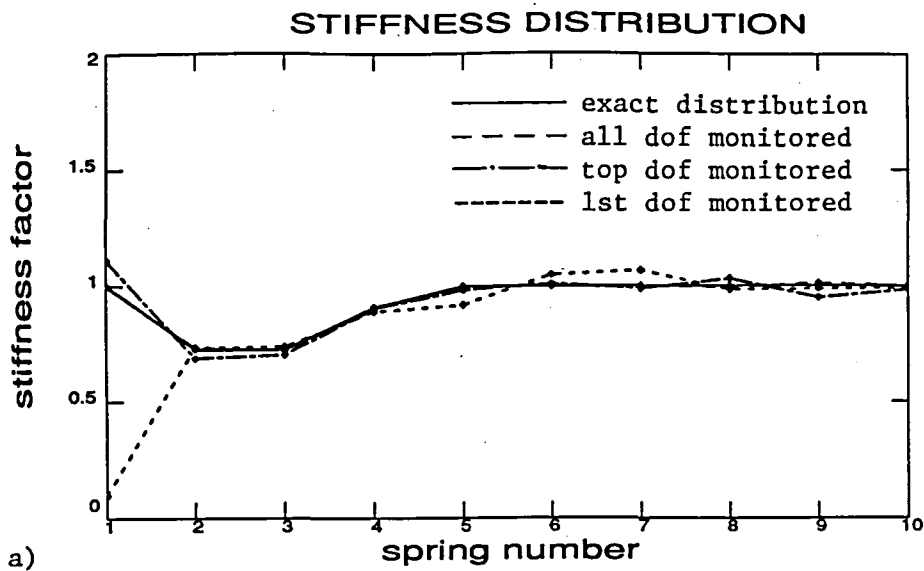
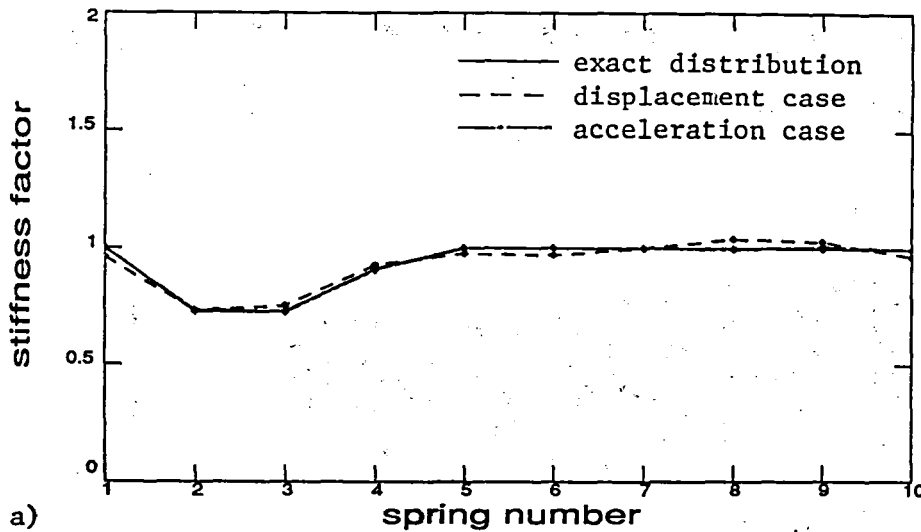


Figure 8.

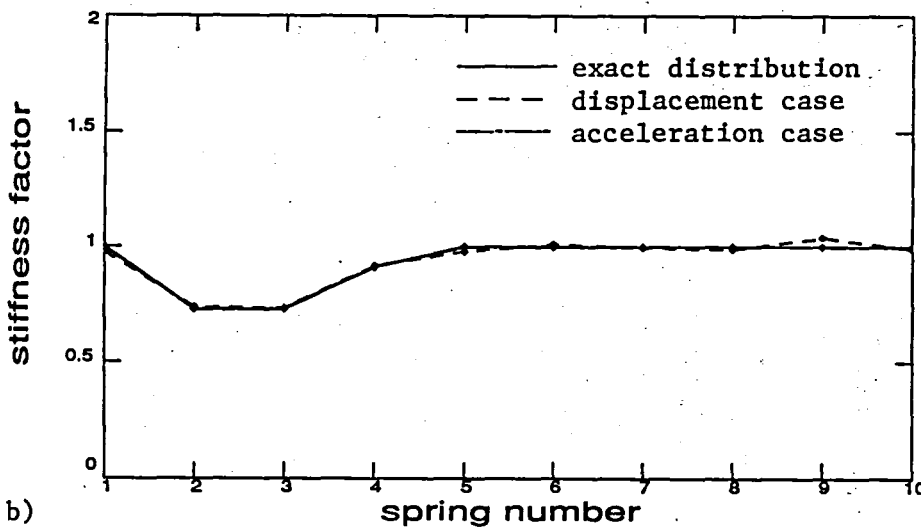
Measurement of signals at different locations within the structure may yield inaccurate results if the input-output combinations correspond to non-unique configurations. a) Roof-excitation results: large inaccuracies occur when degree of freedom 1 is monitored, otherwise, there is good agreement. b) Base-excitation results: here the results are inaccurate when the topmost degree of freedom is monitored, otherwise, the results are close to the exact.

STIFFNESS DISTRIBUTION



a)

STIFFNESS DISTRIBUTION



b)

Figure 9.

The effect of the monitored quantity on the results are shown for the roof-excitation case (diagram a)) and for the base-excitation case (diagram b)). The displacement-based results are not as close to the true distribution as the results for the case where the accelerations were monitored. The errors were worse for the roof-excitation case but still remained within 2% of the exact.

CONSTRUCTION OF A SIGNAL WITH NOISE

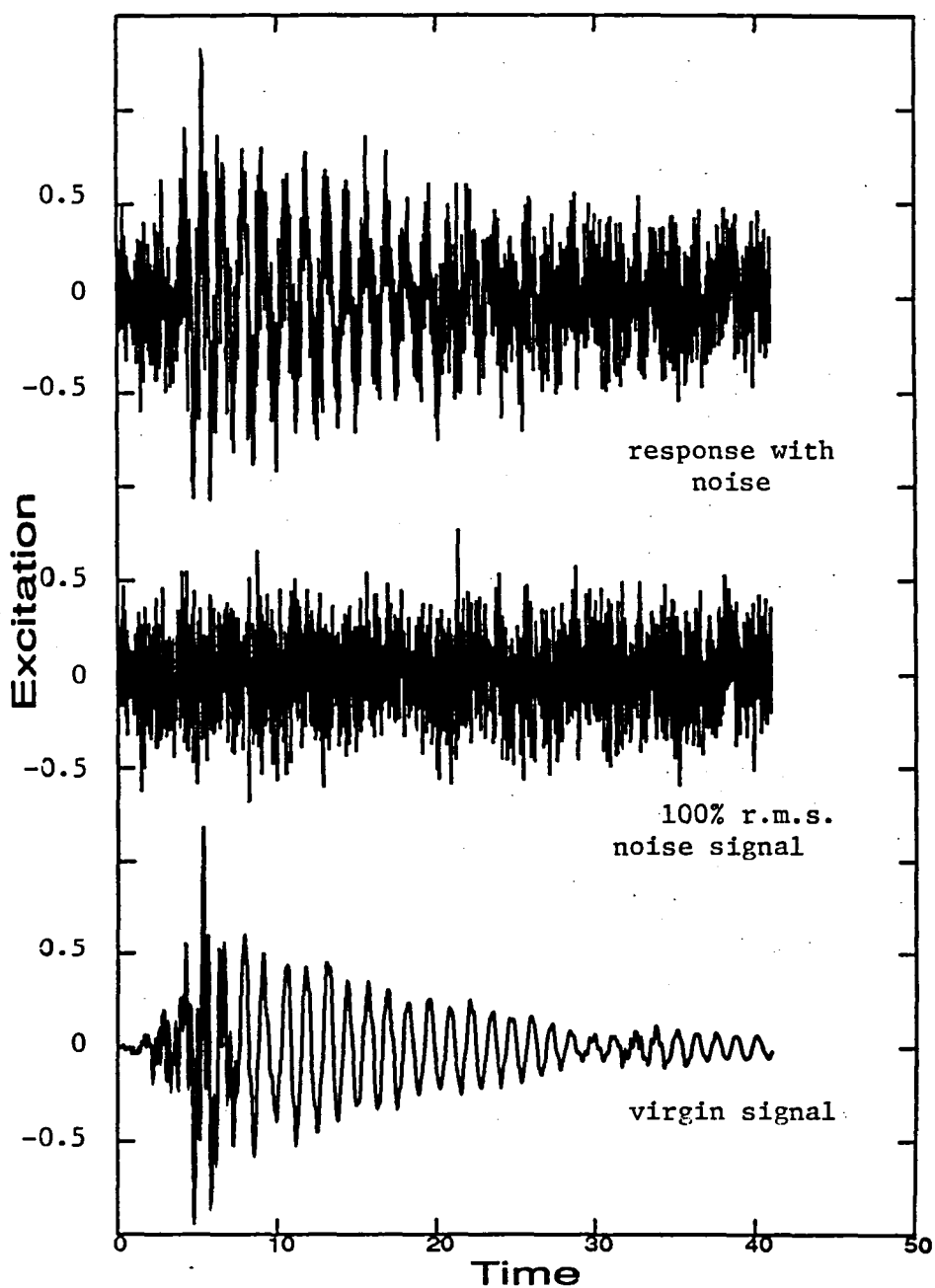


Figure 10.

This diagram shows the method employed to construct the "noisy" signals. Noise in the form of a Gaussian white-noise signal was added to all input and output signals. The size of a noise signal was characterized by its r.m.s. value. This r.m.s. value was predefined as a fraction of the r.m.s. value of the base acceleration (for input signals) or of the r.m.s. value of the roof acceleration (for output signals).

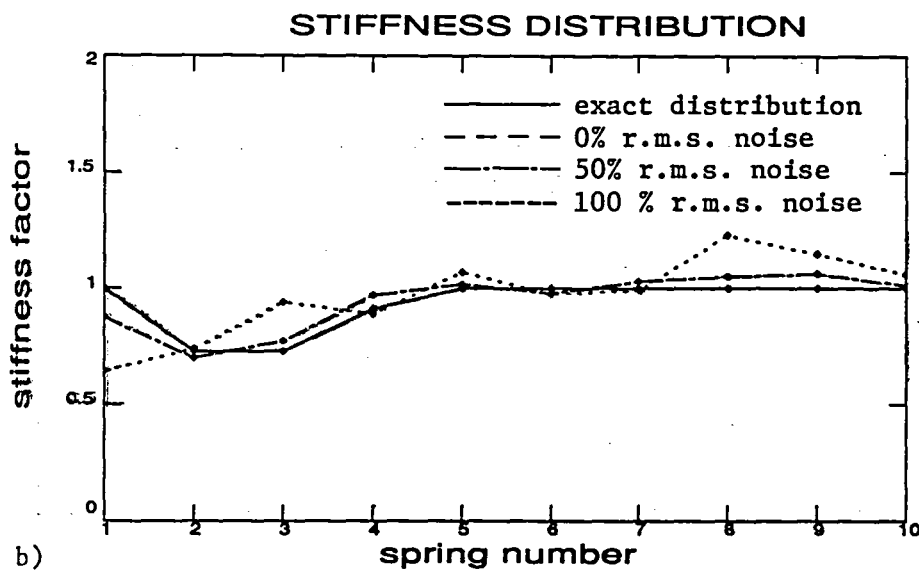
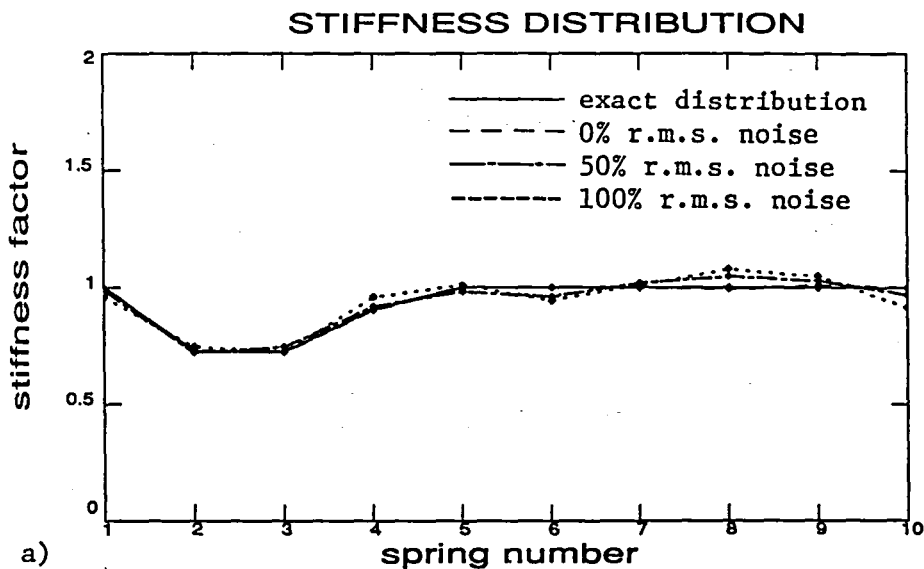


Figure 11.
 The effects of noise on the accuracy of the estimates were smaller than expected. For the extreme case of 100% r.m.s. noise-to-signal ratio, the errors were within 10% of the exact for roof excitation and within 30% for base excitation. For the more realistic case of 50% r.m.s. noise, the errors were within 5% for roof excitation and within 14% for base excitation. a) Roof-excitation results, b) base-excitation results.

STIFFNESS DISTRIBUTIONS

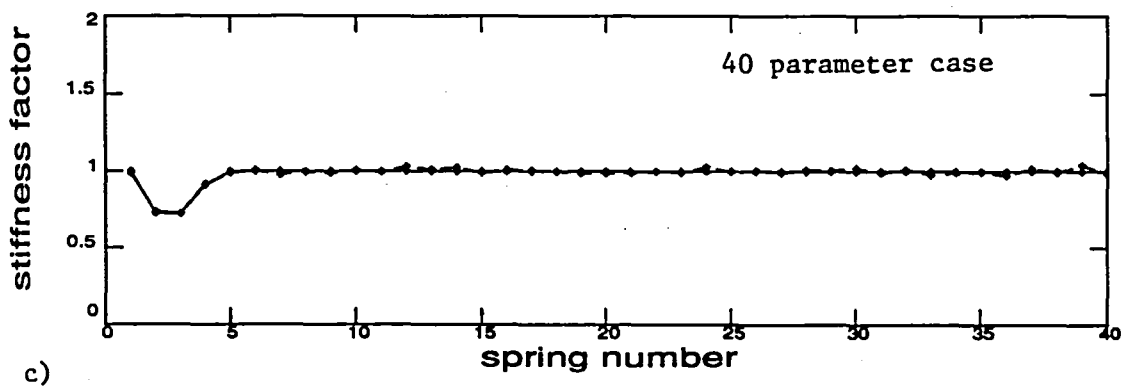
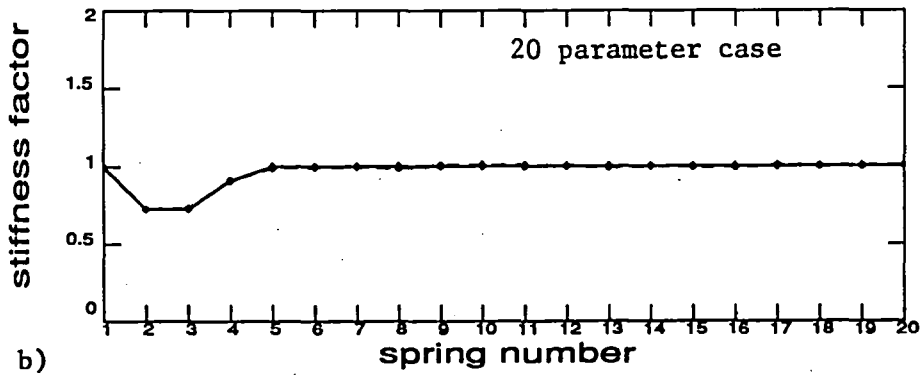
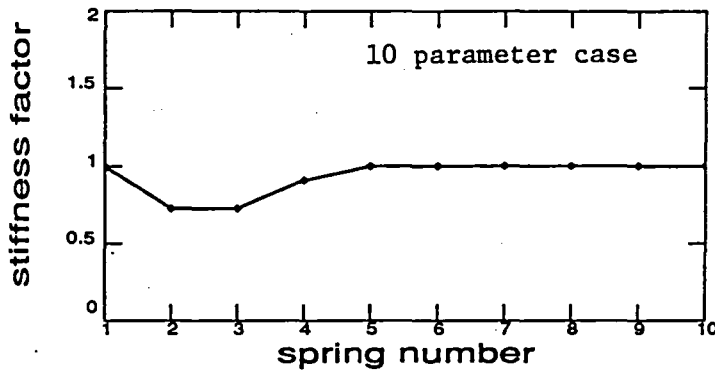


Figure 12.
Identification of the stiffness distribution appear to be insensitive to the number of parameters (i.e. modules) employed. a) 10-parameter case, b) 20-parameter case and c) 40-parameter case.

STIFFNESS DISTRIBUTIONS

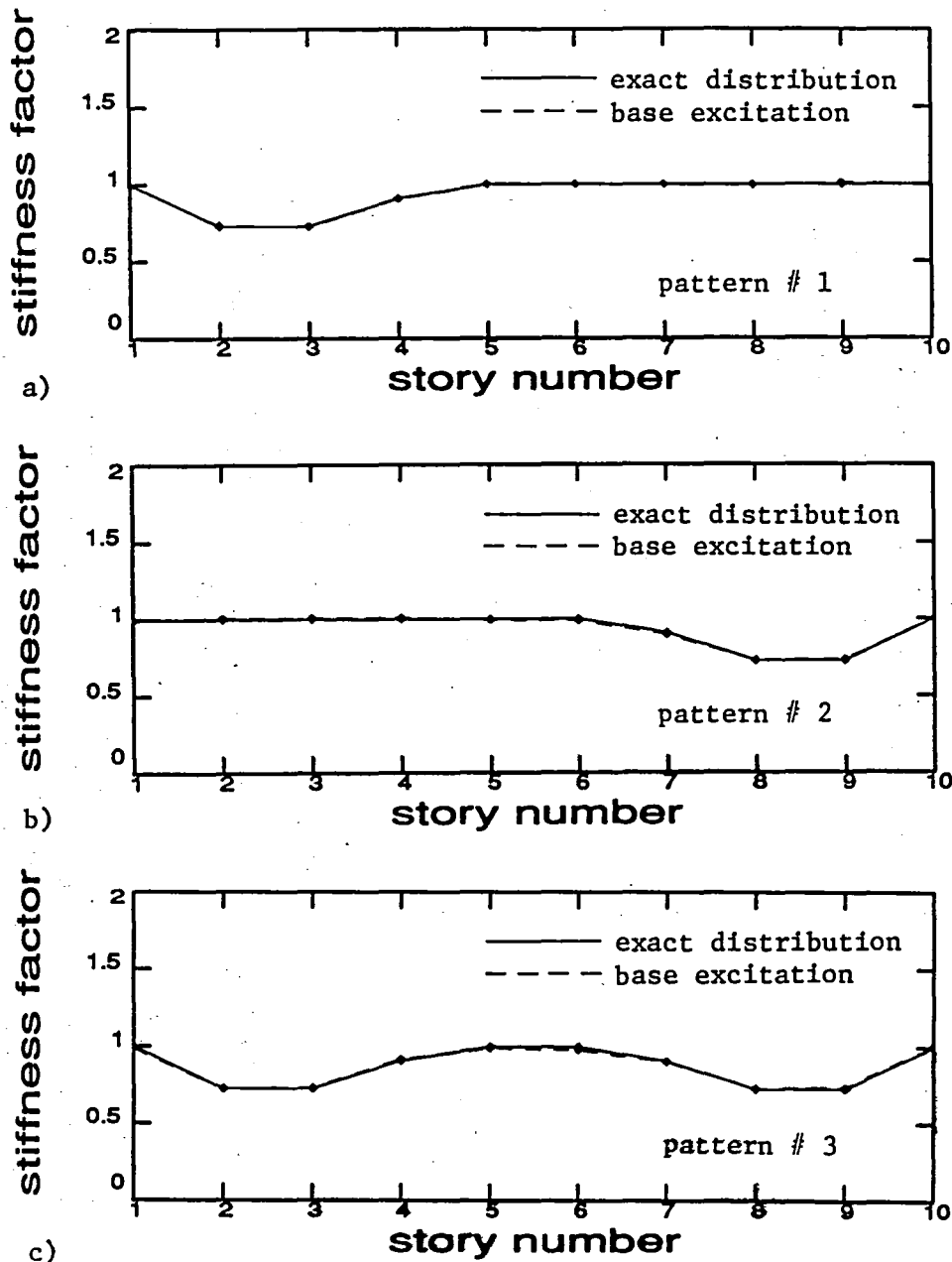


Figure 13.
The effects of the type of damage on the parameter estimation procedure are seen to be small. a) Pattern # 1, b) pattern # 2, c) pattern # 3.

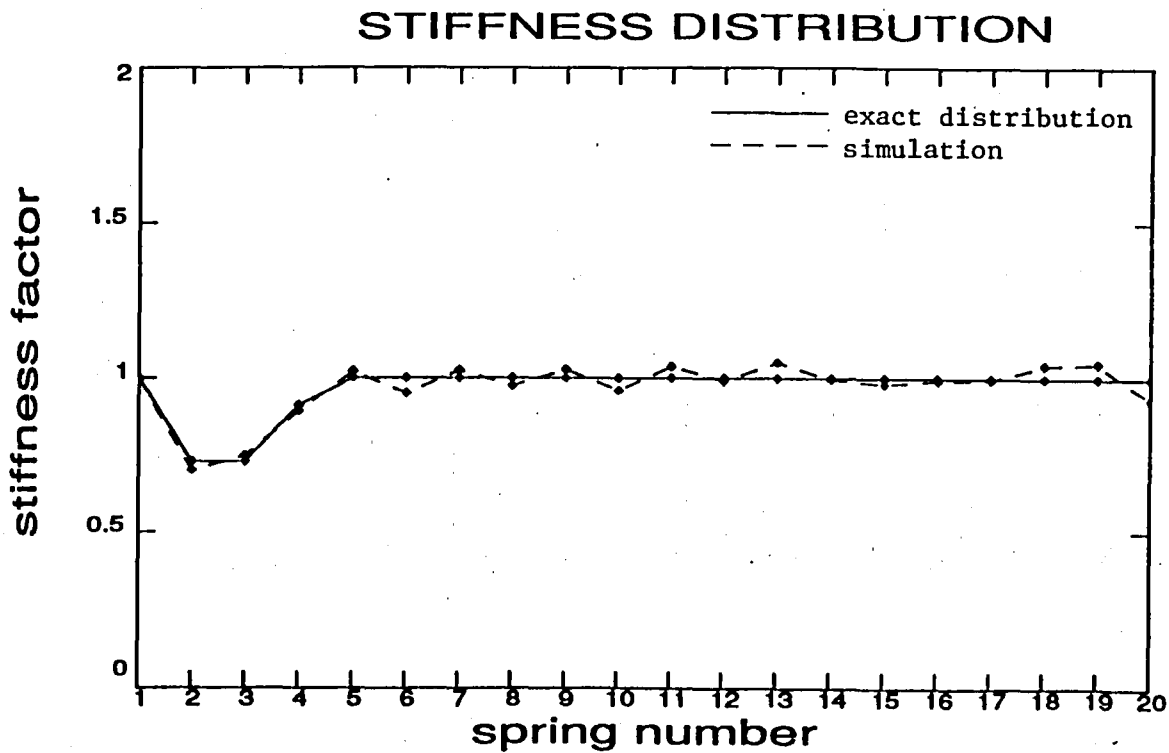


Figure 14.
Comparison between the exact distribution and the results corresponding
to the more realistic simulation. The estimation problem was
characterized by a) excitation at the base, b) monitoring of acceleration
signals at degrees of freedom 1, 10 and 20 and c) 20% r.m.s. noise added
to the input and output signals.

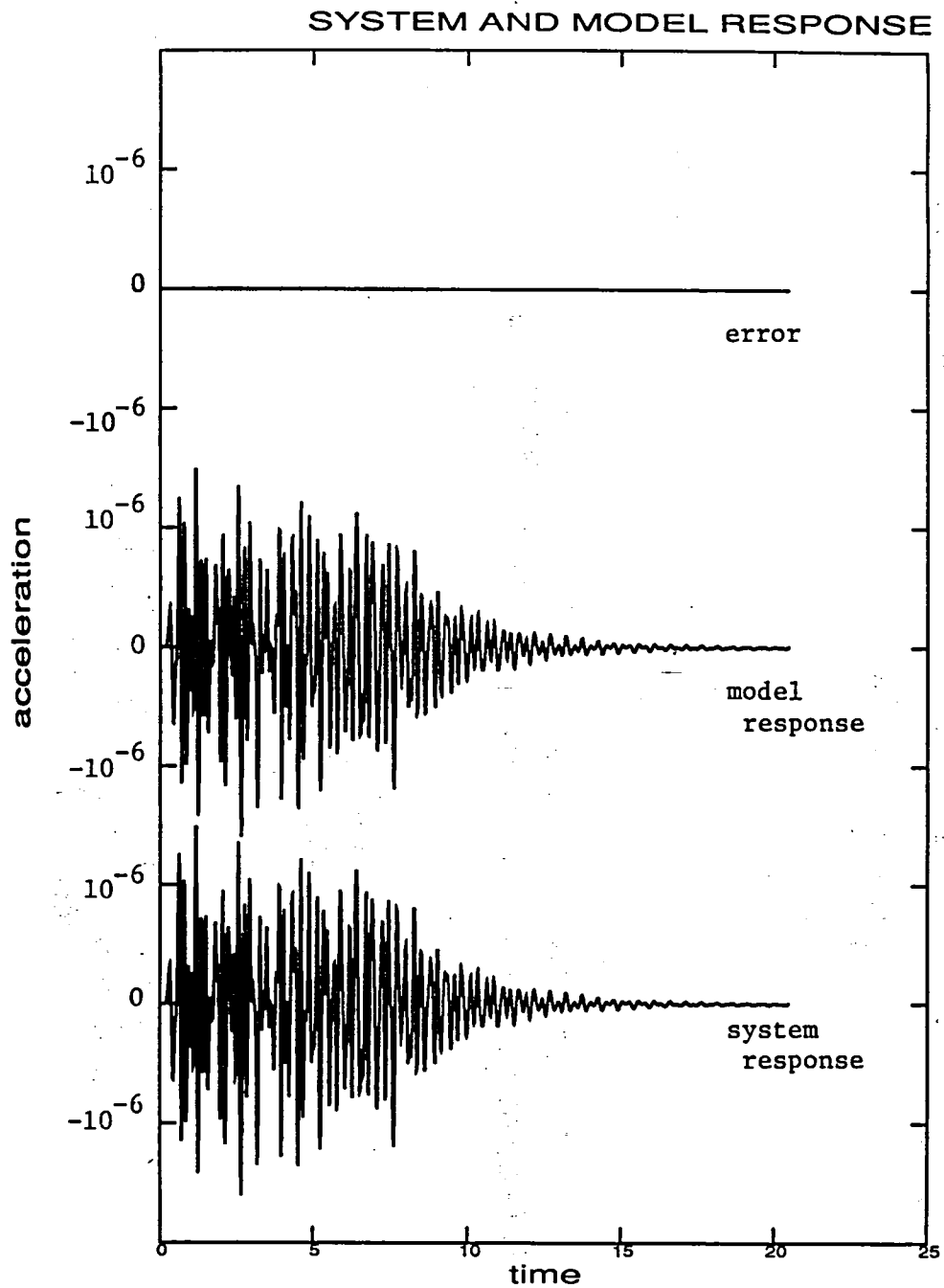


Figure 15.

Matching of the system response by a model response can be quite accurate as seen in the error signal above. The situation corresponds to the roof excited, 1st dof-monitored case of Figure 8a. This accuracy, however, does not always imply a correct stiffness distribution as Figure 8a demonstrates.

5115
16382
P-35
NONPARAMETRIC IDENTIFICATION
EXPERIMENT

Yeung Yam

1222-393-2221
USAF/NASA WORKSHOP ON MODEL
DETERMINATION FOR LARGE SPACE SYSTEMS

JPL

Jet Propulsion Laboratory
California Institute of Technology
March 23, 1988

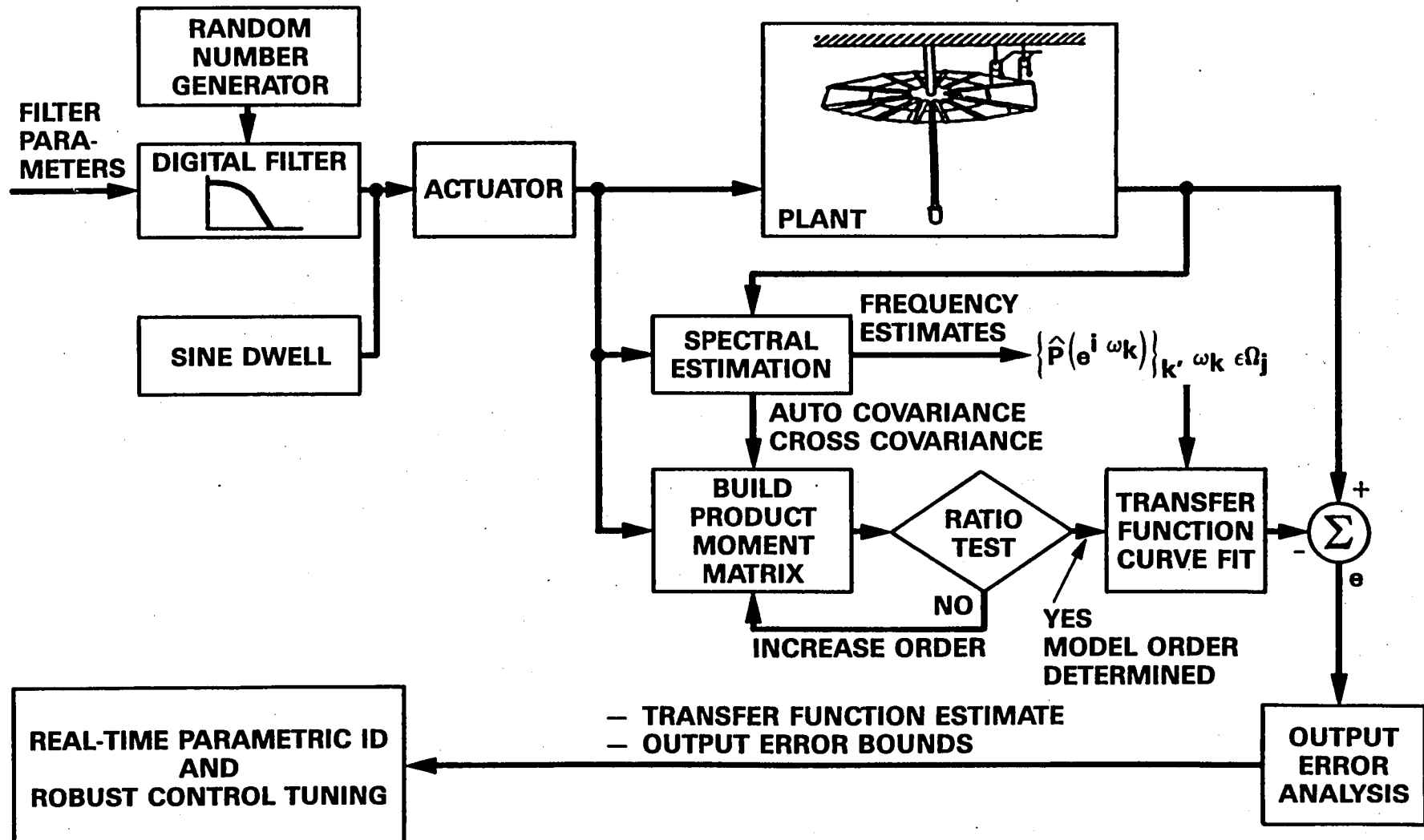
The Nonparametric Identification and Model Determination methodology is shown in this viewgraph. There are three types of excitation input to the plant via the actuator. The first is the wideband excitation in which case the random number generator is fed directly into the actuator and plant bypassing the digital filter. Wideband excitation has an evenly distributed energy spectrum and tends to excite all modes of the plant. The second type is the narrowband excitation obtained by passing the random number generator output through a digital filter to excite the plant modes in a desired frequency range. The third type is the sine dwell. The plant excitation is a sinusoidal input of a particular frequency of interest.

The excitation input and corresponding output of the plant are fed into the spectral estimation algorithm as shown. The spectral estimation algorithm computes the auto- and cross-covariances of the input and output as well as the Fourier transform, i.e., the power spectral density (PSD), of these covariances. The transfer function of the plant is generated as the ratio of the input/output cross-covariance PSD to the input auto-covariance PSD. As transfer function is the Fourier Transform of the plant impulse response function, the plant output due to any general input can in theory be composed based on the transfer function estimates. Hence, at this point, the plant is completely characterized without the need to define and determine any relevant plant parameters. This is the so called nonparametric system identification technique.

In general, however, a knowledge of the plant model/parameters is extremely useful, especially in designing control systems. To facilitate this, a model determination algorithm is thus included in the methodology. There are two parts of the model determination algorithm. The first is the model order determination based on the product moment matrix test. Two options for forming the product moment matrix (PMM) are possible in this work. One generates the PMM directly from the plant input and output. The other assumes statistical stationarity for the process and forms the PMM using the covariances from the spectral estimation. The second option is computationally less intensive but may be less reliable due to the fact that the stationary assumption may not be strictly satisfied. The results to be presented here are generated via the first option.

The determined model order from the PMM test and the estimated transfer function are passed to the transfer function curve fitting algorithm. Based on a least square subroutine, the curve fitting algorithm determines the modal parameters, frequencies and damping coefficients, of the plant. A measure of the quality of this curve fitted modal plant model can be obtained by taking the difference of the actual plant output and the curve fitted plant model and performing the output error analysis. Advanced parametric identification schemes and robust control tuning designs can be performed based on the curve fitted plant model and the output error bounds, which is effectively a measure of the reliability of the curve fitted plant model.

NONPARAMETRIC IDENTIFICATION AND MODEL DETERMINATION



This viewgraph briefly summarizes the present identification technique. There are three kinds of inputs, namely, wideband, narrowband, and sine-dwell. The spectral estimation algorithm computes the covariances and PSD of the plant input and output, and obtains the transfer function by dividing the PSD of input-output cross-covariance by the PSD of the input auto-covariance. In general, from the estimated transfer function obtained for a wideband excitation, frequency ranges or particular frequencies of interest can be selected for narrowband or sine-well experiments. The present experiment software has the ability to put together data from several narrowband and sine-dwell experiments and form the transfer function for a wide frequency range.

The covariances and PSD from the spectral estimation are passed to the PMM test and transfer function curve fitting algorithms, respectively. The product moment matrix determines, directly from the plant input and output or through the covariances, the estimated order for the plant. This information is passed to the curve fitting subroutine as well. The transfer function curve fitting algorithm generates estimated value of the modal frequencies and damping ratio and based on these, the curve fitted transfer function for the plant. This can be done for individual and integrated data sets of wideband, narrowband, and sine-dwell experiments.

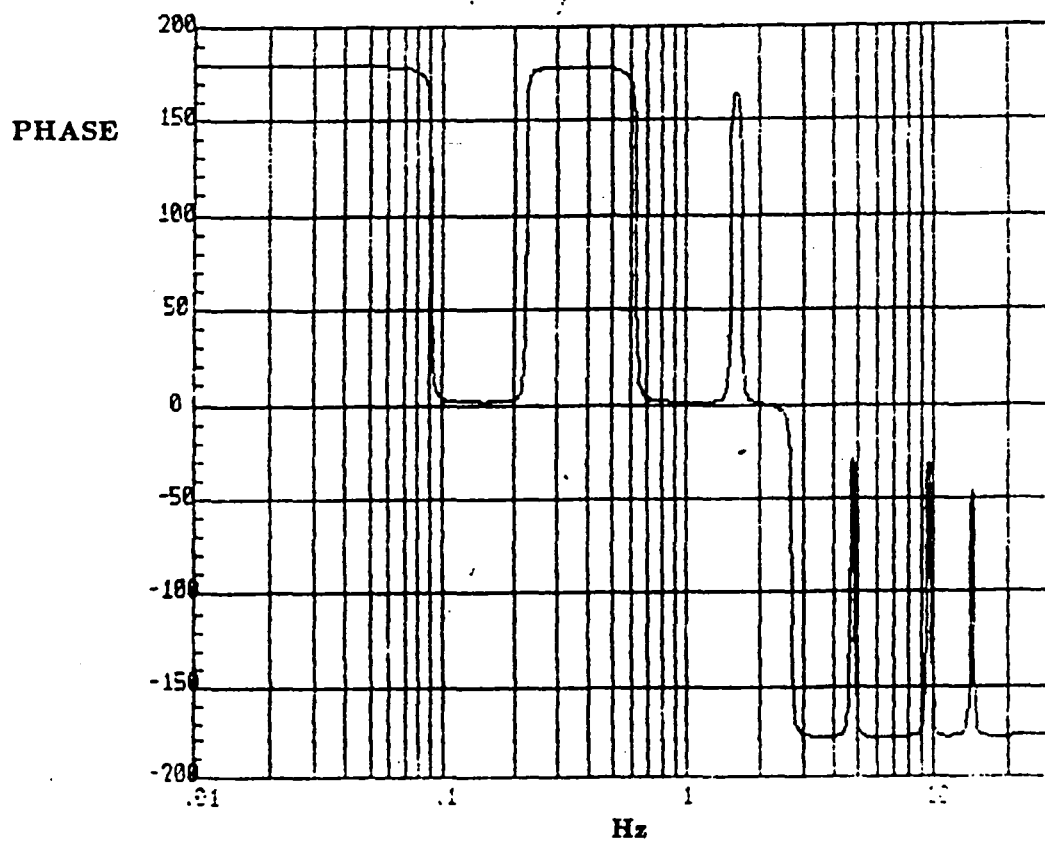
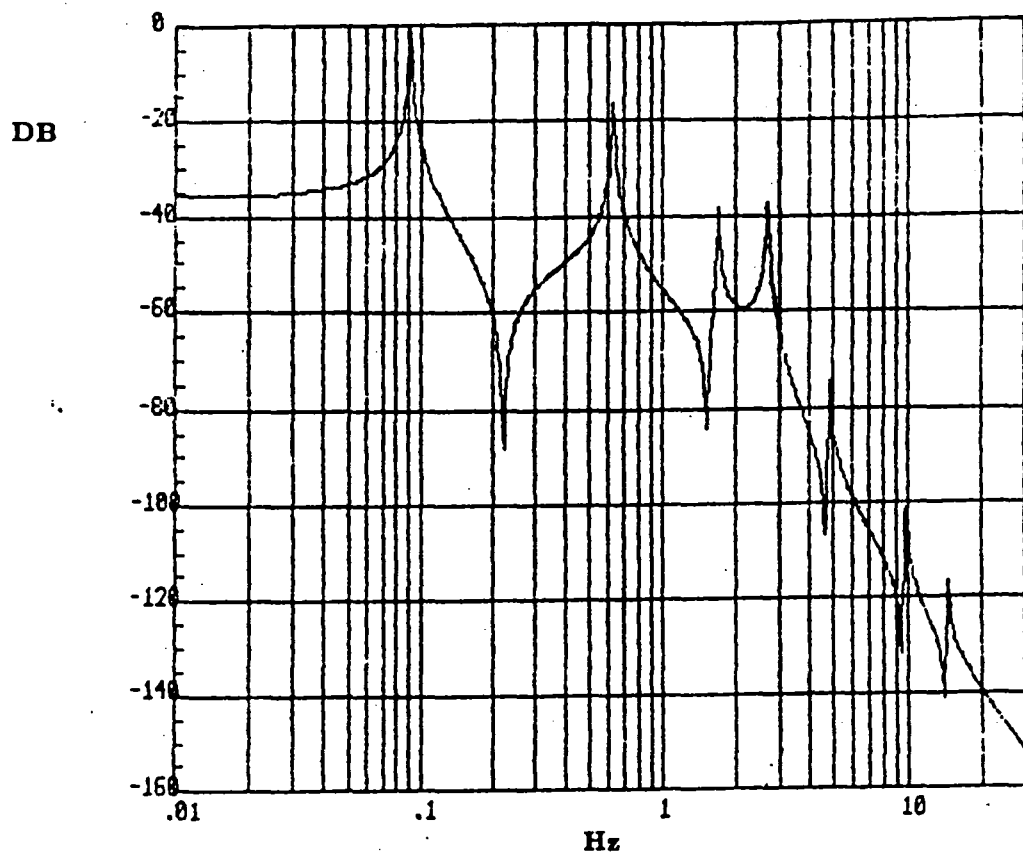
The present approach serves to generate a minimal representation of the plant in the range of frequency of interest and for the relevant set of input/output points. Output error analysis can be facilitated to have a measure of the reliability of the identified plant model. Fine determination of the modal frequencies can be conducted through binary search of the transfer function resonance peaks via sine-dwell excitation. Nonlinear dynamic characterization can be accommodated within the present approach by repeating the sine-dwell and resonance tuning processes with different input amplitudes.

JPL ON-ORBIT NONPARAMETRIC ID METHODOLOGY

- PROVIDES A-PRIORI KNOWLEDGE FOR REAL-TIME PARAMETRIC ID
 - INITIAL FREQUENCY ESTIMATES FOR BLOCK PROCESSING MLE
 - CHOICE OF PREFILTERS IN RECURSIVE ALGORITHMS
 - INSURE SPR CONDITION FOR PSEUDO-LINEAR REGRESSIONS
- SPATIAL AND FREQUENCY DOMAIN PARTITIONS
 - WIDEBAND SURVEY TO ESTABLISH PARTITIONS
 - GLOBAL CHARACTERIZATION OF STRUCTURE
 - FINE RESOLUTION OF CLOSELY SPACED MODES
- WIDEBAND DATA COMPOSED FROM NARROWBAND EXPERIMENTS
 - OVERCOMES ACTUATOR POWER CONSTRAINTS
 - ENSURES EXCITATION OF HIGH FREQUENCY MODES
- OUTPUT ERROR CHARACTERISTION
 - DETERMINES ACCURACY OF CURVE FIT
 - PROVIDES ROBUST CONTROL UNCERTAINTY BOUNDS

The nonparametric identification and model determination experiment software has been developed. Simulation validation of the software has been carried out. Part of the results are to be presented here. This viewgraph shows the analytical model utilized in the simulation. It is the actual designed model developed for the experiment structure with hub torquer as the input point and the boomfeed as the output point. A total of seven modes is included in the simulation. The frequencies are: 0.09 Hz, 0.63 Hz, 1.68 Hz, 2.68 Hz, 4.89 Hz, 9.89 Hz, and 14.6 Hz. The damping coefficient for all modes is 0.007. This will be the transfer function the present identification process attempts to reconstruct/verify.

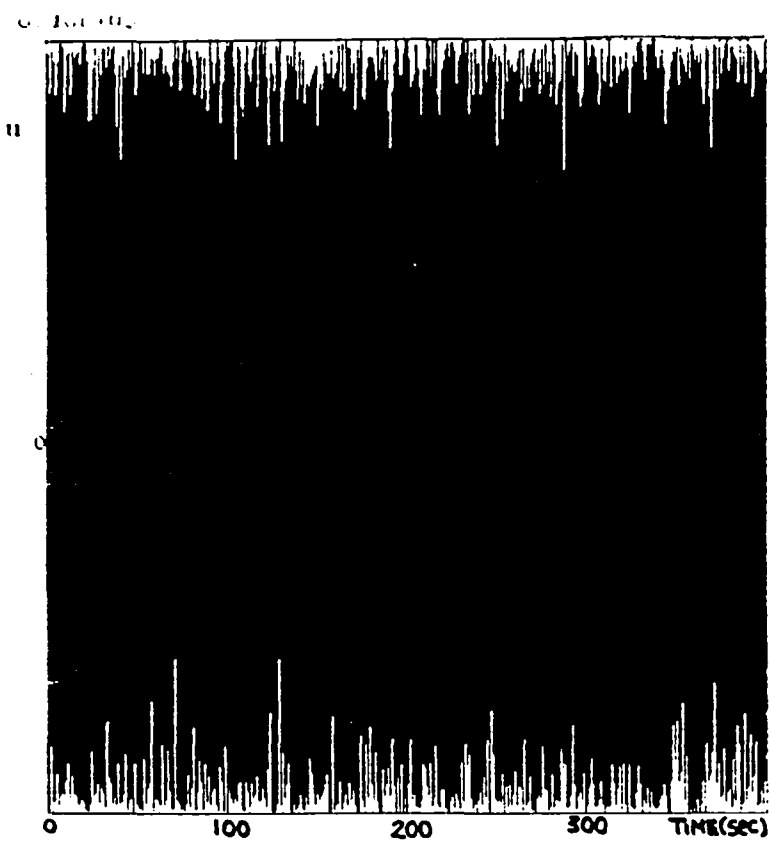
ANALYTICAL MODEL UTILIZED FOR SIMULATION



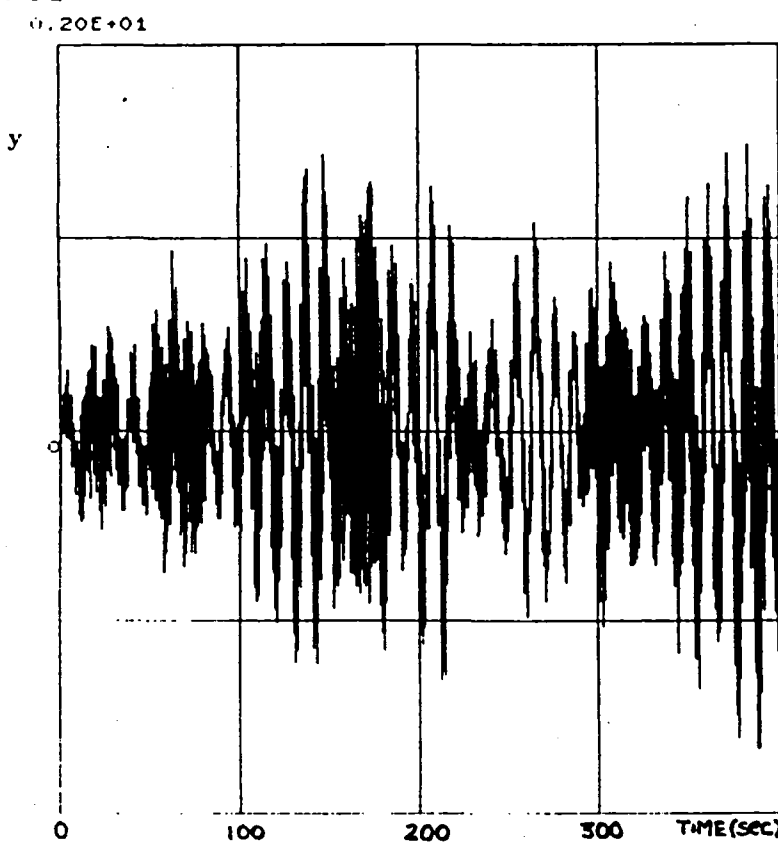
The first case to be presented is the wideband excitation. The plant input and output are shown here. Simulation data of a 1000 second experiment are generated but only 400 seconds of that data are presented here. The plant input and output are fed into the spectral estimation algorithms and the PMM test subroutine for further processing.

WIDEBAND EXCITATION

PLANT INPUT



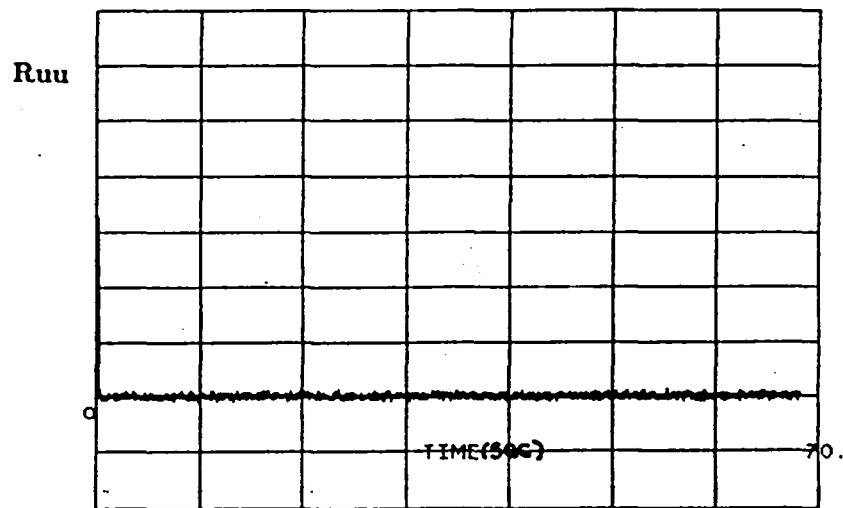
PLANT OUTPUT



This viewgraph presents examples of covariance estimates and the PMM test results. The auto-covariance of the input closely resembles a delta function, as it should be. The covariances estimates are passed into the PMM test subroutines. As mentioned before, the PMM test routine can generate the PMM via direct computation using plant input/output data, or from the covariance estimates assuming a stationary process. The results presented in this work are all generated via the first option. The essence of the PMM test is as follows: If the assumed plant order is larger than the actual order as reflected in the data, the PMM becomes singular and yields a zero value for its determinant. The PMM matrix determinant as a function of the number of assumed modes in the plant is shown here. It indicates that although the simulation is carried out with seven modes in the model, only four of them are reflected in the data.

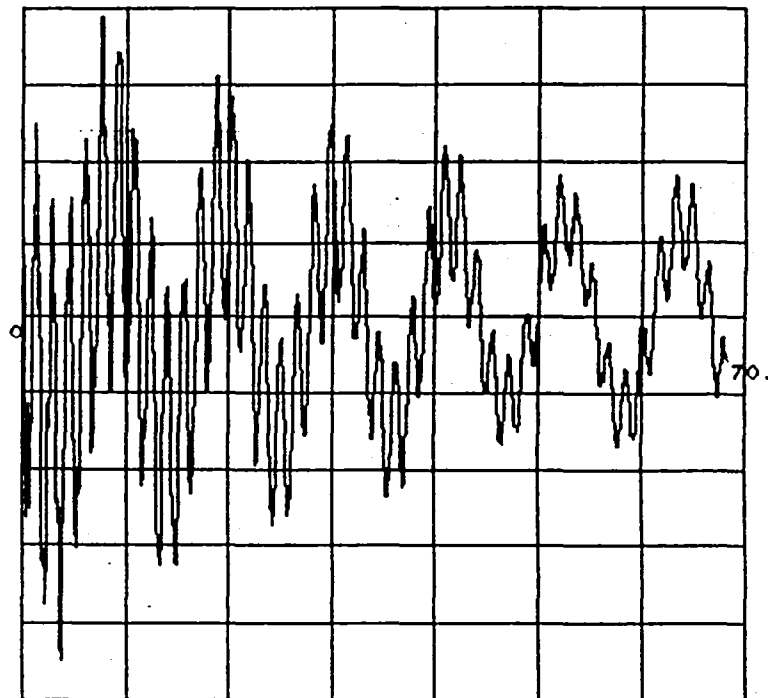
SPECTRAL ESTIMATION: COVARIANCE ESTIMATES

0.35E+04



0.25E+01

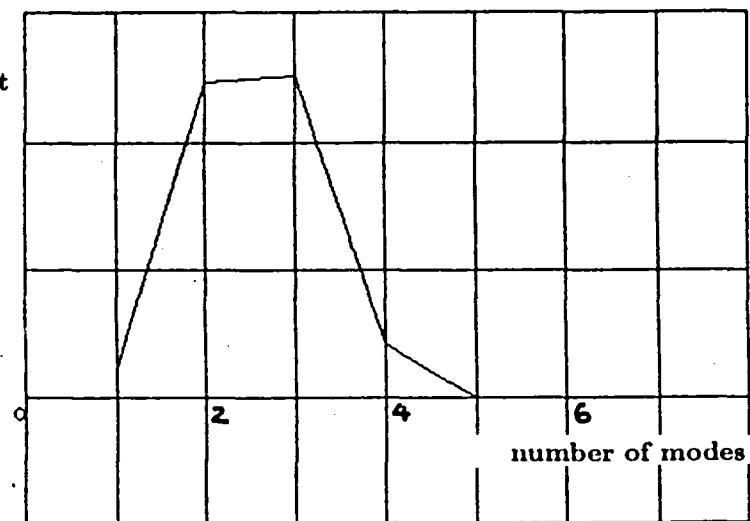
Ruy



PRODUCT MOMENT MATRIX TEST

0.15E+05

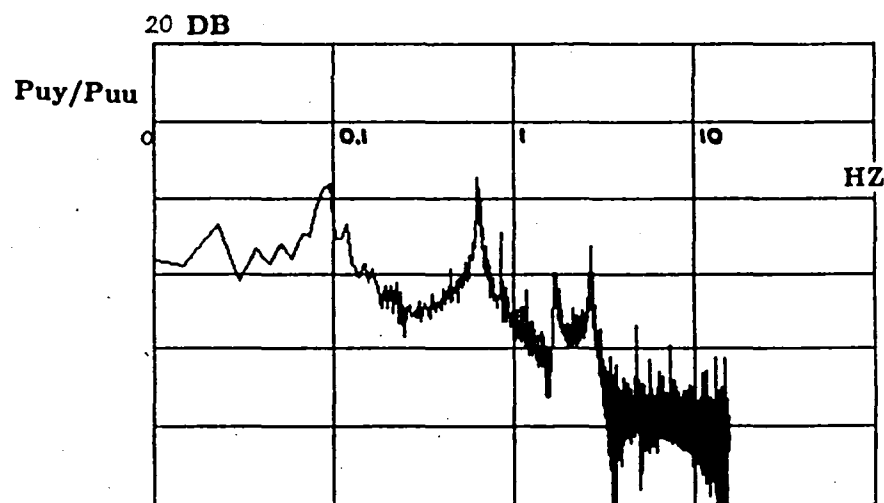
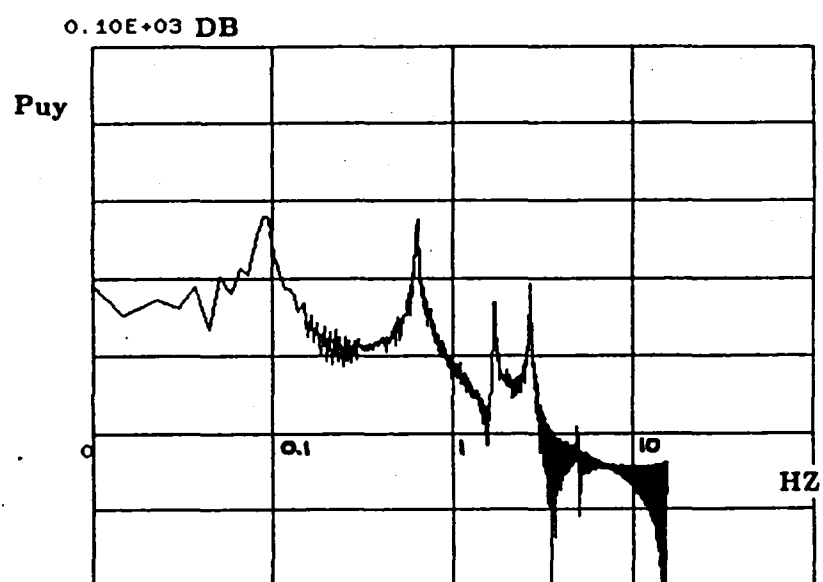
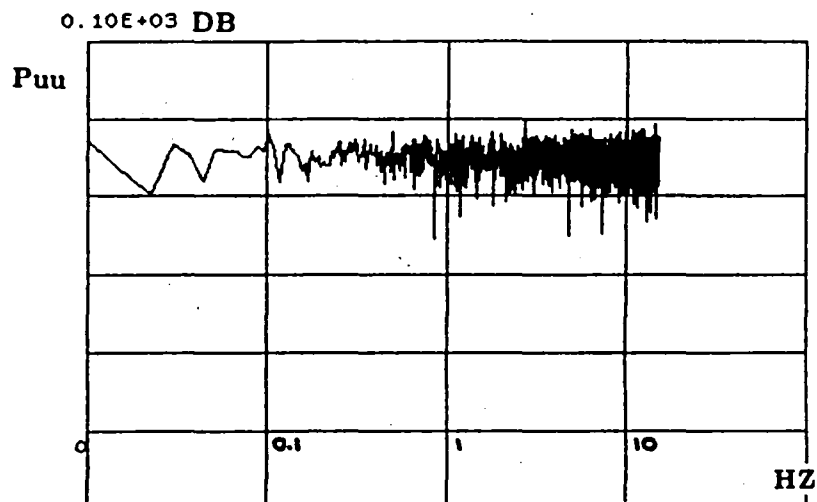
Matrix Determinant



700

The PSD of the input auto-covariance and input/output cross-covariance, together with their ratio which is the estimated transfer function, is shown here. The horizontal axes are in logarithm scale. The PSD of the input is more or less a constant value as the input is a white noise. The resulting estimated transfer function shows that indeed only four of the seven modes, more specifically, the four lowest frequency modes, are apparent from the spectral estimates. This transfer function is passed to the curve fitting subroutine for plant model determination.

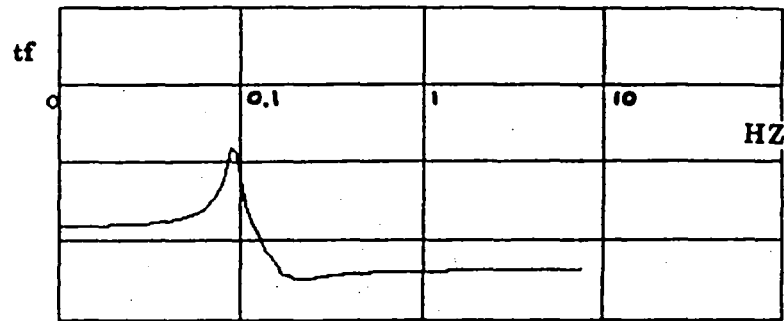
SPECTRAL ESTIMATION: FREQUENCY ESTIMATES



Even for wideband excitation as in this case, the spectral estimated transfer function can be passed to the curve fitting subroutine in whole or in parts. In whole, the estimated transfer function over the full spectrum can be passed. In parts, the transfer function over a few narrow frequency bands of interest can be passed. This viewgraph shows two cases of passing the transfer function in parts. The first passes the data from 0 to 0.15 Hz and the second from 0.15 to 3 Hz. They aim to perform curve fitting on the first mode and the other three observed modes of the plant respectively. The top plot shows the transfer function obtained based on curve fitting results for the first mode. The second plot shows the difference between the spectral estimates and this curve fitted transfer functions. The difference is small in the frequency range of 0 to 0.15 Hz and indicates that the curve fitted transfer function is a good approximation to the actual plant within the frequency range. The case of passing the transfer function data within the frequency range of 0.15 Hz to 3 Hz also shows that the other three observed modes of concern are well estimated, as the difference between the curve fitted and spectral estimated transfer function are small within the frequency range of interest.

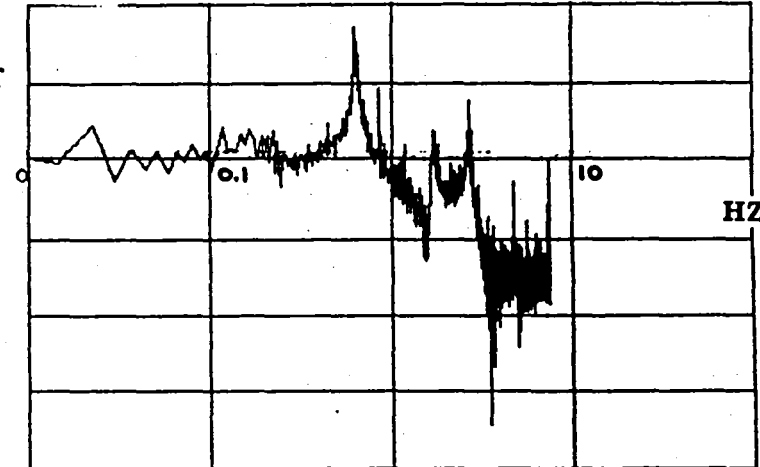
TRANSFER FUNCTION CURVE FIT

20 DB



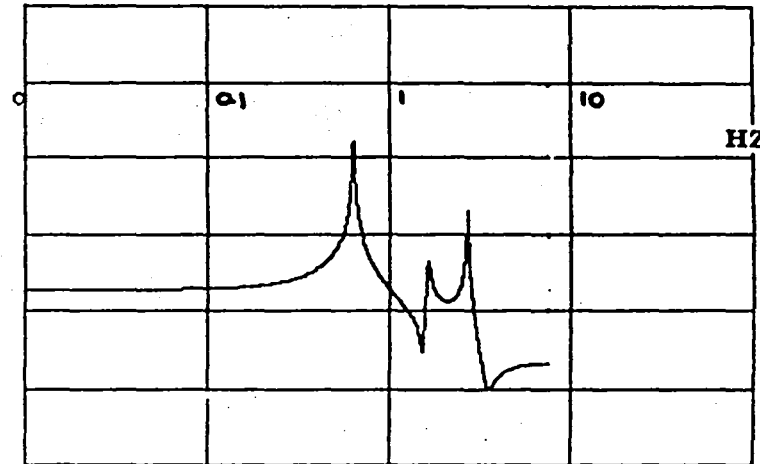
40 DB

$$e = puy / puu - tf$$



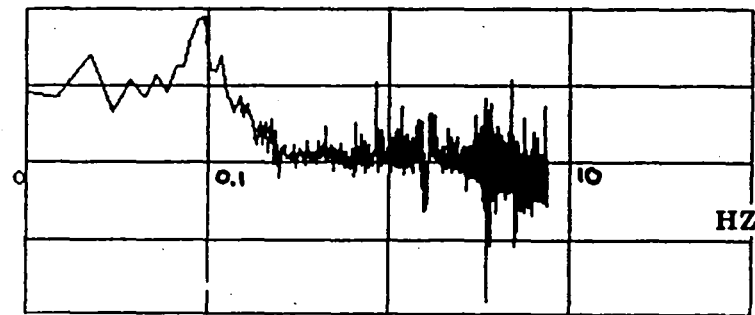
20 DB

tf



40 DB

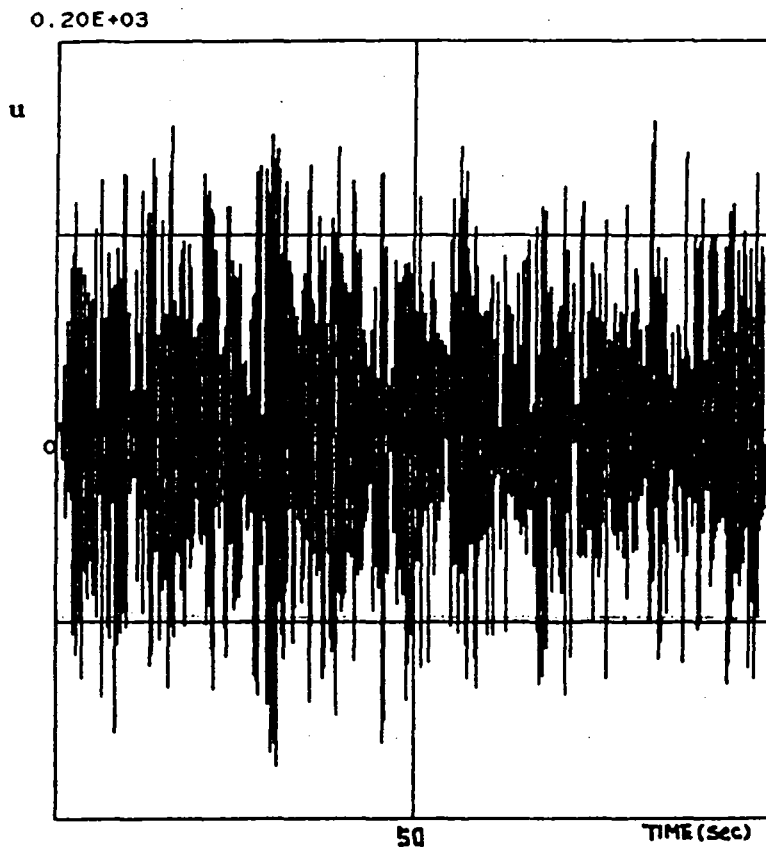
$$e = puy / puu - tf$$



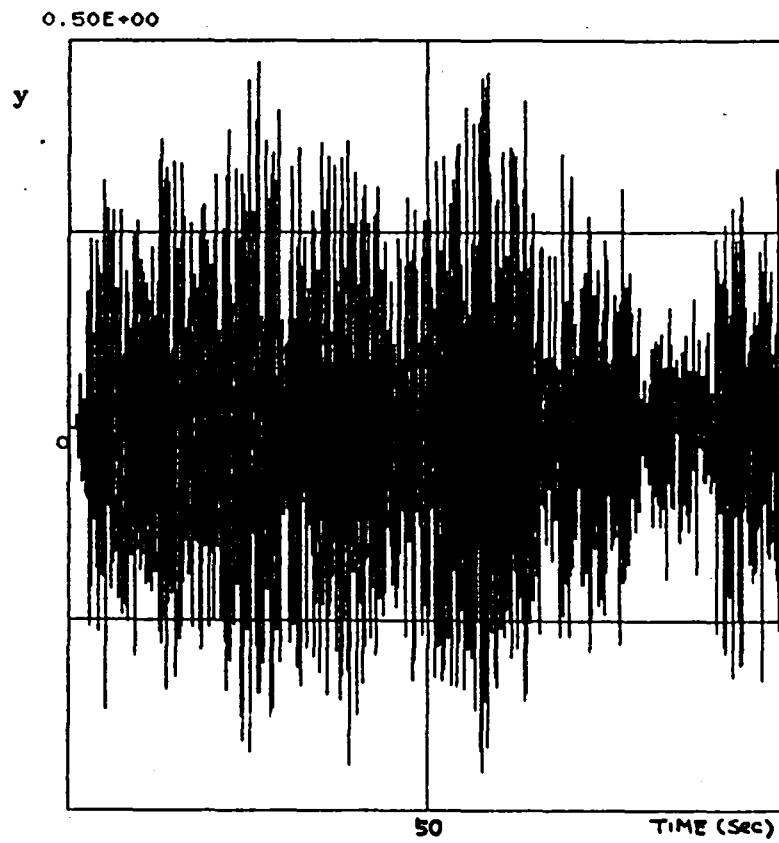
Wideband excitation spreads its energy evenly over the whole frequency spectrum and hence may not be effective in exciting higher frequency modes. Narrowband excitation concentrates the available energy in a smaller frequency range of interest. Plant modes lying within this frequency range will therefore be more effectively excited. Two cases of narrowband excitation will be presented. The first is a narrowband excitation with a passband of 1 to 3 Hz. The plant input and output are shown in this viewgraph. As higher frequency modes allow a more relaxed frequency resolution, data points for a shorter interval are generated. For this narrowband experiment, 300 seconds of simulation data are computed, 100 seconds of which are shown here.

NARROWBAND EXCITATION (1 - 3 HZ)

PLANT INPUT



PLANT OUTPUT

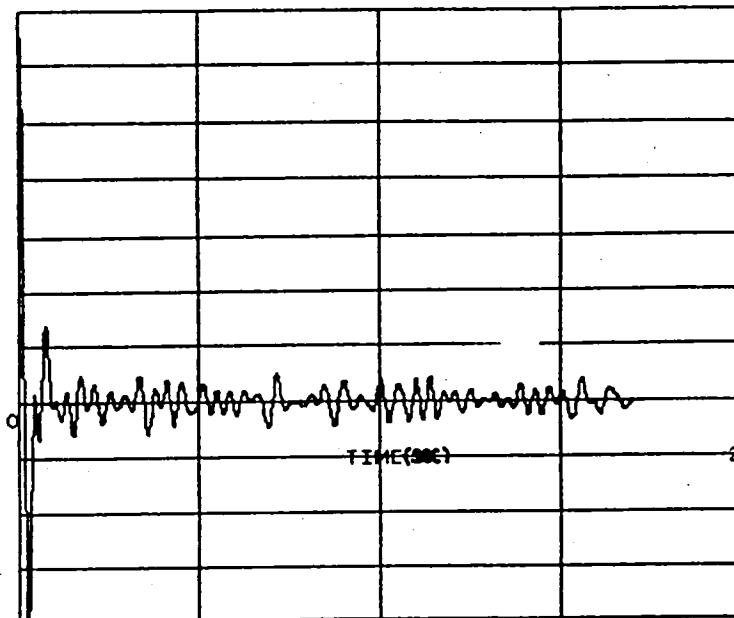


Covariance estimates and PMM test results are shown here. Since the input in this case is not white the auto-covariance of the input deviates from the delta function. Out of the seven modes in the plant, only two of them, specifically, the 1.68 and 2.68 Hz modes, lie in the passband of the present excitation and are expected to be excited. The PMM test clearly picks up this fact as the determinant value becomes very small for assumed mode numbers greater than 3.

SPECTRAL ESTIMATION: COVARIANCE ESTIMATES

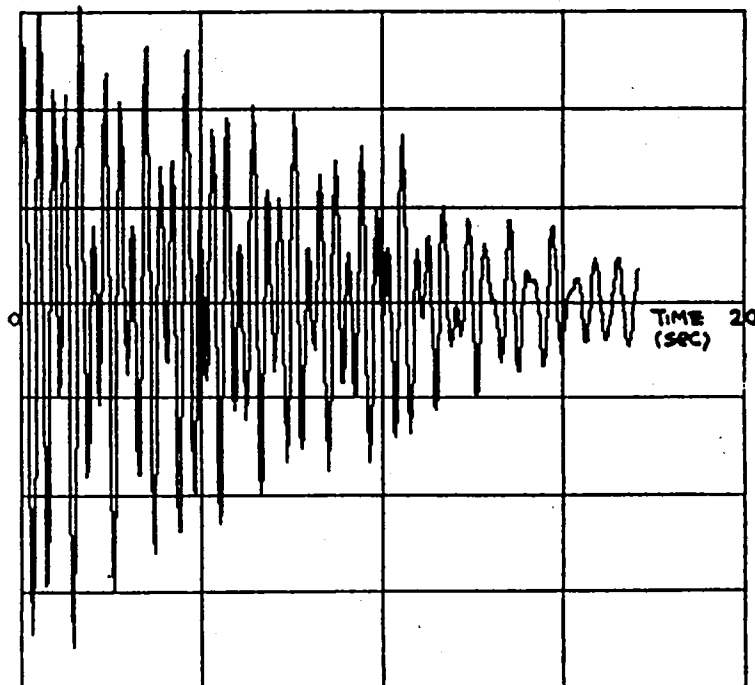
0.35E+04

Ruu



0.35E+01

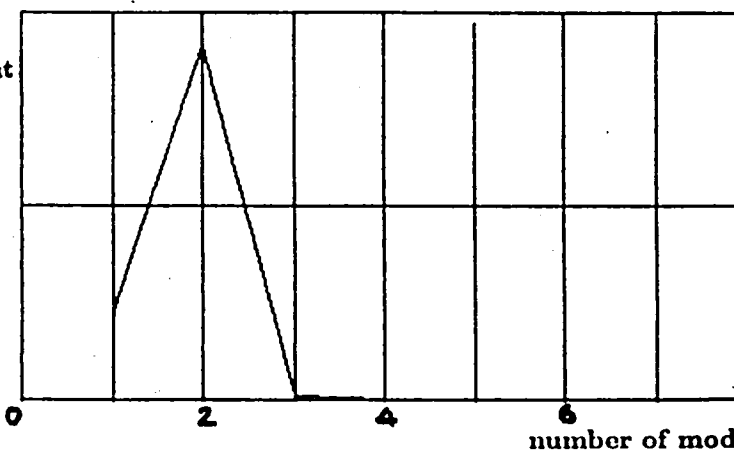
Ruy



PRODUCT MOMENT MATRIX TEST

0.40E+03

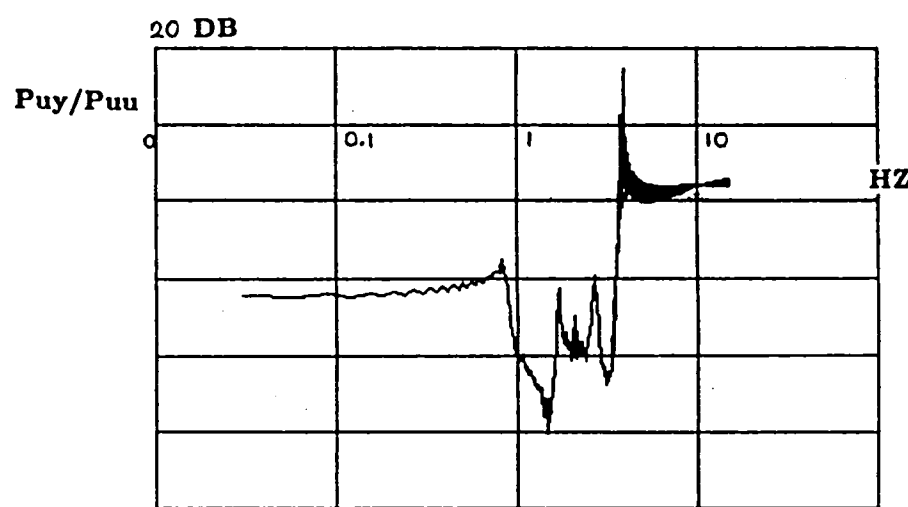
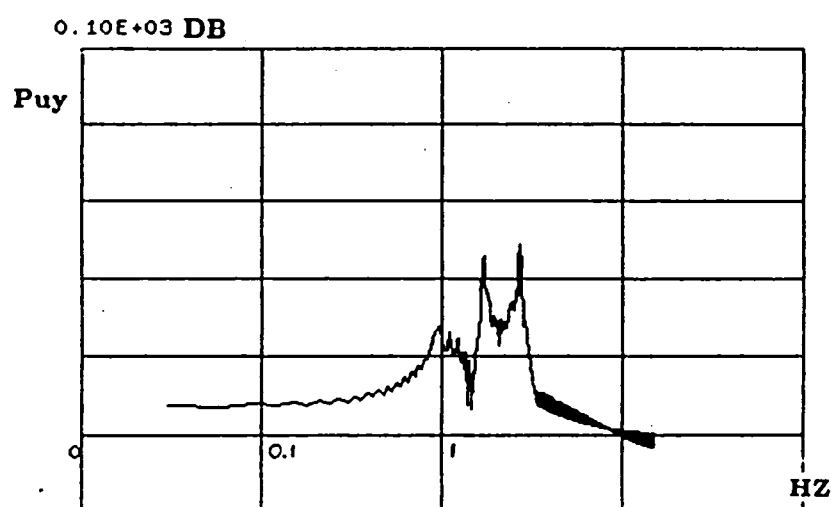
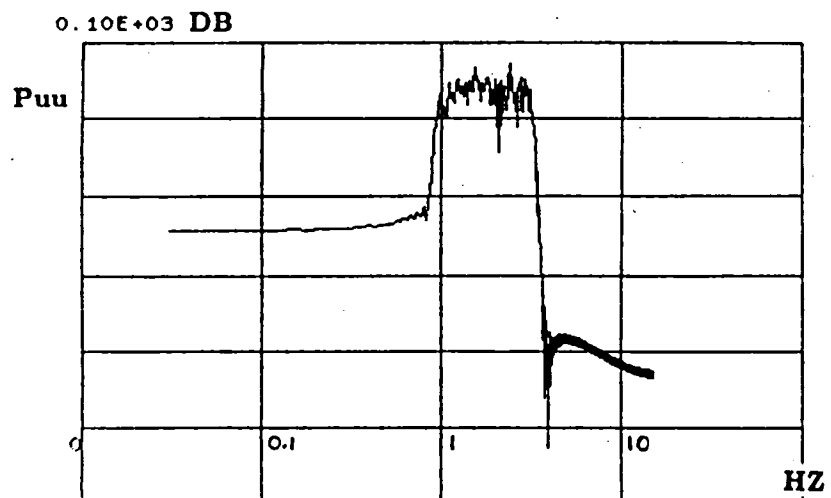
Matrix Determinant



708

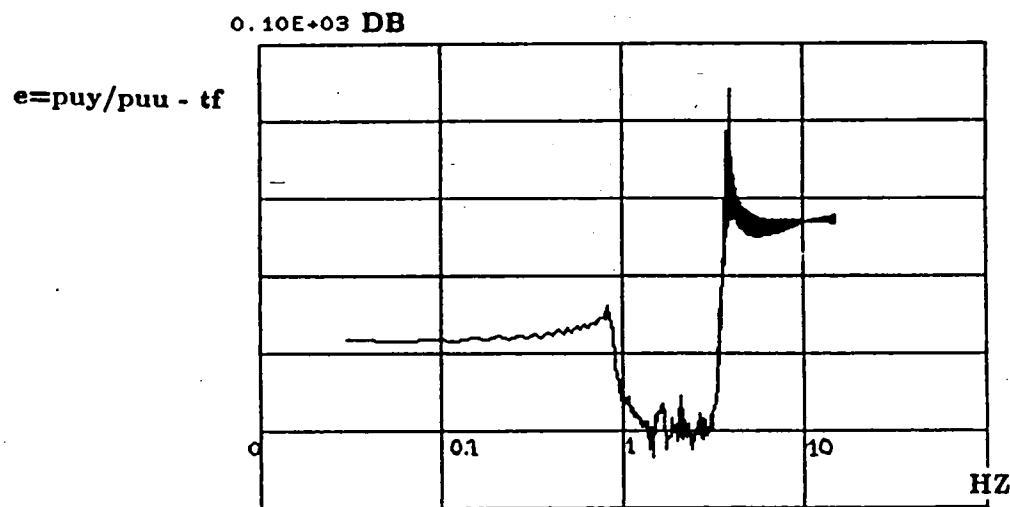
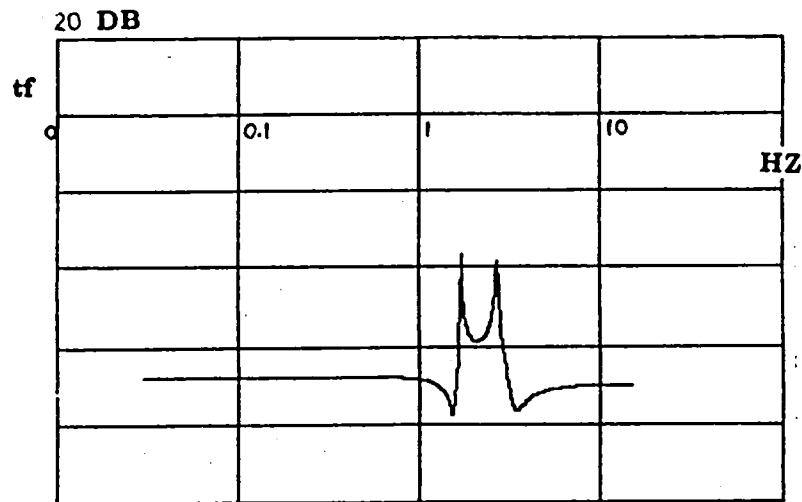
Frequency estimates from the spectral estimation algorithm are shown. The PSD of the input indicates that the input energy is indeed concentrated in the passband of 1 to 3 Hz. Note that for the spectral estimated transfer function, only the values within the passband are meaningful. The results clearly indicate that two modes inside the passband are being excited.

SPECTRAL ESTIMATION: FREQUENCY ESTIMATES



The spectral estimated transfer function within the passband are passed to the curve fitting subroutine. The resulting transfer function based on curve fitting results of modal frequencies and damping coefficients is shown. The quality of the curve fitted transfer function is given in the second plot which shows the difference between the spectral estimated transfer function. The difference shows that the curve fitting result within the passband is quite an adequate approximation of the actual transfer function.

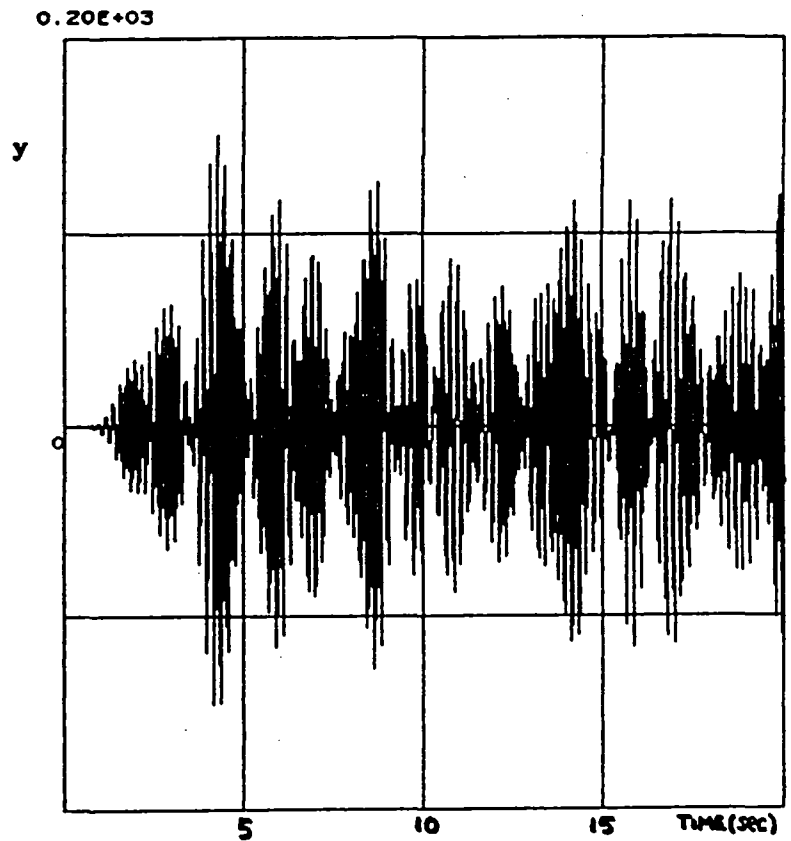
TRANSFER FUNCTION CURVE FIT



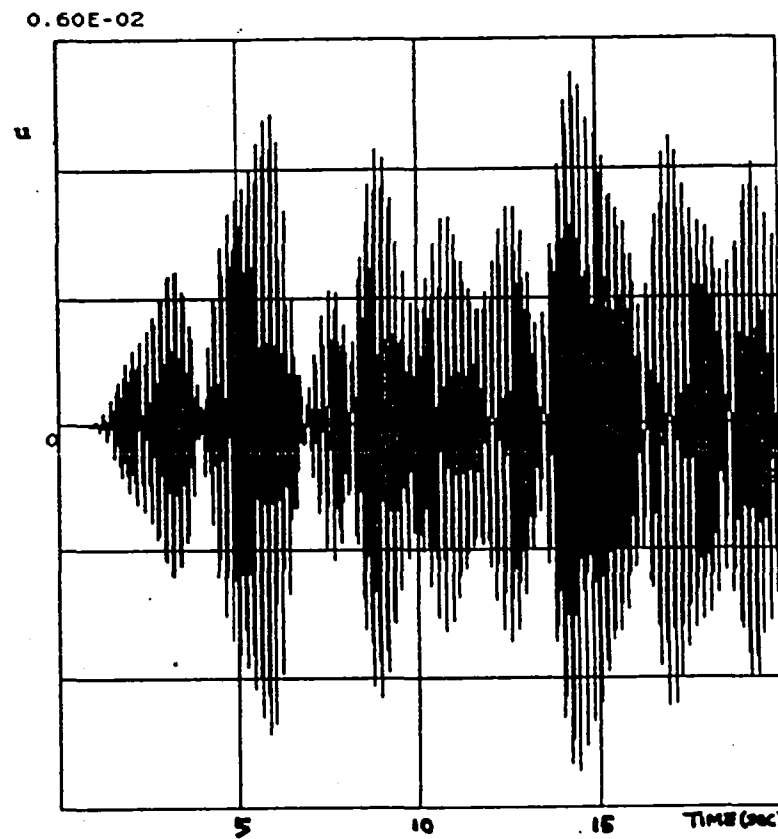
The second narrowband excitation case is presented here. The bandpass frequency is from 4.5 Hz to 5.5 Hz, aiming to excite the 4.89 Hz mode of the plant which was not observed at all in the wideband experiment. This viewgraph shows the plant input and output. Note the small excitation amplitude of the plant output. The 4.89 Hz mode is barely excited. If it were a wideband excitation, the response due to this mode would be obscured by the dominant modal responses.

NARROWBAND EXCITATION (4.5 - 5.5 HZ)

PLANT INPUT

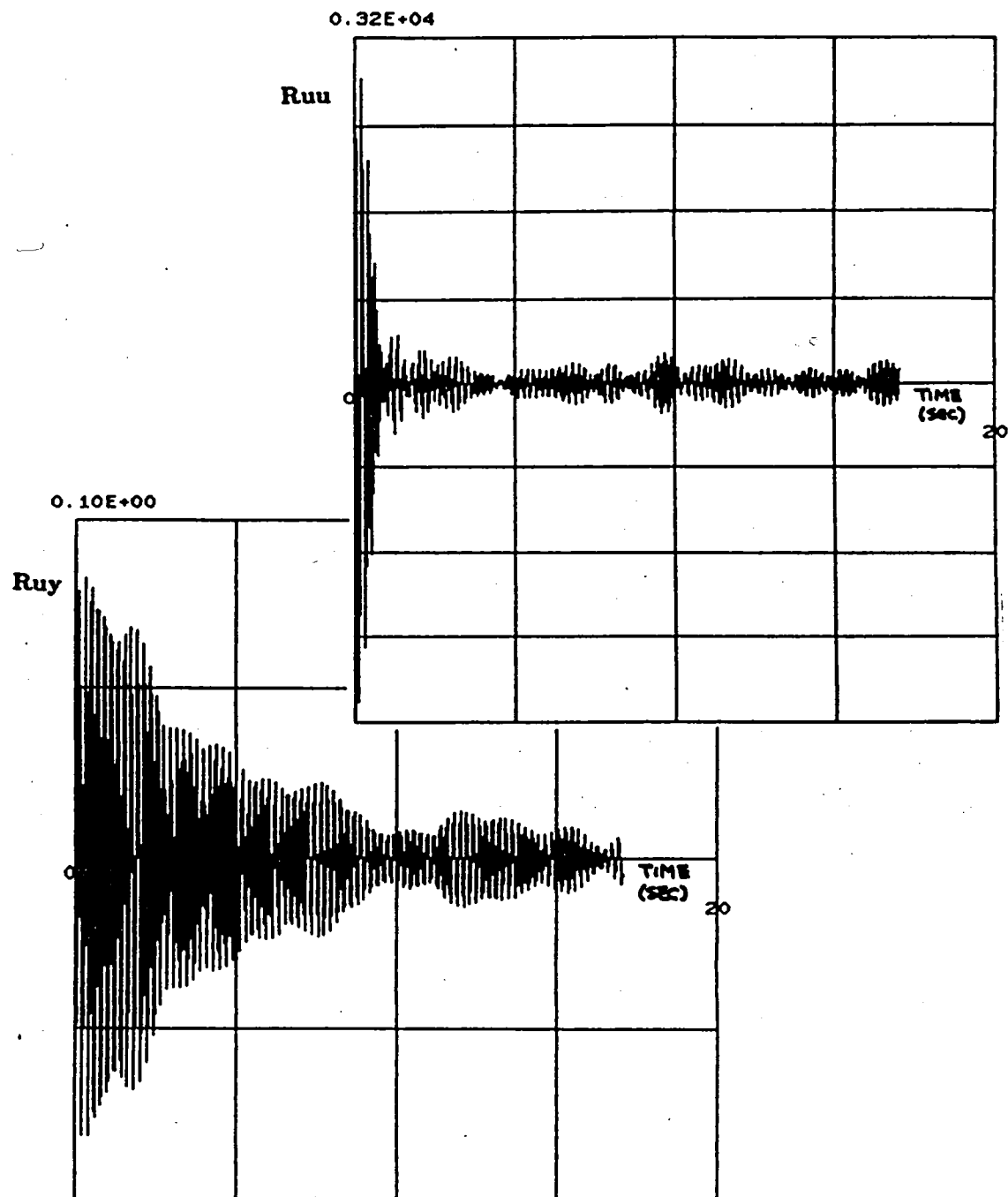


PLANT OUTPUT

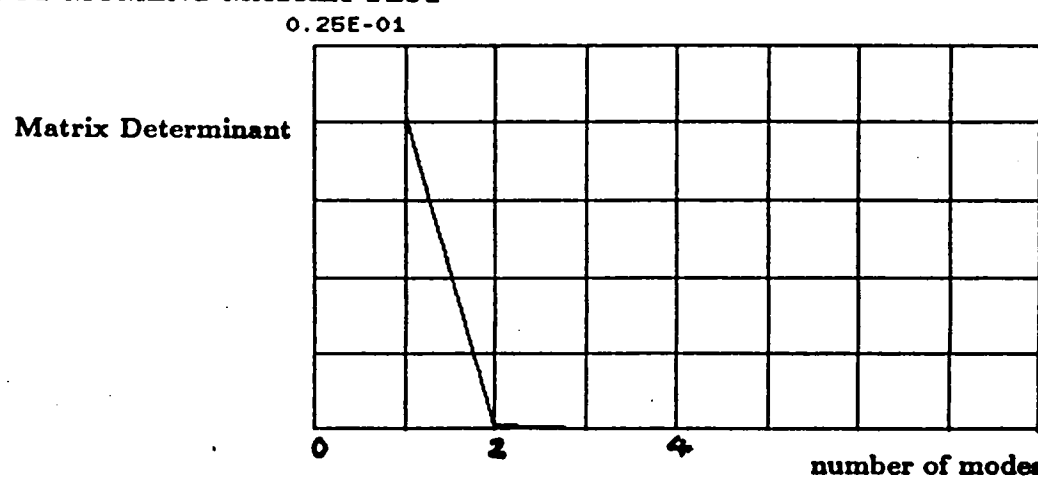


The covariance estimates and PMM test results are shown. As expected, the auto-covariance of the input deviates more from a delta function. It is interesting to note, that even though the 4.89 Hz mode is barely excited, the PMM test still indicates, without ambiguity, that there is just one excited mode reflected in plant input/output data.

SPECTRAL ESTIMATION: COVARIANCE ESTIMATES

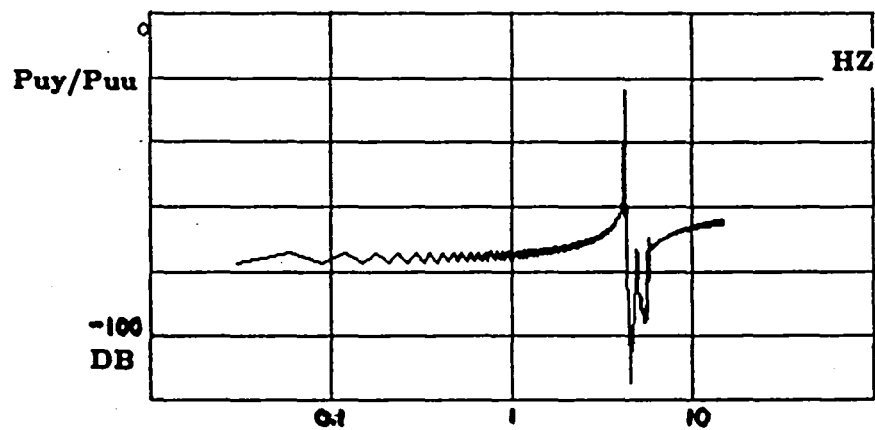
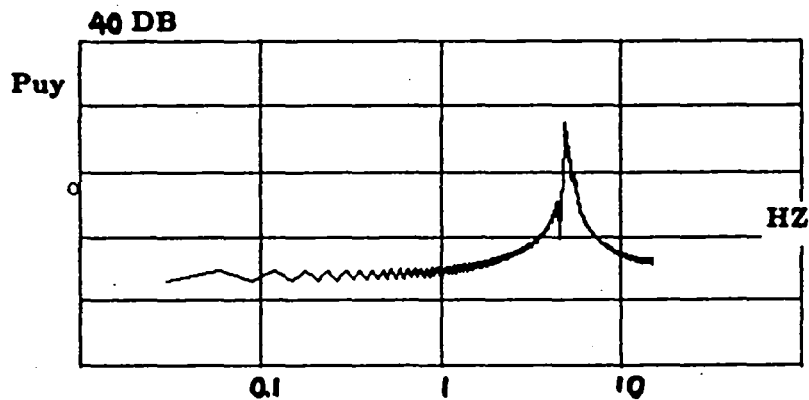
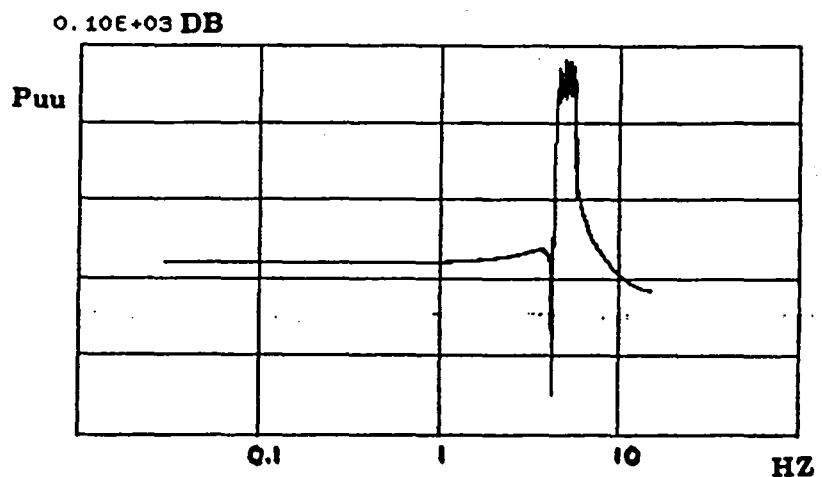


PRODUCT MOMENT MATRIX TEST



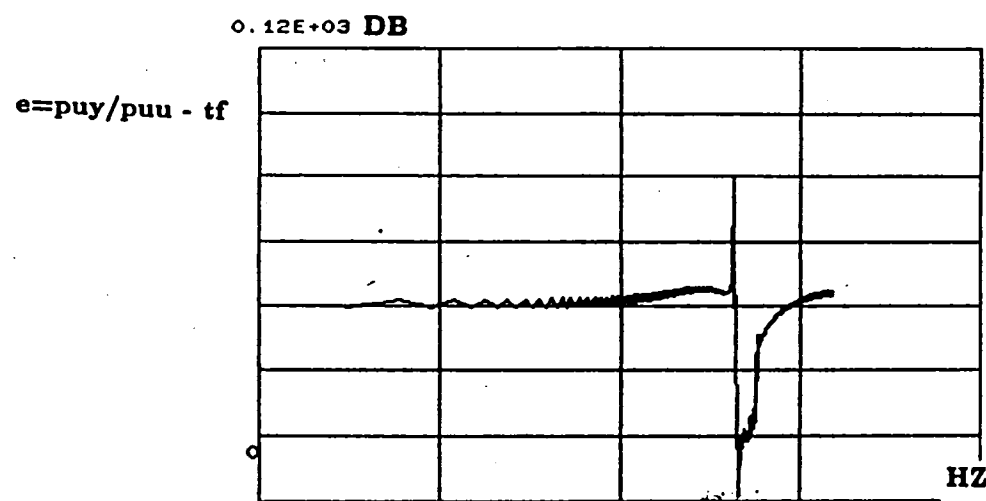
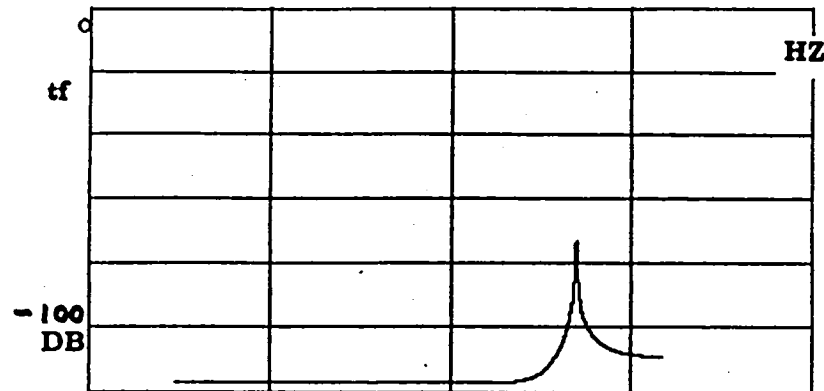
The frequency estimates are as shown. Excitation energy is indeed concentrated within the passband of 4.5 Hz to 5.5 Hz as indicated by the input PSD. The transfer function obtained by dividing the input/output cross-covariance PSD by the input PSD clearly indicates the presence of the 4.89 Hz mode. Again, the numbers are irrelevant outside the passband. Thus, using narrowband excitation, an otherwise obscured mode can be observed.

SPECTRAL ESTIMATION: FREQUENCY ESTIMATES



The transfer function data within the passband are passed to the curve fitting algorithm for the estimation of the modal frequency and damping coefficient of this one mode. The resulting curve fitted transfer function is as shown on the top plot. The difference between the spectral estimated and curve fitted transfer function again indicates that the curve fitting result is a good approximation of the plant within the passband.

TRANSFER FUNCTION CURVE FIT



The merits of the nonparametric identification and model determination technique are summarized in this viewgraph.

The nonparametric identification technique is usually performed preceding any other identification methodology. It provides a-priori knowledge of the plant for more sophisticated real-time parametric identification schemes. This knowledge includes initial frequency and damping estimates, frequency ranges of interest for prefilter design, and strictly positive real conditions to ensure convergence of regression schemes.

The technique adopts spatial and frequency domain partitions to achieve better estimation results and finer resolution of closely packed modes. Narrowband partitions are designed based upon wideband survey. The technique can serve to obtain a global characterization of the plant through transfer function determination on a point by point basis.

The use of narrowband experimentation overcomes the power constraints of the actuator power and also ensures excitation of otherwise obscured high frequency modes. The present technique can also incorporate output error analysis which determines the accuracy of the curve fitted plant model and thus provides uncertainty bounds for robust control design.

NONPARAMETRIC ID PROCESS

- INPUT EXCITATION DESIGN
 - WIDEBAND STATIONARY PROCESSES
 - NARROWBAND STATIONARY PROCESSES
 - SINE-DWELL
- SPECTRAL ESTIMATION
 - WIDEBAND AND NARROWBAND COMPOSED DATA
 - CORRELATION FUNCTIONS AND PSD's
 - HAND-OFF TO TRANSFER FUNCTION CURVE FIT
 - SETS UP PRODUCT MOMENT MATRIX ROUTINE
- PRODUCT MOMENT MATRIX ANALYSIS
 - DETERMINES MODEL ORDER IN SPECIFIED FREQUENCY BANDS
 - DIMENSIONS TRANSFER FUNCTON CURVE FIT
- TRANSFER FUNCTION CURVE FIT
 - INTEGRATES SPECTRAL ESTIMATION AND SINE-DWELL DATA
 - MINIMAL REPRESENTATION FOR CONTROL SYSTEM DESIGN
 - OUTPUT ERROR CHARACTERIZATION
- NONLINEAR DYNAMICS CHARACTERIZATION
 - SINE-DWELL AND RESONANCE TUNING TECHNIQUES

The followings constitutes a summary of this paper:

- On-orbit identification methodology starts with nonparametric techniques for a-prior system determination.
- Development of the nonparametric identification and model determination experiment software has been completed.
- The validation experiments to be performed on the JPL Control and Identification Technology Validation Laboratory have been designed.
- Experiments are to be started in a couple of weeks. In a few months, experimental results will be available.

- **ON-ORBIT IDENTIFICATION METHODOLOGY BEGINS WITH NONPARAMETRIC TECHNIQUES**
- **DEVELOPMENT OF AN INTEGRATED NONPARAMETRIC PROCESSING ARCHITECTURE AND SOFTWARE IS COMPLETED**
- **DESIGN OF VALIDATION EXPERIMENTS ON A PHYSICAL STRUCTURE HAS BEEN ACCOMPLISHED**
- **EXPERIMENTATION IS ABOUT TO GET UNDERWAY**

IDENTIFICATION AND CONTROL

INTEGRATION STRATEGIES

**Mark Milman
Edward Mettler
David Bayard**

**USAF/NASA Workshop on Model
Determination for Large
Space Systems**

**Jet Propulsion Laboratory
California Institute of Technology**

March 23, 1988

163822
128
111

5/2-18
163822
p-25

725

N 93-42222

726

121
INTERVIEWED BY [REDACTED]

PAGE 726
INTENTIONALLY BLANK

727

This paper describes an autonomous control concept for pointing and articulation of science instruments on the Eos (Earth observing system) NASA/NOAA platforms intended to be operational by the late 1990s. Key features of this concept include advanced control adaptation and tuning strategies which provide performance robustness over a wide range of system uncertainties and mission time criticality. System identification-control modification paradigms are synthesized to form an adaptation continuum over this extended regime of autonomous operations.

JPL INTEGRATED PAYLOAD ARTICULATION AND IDENTIFICATION SYSTEM

- IPAIDS CONCEPT IS OUTGROWTH OF EOS AUTONOMY STUDY

OBJECTIVE: ON-BOARD SYSTEM FOR MANAGING NUMEROUS ARTICULATED AND STRAPPED DOWN INSTRUMENTS

- DETERMINE SLEW TRAJECTORIES
- ATTENUATE SLEW INDUCED DISTURBANCES
- AUTONOMOUSLY RESPOND TO CHANGING SCENARIOS/ENVIRONMENT

EOS AUTONOMY STUDY OBJECTIVE: ON-BOARD COMMAND OF ARTICULATED INSTRUMENTS IN RESPONSE TO REAL-TIME TARGETS OF OPPORTUNITY

The Eos platform consists of an Engineering Module and an Instrument Carrier. The JPL Carrier concept includes an integrated autonomy architecture. The Carrier is expected to become increasingly autonomous as the system evolves over its potential lifetime of 20 years.

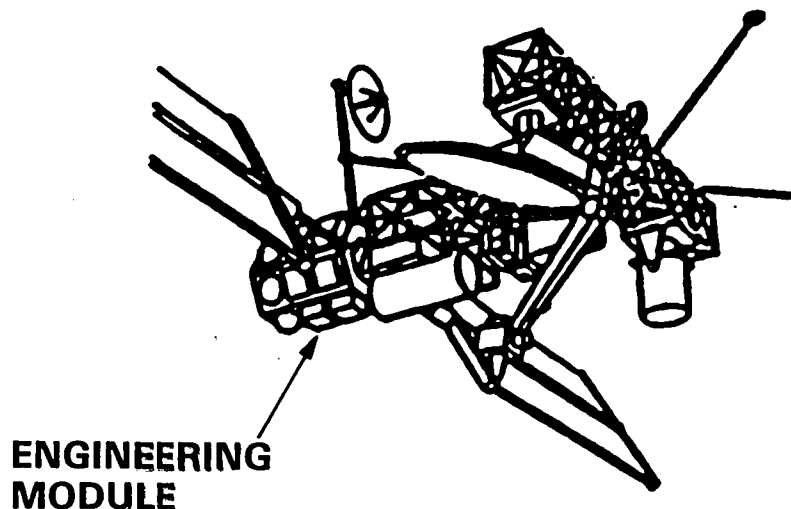
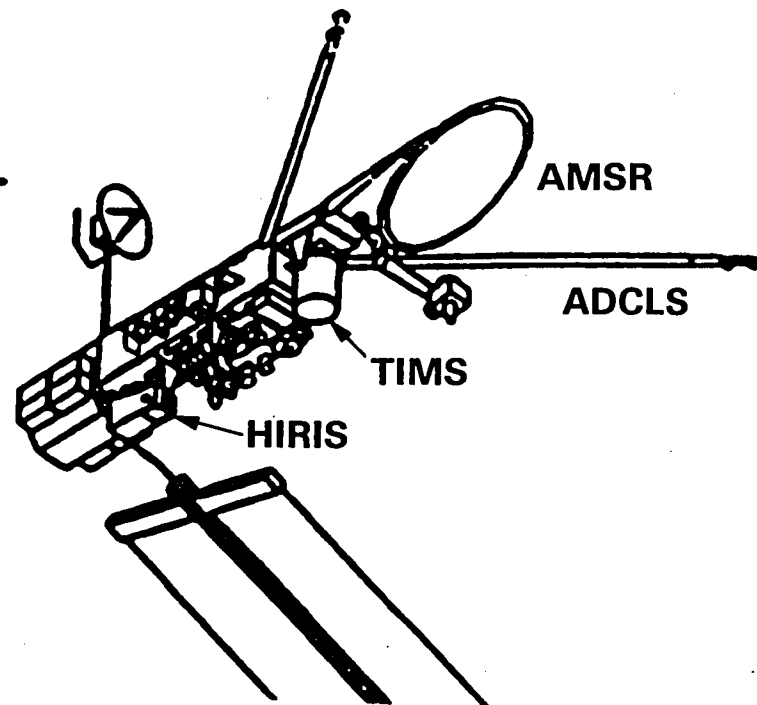
The instruments are carried on platforms orbiting in circular polar orbits of 824-km altitude. The adjacent figure shows representative baseline platform configurations where features relevant to the design of the Integrated Payload Articulation and Identification System (IPAIDS) can be identified. These features include the large solar array. The Engineering Module, which houses the core ACS (e.g., reaction wheels, gyros, star trackers, etc.), the Carrier System where the instruments are attached, and the instruments themselves.

The Engineering Module ACS is assumed to point the Carrier System with the following precision:

- o Pointing accuracy = $108 \text{ } \hat{\text{s}}$ (3-sigma), including rigid-body dynamics and quasi-static errors.
- o Pointing stability = $1.08 \text{ } \hat{\text{s}}/\text{s}$ (3-sigma), primarily representing flex-body dynamics, system noise, and nonlinearities.

Payloads that require more accurate pointing than this will need dedicated precision pointing systems. There are six instruments that fall into this category, with the most demanding having an accuracy of $20 \text{ } \hat{\text{s}}$ and stability (jitter) of $0.06 \text{ } \hat{\text{s}}/\text{s}$.

Eos PLATFORMS AND PAYLOADS

DUAL ARRAY DESIGN**ENGINEERING MODULE****SINGLE ARRAY DESIGN**

POINTING REQUIREMENTS

	<u>ACCURACY, $\text{s}, 3\sigma$</u>	<u>STABILITY, $\text{s/s}, 3\sigma$</u>	<u>SLEW RATE, $^{\circ}/\text{s}$</u>
ACS	108	1.08	N/A
PAYLOADS (MAXIMUM CASE)	20	0.06	1.25 TO 1.87

The Spacecraft dynamic model consists of a rigid engineering core module, and a reduced-order NASTRAN model of the carrier structure, including the solar panels and communication antenna. The various structural modes of the Eos platform are defined on the opposing page.

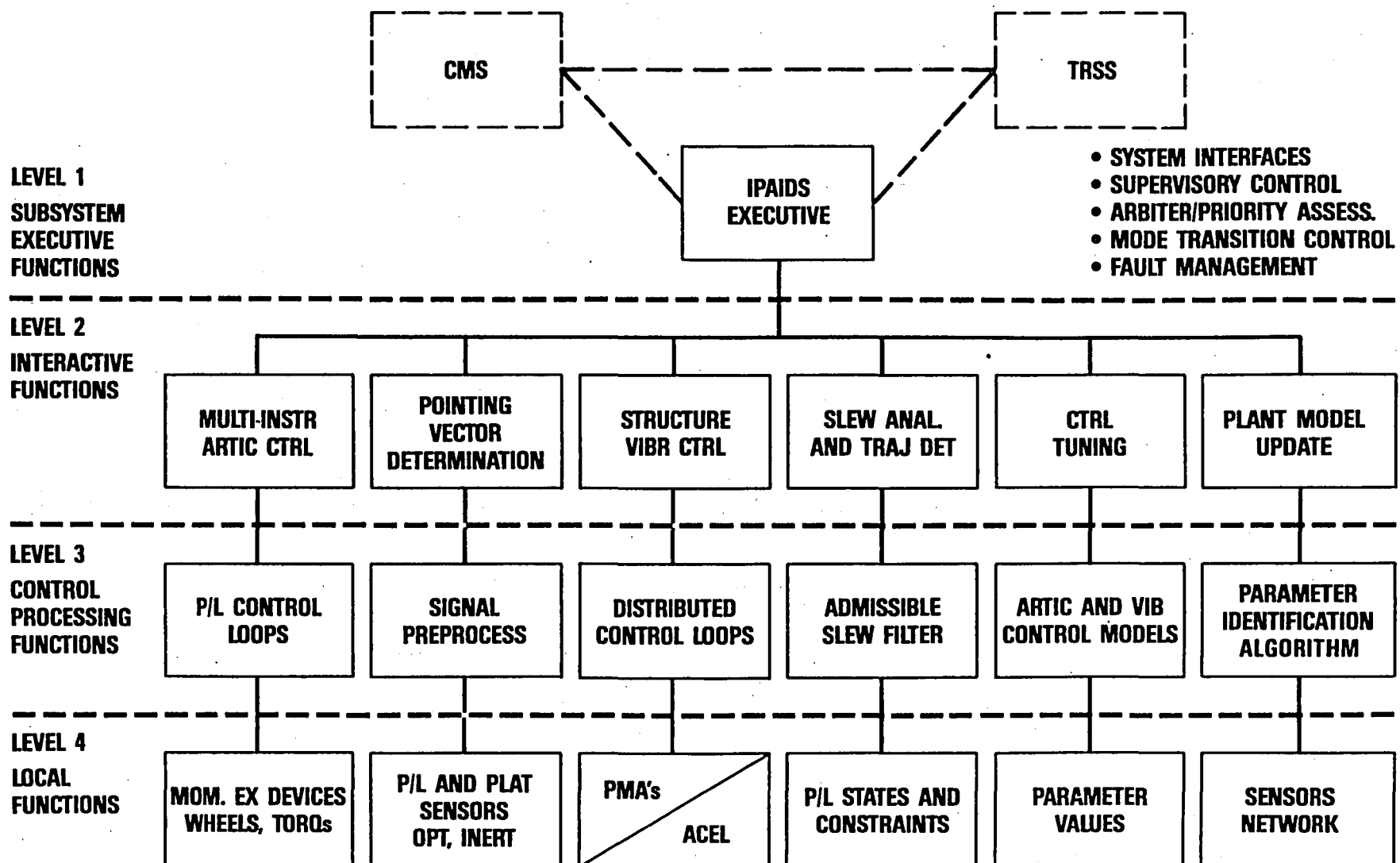
Eos PLATFORM STRUCTURAL MODES

FREQ RANGE	NUMBER OF MODES	TYPE
0.06 Hz TO 0.5 Hz	12	SOLAR PANELS IN TORSION AND BENDING AGAINST PLATFORM CORE (CORE BEHAVES AS RIGID MODE)
0.6 Hz TO 0.9 Hz	8	ADCLS BOOM MODES (CORE BEHAVES AS RIGID MODE)
1 Hz	2	HIGH-GAIN ANTENNA BOOM MODES (CORE BEHAVES AS RIGID MODE)
5 Hz	1	FIRST CORE MODE

The hierarchical structure of the IPAIDS architecture is outlined in the opposite figure. This multilevel architecture has been defined to support the anticipated needs of the multi-instrument carrier. The two main requirements of the architecture are (1) to accommodate a broad spectrum of pointing and stability requirements for various instruments, and (2) to implement a variety of operational scenarios, including scenarios wherein a given instrument may autonomously command the pointing of one or more other instruments.

At the highest level resides the IPAIDS Executive. The secondary level contains the IPAIDS interactive functions that, upon initiation by the Executive, generate the information necessary to begin a multi-instrument slew maneuver, perform post-slew analyses, and effect updates to embedded on-board models. At the third level reside "high-level" utility functions. These are self-contained functions that directly support the elements at the second level. A suite of parameter identification algorithms that act as subroutines when called by a higher-level model-adjust function is an example of a utility function. The fourth level consists of functions or devices that have a narrowly defined localized influence. These devices are commanded by the utility functions that reside at the next higher level.

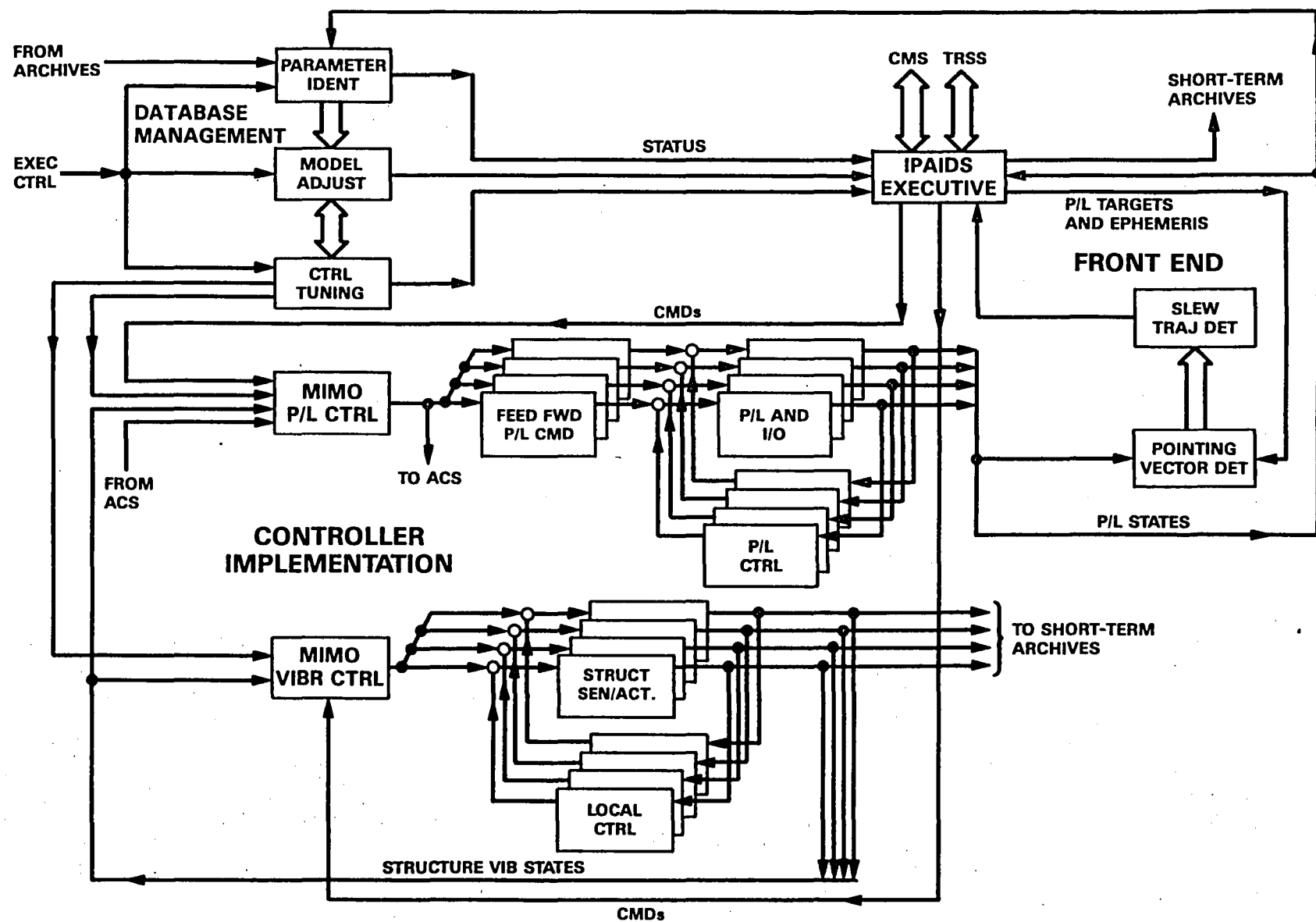
INTEGRATED PAYLOAD ARTICULATION AND IDENTIFICATION SYSTEM FUNCTIONS



The opposing figure depicts the control implementation of the IPAIDS architecture. The implementation architecture consists of four major modules: the IPAIDS Executive, the Front End, the Control Implementation module, and the Database Management module.

The IPAIDS Executive serves as the interface for communications between the IPAIDS and the CMS and TRSS (the other two subsystems that comprise the Payload Executive) and has additional responsibilities that include subsystem architecture, fault management, and supervisory and mode transition control. The primary function of the Front End is to accept and interpret high-level viewing coordinate requests for articulated instruments which are in turn converted into an event time and nominal slew trajectory for the gimballed instrument. The Controller Implementation Module executes slew commands, upon initiation by the executive. A two-tier structure is defined for this module to accommodate the pointing for both articulated and strapped-down payloads. The Database Management Module of the IPAIDS system contains, manages, and updates programmable parameters that are used by the IPAIDS subsystem software and hardware. The active elements of this module include a parameter identification function, a model adjust function, and a control tuning function.

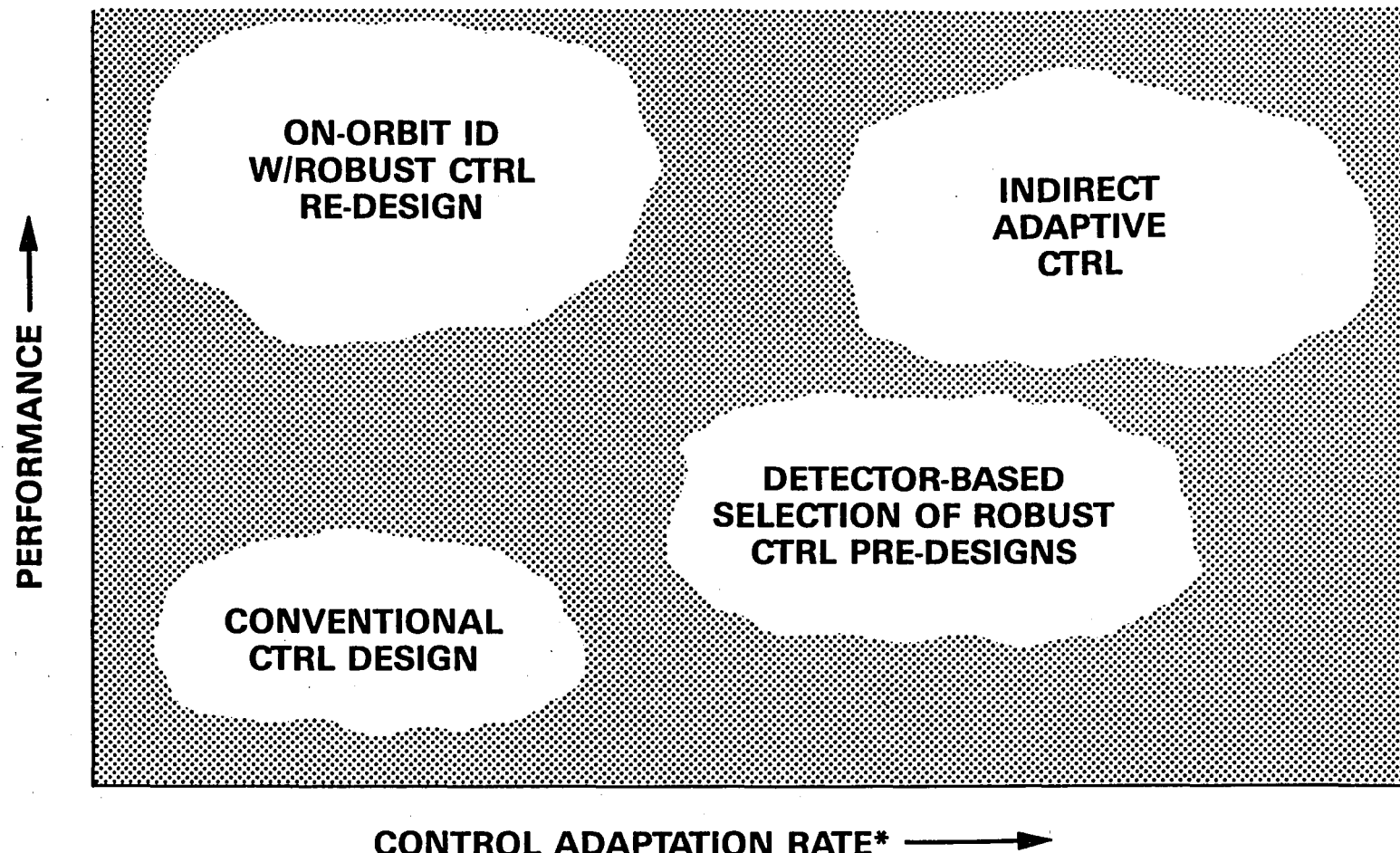
JPL IPAIDS CONTROL IMPLEMENTATION CONCEPT



434

The IPAIDS controller adaptation feature consists of a hierarchy of modification and tuning strategies. These strategies are as follows: (1) operating regime detection with robust controller predesigns; (2) on-orbit system identification with on-line robust control redesign; (3) modern adaptive control. As indicated in the figure, these functions are coordinated to provide maximum performance under a variety of operational scenarios, depending on the degree of performance desired and the relative degree of time criticality involved. In particular, robust controller predesigned changeouts are adequate in scenarios where an immediate control modification action is required, but where high performance is not crucial. In contrast, scenarios which require high performance but allow sufficient time for testing and computation will invoke the on-orbit identification and on-line robust control redesign function. Finally, situations which are critical in both time and performance will require a modern indirect adaptive control approach.

CONTROLLER MODIFICATION STRATEGIES FOR OPERATIONAL AUTONOMY

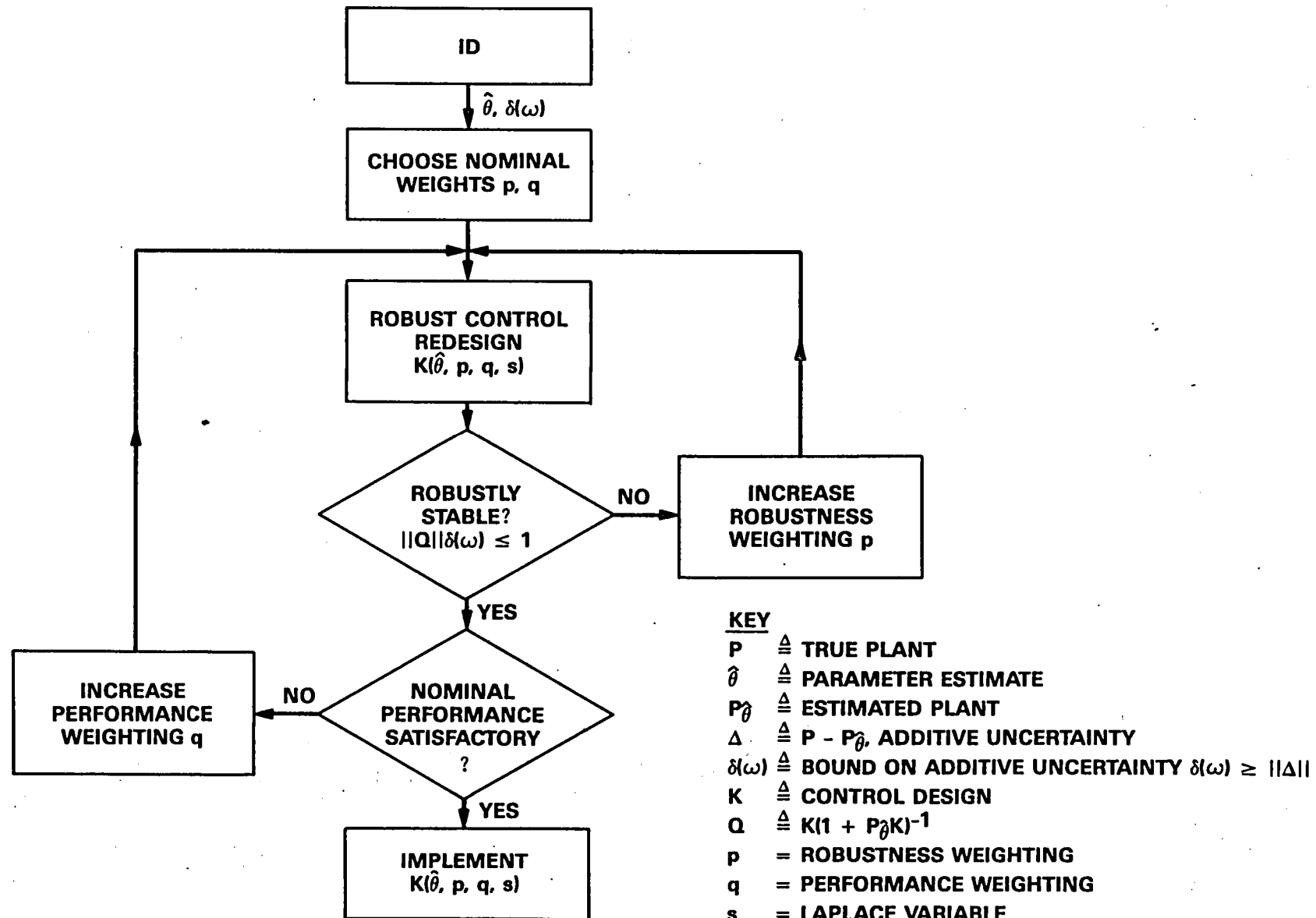


*A FUNCTION OF TIME CRITICALITY AND
PLANT/ENVIRONMENT UNCERTAINTIES

The most basic level of controller adaptation provides predesigned robust controller changeouts supported by a system of detectors. The detection scheme partitions the operational function space into discrete regimes reflecting various operating conditions, fault scenarios, and environmental situations. A detected change of operating regime is passed to the IPAIDS executive, where an appropriate robust control law is chosen from a suite of precomputed designs and switched into operation.

The next level of controller modification involves on-orbit identification in support of robust controller redesign. This level ensures high-performance control by maintaining accurate rendering of plant models, the uncertainties in the identified models, and other uncertainty characteristics in the overall system. The approach utilizes a combination of parametric and nonparametric identification techniques in conjunction with robust control strategies that incorporate H_2 -based tuning heuristics. These heuristics allow for intelligent tradeoffs to be made between control system performance and robustness with respect to confidence levels of the identified parameters. A flow diagram depicting this identification-control paradigm is given in the opposite figure.

ON-ORBIT ID AND ON-LINE ROBUST CONTROLLER REDESIGN



Robust control tuning methodologies can be developed based upon parametric information of plant uncertainty. The opposite figure shows a nominal plant perturbed by unknown but a priori bounded real parameters with given structure (A_j, B_j, C_j) . A first step towards designing a robust feedback controller for this system is to put it in an equivalent feedback perturbation form as shown in the figure.

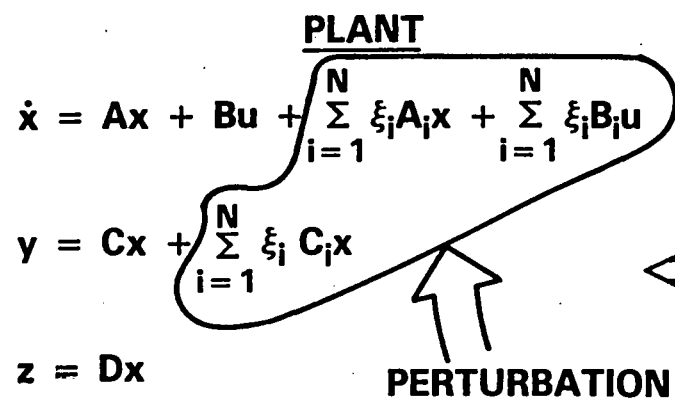
JPL

CONTROL TUNING METHODOLOGY

PLANT

$$\dot{x} = Ax + Bu + \sum_{i=1}^N \xi_i A_i x + \sum_{i=1}^N \xi_i B_i u$$
$$y = Cx + \sum_{i=1}^N \xi_i C_i x$$
$$z = Dx$$

PERTURBATION



PERTURBATION REPRESENTATION

$$\dot{x} = Ax + Bu + F_1 v$$

$$y = Cx + F_2 v$$

$$w = G_1 x + G_2 u$$

$$z = Dx,$$

WHERE F_i, G_i DERIVED FROM A_i, B_i, C_i

$$v = \Delta w$$

$$\Delta = \begin{bmatrix} \xi_1 I_{k_1 \times k_1} \\ \vdots \\ \xi_N I_{k_N \times k_N} \end{bmatrix}$$

Ideally, a computationally efficient synthesis tool is desired to design compensators that optimize both performance and robustness criteria with respect to the perturbation structure. An efficient heuristic for achieving these goals involves minimizing an H_2 transfer function criterion by relating the feedback perturbation form with a standard LQG design problem. This relationship is outlined in the opposite figure.

THE HEURISTIC

$$\dot{x} = Ax + Bu + F_1v$$

$$y = Cx + F_2v$$

$$\tilde{z} = \begin{bmatrix} G_1 \\ D \end{bmatrix}x + \begin{bmatrix} G_2 \\ 0 \end{bmatrix}u$$

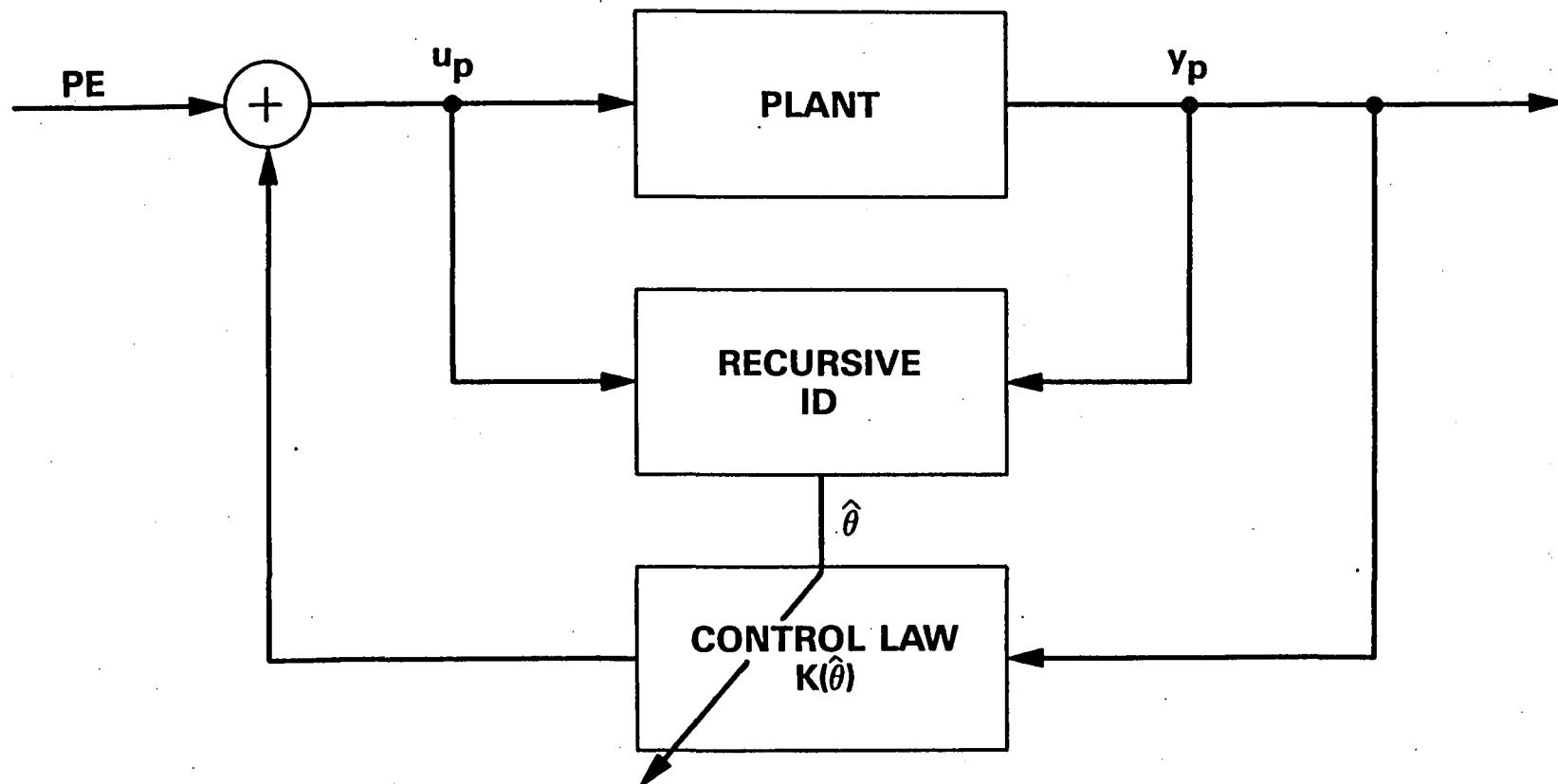
THINK v = WHITE NOISE AND DISREGARD PERTURBATION
CONNECTION BETWEEN \tilde{z} AND v . . .
IN LQG FORMULATION:

- INCREASE STATE WEIGHTING BY $q_1 G_1^* G_1$
- INCREASE CONTROL WEIGHTING BY $q_2 G_2^* G_2$
- INCREASE STATE NOISE BY $q_3 F_1^* F_1$
- INCREASE OUTPUT NOISE BY $q_4 G_2^* G_2$

q_i 's = FREE PARAMETERS

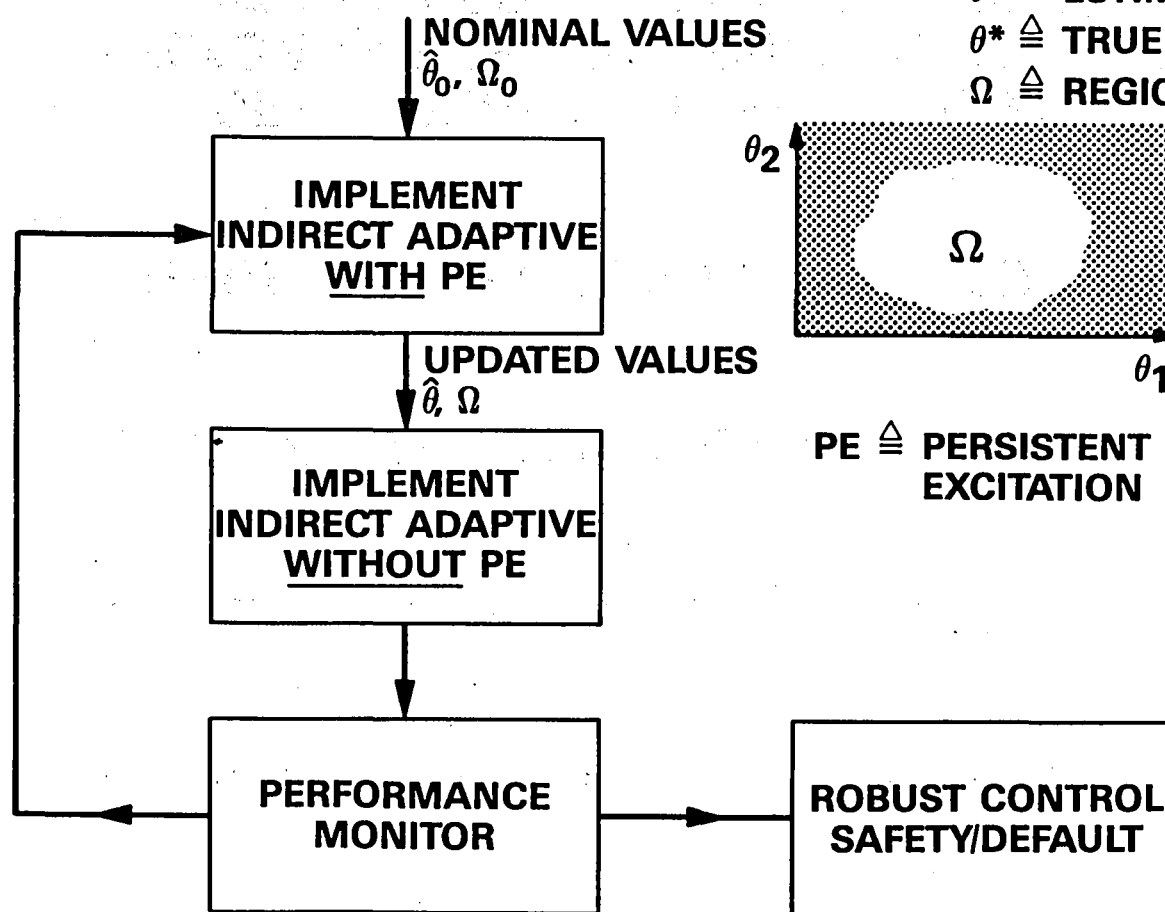
The most sophisticated level of control modification involves the application of modern adaptive control techniques. Present adaptive control schemes can be generally classified in two categories: direct schemes and indirect schemes. Direct adaptive schemes are parameterized by the control gains directly and do not involve the plant parameters explicitly. Indirect adaptive schemes are parameterized by the plant parameters explicitly and essentially involve the continuous tuning of a conventional controller (e.g., pole placement, minimum variance, LQG) by an on-line parameter identification scheme. Presently, a minimal phase condition on the plant restricts the application of most direct adaptive techniques to control of spacecraft with colocated actuator/sensor pairs. In contrast, indirect adaptive control techniques are not restricted in this fashion and can be applied to noncolocated configurations. Furthermore, indirect adaptive schemes contain a recursive identification process and hence can systematically incorporate plant parameter knowledge obtained and supported by the on-orbit ID process. This additional information can be used to advantage to avoid more difficult academic formulations of the adaptive control problem which attempt (ideally) to control a plant with zero a priori knowledge. For these reasons, the proposed methodology will focus on indirect adaptive control approaches.

INDIRECT ADAPTIVE CONTROL ARCHITECTURE

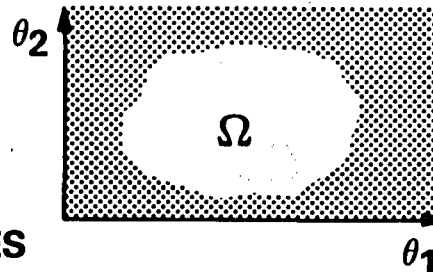


As indicated in the apposite figure, the proposed adaptive control methodology consists of a two-stage process. First indirect adaptive techniques are used which require little a priori plant knowledge. Although these techniques must be supported with PE in the control channel, they insure boundedness of the parameters via a built-in recursive identification process. After the identification process has converged to a reasonably sized (and known) region in parameter space, indirect adaptive methods based on LQG and pole placement which do not require PE are involved. These relatively new techniques guarantee convergence of the tracking error. With this two-stage approach, the undesired effect of PE on the tracking performance endures for only a finite period of time.

TWO-STAGE ADAPTIVE CONTROL



$\hat{\theta} \triangleq$ ESTIMATED PARAMETERS
 $\theta^* \triangleq$ TRUE PLANT PARAMETERS
 $\Omega \triangleq$ REGION SUCH THAT $\theta^* \in \Omega$



PE \triangleq PERSISTENT EXCITATION

- AUTONOMOUS PAYLOAD CTRL ARCHITECTURE
- GENERIC CLASS OF HIGH-PERFORMANCE S/C
- SYNTHESIS OF CONTROL ADAPTATION METHODS
- INTEGRATE ON-ORBIT ID AND ROBUST/ADAPTIVE CTRL
- SATISFY OPERATIONAL PARAMETERS FOR PERFORMANCE, TIME CRITICALITY, AND PLANT/DISTURBANCE UNCERTAINTIES

MIT

Presentation

Entitled

**FORMULATION AND VERIFICATION OF FREQUENCY RESPONSE
SYSTEM IDENTIFICATION TECHNIQUES FOR LARGE
SPACE STRUCTURES**

by

Jerrel R. Mitchell and Victoria Jones

USAF/NASA Workshop

on

"MODEL DETERMINATION FOR LARGE SPACE STRUCTURES"

California Institute of Technology

Pasadena, CA

March 22-24, 1988

5/3-18

163823

P-48

N 93-72773

FORMULATION AND VERIFICATION OF FREQUENCY RESPONSE
SYSTEM IDENTIFICATION TECHNIQUES FOR
LARGE SPACE STRUCTURES

by

Jerrel R. Mitchell, Victoria L. Jones and Charles Plant

OUTLINE OF PRESENTATION

I. Introduction

II. MIMO Frequency Response System ID

III. Techniques for Improving System ID in
the Presence of Noise

IV. Experimental Validation of Techniques

V. Conclusion

INTRODUCTION

"Bottom-Line" on Designing High Performance Control Systems for LSS's: Accurate Model

Design-to-Performance Philosophy:

- (1) Excite the System with Control System Actuators
- (2) Collect Data with the Control System Sensors
- (3) Determine Sampled-Data Control System Models
- (4) Redesign or Fine-Tune the Control System Using the New Model

MIMO SYSTEM IDENTIFICATION

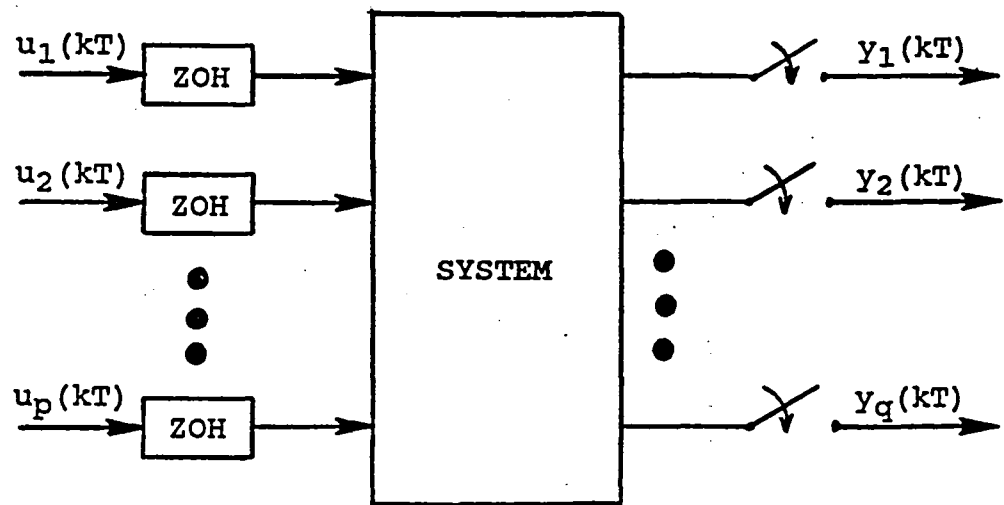


Figure 1: MIMO Sampled-Data System

$$Y(z) = \begin{bmatrix} H_{11}(z) & \dots & H_{1p}(z) \\ \vdots & \ddots & \vdots \\ \vdots & \ddots & \vdots \\ H_{q1}(z) & \dots & H_{qp}(z) \end{bmatrix} U(z) \quad (1)$$

where

$$U(z) = \begin{bmatrix} U_1(z) \\ \vdots \\ U_p(z) \end{bmatrix}, \quad (2)$$

$$Y(z) = \begin{bmatrix} Y_1(z) \\ \vdots \\ Y_q(z) \end{bmatrix} \quad (3)$$

Relationship between the i -th input and the j -th output is

$$Y_j(z) = H_{ji}(z) U_i(z) \quad (4)$$

Sampled-data frequency responses of the transfer functions between the i -th input and each output

$$H_{pi}(e^{j\omega T}) = \frac{\sum_{k=0}^{\infty} y_p(kT) e^{-j\omega kT}}{\sum_{k=0}^{\infty} u_i(kT) e^{-j\omega kT}}, \quad p = 1, 2, \dots, q \quad (5)$$

$u_i(kT)$ and $y_p(kT)$ are input and output sequences

Problem with (5):

Ratio of two infinite series

Facts:

- (1) If all poles of both signals are inside the unit circle, both are converging series.
- (2) Since the input sequence is selectable, there is no problem
- (3) Output sequence converges, provided the system is stable, i.e., all z-domain poles lie inside the unit circle.

With Stable System and Input Sequence
with All Poles Inside the Unit Circle

$$H_{pi}(e^{j\omega T}) = \frac{\sum_{k=0}^N y_p(kT) e^{-j\omega kT}}{\sum_{k=0}^N u_i(kT) e^{-j\omega kT}}, \quad p = 1, 2, \dots, q \quad (6)$$

N is selected to minimize the error due to the truncation

Good results are achieved if N is selected so that NT is greater than twice the largest time constant of the system or the input signal.

Practical choice of N : Selected so that NT is greater than the time where each outputs' magnitude is roughly 10% or less of the maximum magnitude of the corresponding output.

Practical System ID: Noise Problems

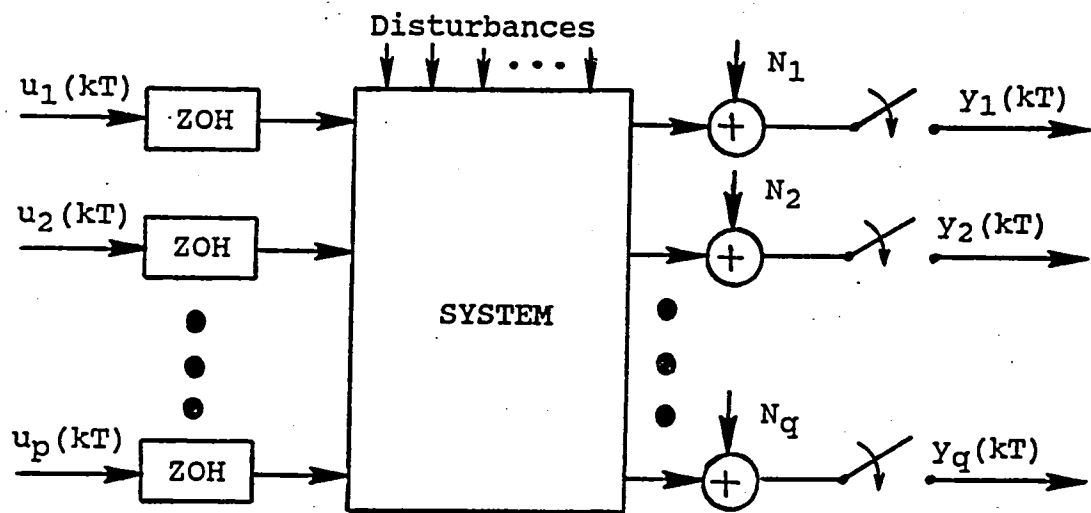


Figure 2: MIMO System with Noise and Disturbance Inputs

System ID with Noise

$$\hat{H}_{pi}(e^{jwT}) = \frac{Y_p(e^{jwT}) + N_p(e^{jwT})}{U(e^{jwT})} \quad (7)$$

TECHNIQUES FOR IMPROVING THE MIMO SYSTEM ID PROCESS

Signal-to-Noise-Ratio for Measuring "Goodness"

$$\text{SNR} = \frac{| Y(e^{j\omega T}) |}{[S_N(e^{j\omega T})]^{1/2}} \quad (8)$$

Facts: (1) Definition of SNR that is a function

- (2) If the power spectrum of the noise is known, the corruption of measurements of various signals can be computed and compared on a frequency by frequency basis.
- (3) If the noise is not known relative comparisons of various signals for improvement of the SNR on a frequency by frequency basis can be made.

Four Basic Ways to Improve SNR

1. Increase the magnitude of the input excitation
2. Increase the input duration
3. Apply shaped inputs
4. Average the results of several tests.

Increasing Input Magnitudes

Increased Input by Constant A,
then the SNR will be increase by A.

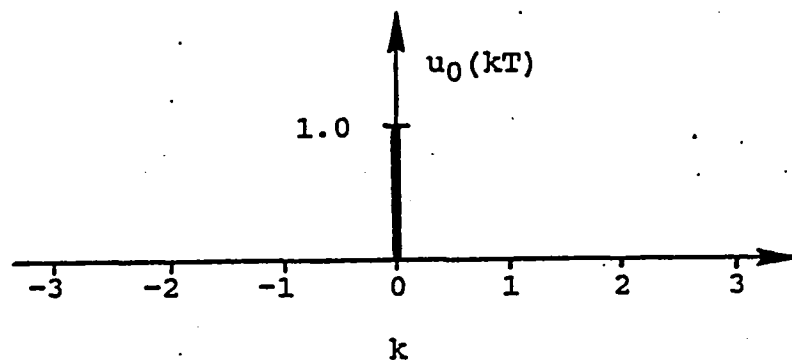
Problems: (1) Saturation of Actuator and/or Sensor
(2) Response of System Dominated by
Nonlinear Structural Effects

Increasing Input Duration

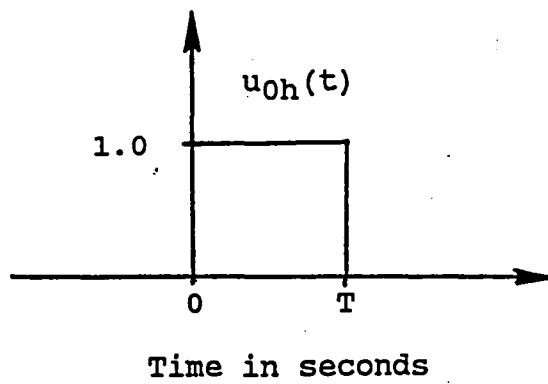
Assumption: No Input Sequence Value Exceeds Unity

Sequences of Ones:

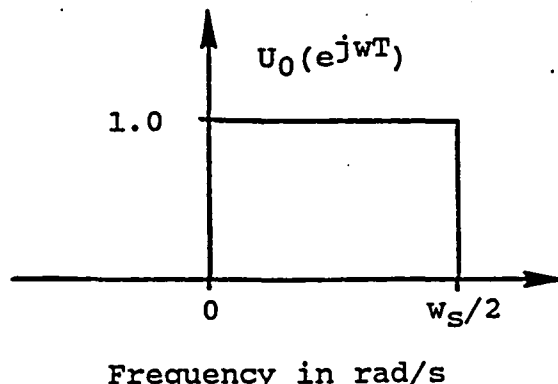
$$u_n(kT) = \begin{cases} 1 & k = 0, 1, 2, \dots, n \\ 0 & k < 0 \\ 0 & k > n \end{cases} \quad (9)$$



(a) Digital One Sequence



(b) Held Digital One



(c) Spectrum of Digital One

Figure 3: Characteristics of the Digital One

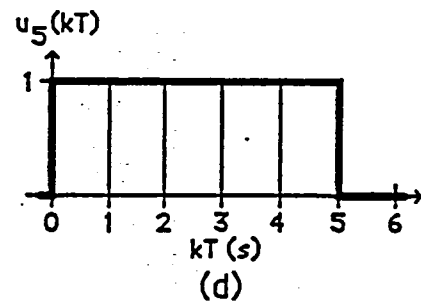
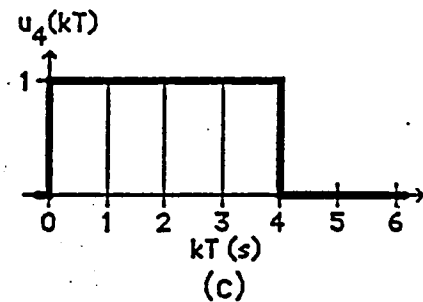
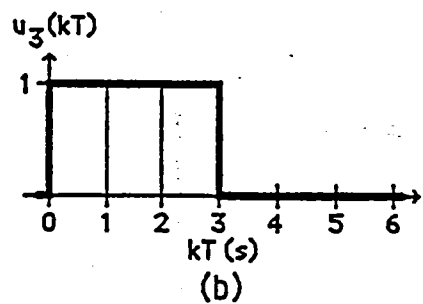
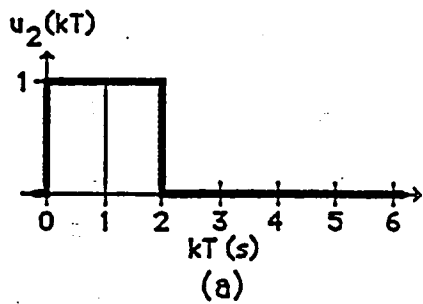
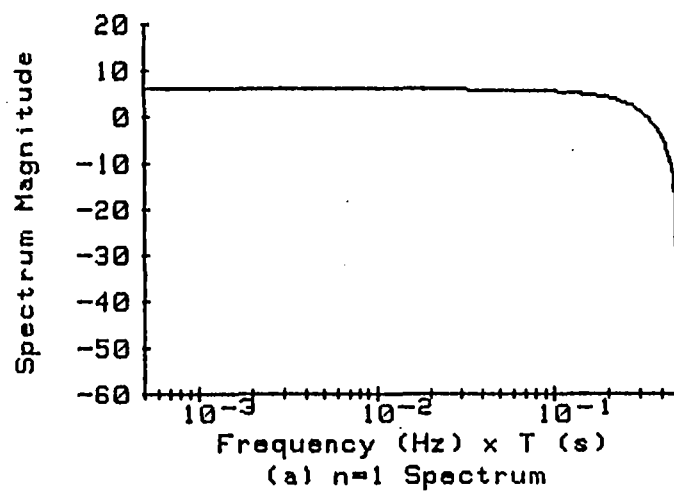
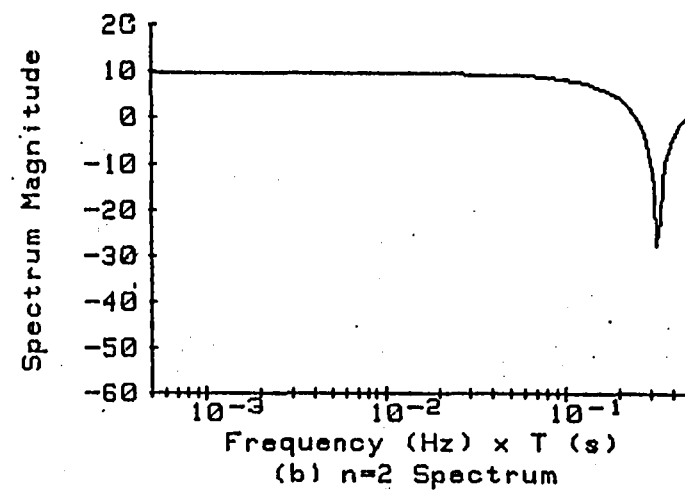


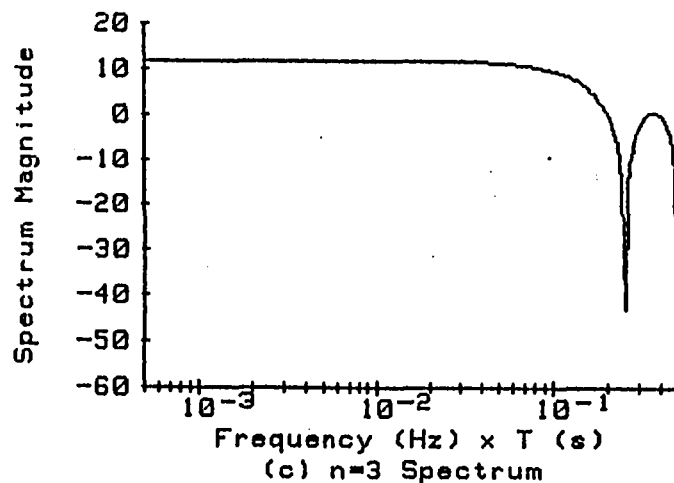
Figure 4: Protracted Pulses for Digital One Sequences of Two, Three, Four and Five.



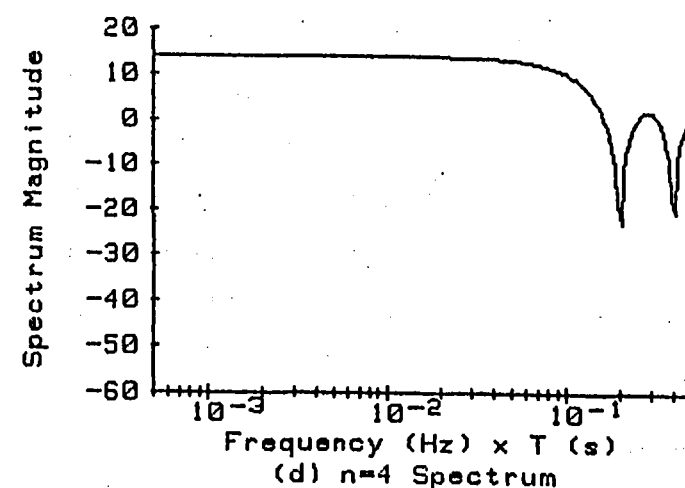
(a) $n=1$ Spectrum



(b) $n=2$ Spectrum



(c) $n=3$ Spectrum



(d) $n=4$ Spectrum

Figure 6: Spectra for Several Digital Ones Sequences

Table 1: Summary of Characteristics of Several Digital Ones Sequences

Order (n)	Signal z-Transform	Null Freq.'s (Hz) x T	d.c. SNR Improvement
1	$\frac{z + 1}{z}$	1/2	2
2	$\frac{z^2 + z + 1}{z^2}$	1/3	3
3	$\frac{z^3 + z^2 + z + 1}{z^3}$	1/2, 1/4	4
4	$\frac{z^4 + z^3 + z^2 + z + 1}{z^4}$	2/5, 1/5	5
...			

Shaped Input Sequences

Assumption: No Element of Sequence Exceeds Unity

Class of sequences that have reasonable wide-band spectra:

$$U_n(z) = K \frac{(z+1)^n}{z^n} \quad (10)$$

Scale Factor:

$$K = (n-k)! k! / n! \quad (11)$$

where k is the integer part of $(n+1)/2$.

General Form of the Shaped Sequences

$$u_n(iT) = \begin{cases} \frac{[(n-k)! k!]}{[(n-i)! i!]} & i = 0, 1, \dots, n \\ 0 & i < 0 \\ 0 & i > n \end{cases} \quad (12)$$

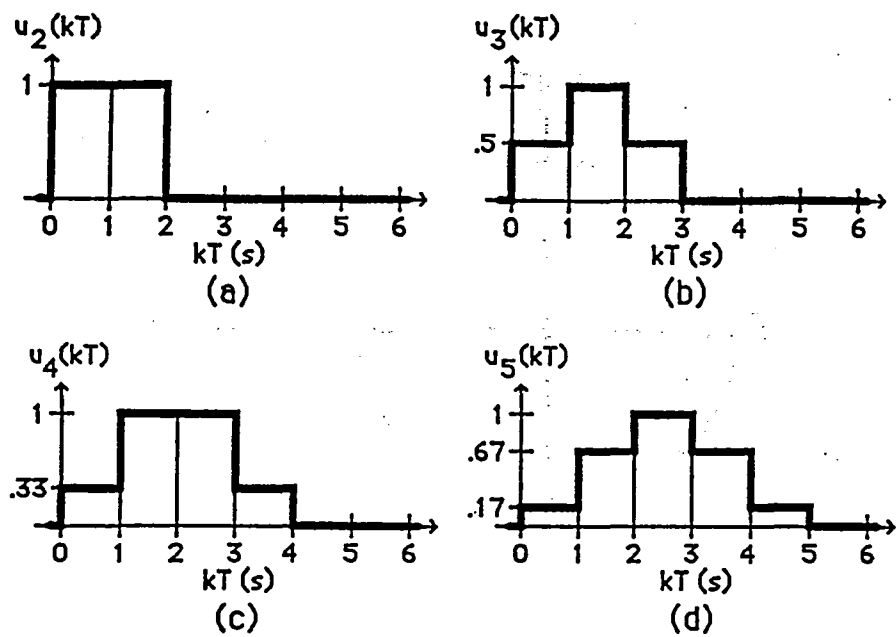


Figure 7a: Held Version of Normalized Binomial Sequences

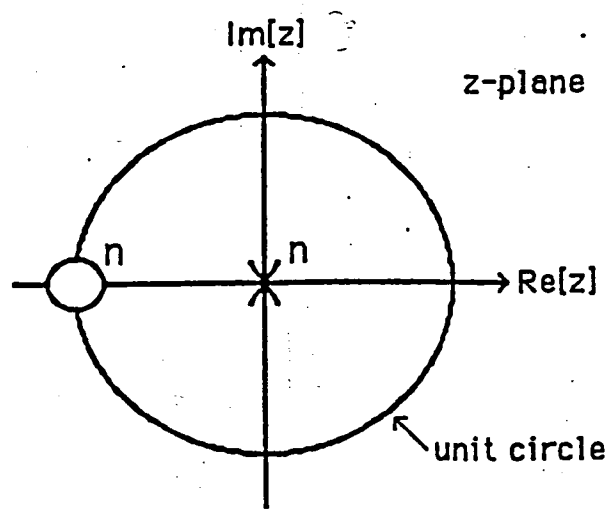


Figure 7: General Pole-Zero Constellation of Shaped Sequences

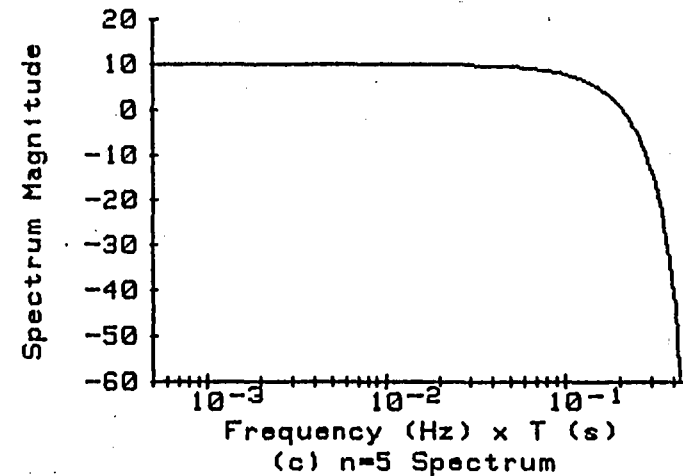
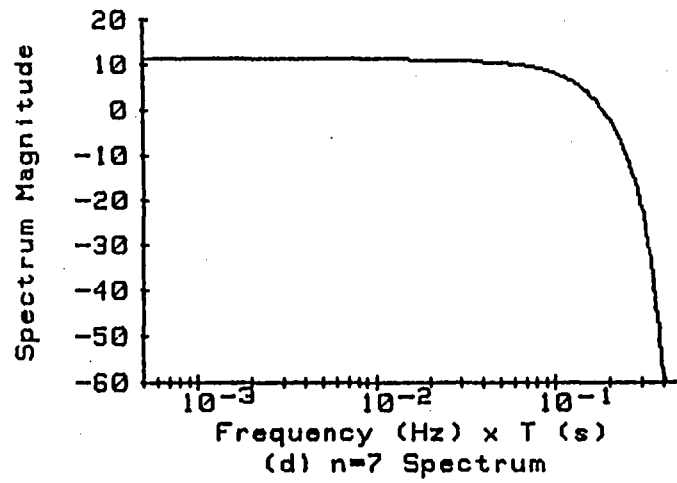
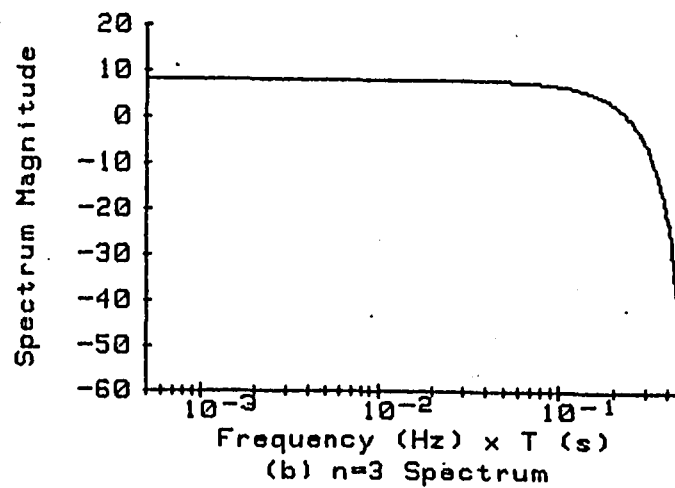
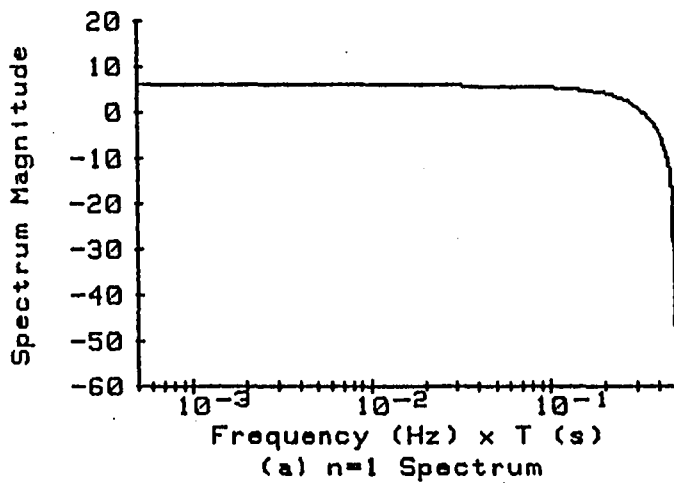


Figure 8: Spectra for Several Shaped Sequences

Maximum SNR Improvement by Shaped Sequences:

$$u_n(1) = (n - k)! k! \sum_{i=0}^n \frac{1}{(n - i)! i!} \quad , \quad (13)$$

Cutoff Frequency of Shaped Sequences:

$$f_c = \frac{1}{6.2832 T} \cos^{-1} [-1 + 1/(2 K^{1/n})] \quad . \quad (14)$$

Table 2: SNR Improvement, Cutoff Frequencies,
and Percent of Cutoff Frequency to
Half Sample Rate for the Shaped Inputs

n	U(1)	$f_c \times T$	f_c/f_{s2}	3 decades
0	1.0000	0.5	100 %	100 %
1	2.0000	0.25	50 %	89 %
3	2.6667	0.177	35 %	83 %
5	3.2000	0.151	30 %	81 %
7	3.6571	0.135	27 %	79 %
9	4.0635	0.125	25 %	78 %
11	4.4329	0.116	23 %	76 %
13	4.7739	0.109	22 %	75 %
15	5.0921	0.105	21 %	75 %
64	10.0658	0.060	12 %	66 %

Averaging the Results of Testing

Well-known Fact: SNR can be improved by averaging the results from several identical tests.

Assumptions: (1) the noise is zero-mean and stationary

(2) There is no correlation between the corrupting noise from one test to another.

Fact: SNR is improved by a factor equal to the square of the number of test results averaged

Recommendation: In any situation where tests can easily be repeated averaging should be done.

Advantages: (1) SNR can be improved by a factor of two with as few as four measurements.

(2) From the test results periodograms can be computed, and, using as few as two of these, estimates of coherence functions can be obtained.

EXPERIMENTAL VERIFICATION

1. Base Excitation Table
2. 3 Axis Base Accelerometers
3. 3 Axis Gimbal System
4. 3 Axis Base Rate Gyros and Counterweight
5. 3 Axis Tip Accelerometers
6. 3 Axis Tip Rate Gyros
7. Optical Detector
8. Mirrors
9. Laser
10. 2 Axis Pointing Gimbal System
11. LMED System

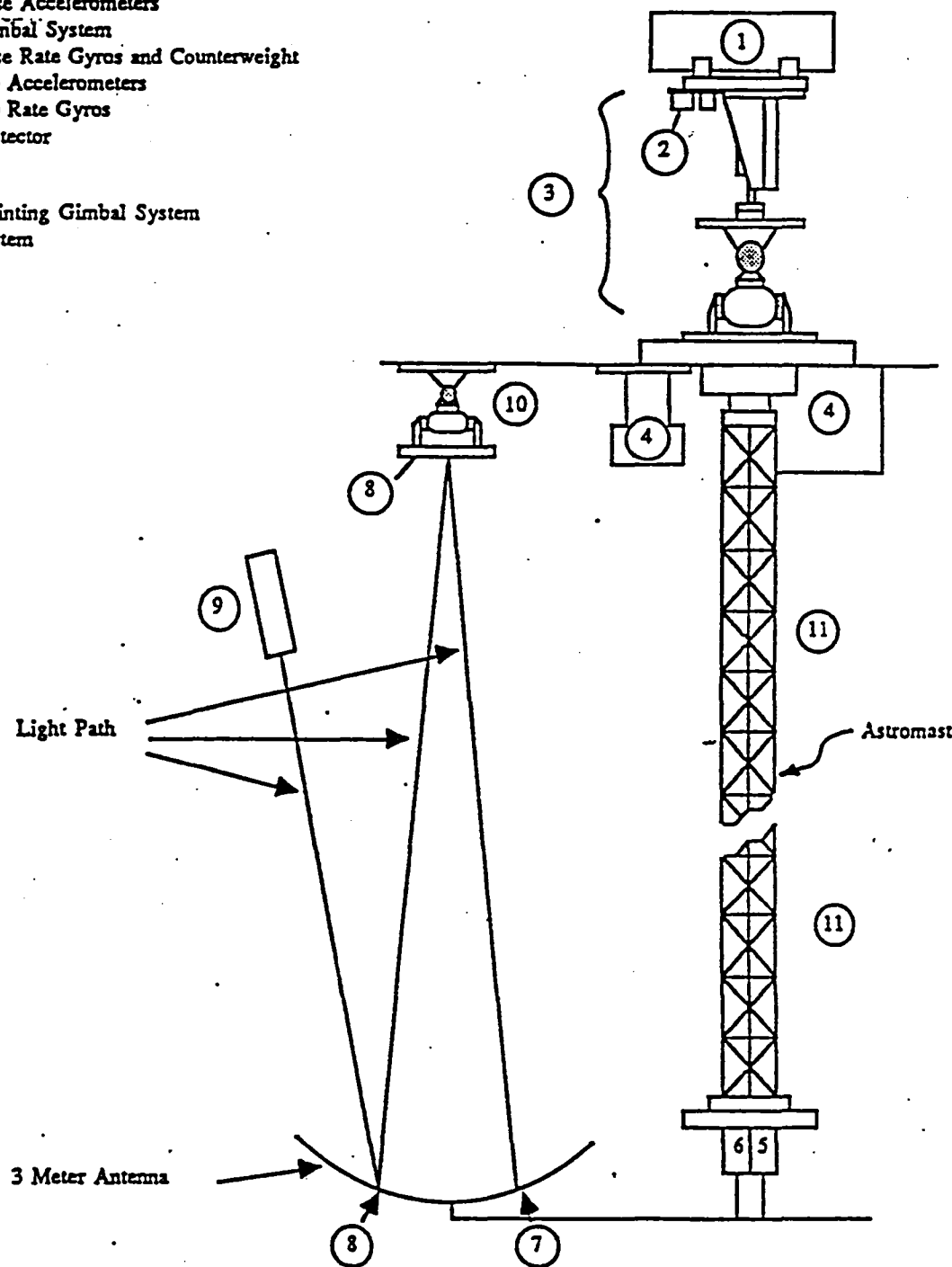


Figure 9: LSS Ground Test Facility at Marshall Test Flight Center

Sample Results of System ID

Inputs Applied:

- (1) Sequences of Ones of Two,
Three, and Four
- (2) Shaped Input of Order Three
- (3) Noise Input

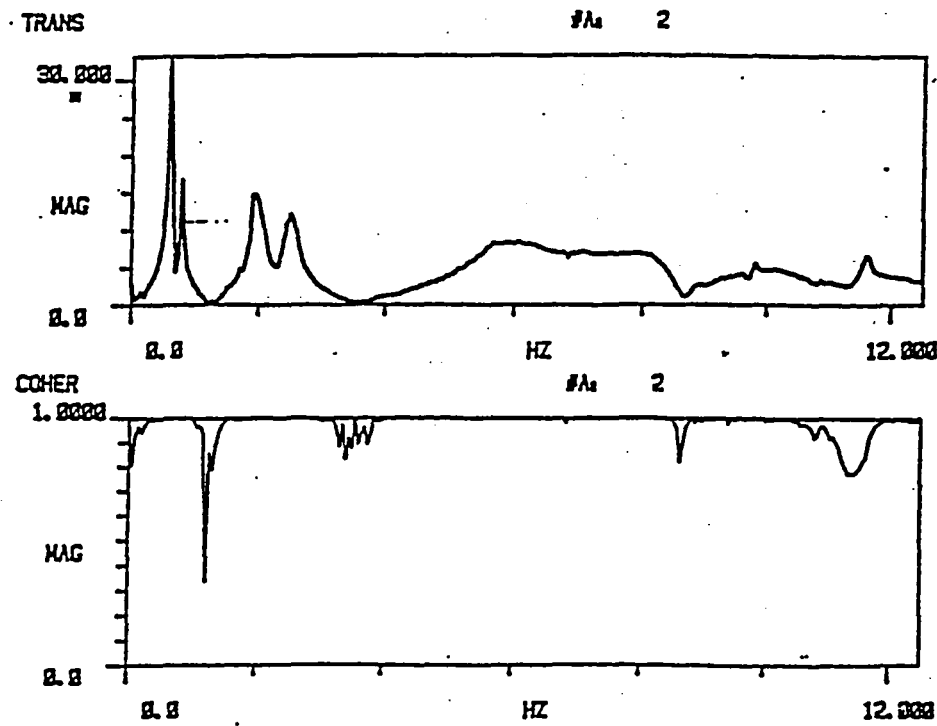


Figure 10: Magnitude and Coherence Estimates for $n=2$ Sequence of Ones Using Two Averages

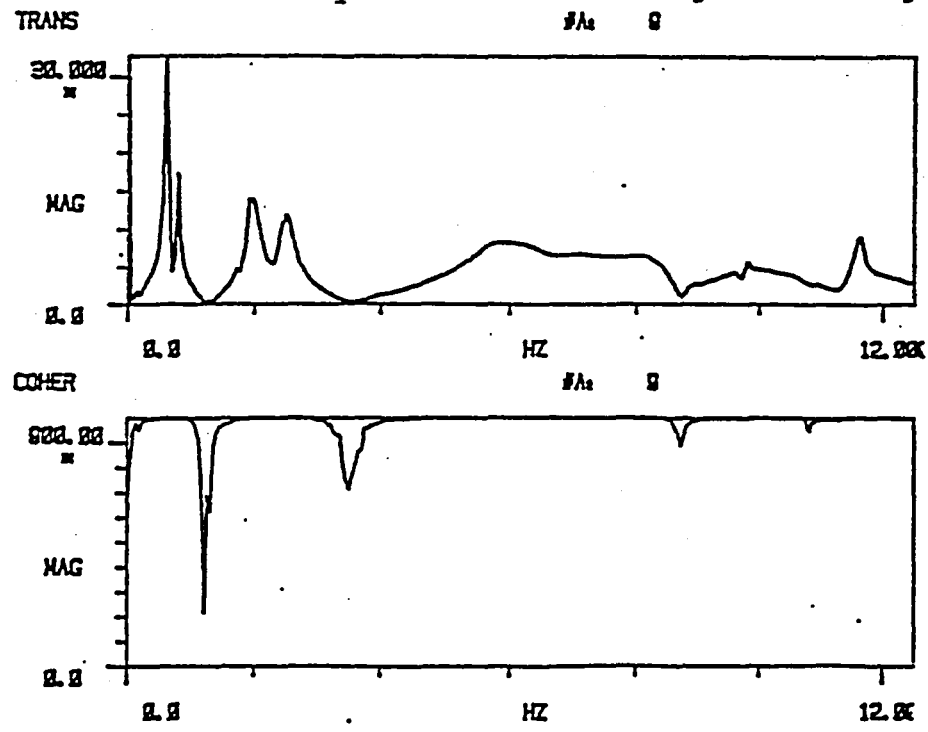


Figure 11: Magnitude and Coherence Estimates for $n=2$ Sequence of Ones Using Nine Averages

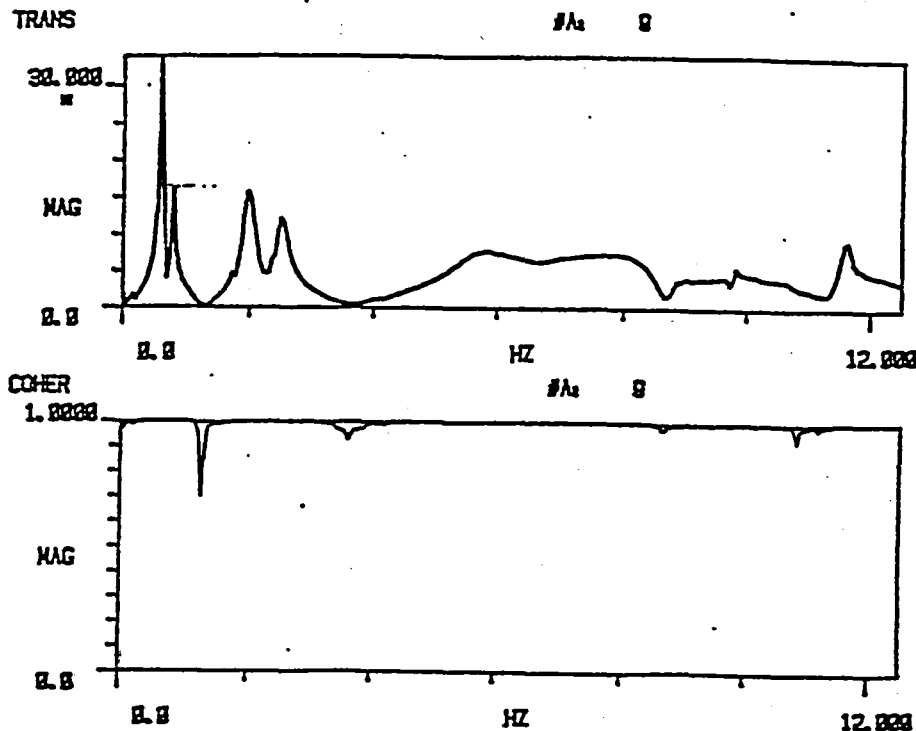


Figure 12: Magnitude and Coherence Estimates for
n=3 Sequence of Ones Using Nine Averages

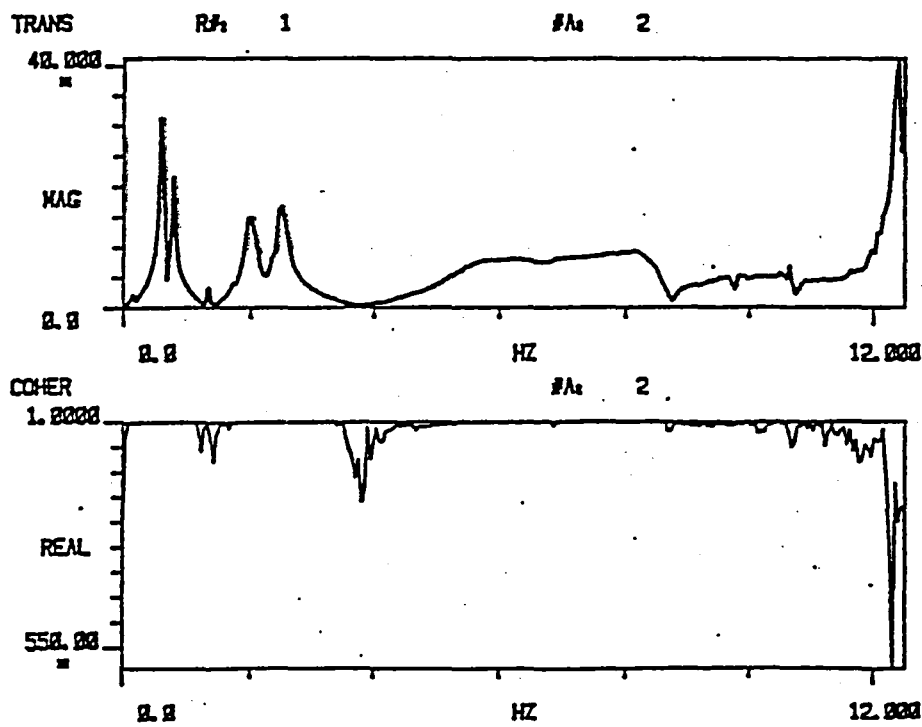


Figure 13: Magnitude and Coherence Estimates for
n=4 Sequence of Ones Using Nine Averages

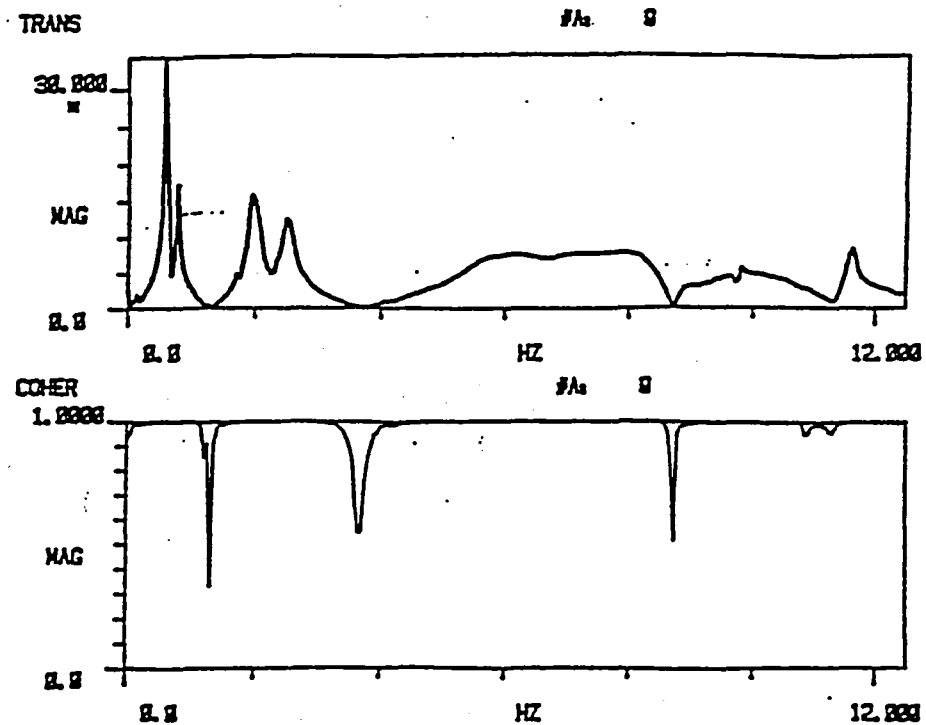


Figure 14: Magnitude and Coherence Estimates for $n=4$ Shaped Sequences using Nine Averages

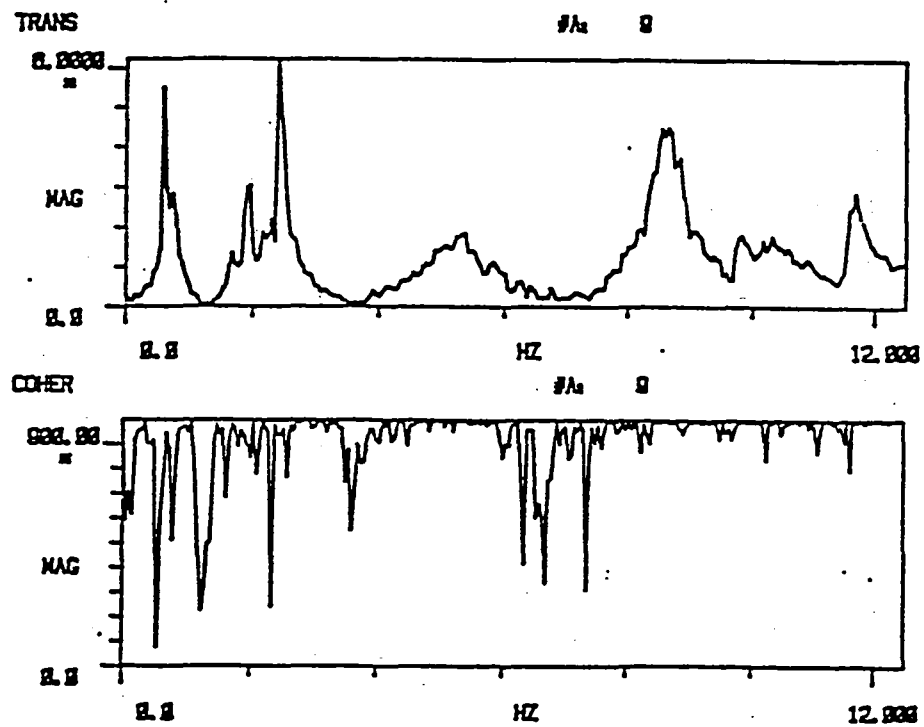


Figure 15: Magnitude and Coherence Estimates for Random Sequences Using Nine Averages

CONCLUSION

Techniques for Improving the SNR in Frequency Response System ID:

- (1) Increase Input Amplitude
- (2) Sequences of Ones
- (3) Shaped Inputs

Testing and Validation of System ID Techniques:

LSS Ground Test Facility at MSFC

"Bottom-Line":

Results are Good.

Looking for Another Facility for Testing

OVERHEAD #1: TITLE AND ABSTRACT

FORMULATION AND VERIFICATION OF FREQUENCY RESPONSE
SYSTEM IDENTIFICATION TECHNIQUES FOR
LARGE SPACE STRUCTURES

Jerrel R. Mitchell¹ and Victoria L. Jones²

Abstract

For the past several years much effort has been given to the development of techniques for designing control systems for large space structures (LSS's). The main objective of these efforts has been to develop a LSS control methodology that produces designs that meet strenuous performance requirements and are robust to model inaccuracies. Unfortunately, performance and robustness are conflicting requirements. Because LSS's can not be fully tested on ground, it has become an accepted fact that the design of LSS control systems to meet performance requirements can not be completed until the LSS is placed on-orbit and tested and an accurate model is extracted from on-orbit test results. Modern MIMO sampled-data frequency response design techniques are viable candidates for designing LSS control systems. First, this paper presents techniques for performing MIMO system identification (ID) from test data. Then, techniques for improving the performance of the system ID process in the presence of noise are presented. Finally, practical utility of the system ID approaches are validated by the presentation of results obtained from application on the LSS Ground Test Facility at Marshall Space Flight Center.

¹Professor and Chairman, Electrical and Computer Engineering, Ohio University, Athens, OH 45701

²Staff Engineer, Control Dynamics Company, Huntsville, AL 35802

OVERHEAD #2 - OUTLINE OF PRESENTATION

First, a brief introduction of the subject material is presented along with justifications for the research being reported. Then, MIMO sampled data frequency response system ID techniques for control systems are outlined. Techniques for improving the system ID process in the present of noise is presented next. Results from application on the Large Space Structure Ground Test Facility at Marshall Space Flight follows. Finally, results and conclusions are summarized and future plans are indicated.

OVERHEAD #3: INTRODUCTION

Future large space structures (LSS's), such as the NASA Space Station, will be constructed from the interconnection of many long, flexible, light-weight beams. Control systems for LSS's will be required for attitude control and vibration suppression. Two key requirements for successfully designing these control systems are the accuracy and fidelity of the LSS dynamical models. State-of-the-art modeling techniques do not produce trusted results past the first few modes, and LSS's can not be completely tested on ground. As a consequence, designing attitude and vibration suppression control systems, that will meet required performance criteria, will not be completed until the structure is placed on-orbit and models have been derived or fine-tuned from on-orbit test results.

Design-to-Performance (DTP) is a LSS control system design philosophy in which (1) the system is excited with control system actuators and data is collected at control system sensors, (2) using system identification techniques, sampled-data frequency response models are determined from this data, and (3) using these models and modern, multivariable, frequency response design techniques, attitude and vibration control systems are generated [1]. Candidate design techniques include the 1-CAT [2], MIMO CIP [3] and Positivity [4].

This paper is concerned with the system identification (second) step in the DTP philosophy. First, the theoretical approach for obtaining and characterizing multiple-input, multiple-output (MIMO) systems with sampled-data models is presented. Then, pragmatic solutions for physically obtaining these frequency responses are presented. In particular, obtaining the models when the test data has been corrupted by noise is addressed. Techniques for improving the signal-to-noise ratio are presented, along with pragmatic and theoretical limitations.

OVERHEAD #4: MIMO SYSTEM IDENTIFICATION

System identification is a very generic term. Its definition can run the gamut from the determination of the elements of the matrices in a state variable formulation to the determination of mode shapes, frequencies and damping ratios for modal models [5,6]. The type and planned use of a model define what the product of the system identification process should be. For LSS's the model will be used to fine-tune or redesign the control system for both attitude and vibration control.

The mission of control systems for LSS's will be to achieve attitude control and vibration suppression. The performance requirements of control systems are expected to be strenuous. In order to achieve the performance goals the control strategy for LSS's of the future will include several coupled control loops. The selection of the physical locations of the sensors and actuators for achieving performance goals is critical; however, this is not a topic in this paper. In fact, the scenario for the application of the system ID techniques presented and developed in this paper are (1) the LSS has been placed or assembled on-orbit, (2) the control sensors and actuators of the LSS are in fixed locations, and (3) the performance of the control system (designed using the best data available prior to launch or on-orbit fabrication) is unacceptable.

The above setting is the premise to the DTP philosophy. The approach is to excite the system with the control system actuators, collect data with the control system sensors, determine sampled-data frequency response models using this data, and use these models to fine-tune or redesign the control system. Since the data will be collected with the control system sensors, the data rate will be the same as that of the control system. Models derived from this data will inherently include the effects of the sampling operation of the control system. Also, delays and errors in the control system due to A/D and D/A processes will be inherently taken into account, and expected computational delays can be included. As a consequence, the on-orbit data obtained from exciting the system with the control system actuators and making measurements with the control system sensors is the best data from which control system models can be extracted. Furthermore, because the controllers will be digital, sampled-data models will be needed to accurately design these controllers.

Consider the linear, time-invariant (LTI) MIMO sampled-data system shown in Figure 1. There are p inputs and q outputs for this system; thus, there are pq paths along which inputs can be propagated to outputs.

OVERHEAD #5: EQUATIONS FOR DESCRIBING MIMO SYSTEM

Using a matrix-vector formulation, the relationship between the inputs and outputs is shown where and z is the z -transform variable. From (2) it is easily seen that the relationship between the i -th input and the j -th output as given in equation (4). In fact, the i -th column in the matrix $H(z)$ describes how the i -th input affects each output.

OVERHEAD #6: SAMPLED-FREQUENCY RESPONSE

Suppose that all inputs are set to zero except the i -th and measurements of the input and all output sequences are made. The sampled-data frequency responses of the transfer functions between the i -th input and each output is represented by the given equation.

OVERHEAD #7: PROBLEM WITH EQUATION (5)

Equation (5) is simply a z -domain representation of the output spectrums divided by the input spectrum. The problem with (5) is that it represents the ratio of two infinite series. For signals with all poles inside the unit circle, both are converging series. Since the input sequence is selectable, there is no problem in assuming that the series formed from this sequence converges. In fact, an obvious and pragmatic choice is a finite sequence, that consequently produces a finite series. If the input sequence is convergence or finite, then the series formed from the output sequence converges, provided the system is stable, i.e., all z -domain poles lie inside the unit circle. Of course this is reasonable to expect since the testing of unstable systems is not practical. In regard to LSS's it is well known that all flexible modes are stable, although lightly damped. However, rigid body modes have poles at $z=1$, which are not stable. In order to test systems with unstable rigid body modes, loops must be closed to add damping to these modes. This can easily and safely be accomplished by closing minimum bandwidth loops with collocated sensors and actuators, e.g., a torque actuator and rate sensor located at approximately the same physical location.

OVERHEAD #8: APPROXIMATE SAMPLED-DATA FREQUENCY RESPONSE

Assuming the system to be stable and assuming that the input sequence has all poles inside the unit circle (a finite sequence satisfies this condition), then (5) can be approximated as shown. In (6) the constant N is selected to minimize the error due to the truncation of the infinite series. Good results are achieved if N is selected so that

NT is greater than twice the largest time constant of the system or the input signal. Since the largest time constant is not normally known and/or cannot be estimated, experience has shown that good results are achieved if N is selected so that NT is greater than the time where each outputs' magnitude is roughly 10% or less of the maximum magnitude of the corresponding output.

OVERHEAD #9: PRACTICAL SYSTEM ID (NOISE PROBLEM)

Figure 1 portrays an ideal sampled-data MIMO control system. A practical problem in system identification, not shown in Figure 1, is that the measurements of the outputs are corrupted by noise. Output noise can either result from the measurement process or from disturbances exciting the system. Figure 2 shows the system with these noise inputs. In either case the output is not wholly due to the actuator inputs. The consequence of this is that additional error will be introduced in the system identification process.

OVERHEAD #10: SYSTEM ID WITH NOISE

In fact, it is easily shown that the sampled-data system identification process will produce results as shown in the equation, where $(^)$ represents the estimated value and $N_p(e^{j\omega T})$ is a noise component due to both system and measurement noise [8]. In the system ID problem $y_p(e^{j\omega T})$ can be thought of as the signal. If the noise is too great, no useful results will be produced from the system ID process, i.e., the results will be too noisy to be useful. However, there are various techniques for improving the results of the system ID process, if noise is expected to be a problem (which is the norm).

OVERHEAD #11: TECHNIQUES FOR IMPROVING THE MIMO SYSTEM ID PROCESS

As implied in the last section, the estimated frequency response of a desired sampled-data transfer function can be thought of as the sum of a signal, i.e., the true frequency response, and noise. In order to improve the fidelity and accuracy in the system ID process, the signal-to-noise-ratio (SNR) must be increased. This implies that the ratio of the signal spectrum to the noise spectrum must be improved. For the case at hand, the nature of the signal and noise is very different. The signal results from the measurement of a converging transient response, which makes it an energy type signal. On the other hand, noise is normally assumed to be a power signal, i.e., it has infinite energy. Thus, the signal

to noise ratio, for the case at hand, is defined to be the ratio of the magnitude of the signal spectrum to the square root of the power spectrum of the noise. Equation (8) represents this definition. An interesting and useful feature of (8) is that it presents a definition of SNR that is a function of frequency. If the power spectrum of the noise is known, the corruption of measurements of various signals can be computed and compared on a frequency by frequency basis. If the noise is not known and if the system is linear, (8) can be used to perform relative comparisons of various signals for improvement of the SNR on a frequency by frequency basis. In the system ID problem there is assumed to be no control over the noise. The power spectrum $S_N(e^{j\omega t})$ is assumed to be stationary and can be either known or unknown. Then, from (8) the only way to improve the SNR is to increase the magnitude of the signal spectra.

OVERHEAD #12: Four Basic Ways to Improve SNR

The four basic ways for improving the SNR are presented on the slide. In the following, the rationale and physical implementation of each of these, along with advantages and disadvantages, are presented [8].

OVERHEAD #13: INCREASING INPUT MAGNITUDES

If in the system ID process an input is increased by a constant multiplier, A , then the signal magnitude spectrum will be increased by A . Hence the SNR will increase by A . Although this is an obvious and easily implemented approach for increasing the SNR, there are some practical limitations. First, there will be some level of excitation that results in the actuator and/or sensor becoming saturated. Second, the system can be driven so hard that nonlinear structural effects will dominate. In either case the system ID process may produce results that will be of little utility in design and can even be misleading or incorrect.

OVERHEAD #14: INCREASING INPUT DURATION

The ideal inputs for system identification are signals with flat spectra. Such inputs are ideal because all modes, regardless of frequency, receive equal excitation. As a consequence, the best excitation for determining sampled-data frequency responses is the digital one (shown on the slide when $n=0$). The digital one has a flat spectrum from zero to the half-sample frequency, the maximum frequency that need be considered in the sampled-data case.

OVERHEAD #15: CHARACTERISTICS OF THE DIGITAL ONE

The digital one is simply a one occurring $t=0$ zero. The held version of a digital one is a pulse of duration T seconds. The magnitude spectra of the digital one is flat.

OVERHEAD #16: SEVERAL DIGITAL ONES SEQUENCES

Unfortunately, there is no other digital input that possesses a flat spectrum like the digital one. However, there are digital signals with amplitudes less than or equal to the digital one which have spectra significantly greater than the digital one over a broad band of frequencies. One class of such signals is generated by applying a sequence of ones, rather than a single one. The held versions of these sequences (called protracted pulses) of one, two, three, and four ones are shown in Figure 4. For each respective higher order sequence the physical system simply sees a corresponding protracted pulse of longer duration.

OVERHEADS #17 & 18: MAGNITUDE SPECTRA AND SUMMARY TABLE OF SEVERAL DIGITAL ONES

The magnitude spectra of several digital ones sequences are, shown. As the order of the sequence increases, the low frequency portion of the magnitude of the spectrum is increased by an amount equal to the order plus one. The regimes where the plots exceed unity are where improvements result in the SNR, in comparison to the digital one. As the order increases so does the number of null points, and as the order increases null points occur at lower and lower frequencies. In the frequency regimes in the vicinity of the nulls the identification will significantly degrade. The maximum improvement in the SNR results at d.c. Table 1 shows the low frequency SNR improvement and the null frequencies for the first four digital ones sequences. Because of the nulls the use of high order sequences of digital ones to improve the SNR must be used with care.

OVERHEAD #19: SHAPED INPUT SEQUENCES

An alternative to the digital ones sequences, for increasing uniformly the magnitude of the spectra of the output signals with respect to frequency, is to apply shaped inputs. Classically this has been accomplished by generating sequences with uniform, white, random number generators on the interval $[-1,1]$. The difficulty with this approach is that even very long sequences of random numbers

do not produce flat spectra. (The reason being that the z-transforms of finite, random sequences have randomly located zeros.)

A class of sequences, called normalized binomial or Pascal sequences, that have reasonable wide-band spectra has z-transforms of the following as present in equation (10), where n denotes the order of the respective sequence. In fact, when n is zero, the digital one sequence is generated. In (10) K is used to scale the sequence so that the maximum value generated will not result in saturation of the actuator. Again, without loss of generality, it is assumed that K is selected so that no element of the sequence exceeds unity in magnitude. For this class of signals K is as shown in equation (11), where k is the integer part of $(n+1)/2$. Then, the general form of the shaped sequences is presented in equation (12).

OVERHEADS #20 & 21: HELD BINOMIAL SEQUENCES AND POLE ZERO CONSTELLATION

The spectra of sequences from this class can be anticipated by looking at the pole-zero constellation of the signal, shown in Figure 7. In particular, inputs of this type have all poles at the origin and all zeros at $z=-1$. Hence, each spectrum will be approximately flat in the low frequency range and will roll-off as frequency approaches the half sample rate. The roll-off rate is directly proportional to the order of the sequence. An interesting characteristic of these signals is that in the low frequency regime every other spectrum increases in magnitude as the order of the sequence is increased. The maximum increase in the spectrum occurs at d.c., i.e., zero frequency.

OVERHEAD #22: SPECTRA OF SHAPED SEQUENCES

The spectra for $n = 1, 3, 5$ and 7 are shown in Figure 8. As mentioned above, as n increases so does the low frequency portion of each spectra. It is, also, seen that the spectra rolls-off rapidly as frequency approaches the half sample rate and that the roll-off rate increases with n . As with the sequences of digital ones, the SNR, with respect to the digital one, is better in the regimes where the magnitudes of the spectra is greater than unity. Different from the digital one sequences, all nulls occur at the half sample frequency. As the order of the sequence increases so does the order of the null. As a consequence, the band over which an SNR improvement occurs decreases as the order of the sequence increases.

OVERHEAD #23: SNR IMPROVEMENT AND CUTOFF FREQUENCY FOR SHAPED SEQUENCES

Maximum improvement in the SNR for the shaped sequences is given by equation (13). The frequency where the magnitude of the sequence is equal to one is defined to be the cutoff frequency. The cutoff frequency, f_c , in Hz can be computed from equation (14).

OVERHEAD #24: TABLE SUMMARIZING SEVERAL SHAPED SEQUENCES

Table 2 shows the spectra magnitudes at d.c. and corresponding normalized cutoff frequencies for several sequences of this type. It should be noted that short sequences can produce reasonable improvements in the low frequency SNR, i.e., a factor of two to three. However, to get dramatic improvements in the SNR, e.g., a magnitude or better, a long sequence is needed. An obvious price paid for using the long sequences is the short effective bandwidths, i.e., zero to f_c , that are presented on a percentage basis in the third column. In the case of the sequence of order sixty-four, Table 2 shows that the effective bandwidth for a magnitude improvement in the SNR is only 12% of the half sample frequency, f_{s2} . However, it should be noted that in most control system work spectra and frequency response data are normally viewed as a function of log frequency. When viewed in this way, the decrease in bandwidth is less severe. The fourth column shows the effective signal bandwidth on a percentage basis for a three cycle log scale. This is also reemphasized by looking at the plots in Figure 8.

The lengths of the long sequences do not pose a realizability problem. However, the dynamic range of the numbers in the long sequences can be a problem. In particular the dynamic range of the numbers in the 64-th order sequence is well beyond the dynamic ranges of current state-of-the-art D/A converters, e.g., 12, 16 or 24 bit converters.

OVERHEAD #25: AVERAGING THE RESULTS OF TESTING

When dealing with signal detection or measurement problems in which a signal has been corrupted with noise, it is well-known that the SNR can be improved by averaging the results from several identical tests. The basic assumption that must be made is that the noise is zero-mean and stationary and there is no correlation between the corrupting noise from one test to another. The averaging can be done in the time domain or the frequency domain. If n tests are made

and the results are averaged, it is well-known that the SNR is improved by a factor equal to the square root of n [7].

In any situation where tests can easily be repeated averaging is highly recommended, regardless of the system ID technique used. First, with as few as four tests, the SNR can be improved by a factor of two. Second, from the test results periodograms can be computed, and, using as few as two of these, estimates of coherence functions can be obtained. The estimates of the coherence functions provide strong evidence on how well a system ID process is working. In particular, if the estimated coherence is near one for various frequency ranges, there is a strong indication that the signal dominates in the output measurements in these frequency ranges. On the other hand, if the coherence function drops significantly below one over various frequency ranges then the output measurements are dominated by noise over these ranges. If there are no ranges in which the coherence function is near one, then the output is probably dominated by nonlinear effects. Therefore, the estimate of the coherence function is a valuable tool in assessing the results in system ID [7].

OVERHEAD #26: EXPERIMENTAL VERIFICATION

OVERHEAD #27: LSS GROUND TEST FACILITY AT MSFC

Experimental verification of the model improvement schemes proposed was performed at the LSS GTF (Ground Test Facility) at Marshall Space Flight Center. The structure tested is shown in Figure 9. The structure is representative of an LSS in that it is a large, flexible structure with many closely spaced, lightly damped, low frequency modes. The objective of the LSS GTF is to examine the control and dynamics of LSS's. The structure consists of a 45 ft lightweight beam, a measurement system, an actuation system, a mirror and laser system, an antenna, a computer system (for data acquisition and structural control), and a disturbance excitation system. The measurement system consists of two three-axis accelerometer packages, two three-axis rate gyroscopic packages, two two-axis accelerometer packages, and a two-axis laser detector. The actuation system consists of three control gimbals, four linear momentum exchange devices, and two mirror control gimbals. Several representative sampled-data frequency responses obtained from testing the structure were extracted using the schemes presented previously [9].

The system identification concepts described in this paper were experimentally applied at the LSS GTF. The concepts of input amplitude maximization, frequency domain

averaging, digital one sequences, and shaped sequences were each employed. A representative transfer function was chosen as the standard for the comparisons. The transfer function from the control gimbal (x-axis torque) to the base gyro (x-axis angular rate) was experimentally determined.

An HP 5423 Spectrum Analyzer was utilized to calculate the transfer function from the actuator input and sensor output time responses. It was desired to perform the system ID over a bandwidth from zero to 12.5 Hz. The spectrum analyzer used a sample rate of 50 Hz, which is identical to the sampling period of the computer system used for control. An exponential window was applied to the output time response due to the very low frequencies and low damping values. The spectrum analyzer assumes the time response has decayed to zero at the final time (20.5 sec); thus, the window was used to shape the time histories to be consistent with this assumption. Care was taken to ensure that the structure response had died out before proceeding to the next test.

OVERHEAD #28: SAMPLE RESULTS OF SYSTEM ID

Several input signals were applied to the control actuator in order to identify the sampled-data transfer function. The input signals included white noise, a shaped sequence of length four units, and digital ones sequences of lengths two, three and four. Averaging was employed for each input signal. The transfer function corresponding to each input signal was determined using two, five, and nine averages. A maximum amplitude of approximately 30 N-m was used for the shaped and digital ones sequences. This amplitude was prudently chosen to be as large as possible without saturating any actuators or sensors during the tests.

The experimental results support the analytical system identification techniques presented above. The coherence functions for each transfer function were excellent. The techniques were simple to apply, and the transfer functions did not require a great deal of time to generate.

OVERHEAD #29: FIGURES 10 & 11

The digital ones sequence of length two was the input signal used to generate the transfer function whose magnitude is shown in Figure 10 (a). The plot in Figure 10 (b) is the estimated coherence function for this case. The units for the magnitude response are $(\text{rad/s})/(\text{N-m})$. Two averages were employed to estimate the transfer and coherence functions. The estimated coherence function indicates that the system ID process has worked well at most frequencies. As expected,

the coherence value is low for frequencies where the magnitude frequency response is effectively zero. This is expected since the SNR will be low for such cases. This shows that the system ID process will not produce accurate results in the vicinity of a system null (lightly damped zero). It should be noted that in the design of control systems accuracy of the model in the vicinity of a null is not crucial.

Figure 11 is the estimated magnitude response of the transfer function generated with the same input signal but with nine averages. The additional averages improve the SNR by a factor greater than two. This improvement is seen in both the estimate of the coherence function and the estimate of the magnitude response of the transfer function.

OVERHEAD #30: FIGURES 12 & 13

A sequence of ones of length three was used as the input to estimate the magnitude response and the coherence function in Figure 12. Comparison of the results for the $n=2$ and $n=3$ cases reveals a small degree of improvement in the coherence function for the longer sequence. This is expected since there is an SNR improvement of 1.5.

A sequence of ones of length four was the actuator input utilized to produce the estimate of the magnitude response in Figure 13 (a). Figure 13 illustrates the fact that the frequency response of the longer sequence ($n=4$) has the disadvantage of having a null at 12.5 Hz. This null the erroneous pole at approximately 12.5 Hz and, as seen in Figure 13 (b), a correspondingly low coherence near this frequency. The values of the estimated coherence function provide a warning that the results near 12.5 Hz should not be trusted.

OVERHEAD #31: FIGURES 14 & 15

A shaped sequence of length four was the excitation signal used to estimate the magnitude response shown in Figure 14 (a). The data presented in Figures 11, 12, 13, and 14 show similar results. An advantage of using shaped sequences are that the signals applied to the actuator are more gradually applied than the digital ones sequences. In the case at hand, the input signal null did not interfere with the estimation of the magnitude of the transfer or coherence functions.

As mentioned previously a classical approach to frequency response system ID is to use pseudo, random

sequences as inputs. Supposedly, these sequences have flat spectra; however, since they are finite in length, this is not possible. Therefore, for this approach to work, averaging must be used. Such an approach was used here. Nine pseudo random noise sequences were applied to the control actuator and averaging was used to produce the estimates of the magnitude response and coherence function in Figure 15. A comparison of Figures 11, 12, 13, and 14 to Figure 15 shows that the sequences of ones and the shaped inputs produced much more accurate estimates of the magnitude response. The estimated coherence function for the noise input case also indicates that the estimated magnitude response is questionable, especially at low frequencies. A test case was also run with fifty pseudo, random sequences. As would be expected the estimate of the coherence function showed an improvement, but there were still low coherence levels at many frequencies.

OVERHEAD #32: CONCLUSIONS

There are many advantages to designing control systems for LSS's using (non-analytical) frequency-domain models extracted from empirical (time) data. The most salient advantage of this procedure is convenience. The tedium of analytical modeling can be obviated. This is especially true for LSS's since these highly flexible structures theoretically have an infinite number of modes. Moreover, the analyst can avoid making decisions as to which modes are significant. Another advantage to this procedure is that it can lead to robust designs. This is due to the fact that the controls engineer can relax performance criteria at frequencies where the model is somewhat uncertain. Some more advantages are that the effects of sampling and transport-lag are automatically accounted for by using this procedure.

Classical system identification using deterministic inputs (SIUDI) is a viable method of obtaining frequency-domain, sample-data models; however, steps should be taken to ensure that the models obtained have sufficient accuracy as well as adequate fidelity. (Additional information regarding classical system identification can be found in, for instance, Bendat and Piersol. [5]) Models can be enhanced using the schemes presented, and a combination of the schemes can be applied so that the SNR problem is attacked from more than one angle. The analyst should evaluate the particular problem at hand and determine what combinations of schemes for improving SNR are appropriate.

There are limitations to the schemes presented. Nonlinearities can reduce the effectiveness of the schemes. For example, hysteresis can cause nonrepeatability of dynamic

tests. This can compromise the effectiveness of frequency response averaging and possibly prevent or delay convergence. Additionally, the effects of signal quantization (which are unavoidable when analog-to-digital converters are used) can cause false high-frequency modes to appear. The analyst should be cognizant of the criteria that are necessary for the schemes presented to provide benefits. *Caveat emptor.*

The schemes presented can be applied to problems other than the control of LSS's. The use of classical SIUDI should be considered whenever a dynamic process that does not lend itself to analytical modeling is being analyzed.

ACKNOWLEDGEMENTS

This research was funded in part by the National Aeronautics and Space Administration (Office of Aeronautics and Space Technology and Marshall Space Flight Center), contract number NAS 8-35835. Credit is due Control Dynamics Company and Ohio University for their cooperation in the preparation of this paper. Special thanks are due Dr. Henry B. Waites (of NASA) who provided helpful criticism and encouragement.

REFERENCES

1. J.R. Mitchell and V.L. Jones, "LSS Control System Design and System Identification Using Design-to-Performance," Final Report, Submitted by Control Dynamics Company to The National Aeronautics and Space Administration, George C. Marshall Space Flight Center, Contract No. NAS 8-36673, AL, April 1986.
2. L. L. Gresham and J. R. Mitchell, "The Compensator Program as an Aid for Designing Multivariable Control Systems", AIAA Journal on Guidance and Control, Vol. 3, No. 4, July 1980.
3. J.R. Mitchell, S.M. Seltzer, and D.K. Tollison, "1-CAT (One-Controller-at-a-Time): A Frequency-Domain Multi-Input Multi-Output Design Approach," Proceedings of the 1984 AIAA Guidance and Control Conference, Seattle, WA, August 1984.
4. "ACOSS Fourteen (Active Control of Structures)", Final Report, TRW, Sponsored by DARPA, Contract No. F30602-81-0194, November 1982.
5. J. M. Mendel, Parameter Estimation: The Equation Error Formulation, Marcel Dekker, New York, NY, 1980.
6. H. W. Sorenson, Parameter Estimation, Marcel Dekker, New York, NY, 1980.
7. J.S. Bendat and A.G. Piersol, Random Data: Analysis and Measurement Procedures, Wiley-Interscience, New York, 1971.
8. C.P. Plant, "Schemes for Improving the Fidelity of Empirical Sampled-data Frequency-domain Models of Large Space Structures," Masters thesis, Mississippi State University, May 1987.
9. H.B. Waites and H.E. Worley, "Large Space Structures Testing," NASA TM-100306, George C. Marshall Space Flight Center, AL, June 1987.

3/4/88

N93-72774

163824

f. 21

Modal Model Reduction
or
Model Reduction of Large Space
Structures in Frequency Domain

by

Ruan Mifang
Graduate Student

and

A.S.S.R. Reddy
Assistant Professor
Department of Mechanical Engineering
Howard University
Washington, D.C. 20059

Presented at the Workshop on

Model Determination for Large Space Systems
at California Institute of Technology
Pasadena, California
March 22-24, 1988

Contents

- **Introduction**
- **Assumptions**
- **Formulation**
- **Optimization Method**
- **Examples**
- **Remarks**
- **Conclusions**

INTRODUCTION

- Large space structures are characterized by large number of modes, grouped frequencies, small inherent damping.
- Model reduction techniques in time domain may not be effective due to small damping.
- Model truncation method is generally used. This method can not solve the problem of grouped frequencies, and will lose all the information about the higher order modes.
- A new method developed in this paper, which tries to minimize the error of interested transfer functions, makes use of all the informations of the original system, and achieves improvement not only from smaller error of transfer functions but also from better frequency distribution.

Assumptions

- Proportional Damping is assumed
- System is expressed by a set of linear, constant coefficient, second order differential equations.

Structural Dynamic Model:¹
(FEM)

$$\ddot{M}\ddot{X} + KX = F \quad (1)$$

$M = NXN$ mass matrix

$K = NXN$ stiffness matrix

$X = NX1$ generalized coordinate vector

$F = NX1$ external force vector

Modal Analysis:

$$X = \phi q \quad (2)$$

$$\phi^T K \phi = \begin{bmatrix} \omega_1^2 & & \\ & \ddots & \\ & & \omega_N^2 \end{bmatrix} = [\omega^2] \quad (3)$$

$$\phi^T M \phi = I \quad (4)$$

$\omega_1, \omega_2, \dots, \omega_N$ are natural frequencies of vibration

or: solution of the eigen value problem

$$\omega_i^2 M \phi_i = K \phi_i \quad (5)$$

Modal Coordinate Equations of Motion:

$$\ddot{q} + [\omega^2] q = \phi^T F \quad (6)$$

Experimental Modal Analysis:²

$$s^2 q(s) + [\omega^2] q(s) = \phi^T F(s) \quad (7)$$

$$q(s) = [s^2 I + [\omega^2]]^{-1} \phi^T F(s) \quad (8)$$

$$x(s) = \phi [s^2 I + [\omega^2]]^{-1} \phi^T F(s) \quad (9)$$

$$H(s) = \phi [s^2 I + [\omega^2]]^{-1} \phi^T \quad (10)$$

$$H_{ij}(s) = \frac{x_i(s)}{F_j(s)} \Big|_{F_i(t)=0} = \sum_{k=1}^N \frac{\phi_{ik} \phi_{jk}}{(s^2 + \omega_k^2)} \quad (11)$$

$i \neq j$

$$H_{ij}(s) = H_{ji}(s) \quad (12)$$

with proportional damping:

$$H_{ij}(s) = \sum_{k=1}^N \frac{\phi_{ik} \phi_{jk}}{(s^2 + 2\zeta_k \omega_k s + \omega_k^2)} \quad (13)$$

$$H_{ij}(\omega) = \sum_{k=1}^N \frac{\phi_{ik} \phi_{jk}}{(-\omega_k^2 + \omega_k^2 + 2\zeta_k \omega_k \omega)} \quad (14)$$

$$i = \sqrt{-1} \quad (\text{imaginary})$$

$x_i(t)$ is measured for given input $F_i(t)$

$F_i(t)$ = impulse or sinusoidal

Fast Fourier Transform of:

$$x_i(t) \longrightarrow x_i(\omega) \quad (15)$$

$$F_i(t) \longrightarrow F_i(\omega)$$

are calculated.

From experimental $H_{ij}(\omega)$'s, ω_k , ζ_k , ϕ_{ik} , ϕ_{jk}

for $k = 1, 2, \dots, n (< N)$, $i, j = 1, 2, \dots$ are evaluated.

Redundant information is used to prune ϕ_{ik} and ϕ_{jk} values.

Model Reduction³

Original transfer function:

$$\begin{aligned}
 H_{ij}(\omega) &= \sum_{R=1}^n \frac{\phi_{ik} \phi_{jk}}{((\omega_k^2 - \omega^2) + I 2\zeta_k \omega_k \omega)} \\
 &= \sum_{k=1}^n \frac{\phi_{ik} \phi_{jk} (\omega_k^2 - \omega^2)}{\Delta(\omega)} - I \frac{2\phi_{ik} \phi_{jk} \zeta_k \omega_k \omega}{\Delta(\omega)} \quad (16)
 \end{aligned}$$

where

$$i = 1, 2, \dots, n$$

$$j = 1, 2, \dots, n$$

$$\Delta(\omega) = (\omega_k^2 - \omega^2)^2 + (2\zeta_k \omega_k \omega)^2$$

Reduced transfer function:

$$\begin{aligned}
 H'_{ij}(\omega) &= \sum_{k=1}^m \frac{\phi'_{ik} \phi'_{jk}}{((\omega'_k^2 - \omega^2) + i 2\zeta'_k \omega'_k \omega)} \\
 &= \sum_{k=1}^m \frac{\phi'_{ik} \phi'_{jk}}{\Delta'(\omega)} - I^2 \frac{2\phi'_{ik} \phi'_{jk} \zeta'_k \omega'_k \omega}{\Delta'(\omega)} \quad (17) \\
 \Delta'(\omega) &= (\omega'_k^2 - \omega^2)^2 + (2\zeta'_k \omega'_k \omega)^2
 \end{aligned}$$

ω'_k , ζ'_k , $k=1, 2, \dots, m$ are assumed.

Error:

$$\begin{aligned} e_{ij}(\omega) &= \|H_{ij}(\omega) - H_{ij}'(\omega)\|^2 \\ &= (H_{ij}(\omega) - H_{ij}'(\omega))(H_{ij}(\omega) - H_{ij}'(\omega))^* \end{aligned} \quad (18)$$

$$E_{ij} = \int_{\Omega_1}^{\Omega_2} r_{ij}(\omega) e_{ij}(\omega) d\omega \quad (19)$$

Ω_1, Ω_2 = lower and upper limits of frequency of interest.

$r_{ij}(\omega)$ = weighting function

Total Error on all the transfer functions:

Method I:

$$E = \sum_{i=1}^{n_s} \sum_{j=1}^{n_a} E_{ij} \quad (20)$$

n_a = number of force locations

n_s = number of sensor locations

Thus E is a function of ϕ'_{ij} 's.

As E is a non-linear function of ϕ'_{ij} 's, the optimization algorithms are used to minimize E and thus selecting ϕ'_{ij} 's.

Method II:

$$E_{ij} = \int_{\Omega_1}^{\Omega_2} r_{ij}(\omega) e_{ij}(\omega) dw \quad (21)$$

E_{ij} is a function of ϕ'_{ij} 's where $\phi'_{ik}\phi'_{jk}$ occur in pairs. A new variable B_k^{ij} is defined as

$$B_k^{ij} = \phi'_{ik}\phi'_{jk} \quad (22)$$

Thus E_{ij} is a quadratic function in B_k^{ij} and the minimization of E_{ij} with respect to B_k^{ij} results in m linear equations in m unknowns $B_1^{ij}, B_2^{ij}, \dots, B_m^{ij}$ and thus can be solved for unique solution. The modified eigen vector components ϕ'_{ij} for $i = 1, 2, \dots$; $j = 1, 2, \dots, m$ will be evaluated by minimizing E_{ij} for $i = 1, 2, \dots, j = 1, 2, \dots$.

Let $i = 1, 2, 3$; $j = 1, 2, 3$; and $m = 2$. As $E_{ij} = E_{ji}$, the following table demonstrates the redundant ϕ_{ij} 's evaluated

Error function	Corresponding ϕ_{ij}	
E_{11}	ϕ'_{11}	ϕ'_{12}
E_{22}	ϕ'_{21}	ϕ'_{22}
E_{33}	ϕ'_{31}	ϕ'_{33}
E_{21}	ϕ'_{21}/ϕ'_{11}	ϕ'_{22}/ϕ'_{12}
E_{31}	ϕ'_{31}/ϕ'_{11}	ϕ'_{32}/ϕ'_{12}
E_{32}	ϕ'_{31}/ϕ'_{21}	ϕ'_{32}/ϕ'_{21}

ϕ'_{ik}/ϕ'_{jk} indicates that ϕ'_{ik} is evaluated if previous ϕ'_{jk} is used or vice versa.

This kind of redundant information is common with Experimental Modal Analysis and techniques used in literature to harness this extra information can be used here.

Example: Space Station:⁴

FEM Structural Dynamic Model:

- 112 Nodes, each node has 6 degrees of Freedom thus M and K are 672×672 matrices
- NASTRAN was used and 60 natural frequencies of vibration (including the six rigid body modes) and the corresponding eigen vectors or mode shapes (with mode shape values in 672 degrees of freedom) are supplied by NASA.
- The structural damping is not modelled, but an equivalent proportional damping is assumed.
- Frequency distribution is shown in Fig. 3
- Typical node locations are shown in Fig. 2
- Space Station Initial operation configuration is shown in Fig. 1.

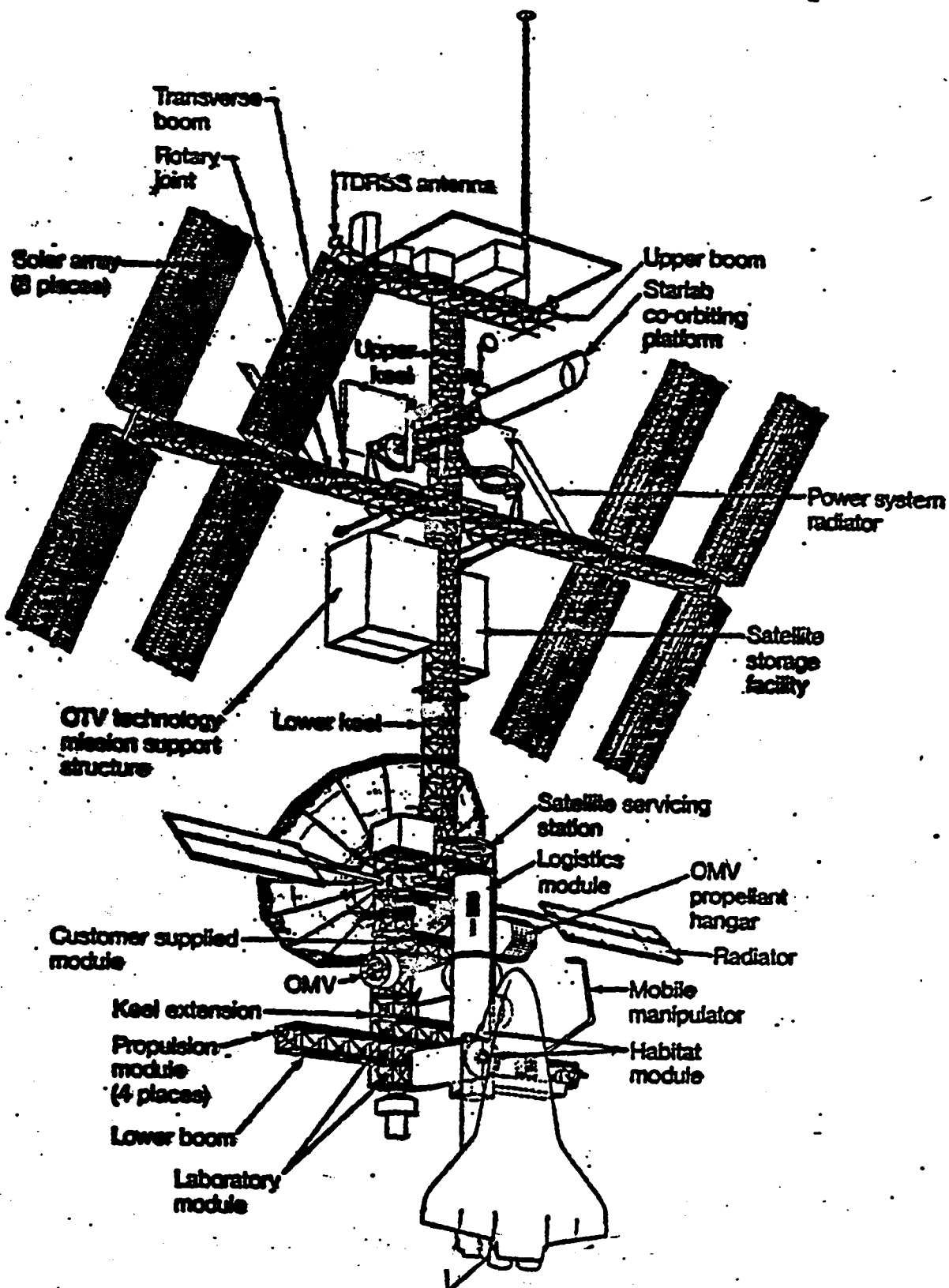


Figure: 1.1; Initial Operation Configuration (IOC) for Space-Station.

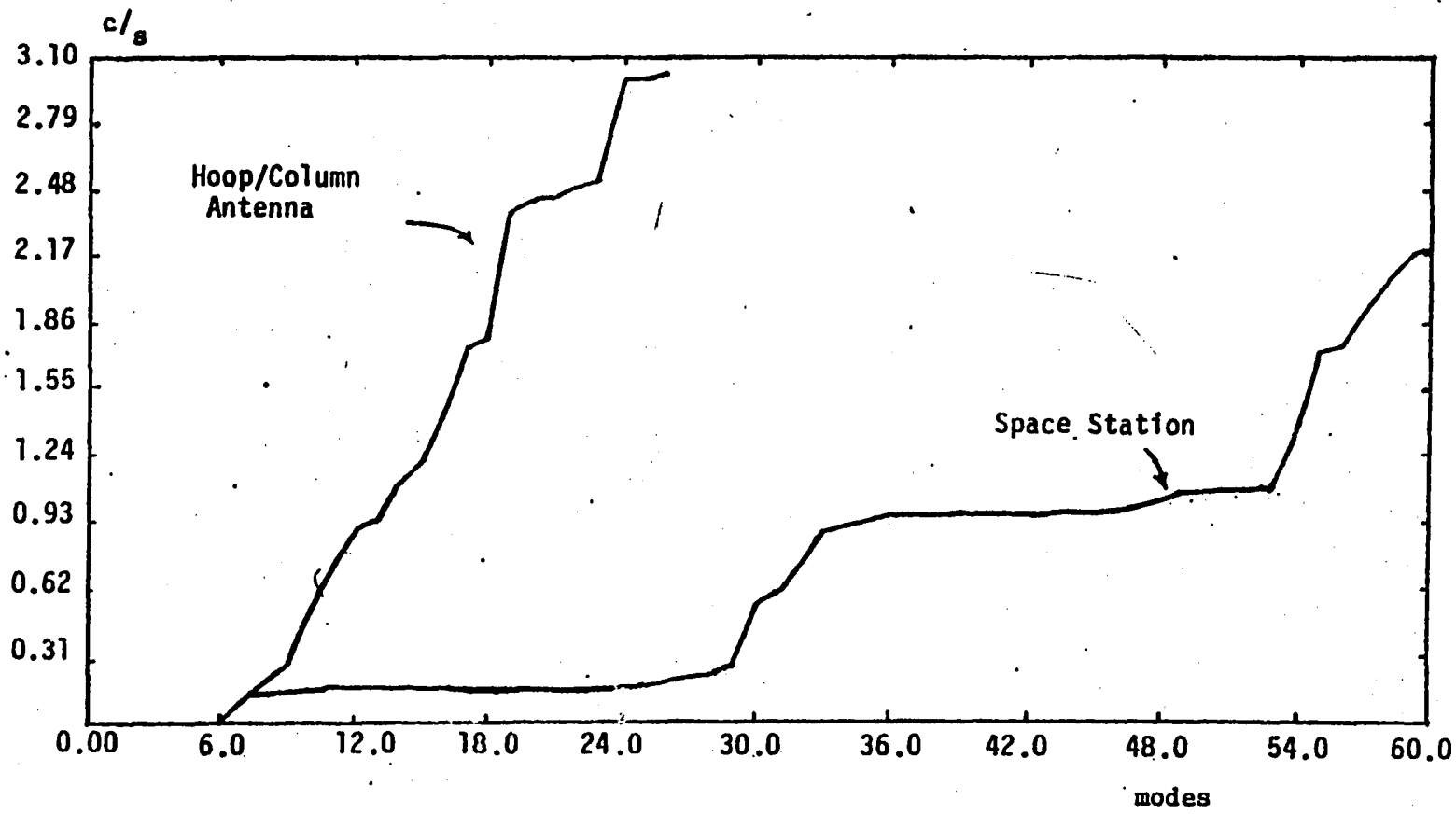
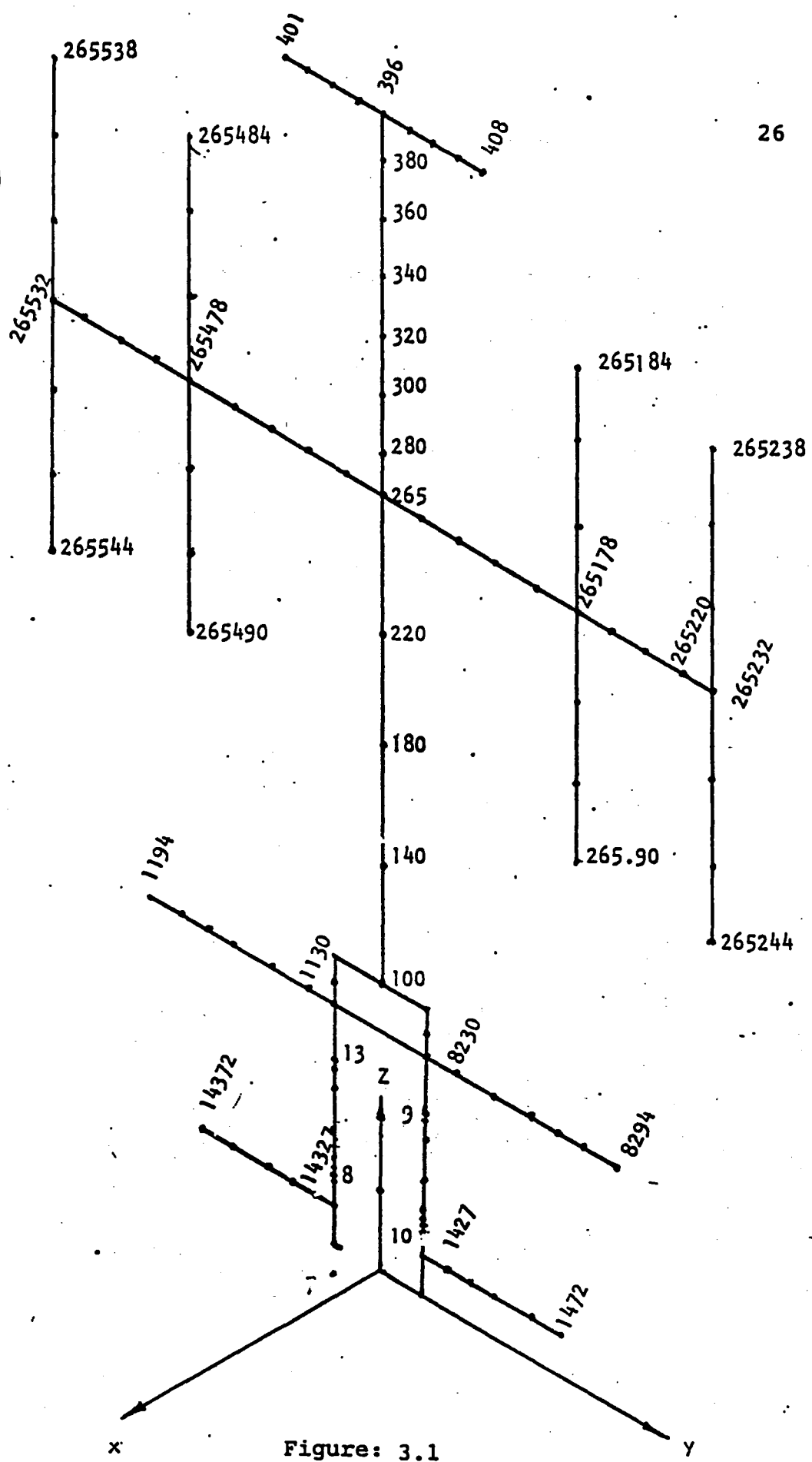


Figure 2.1: Modal Frequencies of Space Station.



Examples

- **Systems:** All examples refer to the system shown in Fig. 1.
- $n = 8, m = 3, \omega_{\max} = 6.0, r(\omega) = -\frac{1}{\omega_{\max}} \omega + 1$
- Assumed actuator and sensor locations are m_4 and m_7 .
- n = original number of degrees of freedom
- m = reduced number of degrees of freedom

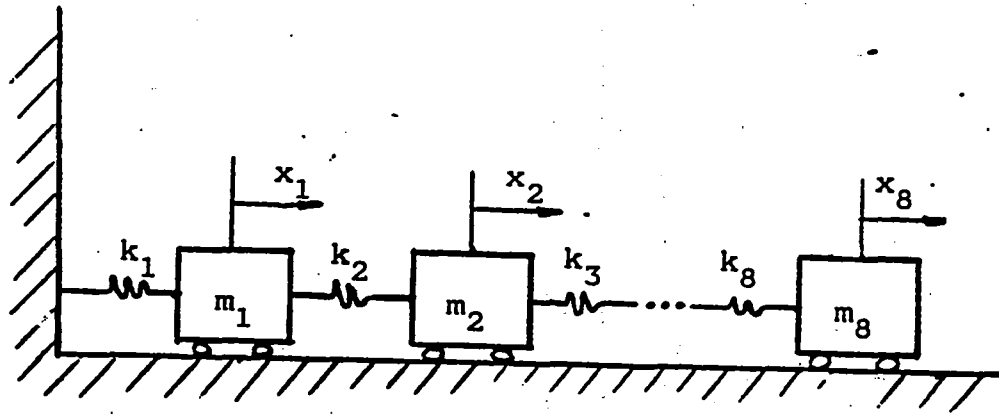


Fig. 1. The Mechanical System for the Examples

Example 1.

• $m_i = 1, k_i = 1, \zeta_i = 1$ ($i = 1, 2, \dots, 8$)

• Frequencies of original system:

$$\omega = \{0.1845, 0.5473, 0.8915, 1.205, 1.478, 1.700, 1.865, 1.966\}$$

• Assigned damping and frequencies:

$$\zeta' = \{1, 1, 1\}$$

$$\omega' = \{0.1845, 0.5473, 0.8915\}$$

Comparison of errors of transfer functions between optimal method and truncation method is listed in Table 1.

Example 2.

• System is same as above, but

$$\omega' = \{0.1845, 0.5473, 1.205\}$$

Comparison of errors is also listed in Table 1.

Table 1. Comparison of Errors of Transfer Functions
For Examples 1 and 2.

i	j	E _{ij}		
		Example 1		Example 2
		optimal	truncation	optimal
4	1	0.00094	0.00264	0.00055
4	2	0.00328	0.00720	0.00137
4	3	0.00379	0.00213	0.00222
4	4	0.01144	0.07656	0.00409
4	5	0.00178	0.01033	0.00137
4	6	0.00037	0.02028	0.00005
4	7	0.00239	0.00049	0.00465
4	8	0.00425	0.00926	0.00480
7	1	0.00087	0.00013	0.00094
7	2	0.00217	0.00032	0.00233
7	3	0.00105	0.00011	0.00110
7	4	0.00239	0.00049	0.00463
7	5	0.00210	0.00318	0.00164
7	6	0.00164	0.00144	0.00109
7	7	0.03142	0.06162	0.02893
7	8	0.01061	0.03013	0.0057
Total		0.08050	0.22634	0.06939
Ratio		35.6%		30.0%

Example 3.

- Resemble the cases of Large Space Structure

- light damping
 - grouped frequencies

- Choose m_i and k_i to get grouped frequencies

$$m = \{1.4403, 1.5996, 0.74633, 0.9905, 1.497, 1.1017, 0.1627, 0.2383\}$$

$$k = \{1.164, 1.493, 1.169, 0.0787, 1.14, 1.271, 0.639, 0.0646\}$$

- original frequencies and damping

$$\omega = \{0.1254, 0.4943, 0.5139, 1.0688, 1.3296, 1.6306, 1.7793, 2.2568\}$$

$$\zeta_i = 0.05 \quad (i = 1, 2, \dots, 8) \\ \text{(assumed)}$$

- Assigned frequencies and damping

$$\omega' = \{0.1254, 0.504, 0.107\}$$

$$\zeta' = \{0.05, 0.05, 0.05\}$$

Comparison of errors of transfer functions is listed in Table 2.

Table 2 Comparison of Errors of Transfer Functions
For Example 3.

i	j	E_{ij}	
		Example 3	
		optimal	truncation
4	1	0.05688	0.01514
4	2	0.12419	0.00659
4	3	0.15614	0.01313
4	4	0.17269	2.86616
4	5	0.25007	0.25108
4	6	0.07469	1.95164
4	7	0.34653	2.94836
4	8	0.16945	0.26322
7	1	0.07626	0.01884
7	2	0.16110	0.00680
7	3	0.20777	0.01869
7	4	0.34653	2.94836
7	5	0.53965	0.55993
7	6	0.81285	2.80350
7	7	21.76417	25.16987
7	8	0.19019	0.36419
Total		25.449	40.2055
Ratio		63.3%	

Fig. 2 shows sum of the errors of the transfer functions vs. frequency for both optimal and truncation cases.

Where error is defined as

$$e_1 = \sum_{i=1}^{N_{act}} \sum_{j=1}^n \|e_{\alpha(i),j}(\omega)\|^2$$

Fig. 3 shows error of the magnitude of H_{78} , defined as

$$e_2 = \|H_{78}\| - \|H'_{78}\|$$

Fig. 4 shows error of phase angle of H_{78} , defined as

$$e_3 = \text{Arg}(H_{78}) - \text{Arg}(H'_{78})$$

Simulation is done based on assumptions

- system decays only under damping
- purpose is to estimate the displacement X
- At $t=0$, every mode of the real system has a displacement 1 and velocity 0. ($\dot{q}_i=0, q_i=1$)
- Two sensors are attached to m_4 and m_7 .
The measurements are perfect.
- Estimator is designed by assumption of perfect measurements and unit plant noise.

- Sampling Ratio = 0.3 sec.
- Initial Conditions of estimator are zeros.

The data flowgraph for simulation is shown in Fig. 5.

Fig. 6 shows the norm of the estimation errors of displacements by both optimal method and truncation method.

Fig. 7 shows the error of x_5 .

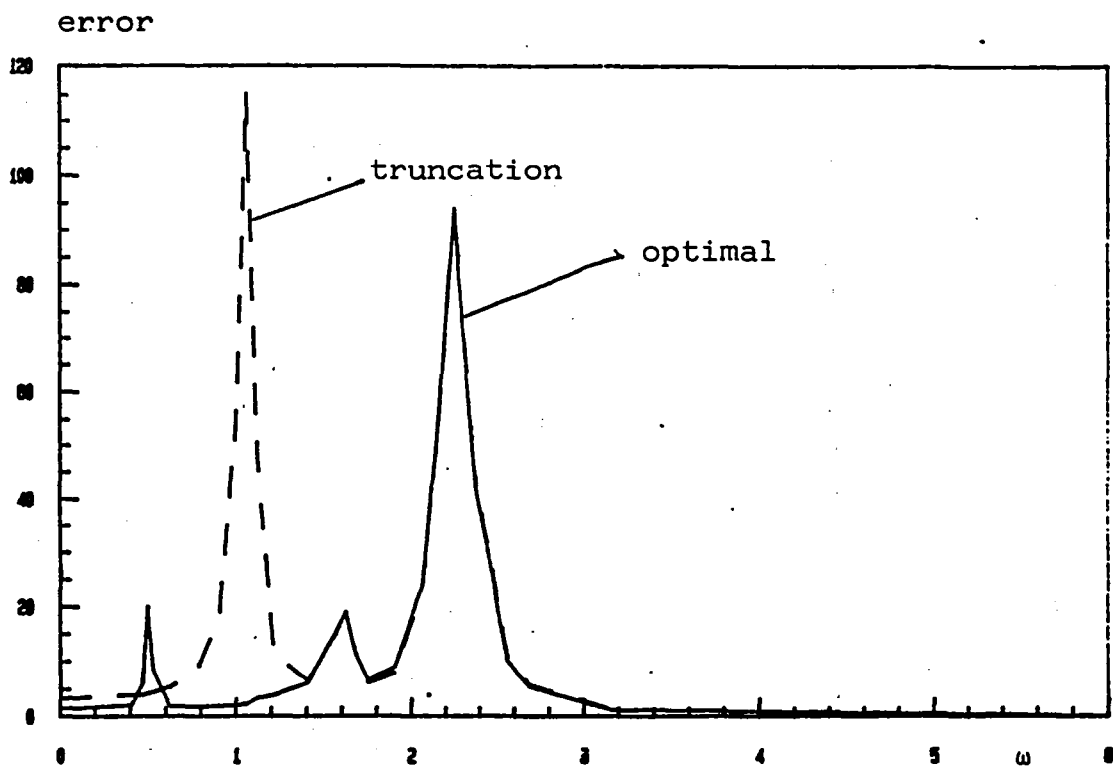


Fig. 2. Sum of errors of transfer functions

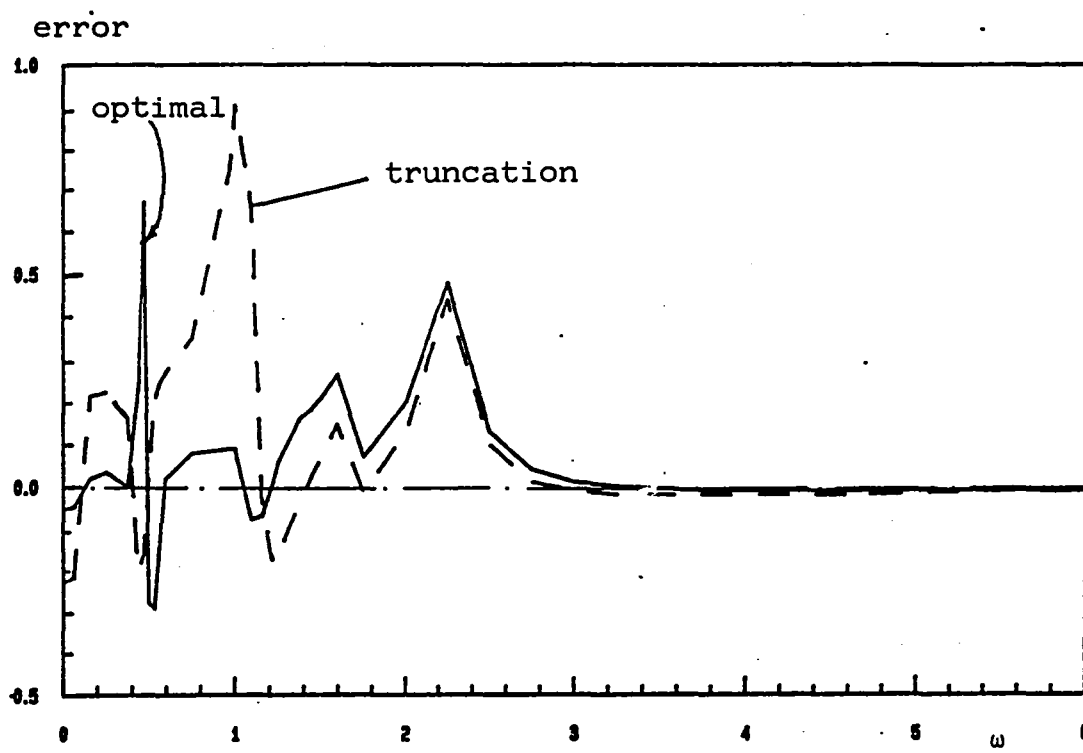


Fig. 3. Error of magnitude of H'_{78}

error

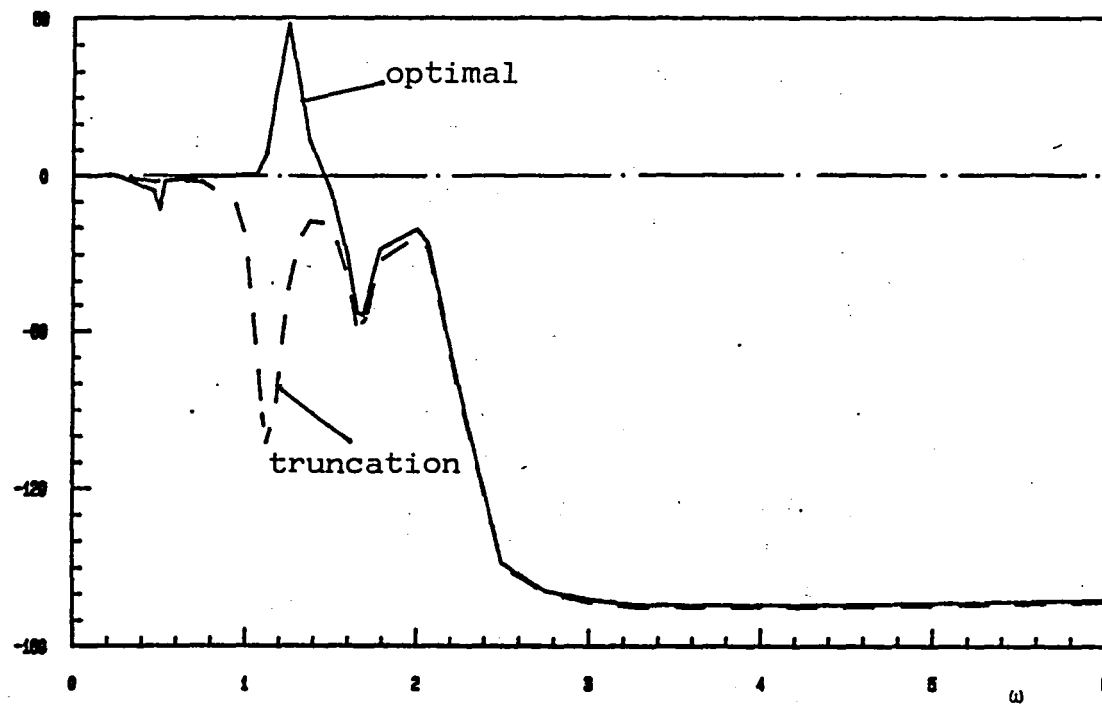


Fig. 4. Error of phase angle of H'_{78}

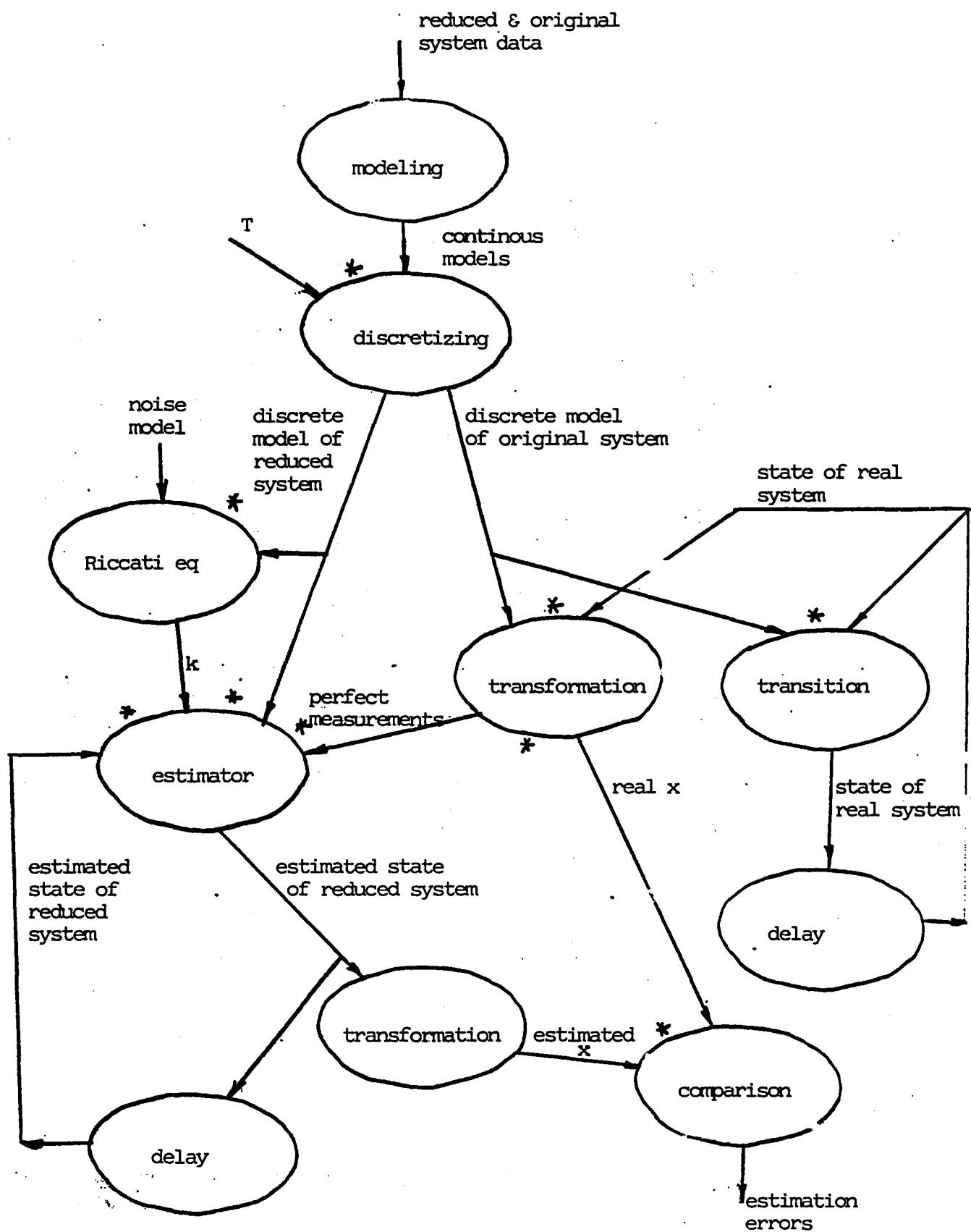


Fig. 7. Data flowgraph for simulation

error

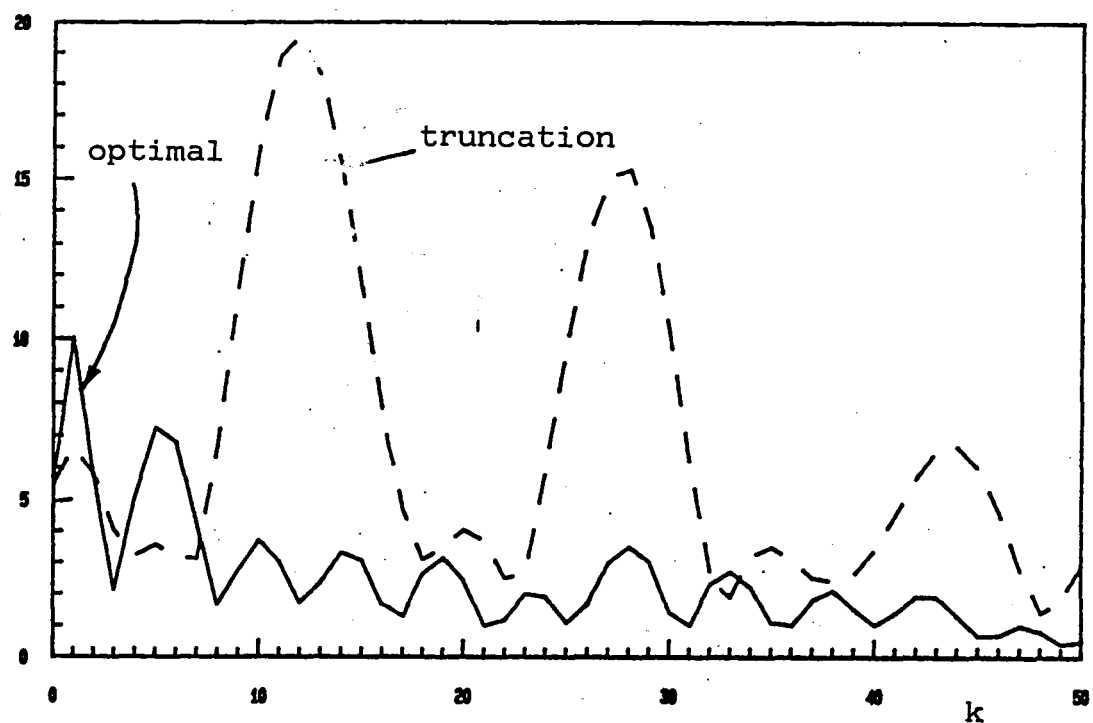


Fig. 5. Norm of estimation errors of X .

error

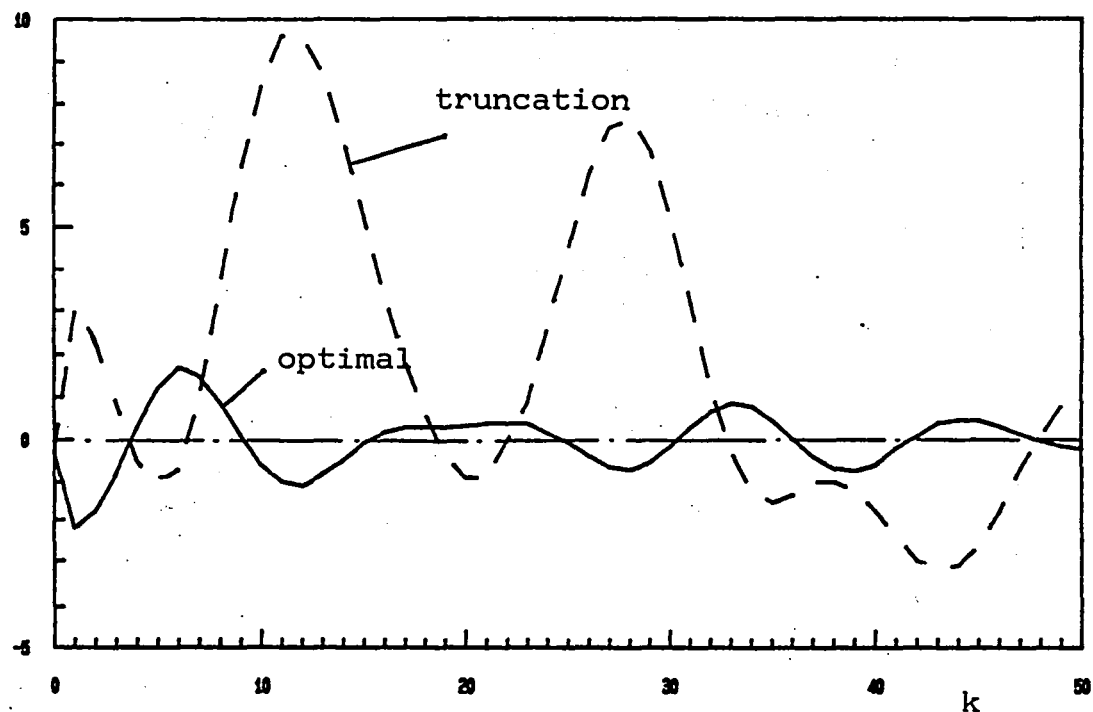


Fig. 6. Estimation error of X_5

CONCLUSIONS

- The transfer function matrix approach, with assumed number of modes, damping, over the frequency range of interest, is used to minimize the errors of the interested transfer functions between the original and the reduced models.
- To achieve better results, less number of transfer functions should be considered. Therefore, actuators and sensors should be co-located.
- The cost function has taken both magnitude and phase angle of the transfer functions into account. But the error of phase angle can be big, where transfer function is small.
- Compare with truncation method, the new method can achieve improvement not only from smaller error of transfer functions but also from better frequency distributions.
- Assumed frequencies and damping for the reduced system can be chosen by a little experience.
- The 1st optimization method(one step method) needs more computational time and memory, but can lead to better results, compare with the 2nd method(two step optimization).

References

1. Bathe, K.J., "Finite Element Procedures in Engineering Analysis"; Prentice-Hall, Englewood Cliffs, New Jersey, 1982.
2. Ewins, D.J., "Modal Testing: Theory and Practice," Research Studies Press Ltd., John Wiley & Sons, Inc., New York, 1984.
3. Jamshidi, M., "Large-Scale Systems: Modelling and Control", Series Volume 9, North Holland, New York.
4. Housner, J.M., "Structural Dynamic Model and Response of the Deployable Reference Configuration Space Station", NASA TM 86386, May 1985.

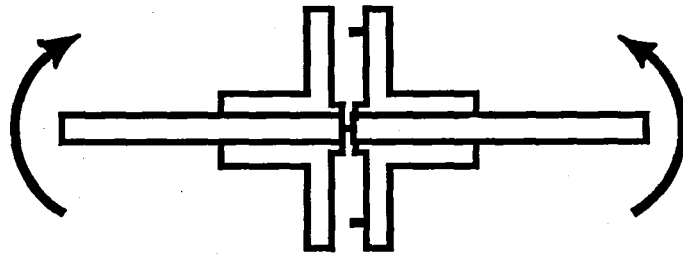
N 93-72775

5/5-18

163825

p. 33

EXPERIMENTAL COMPONENT MODE SYNTHESIS OF STRUCTURES WITH NONLINEAR JOINTS



Gary H. Blackwood and A. H. von Flotow
Department of Aeronautics and Astronautics
Massachusetts Institute of Technology
Cambridge, Massachusetts

Abstract

The accuracy of component mode synthesis is investigated experimentally for substructures coupled by non-ideal joints. The work is based upon a segmented experimental beam for which the free-interface frequency response matrices are measured for each segment. These measurements are used directly in component mode synthesis to predict the behavior of the assembled structure; the segments are then physically joined and the resulting frequency response of the superstructure is compared to the prediction. Rotational freeplay is then introduced into the connecting joint and the new superstructure frequency response is compared to the original linear CMS prediction. The level of accuracy to be expected in component mode synthesis is discussed in terms of the degree of nonlinearity in the joints, mode number and mode shapes.

The ground testing of large spacecraft structures becomes more complicated as the size of the flight structures increases¹. For instance, air damping and the interference of suspension systems with low frequency structural modes must be considered. For those structures too large to test on the ground at full scale, scale models have been proposed¹ to validate on-orbit dynamic behavior. The accuracy of scaling could become questionable, however, particularly when nonlinear joint dynamics such as deadband or hysteresis become important. Structures that will certainly include such "sloppy" joints are deployable trusses, such as the proposed NASA COFS MAST flight structure².

One alternative to testing the entire structure is to test small individual pieces--joints, truss members--and to use these static and dynamic test results to predict the behavior of the assembled structure via finite element analysis³. Such an approach would be at the other end of the "test spectrum" from full scale testing, and one might expect sizeable errors to accrue as hundreds or thousands of elements are assembled analytically. Figures 1 and 2 list possible options in such a "test spectrum".

PREDICTION OF FLEXIBLE SPACECRAFT DYNAMICS BASED ON GROUND TESTS:

WHICH METHOD TO USE?

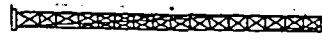
FINITE ELEMENT

FULL SCALE TESTS



SCALE TESTS

LARGE COMPONENTS
(TRUSS BAYS)



INDIVIDUAL PIECES
(JOINTS, TRUSS MEMBERS)

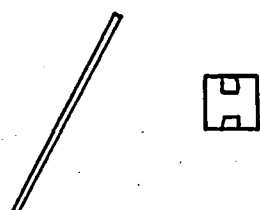


Figure 1: "Test Spectrum" for ground testing of large spacecraft structures

OPTIONS FOR GROUND TESTING OF LARGE SPACE STRUCTURES

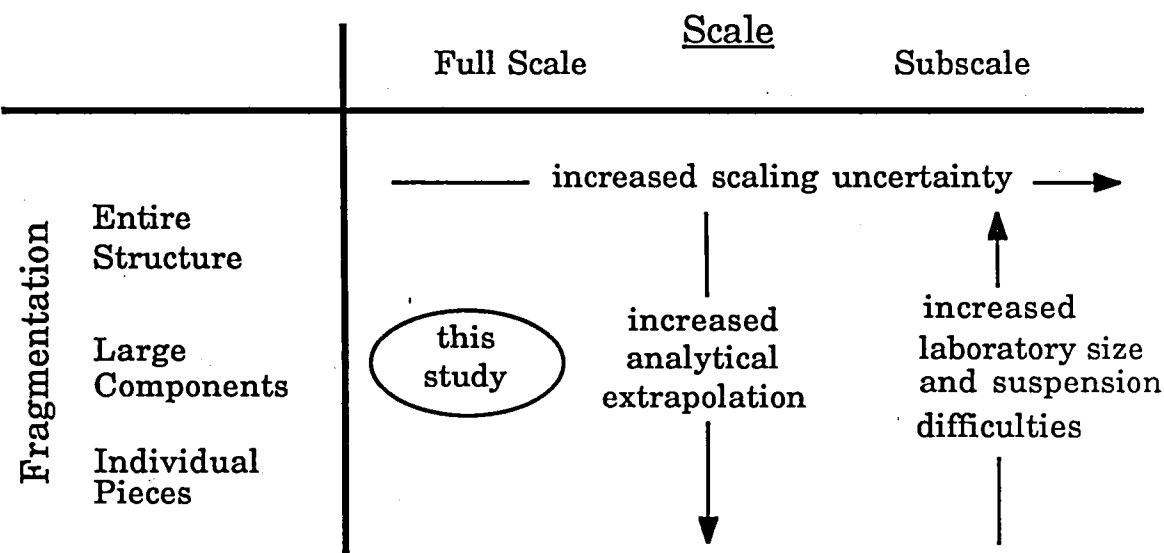


Figure 2: Options for ground testing of large spacecraft structures

Another alternative would be to ground-test full-scale components of a size as large as possible (limited by laboratory space and by component strength requirements), and to assemble these test results analytically. Such an approach would be in the center of the "test spectrum"--in between testing the entire structure and testing small pieces. For a deployable truss structure this might mean one or several bays out of a total of dozens for the entire structure. For a spacecraft consisting of a central bus and flexible appendages, each appendage might constitute a component and be ground tested. The measured dynamic behavior of the components can then, in principle, be used to predict the dynamic response of the entire assembly. The analytical extrapolation would be minimized since the components are chosen to be as large as possible.

COMPONENT MODE SYNTHESIS

TIME DOMAIN (Craig; Martinez, Carne and Miller, Baker)

- dynamic tests of components
- develop state space model (K , M) using complete set of mode shapes
- perform matrix assembly; solve eigenvalue problem of assembled structure

FREQUENCY DOMAIN (Ewins, Geering, Brassard and Massoud)

- dynamic tests of components
- develop modal model for each component in frequency domain
- calculate frequency response of assembled structure by impedance coupling

Procedures for performing analytical assembly of component dynamics are known as component mode synthesis (CMS), and can be implemented using time domain or frequency domain methods⁴. Previous work in analytical component mode synthesis has been extensive; some of the more popular methods include finite element techniques^{5,6}, time domain methods^{5,7}, and frequency domain CMS^{8,9,10,11}. A number of authors have undertaken experimental work in CMS. Bohlen and Gaul⁵ identify the parameters of a nonlinear joint by experiment, and use this model in a finite element analysis to predict the dynamics of two and three member structures connected by pin joints. Martinez, Carne and Miller¹² have developed an adaptation of Craig-Chang CMS techniques to free-interface dynamic testing of components. Ewins^{8,9} has developed an alternative component mode synthesis method in which component frequency response functions, either as raw data or after curve fitting, are used to produce the FRF of the coupled structure. As Craig⁵ has noted, there are strong similarities between this frequency domain CMS formulation and the time domain method, but these relationships are not yet fully explored. The measurement information required for each technique is essentially the same.

Ewins' frequency domain method was used in this research work, and a summary of this CMS formulation is presented here. Figure 3 shows typical components and a coupled structure. The frequency response matrix H^a for component A can be written to relate displacement to force, where x_m and x_p are displacement vectors of interior degrees of freedom (DOF) and x_o is a displacement vector of boundary DOF used in coupling. Forces f_m , f_p and f_o act upon these same interior and boundary DOF. Similar expressions can be written for component B. When components A and B are rigidly connected at interface o , compatibility and force equilibrium conditions can be written.

COMPONENT MODE SYNTHESIS

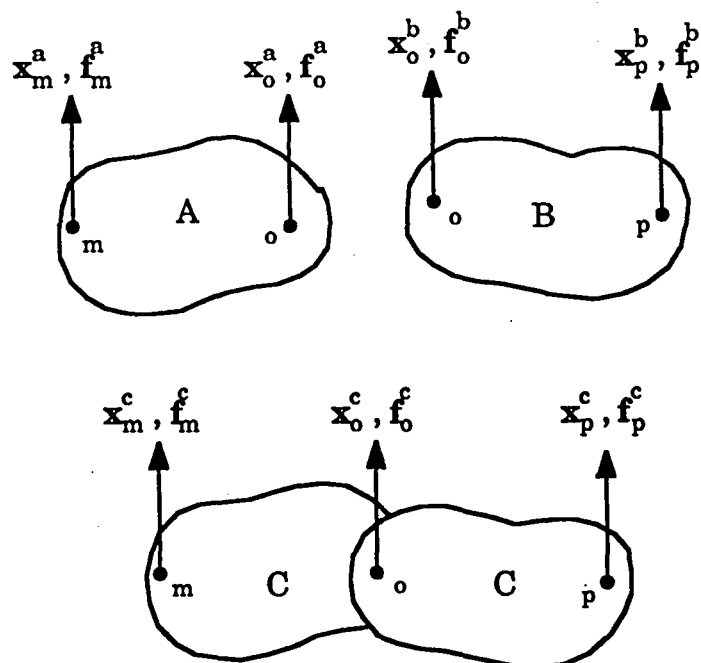


Figure 3: Two hypothetical components A and B are coupled at interface (o) to form superstructure C. Points (m) and (p) are arbitrary interior degrees of freedom.

COMPONENT FREQUENCY RESPONSE MATRIX:

$$\mathbf{x}^a = \mathbf{H}^a \mathbf{f}^a$$

$$\begin{bmatrix} \mathbf{x}_m^a \\ \mathbf{x}_o^a \end{bmatrix} = \begin{bmatrix} \mathbf{h}_{mm} & \mathbf{h}_{mo} \\ \mathbf{h}_{om} & \mathbf{h}_{oo} \end{bmatrix}^a \begin{bmatrix} \mathbf{f}_m^a \\ \mathbf{f}_o^a \end{bmatrix}$$

COMPATIBILITY:

$$\mathbf{x}_o^c = \mathbf{x}_o^a = \mathbf{x}_o^b$$

EQUILIBRIUM:

$$\mathbf{f}_o^c = \mathbf{f}_o^a + \mathbf{f}_o^b$$

COMPONENT MODE SYNTHESIS

MATRIX ASSEMBLY:

$$\mathbf{f}^a = [\mathbf{H}^a]^{-1} \mathbf{x}^a = \mathbf{Z}^a \mathbf{x}^a$$

$$\mathbf{f}^b = [\mathbf{H}^b]^{-1} \mathbf{x}^a = \mathbf{Z}^b \mathbf{x}^a$$

$$\begin{bmatrix} \mathbf{f}_m \\ \mathbf{f}_o \\ \mathbf{f}_p \end{bmatrix}^c = \begin{bmatrix} \mathbf{Z}_{mm}^a & \mathbf{Z}_{mo}^a & 0 \\ \mathbf{Z}_{om}^a & \mathbf{Z}_{oo}^a + \mathbf{Z}_{oo}^b & \mathbf{Z}_{op}^b \\ 0 & \mathbf{Z}_{po}^b & \mathbf{Z}_{pp}^b \end{bmatrix}^c \begin{bmatrix} \mathbf{x}_m \\ \mathbf{x}_o \\ \mathbf{x}_p \end{bmatrix}^c$$

or

$$\mathbf{f}^c = \mathbf{Z}^c \mathbf{x}^c$$

DESIRED FRF MATRIX OF THE ASSEMBLED STRUCTURE:

$$\mathbf{H}^c(j\omega) = [\mathbf{Z}^c]^{-1}$$

The force vectors are written in terms of the inverse frequency response functions \mathbf{Z}^a and \mathbf{Z}^b to permit matrix assembly of the inverse of the frequency response matrix of the coupled structure. The desired frequency response matrix of the superstructure is then determined by matrix inversion. Individual point and transfer FRFs of interest are elements of this superstructure transfer function.

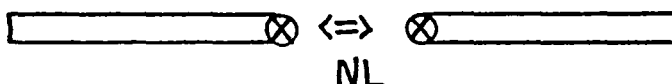
This study examines the applicability of frequency domain component mode synthesis to jointed structures, using experimental frequency response functions. To simulate the problems that might be encountered in the components and joints of deployable spacecraft structures, two beam-like components with joints are built and dynamically tested. In a departure from CMS case studies already in the literature^{8,9,10,11} in which component linearity and full compatibility are assumed, this study relaxes the assumption of compatibility by the introduction of freeplay in the joint between components. The component

ASSUMPTIONS IN COMPONENT MODE SYNTHESIS USING MODAL TEST DATA:

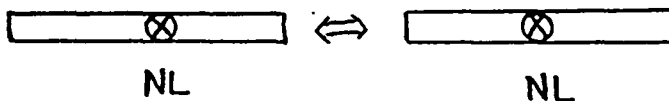
- 1) COMPATIBILITY OF DEFLECTION AT INTERFACE
- 2) LINEAR BEHAVIOR OF COMPONENTS

RESEARCH OBJECTIVES:

- RELAX ASSUMPTION (1) WITH NONLINEAR JOINT AT INTERFACE



- RELAX ASSUMPTION (2) BY TESTING COMPONENTS WITH INTERNAL NONLINEARITY



- RELATE TO GROUND TESTING OF LARGE SPACECRAFT STRUCTURES

experimental frequency response functions (FRFs) are used with component mode synthesis to predict the behavior of the coupled structure. The beams are then physically connected and the actual frequency response of the superstructure is compared to the CMS prediction. Also of interest is the analytical assembly of structures with internal nonlinearities, and of non-linear components via non-linear joints. Such situations are not merely laboratory nightmares, but are needed for pre-flight prediction of the structural dynamics of future deployable spacecraft structures.

It was desired to build an experimental model to address the issues that motivated this research work--the desire to use component mode synthesis to predict the behavior of a multiple bay truss structure, such as the COFS MAST, given the dynamic behavior of components. The MAST flight structure will be characterized by heavy joints and light truss members, will be coupled at many degrees of freedom, may have significant slop in the joints (deadband, hysteresis, nonlinear force deflection curves), and have closely-spaced internal resonances at frequencies well below bending or torsion modes of the bay. These features will strain the accuracy of component mode synthesis, which in the literature to this date has been applied to relatively simple components and coupling.

An experimental coupled beam model was constructed to simulate one of these problems--the effects of a sloppy joint on CMS accuracy. Two identical components A and B were constructed, with lengths of 25.4 inches and with tip masses that serve as joint connections to other components. One of these components is shown in Figure 4. The beam dimensions were chosen in order that bending modes dominate the dynamics of the beam in the frequency range studied, without interference from torsional or shear modes. Components A and B are coupled by a joint to form superstructure C, shown in Figure 5.

COMPONENT:

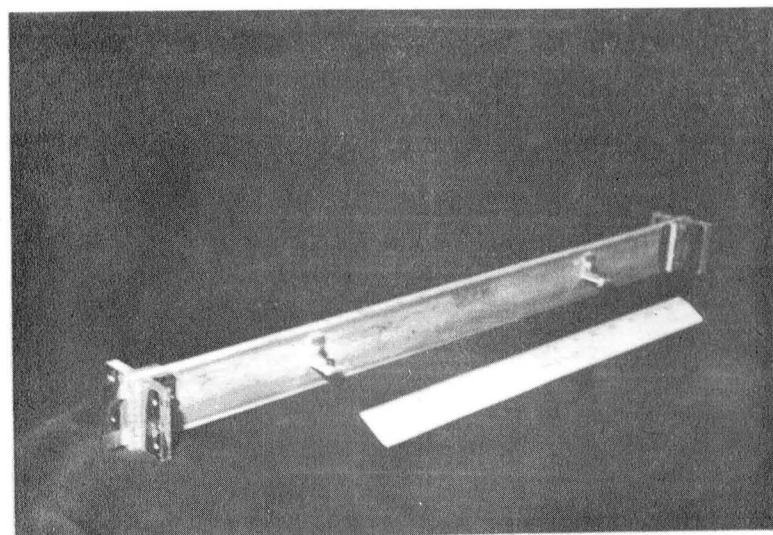


Figure 4: Component used in substructuring

ASSEMBLED STRUCTURE:

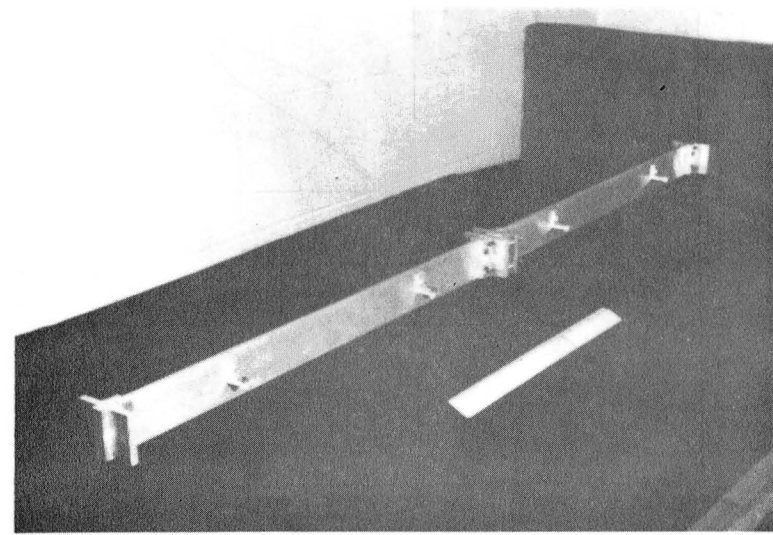


Figure 5: Assembled 2-component superstructure C

JOINT BETWEEN COMPONENTS

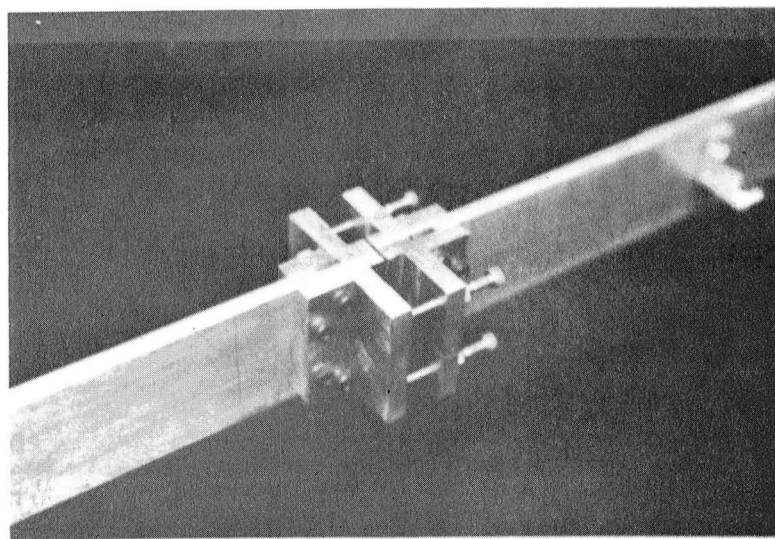


Figure 6: Joint between beam components

LINEAR JOINT

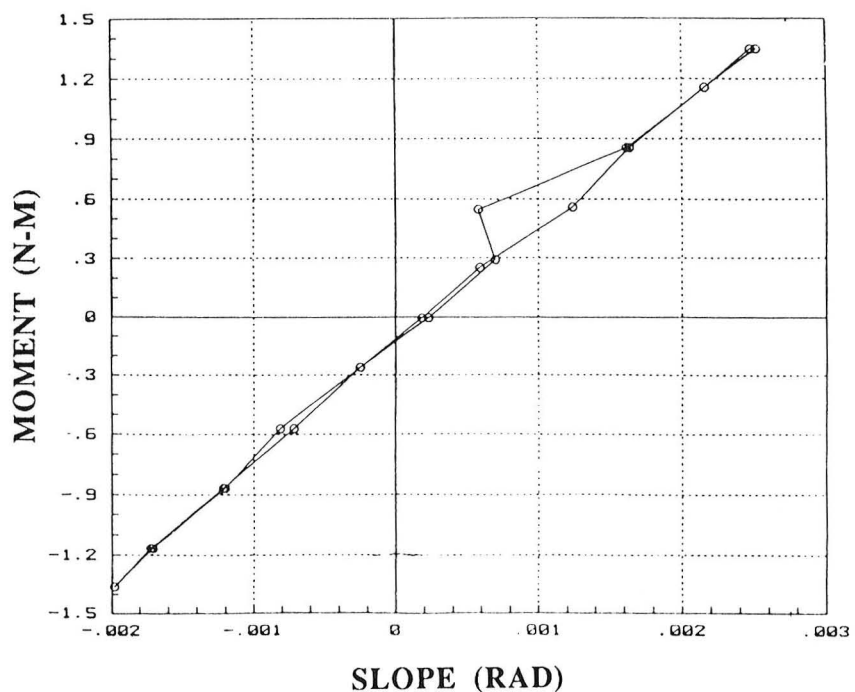


Figure 7: Moment deflection curve of linear joint

Figure 6 shows the joint used to connect components A and B. The joint, which transmits both shear force and moment, can be tightened to appear stiff or loosened to introduce joint rotational freeplay. The joint is made rigid by tightening the bolts (which are tapped into only one component) against the lips of the other component. Thin shimstock maintains alignment of the neutral axis. Rotational freeplay or deadband can be produced by loosening the bolts and letting the joint rotate about the shimstock, which is moderately stiff in shear but weak in bending compared to the beam or joint. No deadband is introduced in the shear deflection--this two degree of freedom joint has deadband in only one degree of freedom.

The experimentally determined moment deflection curve for the rigid joint is shown in Figure 7; note the linearity and lack of measurable hysteresis. The joint is measured to have twice the bending stiffness as an equal length of the rest of the beam. Figure 8 shows the moment deflection curve for the joint with a small deadband introduced. Hysteresis is again not measurable.

JOINT WITH ROTATIONAL FREEPLAY

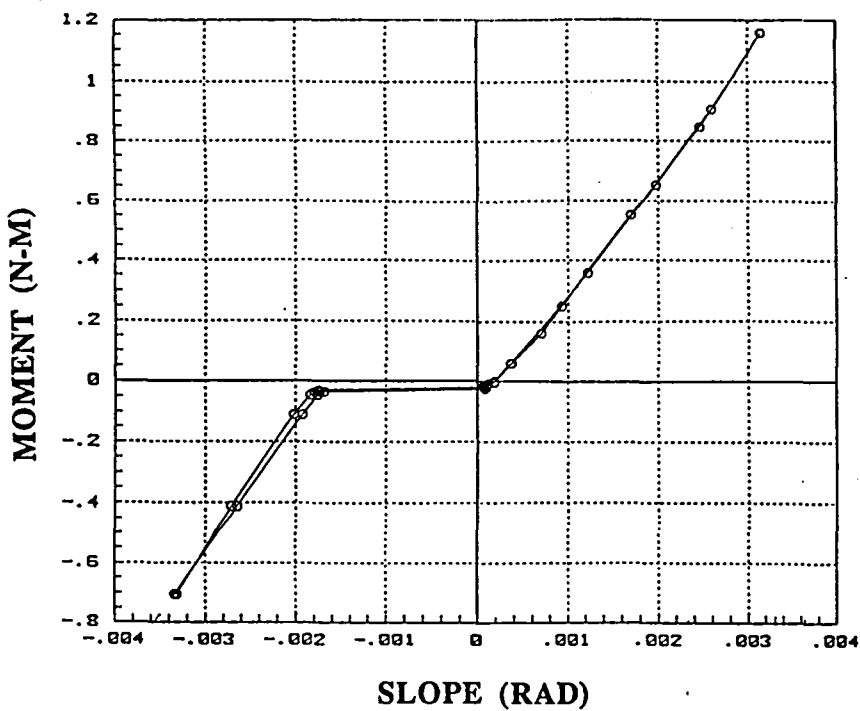


Figure 8: Moment deflection curve of nonlinear joint

Components are suspended by 4 feet of piano wire and are tested in a free-free configuration. Suspension pendulum frequencies of less than 1 Hz are well below the 30 Hz fundamental frequency of the component. Component C is shown suspended in the test configuration in Figure 8. The structure is excited by a shaker, attached to the lip of the structure by a 1mm diameter stinger. Moment excitation is provided by forcing the structure in a direction perpendicular to the lip.

A load cell located between the stinger and the lip measures the force actually applied to the structure. Accelerometers are used to measure translational and rotational accelerations at the beam tips (the desired DOF); rotational accelerations are calculated from translational measurements of the lip lever arm. The structure is excited using broadband burst random excitation. Fifteen averages are used to calculate frequency response functions over the range 0-1000 Hz. Random excitation was selected because of the ease of testing, short time duration of tests, and because it can provide a reasonable linear approximation to the frequency response of a nonlinear structure¹³.

EXPERIMENTAL SETUP

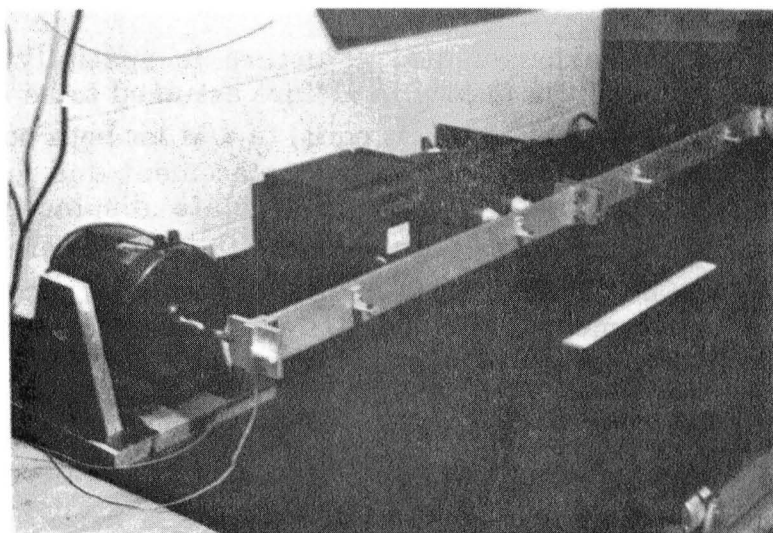


Figure 9: Superstructure C is shown in the free-free test configuration, suspended by 4 feet of piano wire.

FORCE EXCITATION

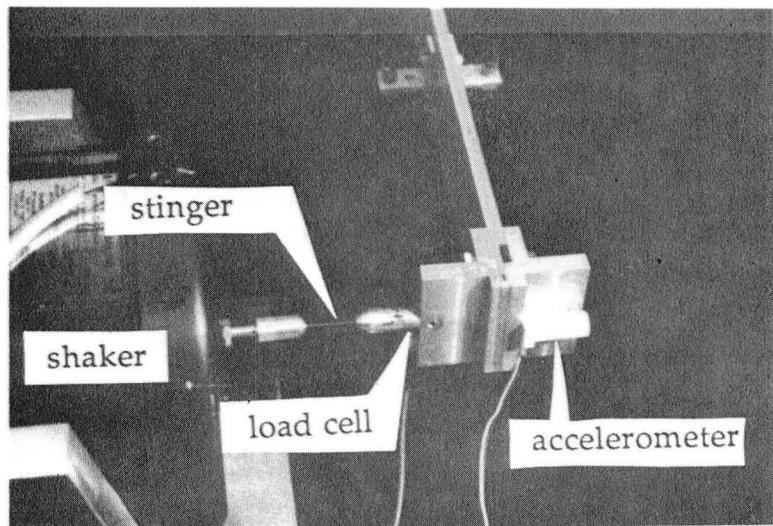


Figure 10: The structure is forced using broadband random excitation applied by the shaker, connected to the joint lip by a flexible stinger (1.2 cm long, 1mm in diameter). A load cell measures the actual force applied; an accelerometer measures a point inertance.

Ewins' frequency domain CMS will now be applied to the experimental component data. Referring to Figure 11, each component has two interior DOF (at point **m**) and two boundary DOF (at point **o**, used in coupling). The two DOF at each point are translation and rotation; each point also is subject to a force and moment. The frequency response matrix $H^a(j\omega)$, or H^a , relates the displacement and force vectors.

Because the experimental structure is spatially symmetric the diagonal partitions of the matrix in H^a are assumed to be identical. It can be shown theoretically⁸ that Θ/F is equal to u/M for both point and transfer receptances (point receptances relate displacement and force at the same geometric point; transfer receptances relate displacement and force between different points). In addition the Θ/M point and transfer receptances can be determined from the u/F and u/M receptances⁸. Thus, four FRF measurements--both point and transfer for u/F and u/M --are sufficient to determine the full 4x4 frequency response matrix H^a .

At this point it is worth noting that during this case study, inertances $a_{ij}(j\omega)$ relating acceleration to force are determined instead of receptances $h_{ij}(j\omega)$ because accelerometers are used as sensors. The receptances $h_{ij}(j\omega)$ can be recovered by

$$h_{ij}(j\omega) = -\frac{1}{\omega^2} \alpha_{ij}(j\omega) \quad (13)$$

The CMS procedure can be implemented as previously described using inertances instead of receptances for the component FRF matrices.

The four experimental FRFs measured for component A are shown in Figure 12. These are the point and transfer inertances for u/F and u/M . Corresponding frequency responses of component B are almost identical. Figure 12(e) also shows one of these FRFs compared to a frequency domain interpolation. Note that the interpolation correctly removes a suspension mode (from the stinger attachment) which is present at around 15 Hz in the measurement. The desirability of such curve fitting is discussed in a subsequent paragraph.

COMPONENT FREQUENCY RESPONSE MEASUREMENTS

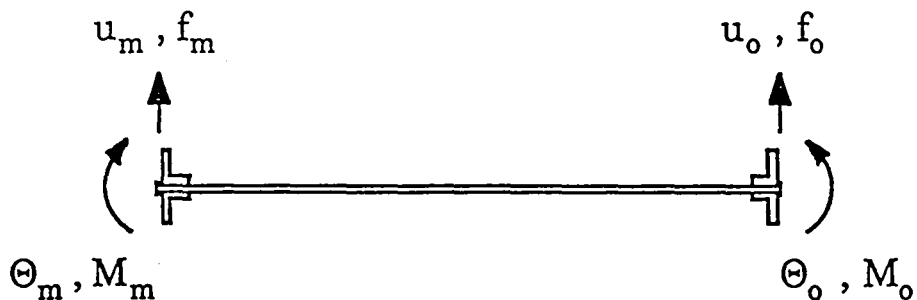


Figure 11: Conventions used to define deflections and forces for the experimental component at interface pt (o) and interior point (m).

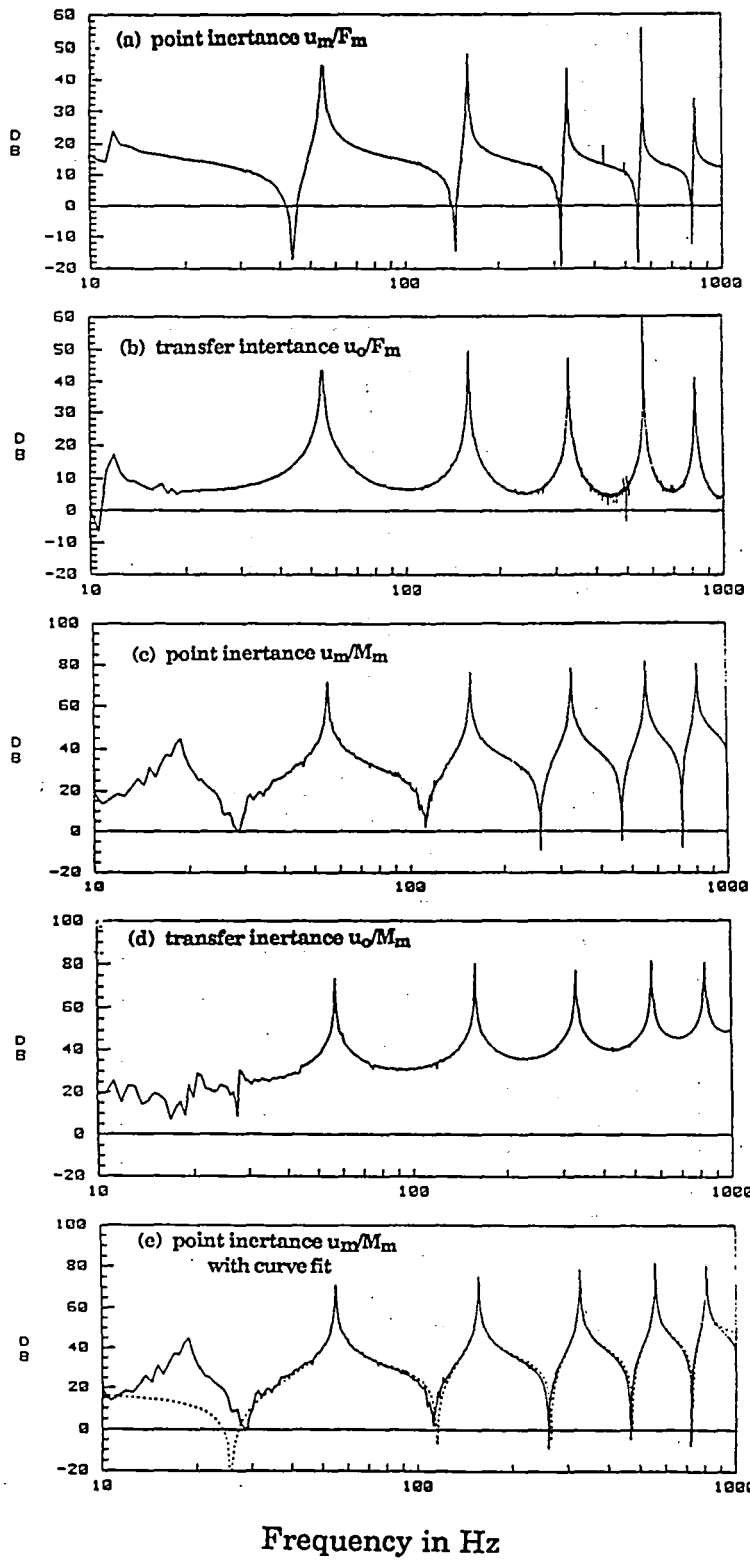
COMPONENT FREQUENCY RESPONSE MATRIX:

$$\begin{bmatrix} u_m \\ \Theta_m \\ \hline u_o \\ \Theta_o \end{bmatrix}^a = \begin{bmatrix} h_{11} & h_{12} & | & h_{13} & h_{14} \\ h_{21} & h_{22} & | & h_{23} & h_{24} \\ \hline h_{31} & h_{32} & | & h_{33} & h_{34} \\ h_{41} & h_{42} & | & h_{43} & h_{44} \end{bmatrix}^a \begin{bmatrix} f_m \\ M_m \\ \hline f_o \\ M_o \end{bmatrix}^a$$

$$\begin{bmatrix} x_m \\ x_o \end{bmatrix}^a = \begin{bmatrix} h_{mm} & h_{mo} \\ h_{om} & h_{oo} \end{bmatrix}^a \begin{bmatrix} f_m \\ f_o \end{bmatrix}^a$$

$$\mathbf{x}^a = \mathbf{H}^a \mathbf{f}^a$$

COMPONENT FREQUENCY RESPONSE MEASUREMENTS



Frequency in Hz

Figure 12: The four experimental inertance frequency response functions used to define the 4x4 FRF matrix for component B are shown in (a) through (d). 12(c) is replotted in (e) along with its curve fit approximation. Zero dB for translational inertances are 1m/sec^2 per Newton; zero dB for rotational inertances are 1m/sec^2 per Newton-meter.

COUPLED STRUCTURE

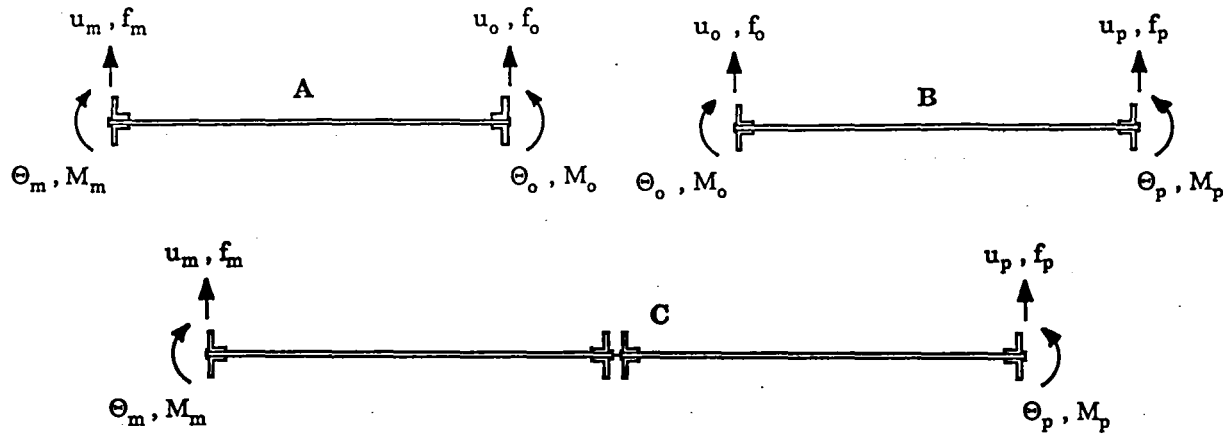


Figure 13: Components A and B are joined at interface (o) to form superstructure C.

COMPATIBILITY:

$$\begin{bmatrix} u_o \\ \Theta_o \end{bmatrix}^c = \begin{bmatrix} u_o \\ \Theta_o \end{bmatrix}^a = \begin{bmatrix} u_o \\ -\Theta_o \end{bmatrix}^b$$

EQUILIBRIUM:

$$\begin{bmatrix} f_o \\ M_o \end{bmatrix}^c = \begin{bmatrix} f_o \\ M_o \end{bmatrix}^a + \begin{bmatrix} f_o \\ -M_o \end{bmatrix}^b$$

Using the measured inertance matrices of each component, the component mode synthesis procedure is carried out, using the equations of compatibility and force equilibrium. Note that compatibility is enforced for both translation and rotation. These compatibility conditions are known to be in error in the presence of rotational freeplay, in which case Θ_o^a does not equal Θ_o^b . The presence of joint freeplay does not alter the validity of the force equilibrium equation.

Figure 14 shows a comparison of u_p/f_m between direct CMS prediction using the measured component FRFs presented in Figure 10 and the actual measurement of the assembled two-component structure. The prediction matches the true FRF well in terms of damping and modal amplitudes, and accurately predicts the frequencies of the seven lowest superstructure modes except the first. Note that there are several incorrect modes and zeros present; these occur at poles and zeros of the component FRFs, and are due to the inconsistencies in the measurements.

Ewins has shown that these errors may be greatly reduced by careful curve-fitting and adjustment of the raw FRFs by means of a consistent modal model⁸. The generic modal model for an inertance FRF is given by

$$\frac{\ddot{x}}{f} = A_0 + \sum_{r=1}^N \left\{ \frac{\omega^2 A_r}{\Omega_r^2 - 2j\Omega_r \zeta \omega - \omega^2} \right\} + \sum_{r=N+1}^{\infty} \left\{ \frac{\omega^2 A_r}{\Omega_r^2} \right\} \quad (16)$$

where N is the number of kept dynamic modes, Ω_r is the natural frequency of the r^{th} mode and ζ is the damping ratio for that mode.

The four component FRFs of Figure 12 were curve fit and reconstructed according to this modal model, excluding the contributions of higher modes. Analytical rigid body modes were substituted for the low frequency asymptote, effectively removing the stinger influence. A further minor adjustment is necessary; the component FRFs must be consistent with a modal model; modal frequencies, damping ratios and residues were all adjusted for consistency. In each case the corrections were only a few percent, and were derived by taking the arithmetic average of the available estimates. Figure 15 shows the results of CMS with these "unified" component FRFs. The improvement over Figure 14 is dramatic. Modes 2 to 6 are very accurately predicted. The first mode is strongly influenced by the rigid-body asymptotic adjustments made to the measured component FRFs, and remains in disagreement with the stinger-corrupted superstructure measurements. Modes 7 to 10 show errors that are likely due to errors in positioning the force transducer and the accelerometers precisely at the end of the components, as documented in Figure 10. This difficulty is generic in experimental component mode synthesis. If significant deflections occur between the measurement location and the actual interface, the measured component FRF's will be in error. This measurement error will increase with frequency. Figure 15 also shows the effect of limited curve-fitting of the component FRFs. The last component mode curve-fit is near 800 Hz; the result is the poor superstructure prediction above that frequency.

The poor match at the lowest mode is believed to be due to an inaccurate measurement of this mode rather than a poor prediction. The structure was excited by an electrodynamic shaker connected to the structure via a "stinger" consisting of a piece of piano wire 1.2 cm long. This stinger resonates in the neighborhood of 15 Hz, coupling with the first structural mode. Since the load cell which measures stinger force has some cross-axis coupling, this stinger lateral vibration leads to a measurement error, significant near 15 Hz. Stinger changes are in progress at time of this writing.

RESULTS OF CMS

RAW DATA:

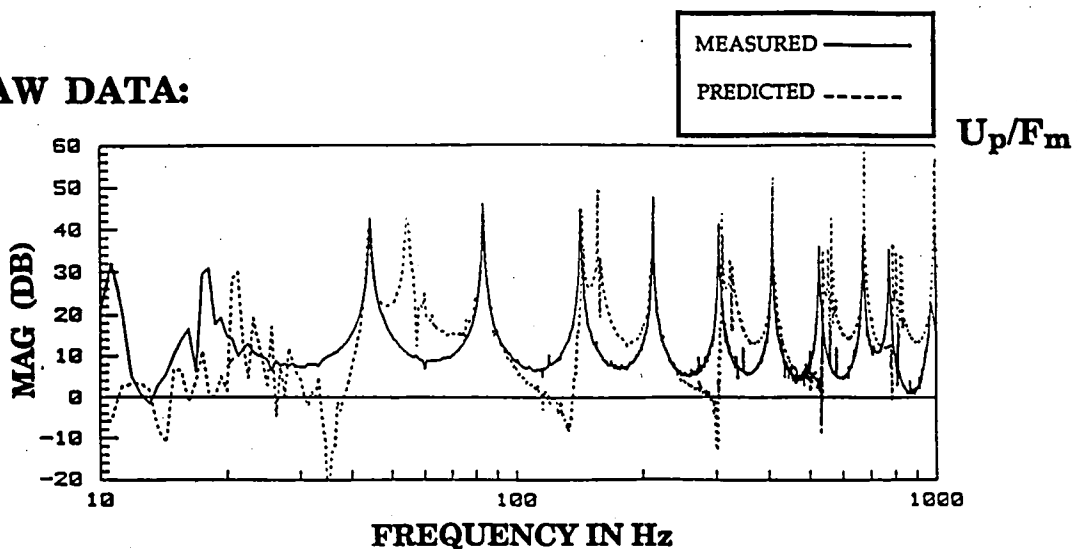


Figure 14: Comparison of the measured FRF u_p/F_m of the physically assembled structure with the CMS prediction using raw data. Spurious resonances occur in the CMS predictions near resonances of the components.

"UNIFIED" MODAL MODEL:

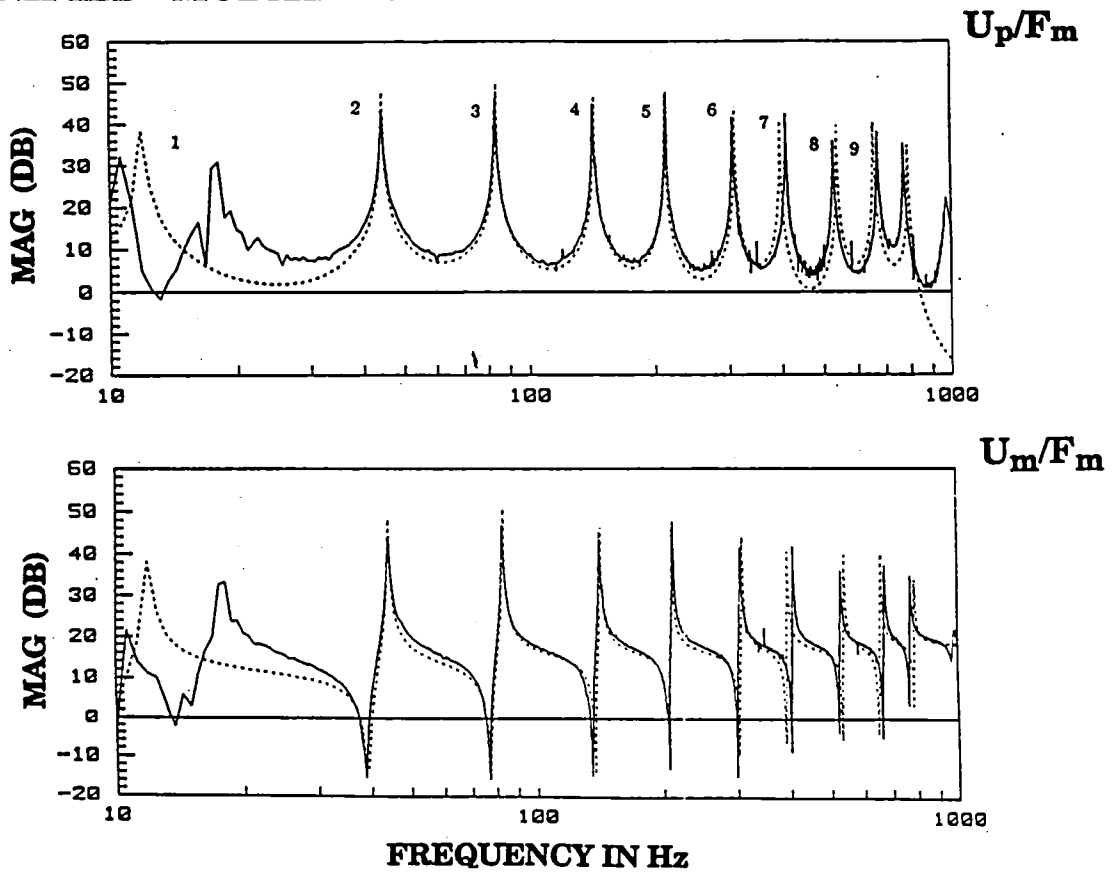


Figure 15: Comparison of the measured FRFs u_p/F_m and u_m/F_m of the physically assembled structure with the CMS prediction using component FRFs derived from a unified modal model.

Various amounts of joint rotational freeplay δ_θ are introduced by loosening the bolts between the lips of the joint, and are measured by saturating the deadband and measuring the deflection change of the joint lips. The deadband δ_θ is defined as the total angle change undergone by the joint in rotating between the two saturation points.

The frequency response of the superstructure with loose joints is then measured. The requirement that the structure be linear for modal test methods to be applicable will be waived for the purpose of identifying the effect of the deadband on the FRF measurement. Since burst random testing is used, the FRFs may be interpreted as the approximate linear response of the nonlinear structure¹³. Although the effect of the gap will clearly be dependent on response amplitude as well as gap size, this study used only a constant force excitation level.

Figure 16 shows the effect of increasing gap size on the FRF of u_p/f_m for the two-component structure. The sizes of the deadband are between 1.5×10^{-3} and 3.5×10^{-3} radians. Several interesting effects occur: firstly, the destruction of the FRF due to the gap occurs first at high modes, while the lower modes appear unaffected and still "linear". The destruction advances down in frequency as the gap size increases. The high frequency effect is understandable, since the rotational deflection of the high modes across the joint is less, and thus the joint nonlinearity will be saturated less of the time. Hunter¹⁴ demonstrated a similar destructive effect on inertance measurements for a four DOF mass spring model. Secondly, the modes appear to be more highly damped, not a surprising result given that significant rattling was heard during the testing, and that the spectrum analyzer has a difficult time constructing a transfer function from noisy and nonlinear data. Thirdly, the mode peaks shift lower in frequency--an effect observed previously in other analytical and experimental studies^{15,16}. However, only the odd modes gain damping and shift in frequency, since the odd mode shapes have an antinode of rotation at the joint and thus excite the deadband. The even mode shapes have a rotational node point at the joint; here the components are coupled only by shear force. These mode shapes do not excite the deadband and therefore the modes are not affected significantly, except when the noise from the other modes becomes excessive and interferes at the even mode frequencies. This dependence on mode shape is consistent with the experimental results of Bohlen and Gaul⁵. Lastly, when the deadband is very large, the FRF resembles noise--a result of a severe breakdown in the assumption of linearity and the superposition principle. Modal analysis is not defined in this regime of structural response.

EFFECT OF INCREASING DEADBAND ON INERTANCE MEASUREMENT:

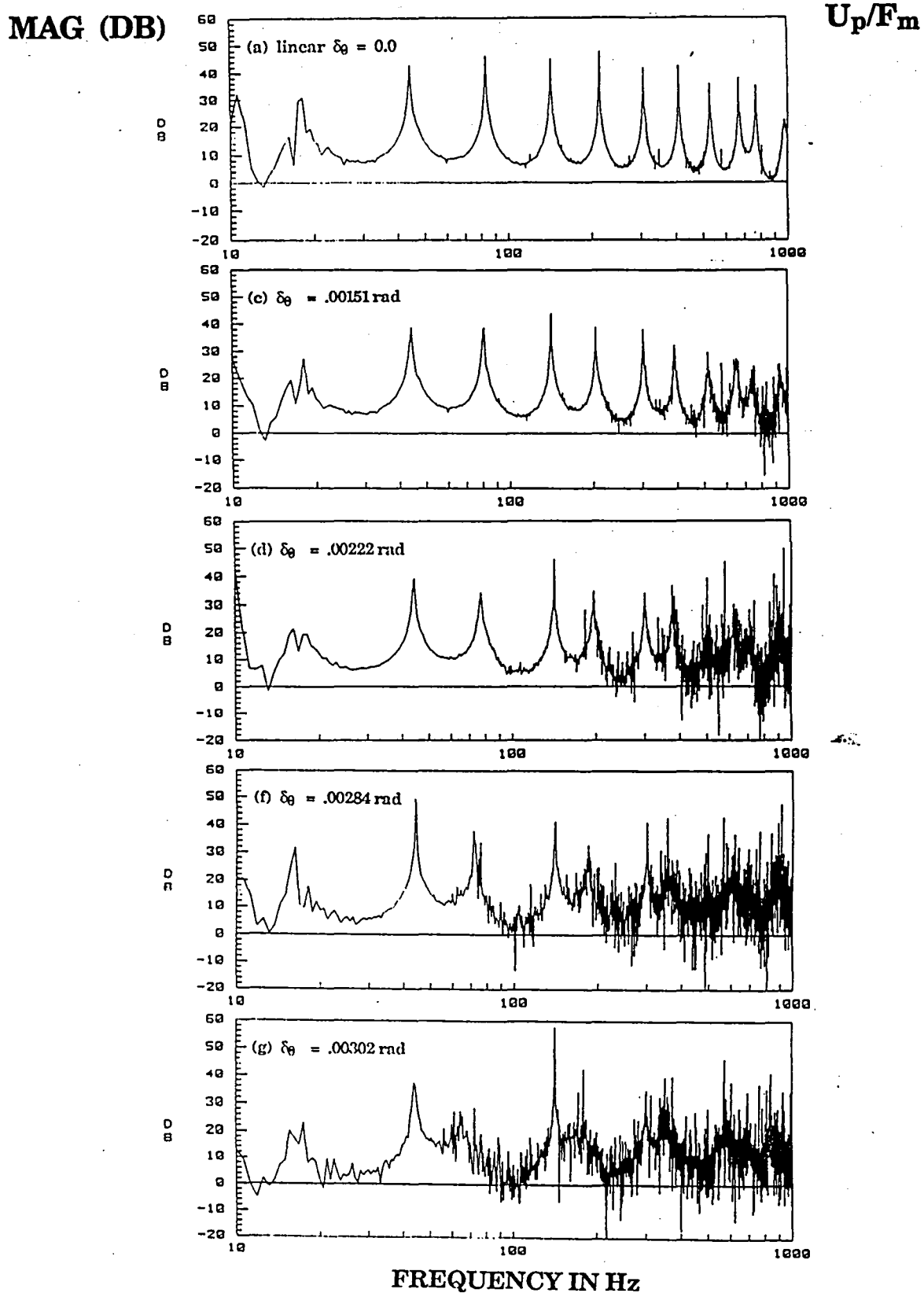


Figure 16: The superstructure inertance U_p/F_m is shown for increasing sizes of deadband in the joint.

The effect of this deadband on the accuracy of the component mode synthesis prediction is now investigated, since the coupling equations assumed a linear, fully compatible joint. Assuming that the CMS prediction is the curve in Figure 15, with an initial error E_0 for the modal quantities, the change in this error ΔE can be calculated by measuring the shift in frequency and damping of the "modes" of the nonlinear structure. Figure 17 provides a visual comparison of CMS predictions with measurements of the non-linear structure.

353

850

ERROR IN CMS PREDICTION

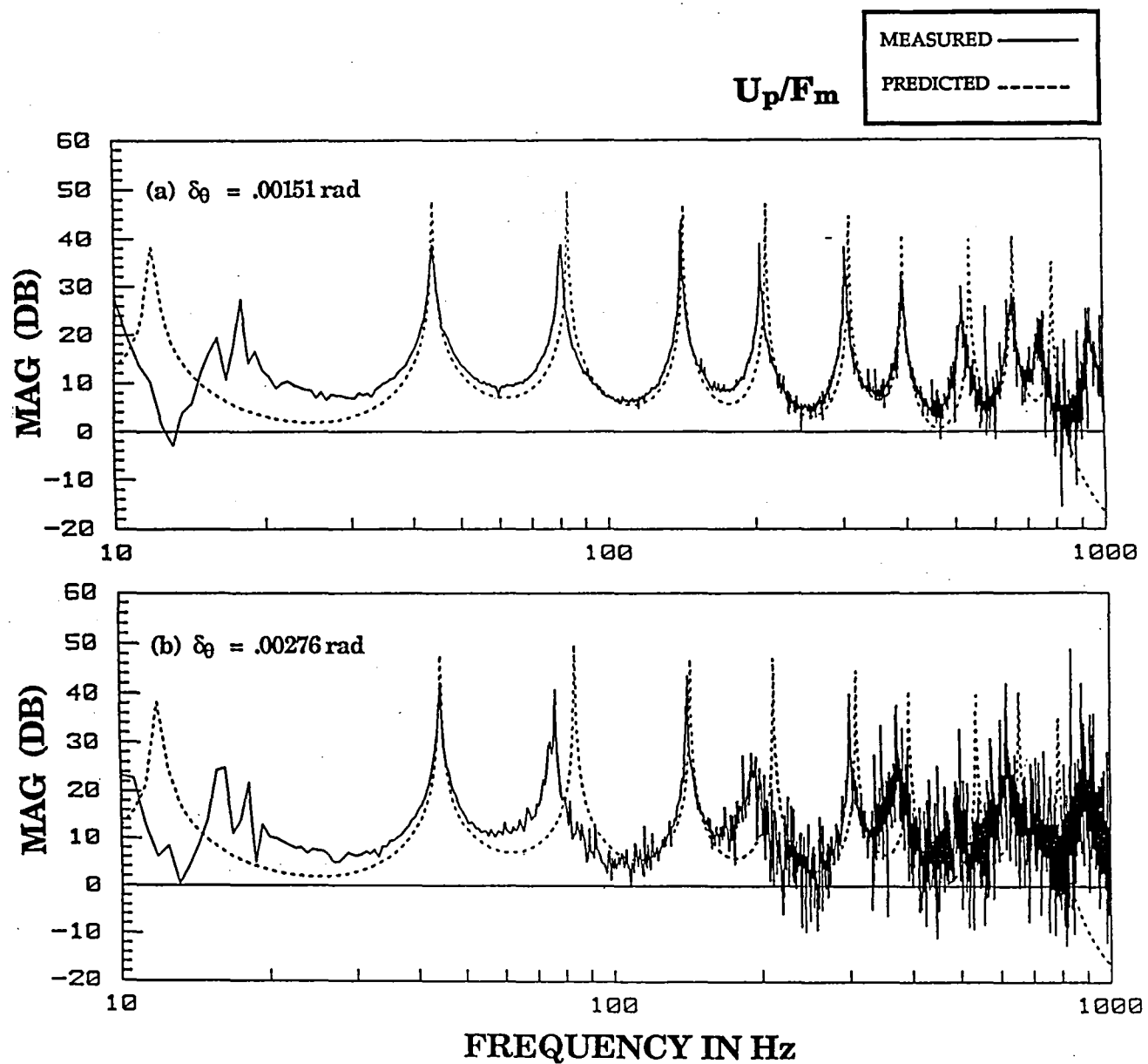


Figure 17: Comparison of linear CMS prediction of the superstructure response u_p/F_m with the actual response of the assembled structure with deadband in the joint.

The percent error in CMS modal frequency prediction due to the gap is plotted versus gap size for the odd modes, 3 and 5, in Figure 18, and the absolute error in damping ratio is plotted versus gap size in Figure 19. The graphs demonstrate an increasing error in frequency and damping prediction as the size of the gap increases. The frequency shift of higher modes is always greater than for lower modes for a given gap size. Note that the frequency error takes a somewhat steep drop at about .0026 radians. This corresponds to the point in Figure 13 when the inertance measurement of mode 3 becomes very noisy.

ERROR IN CMS PREDICTION

Δ ERROR IN MODAL FREQUENCY (%)

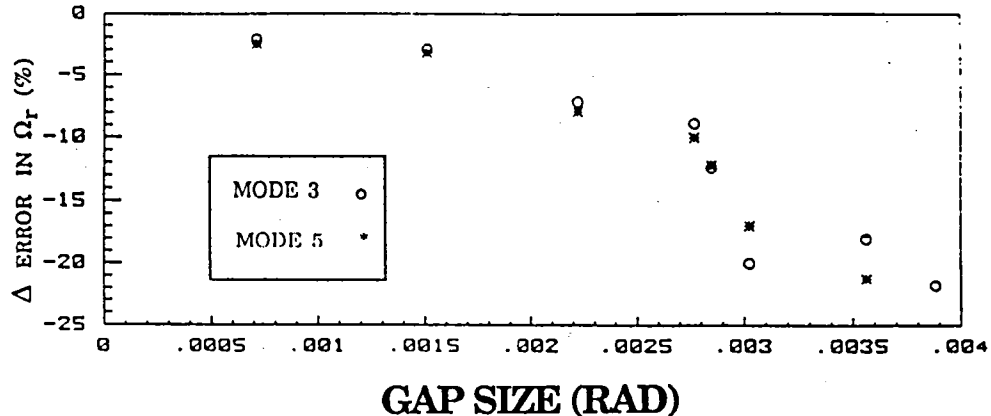


Figure 18: Plot of the error in the CMS prediction of the superstructure modal frequencies 3 and 5 versus the measured gap size in the joint.

Δ ERROR IN % DAMPING

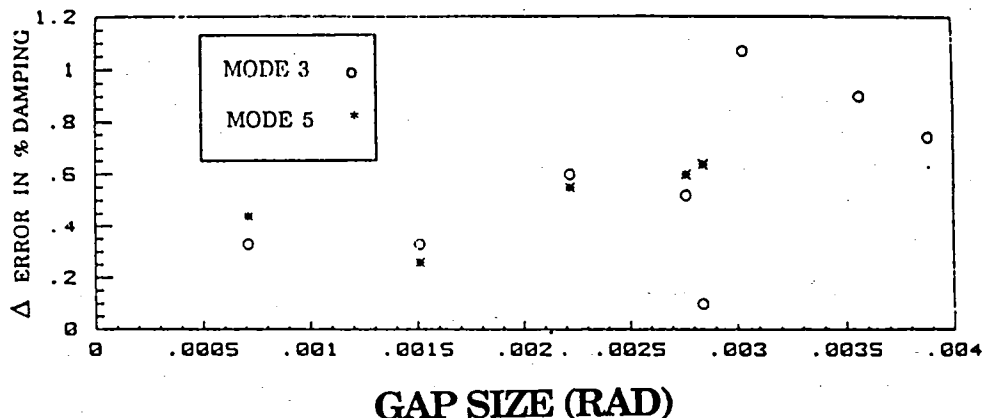


Figure 19: Plot of the error in the CMS prediction of the superstructure damping in modes 3 and 5 versus the measured gap size in the joint.

NON DIMENSIONALIZED DEADBAND

$$\delta_{\theta}^* = \frac{\delta_{\theta}}{\Theta' d}$$

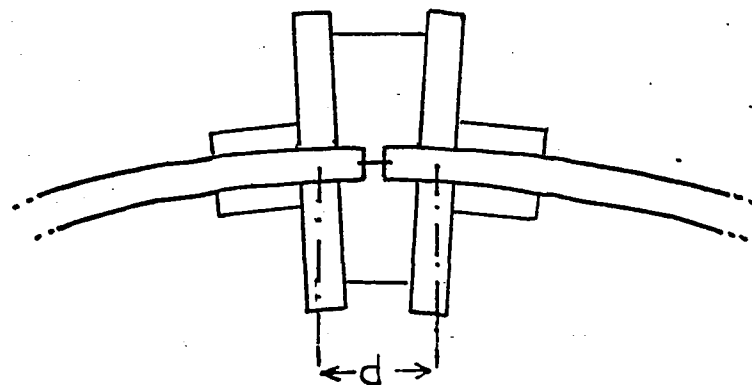


Figure 20: Joint geometry for proposed non-dimensionalization of the gap nonlinearity. The deadband deflection is normalized by the local deflection across the linear joint

An attempt was made to nondimensionalize the deadband gap size. The gap was normalized by the actual rotation due to bending curvature across the length of the joint for the *linear* structure, given the particular excitation force level. This would thus compare the deadband deflection with the local deflection due to local flexibility, a comparison that intuitively would seem to quantify the importance of the gap. The normalized deadband is proposed to be

$$\delta_{\theta}^* = \frac{\delta_{\theta}}{\Theta' d}$$

where d is the distance across the joint along the beam axis, δ_{θ} is the gap size and Θ' is the curvature of the beam at the joint. Work in progress involves expressing the errors in frequency and damping estimates in terms of this nondimensional parameter, which turns out to be very sensitive to the actual force applied to the structure at the mode frequencies.

CONTINUING WORK:

- Generalize results by nondimensionalizing joint nonlinearity
- Incorporate joint dynamics directly into CMS procedure via the describing function technique.
- Investigate relative CMS accuracy when the nonlinear joint is "internalized" inside the component, compared to case when the same joint is at the component interface.

This paper reports only a start into the investigation of applicability of component mode synthesis to structures with non-linear joints. Future work will attempt to generalize these results to other structures by non-dimensionalizing the joint non-linearity. In this way we hope to propose useful guidelines for estimating the fidelity to be expected of ground testing of deployable spacecraft structures. Other planned extensions of this work include introducing explicit non-linear models of joint dynamics into the component mode synthesis procedure, initially via the describing function technique. Also of interest is the analytical assembly of structures with internal non-linearities, and of non-linear components via non-linear joints. These situations are likely to be encountered in the pre-flight prediction of the structural dynamics of future deployable spacecraft structures.

Frequency domain component mode synthesis was conducted for a two-component jointed structure based on the experimental frequency response functions of each component. The CMS predictions of superstructure frequency response were found to be in excellent agreement with the measured response of the physically assembled structure. The accuracy of this prediction is dependent on using component FRF data derived from a consistent modal model, based on experimental frequency response measurements.

The presence of the linear, fully compatible joint influences CMS accuracy since it prevents the accurate measurement of component FRFs at the exact interface degrees of freedom of the components. This affected the CMS prediction of the higher modes of the assembled structure by a few percent. Inaccuracies in the prediction, and measurement, of the first mode of the assembled structure occur because of dynamic interaction with the forcing stinger, a problem which can be overcome by judicious stinger design.

The effect of a nonlinear joint with deadband was demonstrated to reduce the accuracy of the CMS prediction. Mode frequencies are overestimated on the order of 5% to 10% for even small amounts of joint freeplay, and damping values are underestimated. There is little or no error induced in either mode frequency or damping when the superstructure has a strain anti-node at the joint. Errors in mode frequency prediction increase with mode number for any given deadband. The qualitative effect of the joint gap on inertance measurements of the superstructure was also shown. Pollution of the FRF due to joint non-linearity occurred first at high frequencies, destroying modes in this region, and then at progressively lower frequencies as the gap size increased. Small amounts of deadband did not affect the accurate measurement of the lower modes, but did result in small shifts in frequency and damping for these modes.

SUMMARY

- Linear joint affects CMS accuracy by preventing accurate measurement of component FRFs at interface DOF
- Prediction error in frequency and damping is significant when deadband joint is present between components
- Amount of error depends on mode shape
- Component Mode Synthesis reasonably easy and accurate for simple, linear laboratory structures; could be useful for ground testing of large space structure components.

Acknowledgements

This research was supported in part by NASA Grant NAGW-21, monitored by Mr. Samuel Venneri, and in part by an AFOSR Instrumentation Grant, 87-0031, monitored by Dr. Anthony Amos.

References

1. Ashley, H, "Some Considerations on Earthbound Dynamic Testing of Large Space Structures", AIAA Paper # 86-0908.
2. Card, M. F., Anderson, M. S., Walz, J. E., "Dynamic Response of a Flexible Space Beam", NASA Technical Memorandum 86441, May 1985.
3. Crawley, E. F., and O'Donnell, K. J., "A Procedure for Calculating the Damping in Multi- Element Space Structures", Acta Astronautica, Vol. 15, No. 12, 1987, pp. 987-996.
4. Craig, R.R., "A Review of Time-Domain and Frequency-Domain Component Mode Synthesis Method", Combined Experimental Analytical Modeling of Dynamic Structural Systems, ASME, AMD-Vol. 67, June 1985, pp. 1-30.
5. Bohlen, S., and Gaul, L., "Vibrations of Structures Coupled by Nonlinear Transfer Behaviour of Joints; A Combined Computational and Experimental Approach", Proceedings of 5th International Modal Analysis Conference, April 1987, pp. 86-91.
6. Abanshman, M., "Dynamic Modeling of Automobiles Using Combined Analytical/ Experimental Methods", Combined Experimental/ Analytical Modeling of Dynamic Structural Systems, ASME , AMD-Vol. 67, June 1985, pp. 139-153.
7. Baker, M., "Component Mode Synthesis for Test Based, Rigidly Connected, Flexible Components", AIAA/ASME/ASCE/AHS 25th Structures, Structural Dynamics, and Materials Conference, May 1984, pp. 153-163.
8. Ewins, D. J., and Gleeson, P.T., "Experimental Determination of Multidirectional Mobility Data for Beams", Shock and Vibration Bulletin 45, #5, June 1975, pp.153-174.
9. Ewins, D. J., "Modal Test Requirements for Coupled Structure Analysis Using Experimentally-Derived Component Models", Combined Experimental Analytical Modeling of Dynamic Structural Systems, ASME, AMD-Vol.67, June 1985, pp. 31-47.

10. Brassard, J., and Massoud, M., "Identification of a Complete Mobility Matrix of a Synthesized System From Component Mobility Measurements", Proceedings of 5th International Modal Analysis Conference, April 1987, pp. 319-323.
11. Geering, H. P., "New Methods in Substructuring", AIAA/ASME/ASCE/AHS 21st Structures, Structural Dynamics, and Materials Conference, May 1980, pp. 801-808.
12. Martinez, D.R., Carne, T. G., and Miller, A. K., "Combined Experimental/Analytical Modeling Using Component Mode Synthesis", AIAA/ASME/ ASCE/AHS 25th Structures, Structural Dynamics, & Materials Conference, May 1984, pp. 140-152.
13. Goyder, H.G.D., "Foolproof Methods for Frequency Response Measurements", 2nd International Conference on Recent Advances in Structural Dynamics, University of Southampton, England, 1984.
14. Hunter, N. F., "An Investigation of the Time History and Modal Responses of Some Simple Linear and Nonlinear Systems", Proceedings of 3rd International Modal Analysis Conference, Orlando, FL, 1985, pp. 410-418.
15. Mertens, M., et al., "Detection of Nonlinear Dynamic Behaviour of Mechanical Structures", Proceedings of 4th International Modal Analysis Conference, Los Angeles, CA, February 1986, pp.712-719.
16. Coyner, J. V., and Bachtell, E. E., "Box Truss Antenna Technology Status", NASA/DOD Control/ Structures Interaction Technology, Norfolk, VA, November 1986, pp. 717-736.